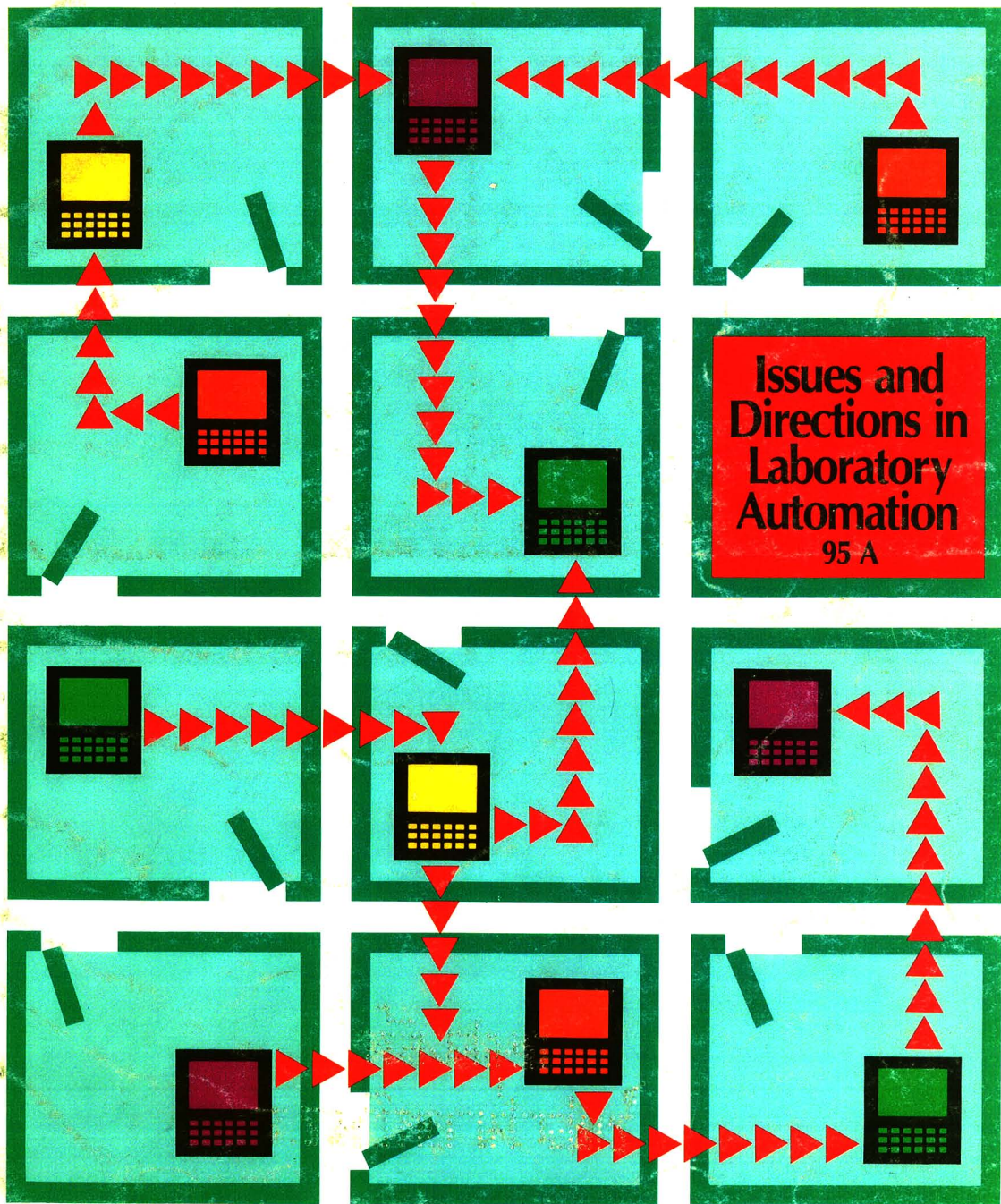
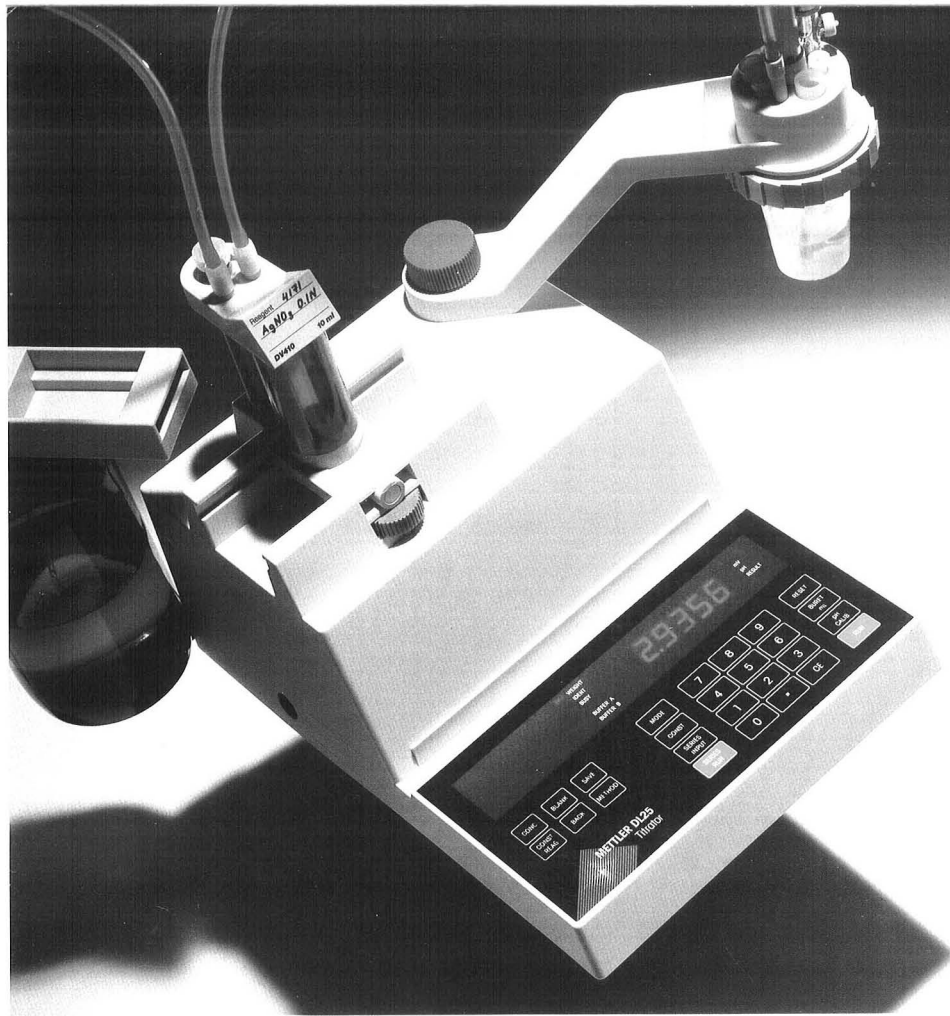


JANUARY 15, 1988

# Analytical

## CHEMISTRY





Staying ahead at the leading edge in **performance**  
and **versatility**, at yesteryears' lower prices...

Introducing the **new DL25 and DL21 Titrators**

- designed to meet your specific needs
- extensive automation possibilities
- available with new PC software
- exclusive two-year **METTLER Service Plus®** Protection:  
on-site repair or a loaner unit guaranteed within 48 hours

**METTLER**, whenever titration is your concern.

CIRCLE 94 ON READER SERVICE CARD

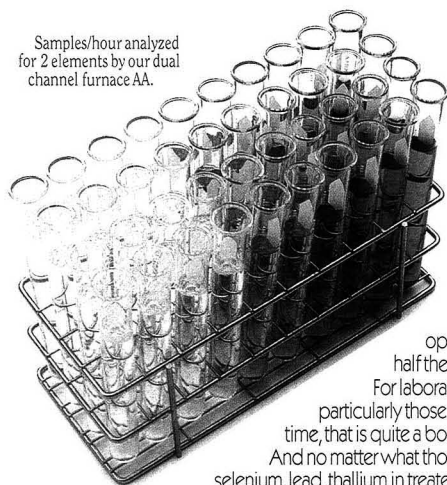
Mettler Instrument Corporation, Box 71, Hightstown, N.J. 08520  
Phone 1-800-METTLER, in New Jersey 609-448-3000

**METTLER**



# Why buy an AA that analyzes tough samples two elements at a time?

Samples/hour analyzed for 2 elements by our dual channel furnace AA.



The Smith-Hieftje 22 was built for environmental and other laboratories for whom productivity, unit cost of analysis and accuracy of results are key concerns.

This dual channel Flame/Furnace AA spectrophotometer with Prep Station and Sample Changer costs approximately the same as a comparable single channel instrument, and yet, in the hands of a single operator, it can do twice as many determinations per day, at half the cost per determination.

For laboratories with a fixed or growing sample load, particularly those who are concerned about turn around time, that is quite a boon.

And no matter what those laboratories are measuring—arsenic, selenium, lead, thallium in treated water, seawater or sludge—the determinations will be accurate every single time.

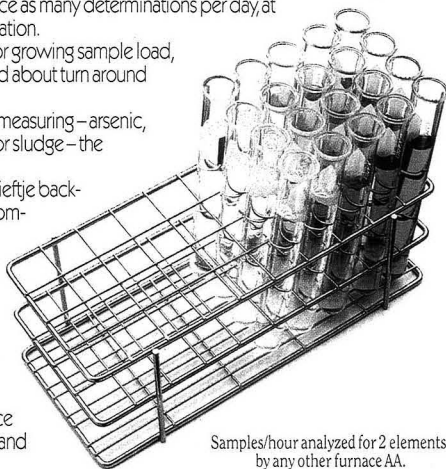
That's because the Smith-Hieftje 22 employs the Smith-Hieftje background correction system—vastly superior to deuterium and recommended by the EPA\*—and is equipped with the Delayed Atomization Cuvette (DAC) and aerosol sampling device, innovations which virtually eliminate vapor and solid phase matrix interferences.

Method development, run initiation, and the display and printing of results are all menu-driven, and, therefore, can be quickly learned even by a novice operator, and sophisticated software allows for overnight unattended operation.

And the Smith-Hieftje 22 comes complete with a full program of service and support including installation, documentation, user training, warranty and field service.

For an appointment to see our new Smith-Hieftje 22 AA Spectrophotometer in operation, call (617) 520-1880. Or write Thermo Jarrell Ash Corporation, 8 E Forge Parkway, Franklin, MA 02038-9101.

\*EPA Test Methods for Evaluating Solid Waste, Vol 1A, two-17, Sept. 1986



Samples/hour analyzed for 2 elements by any other furnace AA.



Smith-Hieftje 22 Flame/Furnace AA Spectrophotometer With Prep Station & Sample Changer

Correction Method	Arsenic True Value	Arsenic Determined Value
Smith-Hieftje	32.4 ppb	32.1 ppb
Deuterium	32.4 ppb	56.0 ppb

The EPA recommends Smith-Hieftje background correction over deuterium, largely on the basis of performance evaluation results such as shown here.

**Thermo Jarrell Ash Corporation**

A Division of Thermo Instrument Systems, Inc.

CIRCLE 156 ON READER SERVICE CARD



**Colorimetry  
made easy.**

Try the Brinkmann  
Immersion Probe  
Colorimeter 14 days—  
FREE. You'll go straight  
to the solution.

**Simplify any colorimetric determination.**

Take the Brinkmann Probe Colorimeter directly to your solutions for simple, accurate, versatile colorimetry. Widely used in industry and educational institutions, it eliminates cuvette breakage and cleaning because no sample transfer is required. The fiber optic probe is dipped directly into any size container—test tube, vat, or permanently installed into a pipeline for process monitoring. Readout (digital or analog) is instantaneous. And because only the probe tips come in contact with the solution, there's no measurable carryover or sample contamination between tests. Built-in filter wheels for applications at six specific wavelengths, interchangeable filters for single or multi wavelengths, and accessories to customize your colorimeter for specific applications are also available.

**A FREE 14-day trial is just the beginning of your savings.**

To enjoy the savings in time and dollars this economical unit can give you, get your FREE trial now. For more information: call 800-645-3050; in New York, 516-334-7500. Or write Brinkmann Instruments, Inc., Cantiague Road, Westbury, NY 11590. (In Canada: 416-675-7911; 50 Galaxy Blvd., Rexdale, Ont. M9W 4Y5)

Shaping the future. **Brinkmann**  
INSTRUMENTS, INC.

BRK-5465





ANCHAM  
 60(2) 59A-102A/97-192 (1988)  
 ISSN 0003 2700

**Registered in U.S. Patent and Trademark Office;  
 Copyright 1988 by the American Chemical Society**

**ANALYTICAL CHEMISTRY** (ISSN 0003-2700) is published semimonthly by the American Chemical Society at 1155 16th St., N.W., Washington, D.C. 20036. Editorial offices are located at the same ACS address (202-872-4600; TDD 202-872-8733). Second-class postage paid at Washington, D.C., and additional mailing offices. Postmaster: Send address changes to **ANALYTICAL CHEMISTRY** Membership & Subscription Services, P.O. Box 3337, Columbus, Ohio 43210.

**Claims for missing numbers** will not be allowed if loss was due to failure of notice of change of address to be received in the time specified; if claim is dated (a) North America: more than 90 days beyond issue date, (b) all other foreign: more than one year beyond issue date, or if the reason given is "missing from files."

**Copyright Permission:** An individual may make a single reprographic copy of an article in this publication for personal use. Reprographic copying beyond that permitted by Section 107 or 108 of the U.S. Copyright Law is allowed, provided that the appropriate per-copy fee is paid through the Copyright Clearance Center, Inc., 27 Congress St., Salem, Mass. 01970. For reprint permission, write Copyright Administrator, B&J Division, ACS, 1155 16th St., N.W., Washington, D.C. 20036.

**Registered names and trademarks, etc.,** used in this publication, even without specific indication thereof, are not to be considered unprotected by law.

**Advertising Management:** Centcom, Ltd., 500 Post Rd. East, Westport, Conn. 06880 (203-226-7131)

**1988 subscription rates include air delivery outside the U.S., Canada, and Mexico**

	1 yr	2 yr
<b>Members</b>		
Domestic	\$ 25	\$ 42
Canada and Mexico	50	92
Europe	78	148
All Other Countries	113	218
<b>Nonmembers</b>		
Domestic	38	64
Canada and Mexico	63	114
Europe	133	242
All Other Countries	168	312

Three-year and other rates contact: Membership & Subscription Services, ACS, P.O. Box 3337, Columbus, Ohio 43210 (614-421-3776).

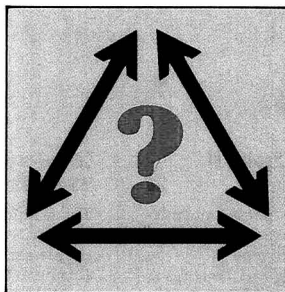
**Subscription orders by phone** may be charged to Visa, MasterCard, Barclay card, Access, or American Express. Call toll free at (800) ACS-5558 from anywhere in the continental United States; from Washington, D.C., call 872-8065. Mail orders for new and renewal subscriptions should be sent with payment to the Business Management Division, ACS, P.O. Box 57136, West End Station, Washington, D.C. 20037.

**Subscription service inquiries and changes of address** (Include both old and new addresses with ZIP code and *recent mailing label*) should be directed to the ACS Columbus address noted above. Please allow six weeks for change of address to become effective.

**ACS membership information:** Bebe Olsen, Washington address.

**Single issues**, current year, \$6.00 except review issue and LabGuide, \$10.00; **back issues and volumes and microform editions** available by single volume or back issue collection. For information or to order, call (800) ACS-5558 or write the Microform & Back Issues Office at the Washington address.

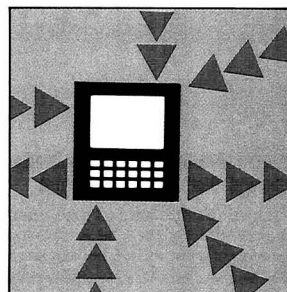
**Nonmembers rates in Japan:** Rates above do not apply to nonmember subscribers in Japan, who must enter subscription orders with Maruzen Company Ltd., 3-10 Nihonbashi 2-chome, Chuo-ku, Tokyo, 103, Japan. Tel: (03) 272-7211.



### REPORT

75 A

**Are Quality and Productivity Compatible in the Analytical Laboratory?** The relationships between quality, productivity, and competitiveness in an environment of changing production practices are explored by Harry S. Hertz of the National Bureau of Standards



### A/C INTERFACE

95 A

**On the cover. Laboratory automation.** Current issues raised by the application of automation systems to the laboratory, including organization, implementation, terminology, communications, and legal issues, are discussed by Joseph G. Liscouski of Digital Equipment Corp.

### BRIEFS

64 A

### LETTERS

70 A

### NEWS

73 A

**Edward S. Yeung** has been appointed an **Associate Editor** of **ANALYTICAL CHEMISTRY**. ▶ **Instrumentation Advisory Panel members** beginning new terms in 1988 are D. Bruce Chase, L. J. Cline Love, and R. Mark Wightman

### MEETINGS

82 A

### FOCUS

87 A

**Howard Malmstadt: An inspiration** for the entire analytical community. The ongoing career of one of the discipline's most influential scientists and educators is recounted

### NEW PRODUCTS & MANUFACTURERS' LITERATURE

92 A

### AUTHOR INDEX

97

## Kinetic Modeling of Fast Atom Bombardment Spectra of Glycerol-Diethanolamine Mixtures

98

A kinetic model based on high-pressure gas-phase ion-molecule reactions gives good agreement with experimental FAB spectra of solutions of diethanolamine in glycerol.

Jan Sunner, Angelina Morales, and Paul Kebarle\*, Department of Chemistry, University of Alberta, Edmonton, Alberta, Canada T6G 2G2  
*Anal. Chem.*, 60 (1988)

## Detection of Ethylene Glycol Dinitrate Vapors by Ion Mobility Spectrometry Using Chloride Reagent Ions

104

Ethylene glycol dinitrate (EGDN) vapors can be detected by ion mobility spectrometry and chloride reagent ions as (EGDN-Cl)<sup>-</sup> ion clusters. The detection limit for a purified air sample is 30 pg, and the optimum operating temperature is 75 °C.

A. H. Lawrence\* and Pavel Neudorfl, Unsteady Aerodynamics Laboratory, National Aeronautical Establishment, National Research Council, Ottawa, Ontario K1A 0R6, Canada  
*Anal. Chem.*, 60 (1988)

## Cluster Ion Formation under Laser Bombardment. Studies of Recombination Using Isotope Labeling

110

Ion formation by recombination in the laser-induced plasma is observed directly by laser microprobe MS in the production of cluster ions from NiS particles deposited on isotopically enriched sulfur thin films.

Inga H. Musselman, Richard W. Linton\*, and David S. Simons, Department of Chemistry, University of North Carolina, Chapel Hill, N.C. 27514, and Center for Analytical Chemistry, National Bureau of Standards, Gaithersburg, Md. 20899  
*Anal. Chem.*, 60 (1988)

## Determination of Dihydroquinghaosu in Blood by Pyrolysis Gas Chromatography/Mass Spectrometry

115

Dihydroquinghaosu, a major metabolite of the antimalarial drug artesunic acid, is assayed by quantitation of its major pyrolysis product with an internal standard method in the low nanogram-per-milliliter range.

Anthony D. Theoharides\*, Michael H. Smyth, Robert W. Ashmore, James M. Halverson, Zhong Ming Zhou, William E. Ridder, and Ai Jeng Lin, Department of Pharmacology, Division of Experimental Therapeutics, Walter Reed Army Institute of Research, Washington, D.C. 20307-5100  
*Anal. Chem.*, 60 (1988)

## Characterization and Selection of Electrolyte Systems for Isotachopheresis of Anions by Cluster Analysis

120

The leading electrolyte system with pH 3 and one with pH between 6 and 10 are found, based on a hierarchical and a nonhierarchical clustering procedure, to be the most favorable binary combination for identification purposes. Ternary combinations are also selected. Additional systems do not increase the identification power.

Ernst Kenndler\* and Gregor Reich, Institute for Analytical Chemistry, University of Vienna, Waehringerstrasse 38, A-1090 Vienna, Austria  
*Anal. Chem.*, 60 (1988)

## Effects of Dilution of Poly(ethylvinylbenzene-divinylbenzene) Adsorbent on the Adsorption of Aliphatic, Alicyclic, and Aromatic Hydrocarbon Adsorbates from Effective Zero to Finite Surface Coverage

124

Relative retentions and heats of adsorption agree to within experimental error with those observed previously for the bulk title adsorbent.

N. M. Djordjevic and R. J. Laub\*, Department of Chemistry, San Diego State University, San Diego, Calif. 92182  
*Anal. Chem.*, 60 (1988)

## Anodic Characterization of Mercury Microelectrodes in Electrolytes at the Micromolar Level

131

Mercury microelectrodes based on platinum disks of either 1- or 12.5- $\mu$ m radius are characterized anodically in various electrolytes at the micromolar level.

Zbigniew Stojek, Department of Chemistry, Warsaw University, Pasteura 1, 02-093 Warsaw, Poland, and Janet Osteryoung\*, Department of Chemistry, State University of New York at Buffalo, Buffalo, N.Y. 14214  
*Anal. Chem.*, 60 (1988)

## Determination of Cephalosporins and Decomposition Products by Liquid Chromatography with Indirect Electrochemical Detection

136

Cephalosporins are determined in standard solutions with detection limits of 0.4-3 ng and a precision of 1.5%. The method is applied to the determination of cefotaxime and its main metabolite in serum and urine, and selectivity is improved compared with that obtained with UV detection.

H. Fabre and W. Th. Kok\*, Laboratory for Analytical Chemistry, University of Amsterdam, Nieuwe Achtergracht 166, 1018 WV Amsterdam, The Netherlands  
*Anal. Chem.*, 60 (1988)

\*Corresponding author



See the JY 24 and other JY ICP instruments at the Pittsburgh Conference, Booths 3026-3031 and 3126-3131.

# Good things come in small packages.

Now...JY brings you the advantages of full-featured ICP analysis in our smallest package.

Just starting spectroanalysis? Converting elemental analysis from AA to ICP? Adding more ICP capacity? The JY 24 was made for you!

The JY 24 packs everything that has made JY the ICP of choice into a single compact space-saving unit — including some not-so-small things like a 40 MHz RF generator!

The JY 24 complements JY's versatile line of ICP units, both sequential and simultaneous, for all your spectroanalytical problems. For information on the complete spectrum of JY spectroanalytical instruments, use the reader service card, or write or call today.



**The New JY 24 Sequential ICP is reasonably priced too!**

**JOBIN  
YVON**



**J-Y Optical Systems  
Instruments SA, Inc.**

6 Olsen Avenue, Edison, NJ 08820-2419 Tel. (201) 494-8660, Telex 844516 FAX (201) 494-8796  
(In Europe:) Jobin Yvon, 16-18 Rue du Canal 91163 Longjumeau, France, Tel. (33) 1.69.09.34.93

CIRCLE 75 ON READER SERVICE CARD

## Measurement of Liposome-Released Ferrocyanide by a Dual-Function Polymer Modified Electrode 142

Liposome-encapsulated potassium ferrocyanide is measured by differential pulse voltammetry following release by surfactant or complement lysis. The electrode used is modified with an anion-exchange polymer film to provide preconcentration of the released ferrocyanide and to protect it from lipid-protein fouling.

Rosanne M. Kannuck and Jon M. Bellama, Department of Chemistry and Biochemistry, University of Maryland, College Park, Md. 20742, and Richard A. Durst\*, Center for Analytical Chemistry, National Bureau of Standards, Gaithersburg, Md. 20899  
*Anal. Chem.*, 60 (1988)

## Simultaneous Determination of Glucose, Fructose, and Sucrose in Mixtures by Amperometric Flow Injection Analysis with Immobilized Enzyme Reactors 147

Response of the sensors is linear between  $2 \times 10^{-5}$  and  $1 \times 10^{-3}$  M. The precision (C.V.) for 10 successive injections at the 1-mM level is better than 1.8% for glucose, 1.8% for fructose, and 1.6% for sucrose. Application of the system to foods is also described.

Kiyoshi Matsumoto\*, Hideaki Kamikado, Hiroaki Matsubara, and Yutaka Osajima, Department of Food Science and Technology, Faculty of Agriculture, Kyushu University 46-09, Hakozaki, Higashi-ku, Fukuoka 812, Japan  
*Anal. Chem.*, 60 (1988)

## Voltammetric Determination of Traces of Nickel(II) with a Medium Exchange Flow System and a Chemically Modified Carbon Paste Electrode Containing Dimethylglyoxime 151

Submicromolar nickel(II) is detected after 30 s accumulation in the deoxygenated system. The electrode is stable for more than 4 h.

Karsten N. Thomsen and Lars Kryger\*, Department of Chemistry, Aarhus University, Langelandsgade 140, 8000 Aarhus C, Denmark, and Richard P. Baldwin, Department of Chemistry, University of Louisville, Louisville, Ky. 40292  
*Anal. Chem.*, 60 (1988)

## Spectroelectrochemical Response and Optical Geometry Optimization of Thin-Layer Flow Detectors with Long Optical Path Lengths: Theory 156

Steady-state current and absorbance responses are quantitatively modeled for thin-layer spectroelectrochemical flow cells. Effects on absorbance of the spatially inhomogeneous sample distribution are treated, and optimum optical geometries are predicted, based on signal-noise considerations.

Lawrence E. Fosdick and James L. Anderson\*, Department of Chemistry, The University of Georgia, Athens, Ga. 30602  
*Anal. Chem.*, 60 (1988)

## Spectroelectrochemical Response and Flow Hydrodynamics in Thin-Layer Flow Detectors with Long Optical Path Lengths and Fiber-Optic or Slab Waveguide Coupling 163

The absorbance and current responses of rectangular, thin-layer spectroelectrochemical flow cells with long optical path lengths show good agreement with theoretical predictions and are used to assess fully developed vs. developing or stagnating laminar flow.

Lawrence E. Fosdick and James L. Anderson\*, Department of Chemistry, The University of Georgia, Athens, Ga. 30602  
*Anal. Chem.*, 60 (1988)

## X-ray Photoelectron Spectroscopy of Silica Surfaces Treated with Polyfunctional Silanes 169

Results of XPS studies of silanized surfaces indicate that base catalysts modify the surface chemistry of reactions involving multifunctional silanes. The extent of surface coverage is also base-catalysis-dependent.

Krishna M. R. Kallury, Ulrich J. Krull, and Michael Thompson\*, Department of Chemistry, University of Toronto, 80 St. George Street, Toronto, Ontario M5S 1A1, Canada  
*Anal. Chem.*, 60 (1988)

## Evaluation of a Nitrosyl-Specific Gas-Phase Chemiluminescent Detector with High-Performance Liquid Chromatography 173

The detector responds linearly to nitrated polycyclic aromatic hydrocarbons between the concentration range of 10 and 1000 ng per compound injected. The HPLC/CD system provides for isocratic and gradient elution in both normal and reversed-phase operation.

Albert Robbat, Jr.\*, Nicholas P. Corso, and Tyng-Yun Liu, Chemistry Department, Tufts University, Medford, Mass. 02155  
*Anal. Chem.*, 60 (1988)

## Determination of Ammonium Ion by Fluorometry or Spectrophotometry after On-Line Derivatization with o-Phthalaldehyde 175

The limit of quantitation for the method is 2 picomoles  $\text{NH}_4^+$ , and the reproducibility is  $\pm 0.3\%$ . An assay time of 1 min is required.

Sham S. Goyal\*, Donald W. Rains, and Ray C. Huffaker, Department of Agronomy and Range Science/Plant Growth Laboratory, University of California, Davis, Calif. 95616  
*Anal. Chem.*, 60 (1988)





"I switched to Ohaus because I needed solid, sensible, rugged balances for QC.

And I couldn't afford to compromise accuracy."

*Chris Kjørhaug  
Corporate Quality Assurance Engineer  
Sewell Plastics, Inc., Atlanta, GA*



See us at  
PITCON '88  
Booths 3020, 3022, 3024

*Solid, sensible balances & scales*

# OHAUS★

The Ohaus GT4000 top-loading balance is easy to use and easy to read. Weighs from 0-4000 g with 0.1 g readability. Features Ohaus FillGuide™, a simple-to-use electronic filling guide. One of nine GT Series precision toploaders ranging in capacity from 210-8000 g with readabilities of 0.001-0.1 g. For more information, call or write Ohaus, 29 Hanover Road, Florham Park, NJ 07932, (800) 672-7722.

Circle 120 for a demonstration. Circle 121 for information.



**The premiere  
research  
publication in the  
environmental  
field.**

Environmental science continues to be one of the fastest growing fields. And ES&T has grown right along with it!

ES&T continues to give you the practical, hard facts you need on this science . . . covering research, techniques, feasibility, products and services.

Essential reading for environmental scientists both in the business and academic world . . . ES&T has increased its emphasis on peer-reviewed research dealing with water, air, and waste chemistry in addition to adding critical reviews of important environmental science issues—all relevant to understanding the management of our natural environment.

Also included are discussions on environmental analyses, governmental regulations, current environmental lab activities, and much more!

**For rate information, and to subscribe, call toll free:**

**(800) 424-6747**

## BRIEFS

### Correspondence

#### Exchange of Comments on the Role of the Interface in Solvent Extraction Processes 180

Henry Freiser, Strategic Metals Recovery Research Facility, Department of Chemistry, University of Arizona, Tucson, Ariz. 85721, and Frederick F. Cantwell, Department of Chemistry, University of Alberta, Edmonton, Alberta, Canada T6G 2G2

*Anal. Chem.*, 60 (1988)

#### Simultaneous Enhancement of Fluorescence and Thermal Lensing by Reversed Micelles 182

Chieu D. Tran, Department of Chemistry, Marquette University, Milwaukee, Wis. 53233

*Anal. Chem.*, 60 (1988)

#### Influence of Porphyrin Structure on Anion Selectivities of Manganese(III) Porphyrin Based Membrane Electrodes 185

N. A. Chaniotakis, A. M. Chasser, and M. E. Meyerhoff\*, Department of Chemistry, The University of Michigan, Ann Arbor, Mich. 48109, and J. T. Groves, Department of Chemistry, Princeton University, Princeton, N.J. 08544

*Anal. Chem.*, 60 (1988)

### Technical Notes

#### Fabrication of Platinum-Disk Ultramicroelectrodes 188

C. D. Baer\*, N. J. Stone, and D. A. Sweigart\*, Department of Chemistry, Brown University, Providence, R.I. 02912

*Anal. Chem.*, 60 (1988)

#### Automated Cryogenic Collection of Carbon Dioxide for Stable Isotope Analysis and Carbon-14 Accelerator Mass Spectrometry Dating 191

C.A.M. Brenninkmeijer, Institute of Nuclear Sciences, Department of Scientific and Industrial Research, Private Bag, Lower Hutt, New Zealand

*Anal. Chem.*, 60 (1988)

#### Correction. Ion-Pair Chromatographic Determination of Anions Using an Ultraviolet-Absorbing Co-Ion in the Mobile Phase 192

Brian A. Bidlingmeyer\*, Carmen T. Santasania, and F. Vincent Warren, Jr., Waters Chromatography Division of Millipore Corporation, 34 Maple Street, Milford, Mass. 01757

*Anal. Chem.*, 60 (1988)



## High-Energy Processes in Organometallic Chemistry

**T**his exciting work is the first of its kind... a comprehensive treatment of the many disciplines and applications of high-energy processes in organometallic chemistry. You'll read about these diverse disciplines and state-of-the-art descriptions

of the methodologies involved. You'll discover the commonalities among seemingly disparate methodologies of high-energy processes, including • metal atom chemistry • plasma chemistry • radiolysis • sonochemistry • electrochemical generation. A wide range of scientists will find this volume helpful because of the extremely multidisciplinary nature of the topic. This book should be of special interest to those involved in organometallic chemistry, microelectronics, colloid chemistry, organic and inorganic syntheses, and physical chemistry.

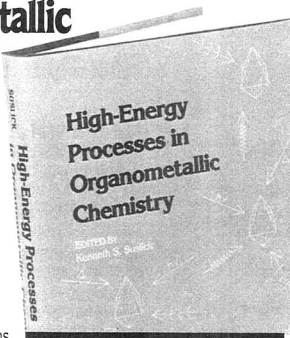
Kenneth S. Suslick, *Editor*

ACS Symposium Series No. 333  
LC 86-32245 ISBN 0-8412-1018-7

336 pages (1987) Clothbound  
US & Canada \$69.95 Export \$83.95

Order from: American Chemical Society, Distribution Office Dept. 44  
1155 Sixteenth St., N.W., Washington, DC 20036

or CALL TOLL FREE **800-227-5558** and use your credit card!



## New Directions in Electrophoretic Methods

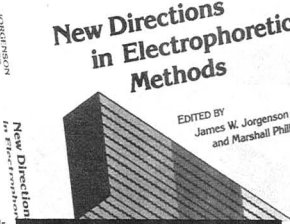
**E**lectrophoresis is the most powerful process available for the separation and analysis of complex mixtures of charged biopolymers. This book offers scientists the latest developments in electrophoretic separations and state-of-the-art electrophoretic technology and applications. It covers both the basic theory and development of electrophoretic methods and the separation and identification tools used by developers. The sixteen chapters in this book focus on several electrophoretic methods • isotachopheresis • zone electrophoresis • isoelectric focusing • two-dimensional electrophoresis • pulsed electrophoresis. Electrophoretic methods play a major role in scientific advances in medicine, agriculture, chemistry, and biotechnology. This book will prove a valuable reference for anyone working with electrophoretic methods.

James W. Jorgenson and Marshall Phillips, *Editors*

ACS Symposium Series No. 335  
LC 87-1777 ISBN 0-8412-1021-7

### New Directions in Electrophoretic Methods

EDITED BY  
James W. Jorgenson  
and Marshall Phillips



284 pages (1987) Clothbound  
US & Canada \$64.95 Export \$77.95

Order from: American Chemical Society Distribution Office Dept. 52  
1155 Sixteenth St., N.W. Washington, D.C. 20036

or CALL TOLL FREE **800-227-5558** and use your credit card!

# Use Gas Chromatography Think Matheson®

**M**atheson's line of special purity carrier gases developed as this instrumentation emerged. Get the best performance from your instrument use, Matheson Purity, U.H.P. and Zero carrier gas. We've kept our specs in step with instrumentation development.

And don't forget you need a high purity regulator like Matheson 3104 (the GC regulator) to get all the purity out of our carrier gases. It's the total system that helps you succeed at GC.

Don't fall behind, ask for our brochure detailing the gas needs to succeed at GC. Use the Reader Service No. or contact us.

## Matheson Gas Products

30 Seaview Drive  
Secaucus, NJ 07096-1587

CIRCLE 96 ON READER SERVICE CARD

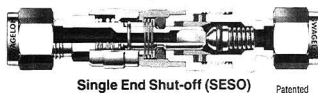


# Swagelok® QUICK-CONNECTS

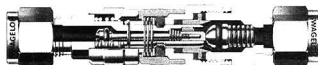
... the easy way to add versatility  
to your fluid systems

## "QC" Series

Push to connect for ease of coupling, single end or double end shut-off, 1/8" to 1/2" hose connector, 37° AN flare, male and female NPT or SWAGELOK Tube Fitting end connections.



Single End Shut-off (SES)



Double End Shut-off (DES)



## "QM" Series Miniature

Finger-tip operation, low dead space, light weight, compact, 1/16" male and female NPT, 1/16" and 1/8" SWAGELOK Tube Fitting end connections.



## "QT" Series TFE Sealed

All 316 stainless steel construction with TFE seals, high flow capacity, single end or double end shut-off, low spillage and air inclusion, push to connect for ease of coupling, safety release button prevents accidental uncoupling, 1/8" to 1" male and female NPT, 37° AN flare or SWAGELOK Tube Fitting end connections.

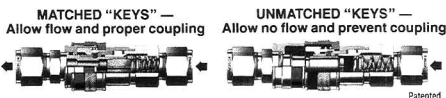
## "QF" Series Full Flow

No orifice restrictions, O-Ring can be changed without disassembling body, 1/4" to 1" male and female NPT or SWAGELOK Tube Fitting end connections.



## "Keyed" Quick-Connect Series

Positive mechanical lockout system prevents coupling of unmatched stems and bodies eliminating accidental mixing of fluids in multi-line systems. Keys are numbered and color coded for easy identification.



## "Keyed QC" Series

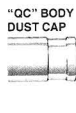


## "Keyed QT" Series



## Accessories

Special devices are available to prevent damage or contamination in the uncoupled position.



Swagelok®  
QUICK-CONNECTS



SWAGELOK Co.  
Solon, Ohio 44139  
SWAGELOK Canada, Ltd., Ontario

CIRCLE 150 ON READER SERVICE CARD

## LETTERS

### Fiber-Optic Biosensors

Sir: I would like to correct an error that appeared in the FOCUS article published in the Oct. 1 issue of the JOURNAL (*Anal. Chem.* 1987, 59, 1161 A-1164 A). The reference to a fiber-optic assay technique in the first paragraph at the top of page 1162 A ("An example of this competitive type of assay is a technique developed by S. M. Angel of Lawrence Livermore National Laboratory...") is in error. I did not develop this technique; it was developed by the late Tomas Hirschfeld during a time when I was doing a post-doc with him. Also, the 10<sup>-12</sup> M detection limit was achieved by Hirschfeld. We have yet to achieve this in our laboratory.

Stanley M. Angel  
Ecosystem and Measurement  
Sciences Section  
Environmental Sciences Division  
Lawrence Livermore  
National Laboratory  
Livermore, Calif. 94550

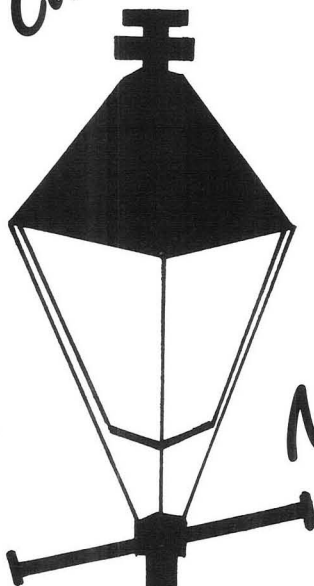
**MOST  
USED**  
...because  
it's the most  
useful.



Published since 1955, the annual *LabGuide* leads all others in advertising pages and in reader usage (22,000 references daily). It's the true one-stop buying source where most manufacturers say with their ads. "Here we are. Compare our products with those of our competitors." That's why in more than six out of ten purchases by the 277,000 users it serves, the *LabGuide* is consulted before the purchase is made.

*Meet  
the  
Pittsburgh Conference*

*in  
New Orleans!*



RUE PITTSBURGH  
**The Pittsburgh Conference**

RUE ORLEANS  
**New Orleans**

*Register EARLY!  
Save \$30*

*February 22-26, 1988*



**The Pittsburgh Conference  
12 Federal Drive Suite 322  
Pittsburgh, PA 15235  
Phone: 412-795-7110**

CIRCLE 125 ON READER SERVICE CARD

# – O.I.C. Advances GC Detector Technology – New PID Now Available for EPA Analyses

O.I. Corporation has developed a new photoionization detector engineered specifically for use with the electrolytic conductivity detector. This new detector has many features not found in any other PID including:

- Hidden window design prevents sample from contacting and fouling lamp window
- Unitized, combo PID/EICD detector system formed when joined to the EICD
- Only one detector port required for PID/EICD combo system
- No transfer line required for serial interface to EICD
- LampSaver circuit extends lamp life
- Custom designs for specific GC models fit into standard detector ports
- Detector vent for venting unwanted eluates prior to detector chamber

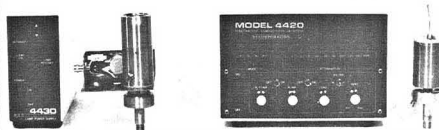
*the Advantage  
in Performance and Flexibility*

## Working Together

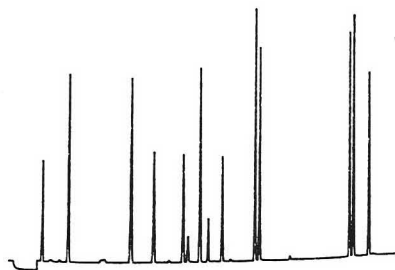


Or

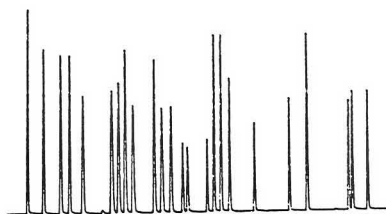
## Working Apart



True capillary performance for EPA 601/602 analyses



4430 PID



4420 EICD

## **O·I·CORPORATION**

Graham Rd. at Wellborn Rd. • P.O. Box 2980 • College Station, Texas 77841-2980  
Telephone (409) 690-1711 • Cable Address: O.I.COSN • TWX No.: 510-892-7944

CIRCLE 123 ON READER SERVICE CARD



## Yeung Named Associate Editor



Edward S. Yeung, professor of chemistry at Iowa State University and senior scientist at Ames Laboratory, has been appointed an Associate Editor of *ANALYTICAL CHEMISTRY*. Yeung will be responsible for peer review of original scientific papers in the area of spectroscopy. He succeeds Fred Lytle of Purdue University, who was an

Associate Editor of the *JOURNAL* for two years. The four other external Associate Editors are Klaus Biemann of the Massachusetts Institute of Technology (mass spectrometry), Georges Guiochon of the University of Tennessee and Oak Ridge National Laboratory (separations), Robert Osteryoung of the State University of New York at Buffalo (electroanalytical chemistry), and John Smith of Harvard Medical School (analytical biotechnology).

Yeung was born in Hong Kong and received an A.B. degree, magna cum laude, from Cornell University (1968) and a Ph.D. degree in chemistry from the University of California, Berkeley (1972), where his research advisor was C. Bradley Moore.

His research interests include analytical spectroscopy, particularly laser-based techniques. He has published more than 100 papers on topics such as photochemistry, nonlinear Raman spectroscopy, atomic and molecular fluorescence, photothermal methods, polarimetry, and chemiluminescence. He is well known for the development of several innovative and sensitive detectors for liquid chromatography, including detectors that monitor optical activity, refractive index (using interferometry), absorbance (using interferometry or photothermal techniques), and fluorescence.

In 1987 he received the ACS Division of Analytical Chemistry Award in Chemical Instrumentation, sponsored by Dow Chemical Co.

## New Instrumentation Panel Members

Three new members have been appointed to serve on the *ANALYTICAL CHEMISTRY* Instrumentation Advisory Panel for three years beginning in 1988. The new members are D. Bruce Chase, E. I. du Pont de Nemours and Co.; L. J. Cline Love, Seton Hall University; and R. Mark Wightman, Indiana University.

Members leaving the board this year are Richard Danchik, Alcoa Laboratories; Thomas Farrar, University of Wisconsin; and John Holland, Michigan State University.

The six members who will continue to serve on the panel are Howard Barth, Hercules Research Center; Richard Browner, Georgia Institute of Technology; James Callis, University of Washington; Joel Harris, University of Utah; Ronald Majors, EM Science; and Linda McGown, Duke University.

Instrumentation Advisory Panel members aid in the selection of appropriate topics and qualified authors for the *JOURNAL*'s *INSTRUMENTATION* feature. They also con-

tribute to a dialogue on the overall aims and scope of the feature, and they are a valuable source of ideas for the other A-page features.

*INSTRUMENTATION* articles focus on chemical measurement systems, including instrument design and specific applications. In contrast to research articles that are written for the specialist, *INSTRUMENTATION* articles are written for the general reader who wishes to broaden his or her knowledge of analytical instrumentation. They are not intended to be comprehensive reviews; instead, they introduce and promote interest in the subject matter. The articles frequently are invited, but unsolicited articles also are considered for publication. Brief biographical sketches of the three new panel members follow.



**D. Bruce Chase** received a B.A. degree from Williams College (1970) and a Ph.D. degree in physical chemistry from Princeton University (1975) before joining the analytical division of the central research department of Du Pont.

Chase's primary research interests include vibrational spectroscopy, FT-IR and Raman techniques, and the

application of these methods to industrial analytical problems. In collaboration with the late Tomas Hirschfeld, Chase developed an FT-Raman spectrometer that demonstrates the utility of near-IR excitation. For this work Hirschfeld and Chase received the 1987 Meggers Award and an IR-100 award. He is currently the president of the Coblenz Society.

**L. J. Cline Love**, professor of chemistry at Seton Hall University, received a B.S. degree from the University of Missouri, Columbia, and a Ph.D. degree from the University of Illinois in 1969. Her recent research interests include applications of organized media, specifically micelles and cyclodextrins, in luminescence and liquid chromatography. She is currently studying the interaction of cyclodextrin media and chiral drugs using nuclear magnetic resonance spectroscopy. In 1984 Cline Love founded the Center for Applied Science at Seton Hall, where she currently is the director.



**R. Mark Wightman** received a B.A. degree (1968) from Erskine College (South Carolina) and a Ph.D. degree (1974) from the University of North Carolina. He carried out postdoctoral research at the University of Kansas under the guidance of Ralph Adams before joining the faculty at Indiana University.

His research interests include electroanalytical chemistry and neurochemistry. Wightman has developed numerous microelectrodes for use in a variety of applications such as the detection of neurotransmitters using *in vivo* sensors.

# The sophisticated LC Gradient Pump with a simple controller



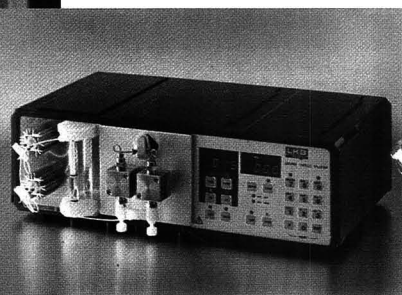
When it comes to routine gradient separations, it pays to focus on the essentials.

Why complicate programming with a variety of options that you'll never use? Why pay extra for a lot of whistles and bells? Why compromise features that really do make a difference in the accuracy and reproducibility of your results?

The new LC Gradient Pump combines all the best flow and mixing features together with self-contained binary or ternary gradient control to ensure quality results. There's no need for additional control components and their added costs.

With the new LC Gradient Pump you get all you really need and more, for a lot less.

Why not simply ask for a demonstration?



*The 2249 LC Gradient Pump.*

## LKB

High Performance LC Division

Pharmacia LKB Biotechnology AB, 751 82 Uppsala, Sweden, Tel. 018-16 30 00, Telex 76070, Telefax 018-14 38 20

LKB products: Box 305, S-16726 Bromma, Sweden, Tel. 08-799 80 00, Telex 10492, Telefax 08-98 63 64

Australia (02)898 36 22 • Austria (0222)69 16 010 • Austria-Eastern European Countries +43(222)92 16 07 • Belgium (02)242 4666

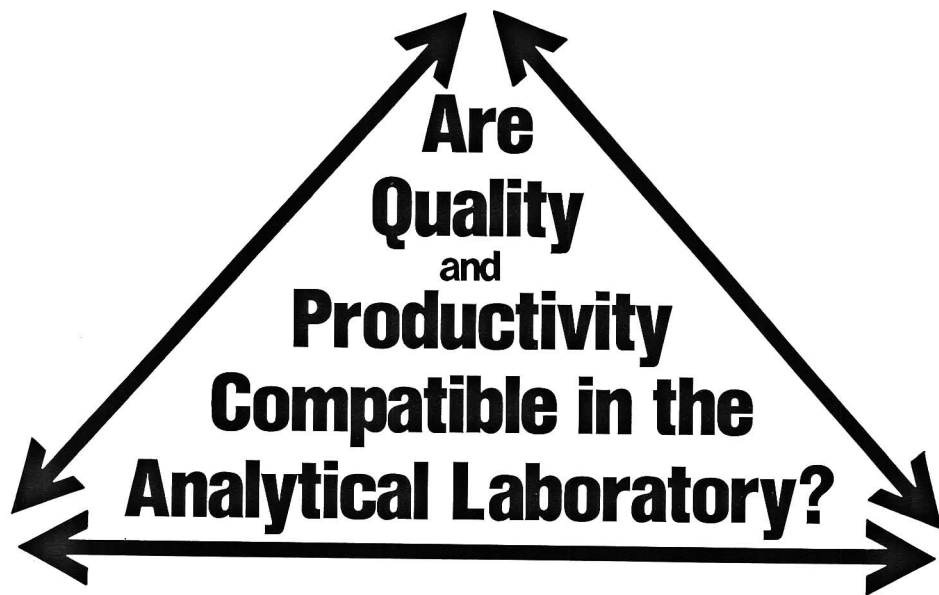
Canada (0514)684 88 81 • Denmark (02)25 52 00 • Finland (021)67 81 11 • France (01)64 46 36 36 • Greece-Middle East +30(1)894 73 96

Great Britain (0908)66 11 01 • Holland (034)80 77 911 Hong Kong-Par East (852)5-814 84 21 • India (0812)57 37 88 • Italy (02)253 913 21 • Japan (03)444-4811

Norway (02)54 90 95 • People's Republic of China (Beijing) 89 06 21 • Soviet Union (095)255-6984 • Spain (03)230 05 01 • Sweden (08)799 80 00

Switzerland (01)821 18 16 • United States (0201)457 80 00 • West Germany (0761)490 30. Over 60 qualified representatives throughout the world

CIRCLE 127 ON READER SERVICE CARD

**Harry S. Hertz**

Center for Analytical Chemistry  
National Bureau of Standards  
Gaithersburg, Md. 20899

In an era in which quality is a buzzword in all discussions relating to competitiveness and productivity, it behooves the industrial production manager to examine the relationships among quality, competitiveness, and productivity. The issues of cost-effectiveness and customer needs are becoming prime motivators in the industrial environment. In fact, many companies now define quality as "meeting customer needs."

In this environment, it becomes necessary to examine the issues of quality and productivity in the analytical laboratory and also to examine the role of quality chemical measurements in overall industrial productivity. These issues are explored in this REPORT. As a result of reflecting on these issues, it is possible to propose a scenario for the future. Although the discussion is somewhat philosophic, I believe the conclusions are inevitable and they provide information about the chemical measurement system of the future.

To put a discussion of quality and productivity in context, one must look at characteristics of chemical measurements, current trends in analytical chemistry, and the current state of the

practice of quantitative measurement. With these considerations in mind, one can explore factors that influence productivity and plan for the future.

**Characteristics of chemical measurements**

As all analytical chemists know, chemical measurements of manufactured goods, process streams, byproducts, and effluent streams are very complex undertakings. The complexity is evident when considering some of the key characteristics of chemical measurements. These measurements are relative in nature; the end result is only as reliable as the calibration material or the calibration curve used as the quantitative basis. Sampling and related material homogeneity problems affect the accuracy of measurements and the interpretation of results, thereby affecting decisions related to processing, marketing, and disposal of a byproduct.

Chemical measurements are multi-method measurements; a given constituent is often measured by various techniques that have different physical bases for measurement and different biases. Particularly at trace levels, chemical measurements are subject to significant interference. Decisions based on unrecognized interferences can have major economic impacts.

Finally, today's chemical measure-

ments usually give only partial information. For example, we can analyze for a trace element, but generally we cannot identify the chemical form (i.e., oxidation state, chemical bonding) in which it exists in a complex material. Greater knowledge of material structure-function relationships will make it important to identify speciation as well as the element present.

**Current trends in analytical chemistry**

With these characteristics in mind, let us examine some of today's driving forces in quantitative analytical chemistry that have an impact on the search for quality and, as measurement complexity increases, on rates of productivity. The first driving force is in response to the fact that most chemical measurements yield only partial information. As we become more aware of relationships between speciation and material performance, there will be an increasing demand for maintenance of very complex speciation information in sample work-up and quantitative analysis.

A second driving force is revealed in the trend toward measurement of lower and lower concentrations of constituents in very complex samples, which places a great burden on the accuracy and quality of measurement. When one looks at industries such as high-technology composite materials and semi-

**Table I. Interlaboratory variability studies**

System studied	No. of samples	No. of labs	Variability (CV)
PCBs in oil	6	18	38-64%
Se in serum	—	27	<sup>a</sup>
$\beta$ -carotene in serum	4	11	100% (per sample) 35% (grand average)
Organic pollutants in water	—	5	500%
Leachates from hazardous wastes <sup>b</sup>	—	—	—

Note. These round robins are representative of many others that could have been reported. They represent data generated under the auspices of NBS, the International Atomic Energy Agency, ASTM, and the chemical manufacturing industry.

<sup>a</sup> Range of results is 38-100  $\mu\text{g/L}$ .

<sup>b</sup> For each of 9 elements studied, the range of results was a factor of 10.

conductor devices, one sees an increasing need for site specificity in analytical chemistry. It is no longer sufficient to know only the bulk concentration of a trace constituent; one must know whether it is homogeneously distributed or, if not, where it is located in a sample (frequently on a micrometer scale).

New measurement instrumentation with increasing automation of chemical measurements is rapidly being introduced. This is a source of danger because sample handling and data manipulation frequently are not under the chemist's control and are unavailable for review or modification by the chemist. To compound the problem, personnel untrained in analytical chemistry, who know less and less about the steps involved in the measurements, are frequently called upon to operate such "black box" instruments.

There is an increasing need for long-term retention of data. The ease of manipulating and storing large databases makes it possible to compare data on similar samples over time, over distance (e.g., at different manufacturing sites), and across international boundaries. The demand on the chemist is to assure that the compositional differences noted are real and not based on analytical bias or imprecision.

### State of the practice

Because modern technology tempts us to compare data generated in different laboratories, analytical chemists must provide accurate information. To substantiate this point, data on various interlaboratory round robins are presented in Table I. I will delve into just the first study that is cited (PCBs in oil). In this study conducted by the National Bureau of Standards (NBS), one of the samples not reported in Table I had no Aroclor (PCB mixture) added. NBS analysis showed that no PCBs were present at the limit of detection, yet

9 out of the 18 laboratories reported the presence of PCBs. One laboratory reported a high value of 113 ppm.

A number of conclusions can be drawn about the state of the practice of quantitative chemical analysis, and one can speculate about the underlying causes of variability leading to results such as those shown in Table I. An obvious conclusion is that the state of the practice is well behind the state of the art. Routine quantitative measurement (if participation in a round robin can be considered routine measurement) falls short of the accuracy and precision achievable under the best of circumstances, which would include qualified chemists, time, and good quality assurance practices. Some of the factors contributing to variability are sample-handling procedures, methodology differences among laboratories, reagent purity and sample contamination, conditions of laboratory facilities, and lack of available reference or calibration materials for standardizing relative measurements.

### Measurement quality and product reliability

A majority of the goods manufactured in the United States is in one way or another affected by the chemical analysis of feedstocks, intermediates, and final products. The key issue in deciding on the level of chemical measurement quality and necessary improvements in this quality is the relationship between chemical measurement and product reliability. As more is understood about compositional variability of materials and the effect this has on performance, product reliability will be improved by better chemical measurement. A few examples of relationships between measurement quality and product reliability from widely varying sectors of the industrial economy demonstrate the potential benefits of improved measurement quality.

- The estimated value of 1985 shipments of U.S. breakfast cereals was \$5.6 billion. In general, vitamins added to breakfast cereals exceed the amounts stated on the packages. This labeling is done for two reasons: to compensate for the degradation of vitamins during the shelf life of the cereal and to compensate for a lack of homogeneity in the distribution of the vitamins and for the variability of subsequent analysis of the nutrient content of the cereals. In a collaborative study conducted several years ago, vitamin C results obtained by 11 food laboratories were compared (1). The results ranged from 3.8 to 293 mg/100 g. What would be the economic impact of reducing this variability? How much could be saved by adding fewer vitamins and distributing them more homogeneously?

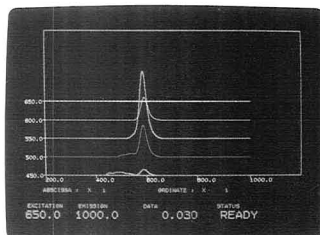
- It is known that oxygen causes failure of bearing steels. The current acceptable level of oxygen in bearing steels is 10 ppm. In a recent round robin of leading producers and users of bearing steels, a steel was distributed with an actual oxygen concentration of 4 ppm (2). Results of the round robin analysis ranged from 2 to 8 ppm—a range of 400% for this critical constituent. What would be the economic impact on steel processing and on manufactured goods using bearing steel if the oxygen content were more consistently and accurately determined?

- The estimated value of U.S.-manufactured electronic products in 1986 was \$47 billion (approximately 1.2% of the gross national product [GNP]). The rejection rate for U.S.-manufactured very large-scale integrated circuits is sometimes 99% (3). On the other hand, for more common integrated circuit devices, the yield frequently must be greater than 90%. It is known that heavy metals ruin device performance. The current allowed level of uranium and thorium in bulk materials for producing these devices is less than 1 ppb. We do not have a measurement capability for determining where uranium and thorium end up in manufactured devices. We cannot perform locationally specific analysis at these levels for heavy metals even though these elements may be present at significantly higher concentrations on a locational rather than a bulk basis. When analytical chemistry can provide such information, product reliability and success rates should improve. In high-technology industries these complex chemical analyses will make the difference in competitiveness and profitability.

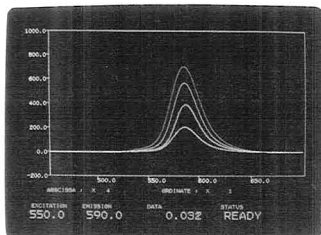
### Economic impact of chemical measurement

It is difficult to obtain a good estimate of the impact of chemical measurement on economic productivity. We do know

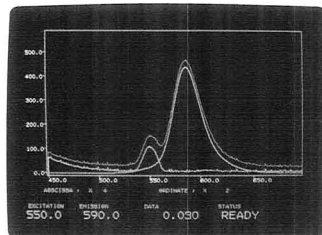




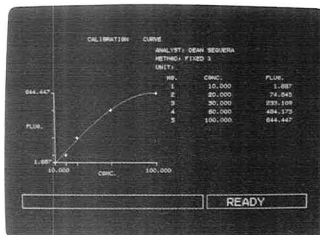
**8:00 AM** Automatic 3D Search for Optimal Excitation and Emission Wavelengths



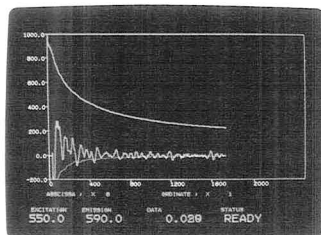
**8:09 AM** Determination of an Optimal Band Pass from 1.5 to 30nm



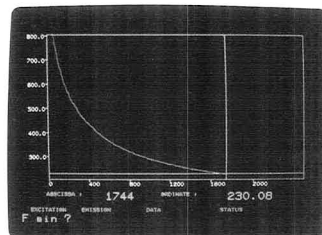
**8:17 AM** Spectral Manipulation Showing Subtraction of the Background with Zooming



**8:26 AM** Quantitation Analysis Using a Higher Order Calibration Curve



**8:37 AM** Kinetic Studies Showing 1st and 2nd Derivatives

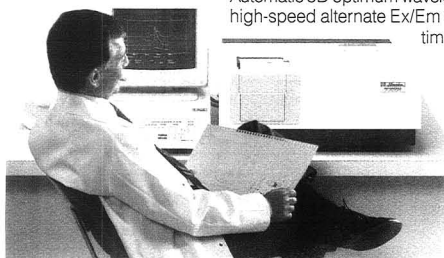


**8:51 AM** Automatic Fura-2 Ca<sup>++</sup> Determination

# Introducing the RF-5000: Fluorescence spectroscopists never had it so easy.

A chemists dream: Convenience, accuracy, sensitivity, speed and great data handling too. Fluorescence spectroscopy used to be slow, cumbersome and full of annoying little problems. It seemed to take forever to find the optimum wavelength for excitation or emission, in order to take a scan. It was cumbersome to correct for Raman or Rayleigh scatter, and quantitation curves were hardly ever linear. Besides, it didn't have quite enough dynamic range, and sensitivity left a lot to be desired. Not anymore.

Shimadzu's new spectrofluorometer RF-5000 does away with all those "little problems". Here's how:  
Automatic 3D optimum wavelength search;  
high-speed alternate Ex/Em wavelength  
time scan



(slews at 9000 nm/min!); quantitative analysis with first through third order curve fits (with linear, log, log-logit axes!); S/N typically found to be over 400 with a 10 nm bandpass (Ex and Em) for the Raman band of H<sub>2</sub>O at 350 nm Ex and 397 nm Em; storage of 15 scans, 4 calibrations, 8 parameter files and 4 time scan files; addition, subtraction and smoothing—even on the fly! And for superior data presentations it comes with a high resolution color video display and a high resolution alphanumeric and graphic printer/plotter.

So, now you can forget all those little problems. The only reservation you should have is with your Shimadzu representative for a demo of the new RF-5000. You never had it so easy. Just call (301) 381-1227.

Shimadzu Scientific Instruments, Inc.,  
7102 Riverwood Drive, Columbia, MD 21046  
In Canada: Tekscience, Inc., (416) 844-1762

See us at  
PITCON '88  
Booths 2816-2831



## SHIMADZU

Shimadzu Corp. International Marketing Div., Tokyo 160, Japan. Tel: Tokyo 03-346-5641  
Shimadzu (Europe) GmbH: F.R. Germany. Tel: (0211) 666371

Circle 152 for a demonstration.

that manufactured goods represent approximately 40% of the U.S. GNP (4). Furthermore, the anecdotal information provided above indicates some of the ties between chemical measurement and product reliability. Better understanding of this link should help to improve competitiveness and productivity.

A conservative estimate of the number of chemical analyses that are repeated in the analytical laboratory today because of suspected contamination, interference, or poor result is 1 in 10. With a conservative estimate of 250 million chemical measurements per day in the United States, at a cost of \$50 billion annually, repeat analyses therefore represent 25 million measurements per day at a cost of \$5 billion annually. At our current level of sophistication, we cannot fully correlate chemical composition with product performance and functional characteristics. In industries in which chemical composition is already tied to product performance, it has been estimated that as many as 30% of the samples must be retested. If one assumes that this relationship holds constant in the future, the cost of repeat analyses alone would be \$15 billion annually or nearly 0.5% of the GNP.

A recent estimate for U.S.-manufactured goods indicated that 10–20% of

domestic sales are for "off-spec" products—manufactured goods sold at a loss or reprocessed to meet specifications (5). Because manufactured goods represent 40% of the GNP, off-spec products represent 4–8% of the GNP. Of course, one cannot conclude that chemical analysis would prevent the manufacture of off-spec goods, but by considering the two cases just presented, it can be estimated that between 0.5 and 8% of GNP is directly affected by the quality of chemical measurement. Even 8% is probably a conservative estimate of the overall impact of chemical measurements on U.S. productivity, because the total impact also includes measurements that qualify or reject feedstock and process streams, resulting in high-quality products.

Certainly as the state of chemical measurement improves and as relationships between chemical composition and product performance are better understood, the impact of quality chemical measurement on U.S. productivity will increase.

#### Laboratory of the future

If one accepts these arguments, one can speculate on how measurements will be made in the laboratory of the future. Laboratory efforts would begin with the accurate measurement of a chemical constituent known to be important

to product performance. The concentration of that constituent would then be varied and the impact on product performance determined. By ascertaining the concentration level at which product performance suffers, one could then set accuracy and precision goals for measuring that constituent in feedstocks, intermediates, and final product. Thus performance characteristics for the product and measurement goals for the chemical and physical testing laboratories could be established simultaneously. Productivity would be maximized both in manufacturing and in the cost-effective quality assurance program in the chemical laboratory.

A discussion of measurement in the future would be incomplete without stating that the laboratory of the future will be closer to the actual production process. Developing more sophisticated chemical sensor technology and providing more immediate feedback to the process stream controller will result in greater use of in-process measurements in industry.

The laboratory of the future will also have a number of analytical aids now being developed to assist in the generation of quality data and to enhance the productivity of the laboratory. The first major contributors will be expert systems capable of providing informa-

**GAIN**

# The Professional Edge

## WITH MEMBERSHIP IN THE AMERICAN CHEMICAL SOCIETY

- Keep up-to-date with weekly copies of *CHEMICAL AND ENGINEERING NEWS*
- Enjoy substantial discounts on subscriptions to ACS's internationally respected, authoritative journals and publications
- Network with your fellow scientists at local, regional and national meetings
- Enhance your career opportunities with ACS employment services
- Save on insurance and retirement plans and tax deferred annuity programs
- Discover the latest advances in your discipline with a first-year-free Division membership

**... and this is just the beginning.**

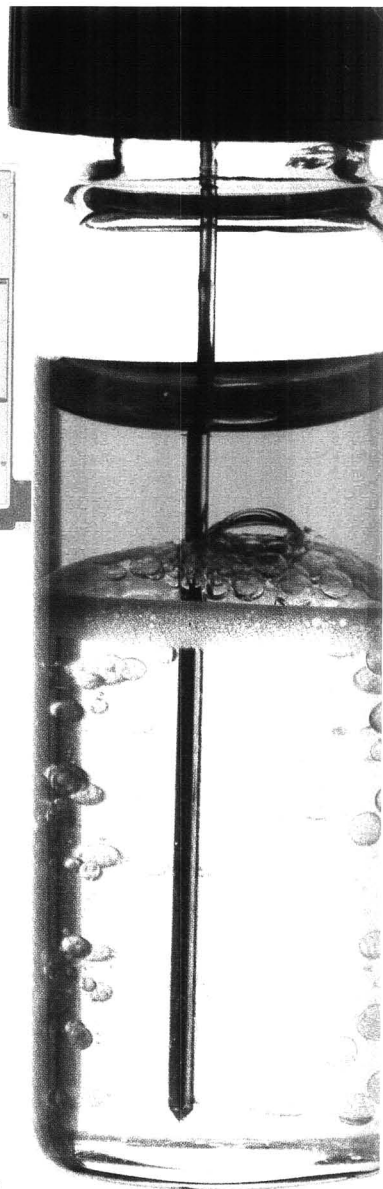
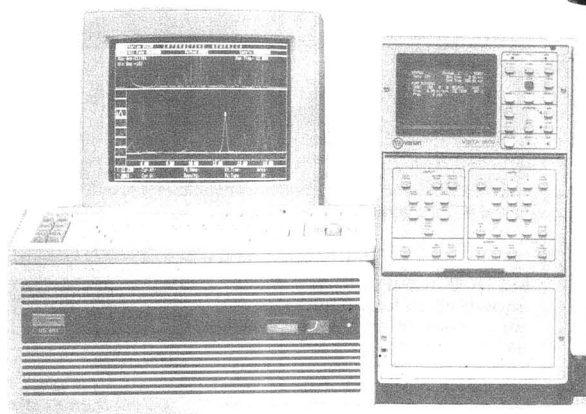
Learn why 9 out of 10 ACS members renew year after year. Gain the Professional Edge: Join ACS now. For further information write or send the coupon below or call TOLL FREE 1-800-424-6747

American Chemical Society  
1155 Sixteenth St., N.W.  
Washington, DC 20036

YES! Please send information on the advantages of joining the ACS.

Name \_\_\_\_\_  
Address \_\_\_\_\_  
\_\_\_\_\_

I am most interested in the following science(s): \_\_\_\_\_  
\_\_\_\_\_



## Automation is more than just injecting a batch of samples

What separates Varian from the rest of the batch is the flexibility of our automated liquid chromatography systems. Our LC 5500 System will automatically prepare a sample using solid phase or liquid-liquid extractions, load the ternary pump program, set the detector parameters, select the desired column, run the sample and report the results. And do it again for over 100 additional vials, using more than 30 different methods.

You don't even have to stand around and watch. You can go on to other tasks, and that adds up to a more productive, cost efficient lab.

Instrumentation is only the beginning. At Varian we don't just sell a single instrument or system, we deliver a whole package. A package that includes expert chemistry and technical support, as well as superior service.

For further information, call 800-231-5772. In Canada, call 416-457-4130.

**Varian is your full-line company for analytical instrumentation**

UV-Visible-NIR

LIMS

Data Systems

Atomic Absorption

Nuclear Magnetic

Resonance

Liquid Chromatography

Gas Chromatography

## Intelligent Solutions

**varian** 

CIRCLE 170 ON READER SERVICE CARD

# WHEATON VACUUM SOURCES

**High technology  
innovations for low  
pressure  
performance**

## Vacumate™

- Nonelectric, explosion resistant vacuum pump
- Whisper quiet operation with no moving parts
- Lightweight and portable — operates at 58 psi compressed air

## A3S Aspirator

- Conserve water — self-contained recirculating water supply requires no water tap hookup
- Compact, safe, and easy-to-operate — perform two independent aspirations simultaneously
- Constant pressure for stable vacuum over a large displacement volume

For more information call  
toll-free 1-800/225-1437.



**WHEATON  
INSTRUMENTS**

*Manufacturers Since 1888*

1301 N. Tenth Street  
Millville, NJ 08332, USA  
Call Toll-Free: 1-800/225-1437  
Ext. 2527

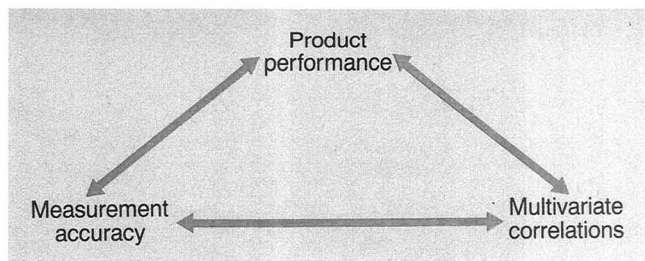


Figure 1. The interaction of quality- and productivity-determining factors.

tion on analytical methods and techniques of choice for performing particular analyses. In the long run, expert systems will control the chemical measurement process in the laboratory. Laboratory robots will initially perform chemical manipulations, and then they will obtain instructions from expert systems programmed by analytical chemists. Finally, chemometrics will be fully incorporated into the operation of the analytical laboratory. Using chemometric approaches, data reduction will include feedback loops to a robot performing chemical manipulations or to an expert system controlling the chemical robot and thus will permit fine-tuning of an experiment to improve analytical data. Furthermore, chemometric approaches will be used more heavily in the initial design of experiments to obtain information on as many constituents as possible in a single experiment.

The laboratory of the future will be governed by a measurement triangle as shown in Figure 1. All three components will interact to assure accuracy of data and sufficient quality to meet product performance requirements. Given the requirements of measurement accuracy and the product performance, multivariate correlations will be made to show the relationships between different chemical constituents and their impact on product performance. Such correlations will further enhance performance and then dictate any improvements needed for measurement accuracy.

It seems logical to conclude that productivity, profitability, and competitiveness will be based on efficient production of high-quality products. Quality products will result from obtaining all information available—both performance- and composition-related. To the extent that compositional information learned early in the manufacturing process can help to avoid manufacture of off-spec products and improve the quality of a product in real time, compositional measurement and the analytical chemist will be vital to industrial productivity.

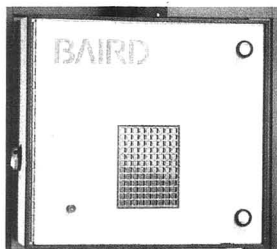
The author gratefully acknowledges many helpful discussions with Curt W. Reimann and Rance A. Velapoldi during the past several years. Their contributions made it possible to create this paper.

## References

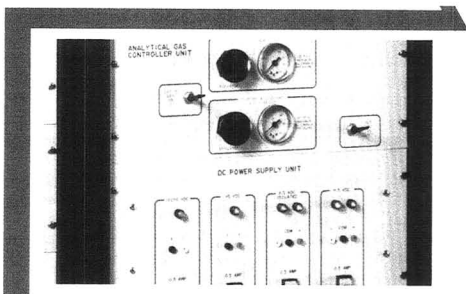
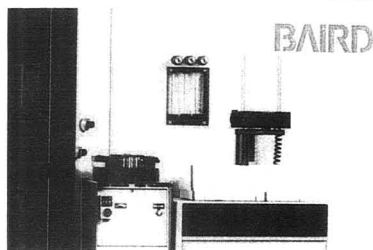
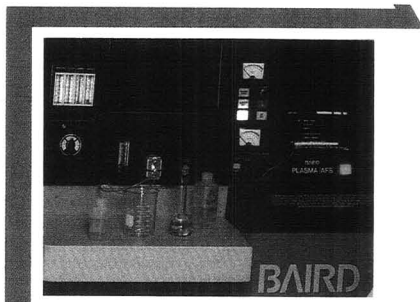
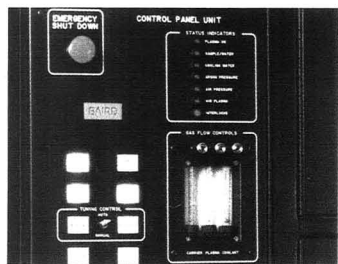
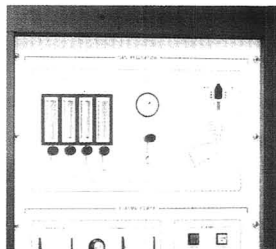
- (1) Egberg, D. C. In *Reference Materials for Organic Nutrient Measurement*; Margolis, S. A., Ed.; NBS Spec. Publ. 635; U.S. Government Printing Office: Washington, D.C., 1982; pp. 8-12.
- (2) Diamondstone, B.; Flinchbaugh, D.; Green, W. *Proceedings of the International Symposium on Effects of Steel Manufacturing Processes on the Quality of Bearing Steels*; American Society for Testing Materials: Philadelphia, Pa., in press.
- (3) Downing, R. G., personal communication.
- (4) *Statistical Abstract of the United States: 1987*, 107th ed.; U.S. Government Printing Office: Washington, D.C., 1986; p. 416.
- (5) Kowalski, B. R., personal communication.



Harry S. Hertz is the director of the Center for Analytical Chemistry at the National Bureau of Standards. He received a B.S. in chemistry from the Polytechnic Institute of Brooklyn (1967) and a Ph.D. in organic chemistry from the Massachusetts Institute of Technology (1971). After spending two years as an Alexander von Humboldt Fellow at the University of Munich, he joined the staff of the National Bureau of Standards. His research has been in the area of organic mass spectrometry, with emphasis on quantitative trace organic analysis. His current interests are in analytical chemical and clinical measurement systems, quality assurance, and future systems for accomplishing quantitative chemical measurements.



Before you choose  
an ICP,  
Examine  
our family  
tree.



Because there are different applications for ICP emission spectroscopy, BAIRD has designed and built a complete family of ICP's from which to choose. Regardless of the industry you are in or your specific need, BAIRD has an ICP that will work for you — **WITHOUT COMPROMISE.**

BAIRD CORPORATION  
125 Middlesex Turnpike  
Bedford, Massachusetts 01730  
617/276-6096

Every spectrometer will provide years of reliable and accurate service and is backed by BAIRD's outstanding field and technical support. This combination has you up and running quickly and with complete confidence. Call us today to find the ICP that's right for you.

**BAIRD**  
The Spectroscopy People

CIRCLE 18 ON READER SERVICE CARD



## Meetings

- **2nd International Symposium on Preparative and Up-Scale Liquid Chromatography.** Feb. 1-3. Baden-Baden, F.R.G. Contact: Gesellschaft Deutscher Chemiker, Abt. Tagungen, Postfach 90 04 40, D-6000 Frankfurt/Main 90, F.R.G.
- **OPTICS/ECOOSA '88.** March 22-25. Birmingham, U.K. Contact: Meetings Officer, The Institute of Physics, 47 Belgrave Square, London SW1X 8QX, U.K.
- **2nd International Symposium on Analytical Methods and Problems in Biotechnology.** March 29-31. Noordwijkerhout, The Netherlands. Contact: Symposium Secretariat, ANABIOTEC '88, c/o QLT Convention Services, Keizersgracht 792, 1017 EC Amsterdam, The Netherlands
- **CANBIOCON '88.** April 12-14. Montreal, Canada. Contact: Rachel Boekman, BCI-BIOTECH CANADA Inc., 100 Alexis Nihon, Suite 875, Montreal QC H4M 2P4, Canada
- **Flow Analysis IV.** April 17-20. Las Vegas, Nev. Contact: G. E. Pacey, Dept. of Chemistry, Miami University, Oxford, Ohio 45056
- **29th Experimental NMR Conference.** April 17-21. Rochester, N.Y. Contact: Judith Watson, ENC, 750 Audubon, East Lansing, Mich. 48823 (517-332-3667)
- **4th International Symposium on Resonance Ionization Spectroscopy and Its Applications (RIS-88).** April 18-22. Gaithersburg, Md. Contact: Kathy Stang, National Bureau of Standards, Room A345, Physics Bldg., Gaithersburg, Md. 20899
- **4th Texas Symposium on Mass Spectrometry: Analysis of Peptides and Proteins.** April 18-20. College Station, Tex. Contact: Catherine McNeal, Dept. of Chemistry, Texas A & M University, College Station, Tex. 77843
- **Handling of Environmental and Biological Samples in Chromatography.** April 27-29. Basel, Switzerland. Contact: R. Frei, Dept. of Analytical Chemistry, De Boelelaan 1083, Vrije Universiteit, 1081 HV Amsterdam, The Netherlands
- **The Analytical Environment—Symposium on Analytical Instrumentation for Environmental Monitoring.** May 9-11. Chicago, Ill. Contact: Robert Zuthis, Infoscience Services, 2970 Maria Ave., P.O. Box 153, Northbrook, Ill. 60065 (312-291-9161)
- **9th International Symposium on Capillary Chromatography.** May 16-19. Monterey, Calif. Contact: P. Sandra, Research Institute for Chromatography, P.O. Box 91, B-8610 Wevelgem, Belgium
- **4th International Conference on Chemometrics in Analytical Chemistry.** May 18-20. Amsterdam, The Netherlands. Contact: H. C. Smit, Laboratory for Analytical Chemistry, University of Amsterdam, Nieuwe Achtergracht 166, 1018 WV Amsterdam, The Netherlands
- **1st International Symposium on Separation of Chiral Molecules.** May 31-June 2. Paris, France. Contact: Société Française de Chimie, 250 Rue Saint-Jacques, 75005 Paris, France
- **36th ASMS Conference on Mass Spectrometry and Allied Topics.** June 5-10. San Francisco, Calif. Contact: Judith Watson, ASMS, P.O. Box 1508, East Lansing, Mich. 48823 (517-337-2548)
- **195th ACS National Meeting and 3rd Chemical Congress of North America.** June 5-10. Toronto, Canada. Contact: B. Hodson, 1155 16th St., N.W., Washington, D.C. 20036
- **ElectroFinnAnalysis.** June 6-9. Turku (Åbo), Finland. Contact: Ari Ivaska, Laboratory of Analytical Chemistry, Åbo Akademi, SF-20500 Turku (Åbo), Finland
- **12th International Symposium on Column Liquid Chromatography.** June 19-24. Washington, D.C. Contact: Symposium Manager, Barr Enterprises, P.O. Box 279, Walkersville, Md. 21793 (301-898-3772)
- **4th Biennial National Atomic Spectroscopy Symposium.** June 29-July 1. York, U.K. Contact: N. W. Barnett, Dept. of Environmental Sciences, Plymouth Polytechnic, Drake Circus, Plymouth PL4 8AA, U.K.
- **11th International EPR Symposium.** July 31-Aug. 5. Denver, Colo. Contact: Gareth Eaton, Dept. of Chemistry, University of Denver, Denver, Colo. 80208 (303-871-2980)
- **NMR Symposium.** July 31-Aug. 5. Denver, Colo. Contact: James Haw, Dept. of Chemistry, Texas A & M University, College Station, Tex. 77843
- **Symposium for Innovation in Measurement Science.** July 31-Aug. 5. Geneva, N.Y. Contact: Marie Long, ISA, 67 Alexander Dr., Research Triangle Park, N.C. 27709 (919-549-8411)
- **9th International Congress on Thermal Analysis.** Aug. 21-26. Jerusalem, Israel. Contact: S. Shoval, Everyman's University, P.O. Box 39328, Tel Aviv 61392, Israel
- **102nd Annual AOAC International Meeting and Exhibition.** Aug. 29-Sept. 1. Palm Beach, Fla. Contact: Margaret Ridgell, AOAC, 1111 North 19th St., Suite 210, Arlington, Va. 22209 (703-522-3032)
- **11th International Mass Spectrometry Conference.** Aug. 29-Sept. 2. Bordeaux, France. Contact: Conference Secretary, 11th International MS Conference, Ecole Polytechnique, F-91128 Palaiseau, France
- **8th Annual American-Eastern European Colloquium and Symposium on Liquid Chromatography.** Sept. 3-7. Szeged, Hungary. Contact: Huba Kalász, Dept. of Pharmacology, Semmelweis University of Medicine, Budapest, Nagyvárad tér 4, 1089 Hungary
- **9th European Congress on Electron Microscopy (EUREM 88).** Sept. 4-9. York, U.K. Contact: Congress Secretariat, The Royal Microscopical Society, 37/38 St. Clements, Oxford, OX4 1AJ, U.K.
- **Computer Applications in Analytical Chemistry—COMPANA '88.** Sept. 5-8. Jena, G.D.R. Contact: K. Danzer, c/o Friedrich Schiller University Jena, Dept. of Chemistry, Steiger 3, Jena, DDR-6900, G.D.R.
- **10th Conference on Analytical Atomic Spectroscopy and 7th Polish Spectroanalytical Conference.** Sept. 5-9. Toruń, Poland. Contact: J. Fijałkowski, Institute for Nuclear Chemistry and Technology, ul. Dorodna 16, 03-195 Warszawa, Poland
- **6th International Symposium on Isotachopheresis and Capillary Zone Electrophoresis.** Sept. 21-23. Vienna, Austria. Contact: E. Kennler, Symposium Chairman, Institute for Analytical Chemistry, University of Vienna, Währinger Strasse 38, A-1090 Vienna, Austria
- **5th International Symposium on Bioluminescence and Chemiluminescence.** Sept. 25-29. Florence, Italy. Contact: M. Pazzagli, Endocrinology Unit, University of Florence, Viale Morgagni, 85, 50134, Florence, Italy

# American Chemical Society

## 1988 Membership Application

1155 Sixteenth Street, N.W., Washington, D.C. • (202) 872-4600

### An Invitation

The American Chemical Society, the world's largest scientific organization, invites you to join in membership with 137,000 other chemists and scientists in allied fields. We hope this application will provide the opportunity for you to take advantage of the many benefits ACS offers to its members.

(Please type or print.)

Mr., Mrs. \_\_\_\_\_  
Dr., Miss, Ms. \_\_\_\_\_  
Mailing Address \_\_\_\_\_

Telephone: Home \_\_\_\_\_ Office \_\_\_\_\_  
Area Code Area Code

### Academic Training

Name of College or University (Including current enrollment)	City and State	Curriculum Major	Years of Attendance	Title of Degree(s) Received or Expected	Date Degree Received or Expected
---	----------------	---------------------	------------------------	---	--

### Courses Completed

*Not required of those with a bachelor's, master's, or doctor's degree in chemistry or a closely related science.*

Please list completed courses (by title) in the chemical sciences (attach separate sheet or transcript if more space is needed). Quarter hour credits should be multiplied by two-thirds. If school did not use a credit hour system, please estimate credits on basis of 15 lecture clock hours or 45 laboratory clock hours as equivalent to one semester hour credit.

Course Title	Semester Hours	Course Title	Semester Hours	Course Title	Semester Hours
_____	_____	_____	_____	_____	_____
_____	_____	_____	_____	_____	_____
_____	_____	_____	_____	_____	_____

*The Admissions Committee will review all applications in accordance with the criteria for membership.*

### Nomination

Nomination by two ACS members is required by ACS Bylaws. If this presents difficulty, we suggest you contact the Washington office. Such nomination is not necessary for former members. Student affiliation does not constitute membership. The requirement of having two nominating signatures may be waived by the Admissions Committee in cases where applicant lives in areas remote from ACS members.

We recommend \_\_\_\_\_ for membership in the American Chemical Society.  
(Name of Applicant)

ACS Member: \_\_\_\_\_  
(Signature) (Printed Name)

ACS Member: \_\_\_\_\_  
(Signature) (Printed Name)

This space for use of  
ADMISSIONS COMMITTEE

Local Section/Division Commission Claim

1 2 3 4 6 N

# Statistical Information

(Please type or print.)

Mr., Mrs. \_\_\_\_\_  
Dr., Miss, Ms. \_\_\_\_\_ Family Name First Middle  
Mailing Address \_\_\_\_\_

Office Use Only

AMC \_\_\_\_\_  
MJR \_\_\_\_\_  
DEL \_\_\_\_\_  
HDL \_\_\_\_\_  
MED \_\_\_\_\_  
CSD \_\_\_\_\_  
PNI **8823Y** \_\_\_\_\_  
TEC \_\_\_\_\_

Date of Birth \_\_\_\_\_ Sex ☐ F ☐ M Telephone: Home \_\_\_\_\_ Office \_\_\_\_\_  
(Information needed for statistical purposes) Area Code Area Code

Previous Membership I have ☐ have not ☐ previously been a member.  
I have ☐ have not ☐ previously been a student affiliate.

## Professional Experience

Job Title: \_\_\_\_\_ Employer \_\_\_\_\_  
Employer City, State, Zip \_\_\_\_\_ Starting Date \_\_\_\_\_ MO/YR  
Nature of Business: ☐ Manufacturer ☐ Academic ☐ Government  
☐ Other \_\_\_\_\_  
(Please specify)

## Dues/Subscriptions/Divisions

☐ **FREE DIVISION MEMBERSHIP FOR NEW MEMBERS FOR ONE YEAR!** Check here if you wish complete information.

There are four start dates for membership: 1 January, 1 April, 1 July, and 1 October. We are anxious to begin your membership as soon as possible and will therefore enroll you immediately upon approval of your application by the ACS Admissions Committee. Dues for 1988 are \$79.00. Your membership will begin at the nearest quarter and you will be billed accordingly. Those entering 1 October will be billed for the three months of the year plus the full dues for the following year (or 15 months dues) or at the new member's option, may pay for the final three months of the current year only. Former members who did not resign will be assessed a \$10.00 reinstatement fee. *Please send no money now.*

### Student Dues

If you are a student majoring in the chemical sciences, a 50% reduction on membership dues is available. To apply you must be registered for a least six credit hours as an undergraduate or be enrolled as a full-time graduate student.

I am ☐ an undergraduate student enrolled as described above.

I am ☐ a graduate student enrolled as described above. \_\_\_\_\_  
Name of College or University

### National Affiliation

National Affiliates pay three-quarters dues (i.e., \$59.25) and likewise will receive a prorated bill based on the quarter National Affiliation begins.

### Husband/Wife Dues

If you are the spouse of a member receiving *C&EN*, 23% (of the prorated amount) will be deducted from your bill. This is the portion that is allotted for *C&EN*. If you are eligible, please give the name of your spouse and his/her membership number.

Spouse's Name \_\_\_\_\_ Membership Number \_\_\_\_\_

If you wish to subscribe to any ACS publications, please list them below.

\_\_\_\_\_  
\_\_\_\_\_

*Remember, send no money now.*

## Agreement

I attest to the accuracy of information on the application. I agree to restrict for my own personal use all publications to which I subscribe at member rates. I understand that membership dues are payable annually unless my signed resignation is received by the Executive Director before January 1 of the year for which my resignation is to take effect.

Date \_\_\_\_\_ Signature of Applicant \_\_\_\_\_

## IUPAC Affiliation

The International Union of Pure and Applied Chemistry (IUPAC) offers individual Affiliation to members of national chemical societies. Recognized by all the sciences and by the national level academies of science as the international representative body for chemistry, IUPAC is the authority on chemical nomenclature, terminology, symbols, atomic weights, and related topics. IUPAC Affiliate dues for ACS members residing in the U.S. are \$20.00 and include a subscription to *Chemistry International* magazine.

☐ IUPAC Affiliation \$20.00 (U.S. members only).



# Howard Malmstadt: An Inspiration

*Honored by FACSS and ANACHEM*

At the annual meeting of the Federation of Analytical Chemistry and Spectroscopy Societies (FACSS), which took place in Detroit, Oct. 4-9, 1987, renowned chemist Howard V. Malmstadt was doubly honored. Malmstadt, professor emeritus at the University of Illinois and provost and senior vice-president at the Pacific and Asia Christian University, accepted the 1987 ANACHEM Award. In addition, more than 50 chemists, all academic progeny of Malmstadt, contributed some 150 technical papers to the conference.

The ANACHEM Award, which is given yearly by the Association of Analytical Chemists, honors Malmstadt's outstanding contributions to analytical research and education. The technical presentations by Malmstadt's former students (and their students, etc.) convincingly demonstrated the wide-ranging influence and importance of the man in both areas.

## A distinguished career

Howard Malmstadt was born in Marionette, Wis., in 1922. He earned his bachelor's degree at the University of Wisconsin in 1943. During a subsequent three-year hitch in the Navy, he studied electronics at Princeton and at the Massachusetts Institute of Technology and served as a radar officer in the Pacific. After the war he returned to the University of Wisconsin, where he obtained his M.S. (1948) and Ph.D. (1950) degrees in analytical chemistry. In 1951 Malmstadt began a long tenure at the University of Illinois, during which he taught, performed research, and authored or coauthored more than 150 technical articles and 10 books. He retired from Illinois in the early 1980s and assumed his current position at the Pacific and Asia Christian University in Kailua-kona, Hawaii.

During his years at the University of Illinois, Malmstadt earned a reputation as an inspirational force in the analytical community. Gary Hieftje, an early student of Malmstadt's, now at Indiana University, recently reflected: "He [Malmstadt] emphasized setting high goals. He would urge his students, by example, to set up standards or ideal characteristics that they would like an instrument to possess. He presented an ideal framework for academic growth. And there is tremendous success among his former students."

## FOCUS

Jim Winefordner, the first of Malmstadt's students to enter academia, and now at the University of Florida, echoed Hieftje: "Possibly he [Malmstadt] produced more Ph.D.'s that pursued academic careers than did any other professor. I think it was something like twenty. In terms of scientific ability, he was brilliant. He always had good suggestions, even though he covered a wide swath of projects." Hieftje concurred: "His students studied everything and went in every direction in analytical chemistry."

Chris Enke, now at Michigan State, has collaborated with Malmstadt on many projects. Enke recently stated, "Instead of just speaking of principles and ideals, Howard has lived them." If one area stands out as being strongly advocated and advanced by Malmstadt, it is electronics. He was an innovator and a leader in the development of modular electronic instruments, and he developed a popular and influential course in electronics for scientists. Stan Crouch, another early student, now at Michigan State, summed it up in this

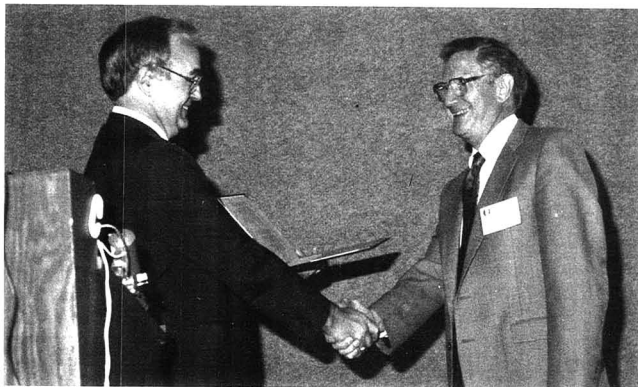
way: "He [Malmstadt] introduced electronics to chemists. He had the vision to see that chemists would be using electronic tools. It is now taken for granted—thanks to Malmstadt—that an analytical chemist will know electronics." Malmstadt's interest in electronics resulted in the 1962 book, *Electronics for Scientists*, coauthored by Enke and E. C. Toren, Jr., and the 1981 book, *Electronics and Instrumentation for Scientists*, coauthored by Enke and Crouch.

Malmstadt is also known for his efforts in the area of kinetic methods. "He promoted and fostered these methods," said Crouch. Another area that has benefited from Malmstadt's influence is spectroscopy. "People forget the spectroscopy part," opined Crouch. "I am creating a spectroscopy text that owes very much to Howard Malmstadt and his course in spectroscopy (that is, the one he developed at the University of Illinois)."

## A host of honors

Malmstadt's professional achievements and past honors are many. He is a former Guggenheim Fellow and was the chairman of the ACS Division of Analytical Chemistry. He has been on the advisory boards of the National Science Foundation, the National Institutes of Health, the National Research Council, and various scientific journals. He has served as a consultant for U.S. industries and the United Nations and has been a visiting professor or guest lecturer at universities and scientific societies in the United States, England, Australia, Brazil, Singapore, India, Japan, and China.

Malmstadt's many awards include the following: the Instrument Society of America Award, the ACS Awards in Analytical Chemistry and Chemical In-



Harry Pardue (left), of Purdue University, presents the 1987 ANACHEM Award to Howard Malmstadt.

strumentation, the Pittsburgh Conference Outstanding Chemist Award, the Fulbright-Hay Distinguished Professor Award, the Isco Award for Contributions in Biochemical Instrumentation, and the ACS Division of Analytical Chemistry Excellence in Teaching Award.

## A celebration and a proposal

In bringing together so many academic relations in one place, the FACSS conference became not just a tribute to the accomplishments of Howard Malmstadt, but also a celebration of the man's spirit. Many of the direct descendants shown in the family tree on page 90 A, as well as many professional colleagues who have worked with Malmstadt through the years, attended the conference. As acquaintanceships were renewed and old times recalled, the participants shared in the themes of respect and enthusiasm for Malmstadt and his work.

The program also featured three half-day symposia, each of which was conducted by former students and colleagues of Malmstadt. These symposia, which explored analytical trends and issues of wider scope, were as follows:

"Emerging Concepts in Instrumentation and Education," "New Concepts in Spectrochemical Analysis," and "Advances in Biotechnological and Clinical Methodology."

Malmstadt closed the first symposium with an address entitled "Technology, Education, and Communities in Need." In this moving oration, he explored profound issues of chemistry in a social context, drawing on his own appropriate experience. Malmstadt envisioned an academic curriculum that would recognize the needs of communities and provide a framework for satisfying those needs through the course of academic study. In this curriculum, the main objectives of education would be ever present, as problems involving energy, the environment, health, sanitation, and engineering would be dealt with literally. Problems would be identified, the skills required to solve them would be determined, and students would be trained appropriately. Students would work in the field so that their experience would result in a mix of the practical and empirical aspects of problem solving together with the ideal and theoretical aspects.

In his role as a teaching professor,

Howard Malmstadt insisted that his students develop and maintain a broad perspective on their discipline. As Gary Hieftje put it, "He taught that students should not lose sight of their heritage, that is, the chemistry." Malmstadt's remarks at the FACSS conference revealed an insistence on an even broader perspective. He now calls upon chemistry students not only to be aware of the wide base of knowledge and the history that surround their work, but also to recognize the responsibilities and possibilities inherent in the relationship between the science and society.

At the Pacific and Asia Christian University, Howard Malmstadt now contributes his knowledge and talents to a program that is meant to help people living in the Pacific Basin area. He has come full circle since that time, some 40 years ago, when he served as a radar officer in the Pacific Theater and was just starting his career in science. In the intervening years, Malmstadt has worked with countless young scientists, instilling in them good values while pointing them in the direction of good science. This man of patience and brilliance and vision has been, and continues to be, an inspiration.

Don Cunningham



At the FACSS convention Malmstadt spoke about "Technology, Education, and Communities in Need."



Some of the first generation of Malmstadt "academic progeny" gather (left to right): Pedro Rodriguez, Rich Timmer, Gary Horlick, Warren Lanier, Jim Howell, Willard Harrison, Ed Piepmeier, Gary Hieftje, Cliff Toren, Harry Pardue, Chris Enke, Howard Malmstadt, Brian Renoe, Malcolm Warren, Stan Crouch, Jim Avery, Sheldon Brunk, Mike Franklin, Milt Karayannis, Ramon Barnes.



## Don't sacrifice GC/MS specificity for sensitivity.

Reach for a new level of sensitivity while scanning the full mass range throughout your GC run. All with a linear dynamic range of over five decades, and the use of internal standards for the highest quantitative precision.

The new Finnigan MAT Model 800 Ion Trap Detector™ gives you positive identification at sample levels as low as 10 picograms, with the confidence level only a full mass scan can offer. To attain equivalent sensitivity, competitive detectors depend on the measurement of a few selected ions, sacrificing specificity for sensitivity.

For molecular weight confirmation, the ITD™ 800 offers chemical ionization (CI) capabilities, a feature previously available only on mass spectrometers costing twice as much as the ITD 800.

As always, the ITD's powerful library search program can match an unknown spectrum in seconds.

Richard A. Yost (University of Florida), William McClennen and Henk L.C. Meuzelaar (University of Utah) put the ITD to the test. Their findings are documented in our Technical Report #209, "Enhanced full scan sensitivity and dynamic range in the Ion Trap Detector." Ask your Finnigan MAT representative for a copy today, and demand to see results like these from *your* next mass spec detector.

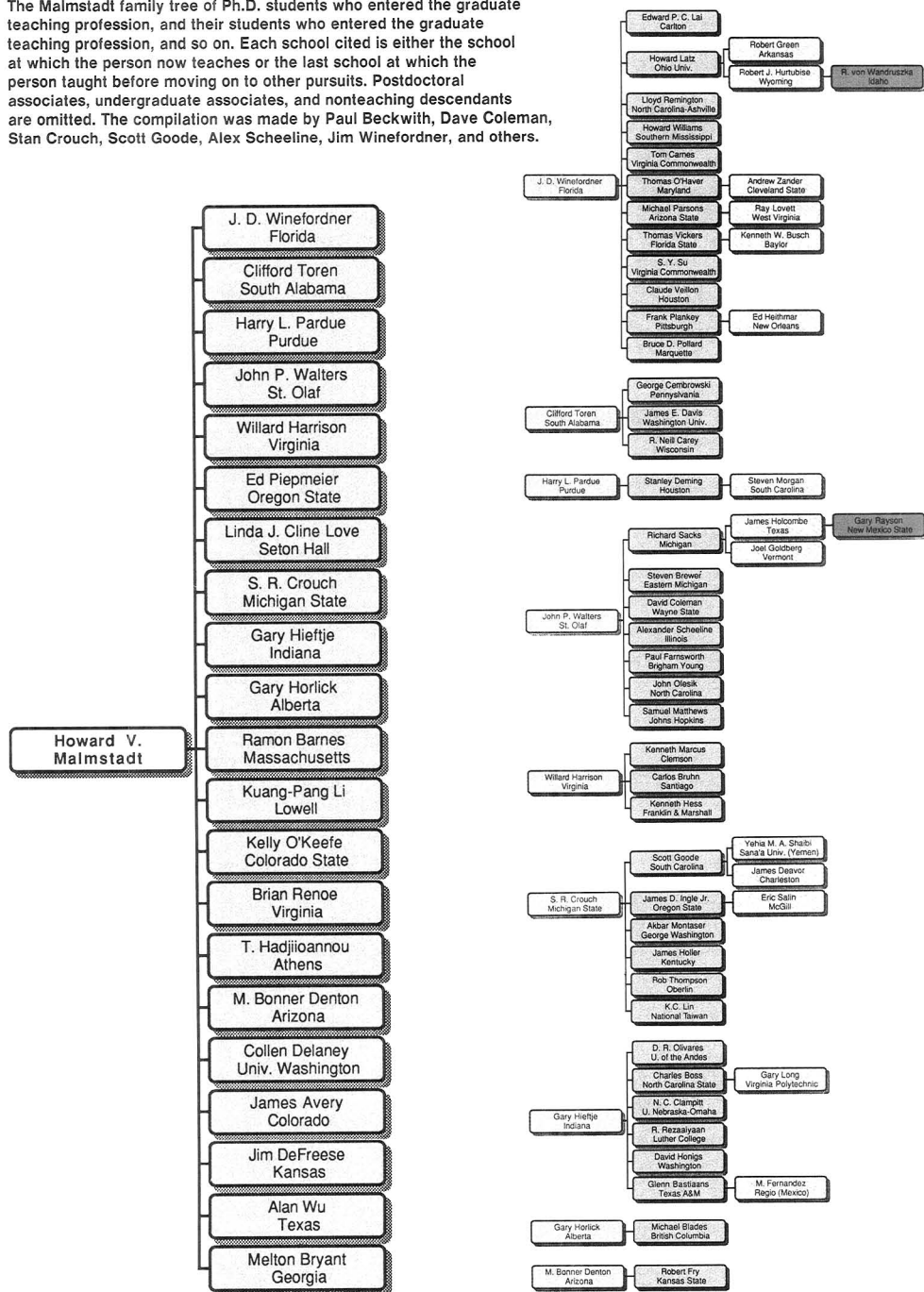
Mass spectrometry:  
We make the difference.



U.S.A., 355 River Oaks Parkway, San Jose, CA 95134, (408) 433-4800  
Germany, Postfach 14-40 62, D-2800 Bremen 14, (0421) 54 93 0  
U.K., Paradise, Hemel Hempstead, Herts HP2 4TG, (0442) 255555  
France, 69, rue de Paris, F-91400 Orsay (1) 69 28 52 53  
Sweden, Amnåstravägen 1C, 117 43 Stockholm, (08) 190480  
Benelux, Landjuwel 7, 3645 PE Veendam, (0855) 27356  
Italy, Via Valadier, 37B, 00183 Rome, (06) 3161000  
Japan, Shirozaki Bldg., 2-7-1 Hirakawa-cho, Chiyoda-ku, Tokyo 102, (03) 221-1001

Circle 50 for literature.  
Circle 51 to have a representative call.

The Malmstadt family tree of Ph.D. students who entered the graduate teaching profession, and their students who entered the graduate teaching profession, and so on. Each school cited is either the school at which the person now teaches or the last school at which the person taught before moving on to other pursuits. Postdoctoral associates, undergraduate associates, and nonteaching descendants are omitted. The compilation was made by Paul Beckwith, Dave Coleman, Stan Crouch, Scott Goode, Alex Scheeline, Jim Winefordner, and others.



# NOW YOU CAN SEARCH RSC JOURNALS ONLINE



The main primary journals published by the Royal Society of Chemistry (RSC) are now searchable online via **CHEMICAL JOURNALS ONLINE (CJO)** – a family of new online files produced by the American Chemical Society and available through STN International.

The RSC journals file (**CJRSC**) includes Chemical Communications, Dalton Transactions, Faraday Transactions (I\* & II), Perkin Transactions (I & II), The Analyst, Journal of Chemical Research,\* Journal of Analytical Atomic Spectrometry, Faraday Discussions.

\*Available from 1988

**CJRSC** may be searched alone or in conjunction with other components of the **CJO** database which includes ACS journals and polymer journals published by Wiley.

The unique Crossover facility from STN enables you to perform the same search on **CJRSC** and **CAS ONLINE** thereby combining the breadth of coverage of Chemical Abstracts with the depth of coverage of RSC journals.

Online access to the RSC journals provides you with a convenient, rapid and economical means of keeping up with the latest significant research in the chemical sciences.

*For more information, call (614) 421-3600, or return the form below to: STN International, c/o Chemical Abstracts Service, 2540 Olentangy River Road, P.O. Box 02228, Columbus, OH 43210.*

Please send me more information on **CJRSC** and the Chemical Journals Online data base.

Name .....

Address .....

.....

.....

**CHEMICAL JOURNALS  
ONLINE**

# NEW PRODUCTS



**GP analyzer** is designed for moisture testing of solids such as grains and pharmaceutical tablets and powders. Moisture content from ~0 to 35% can be measured, and accuracy is within 0.2% for moisture levels up to 20%. Tecator **401**

**Data management.** HP 3359 chromatographic worksystem is a multiple-instrument, multiuser product for laboratory data acquisition, reduction, and reporting. The system can operate as part of a local area network or via modem to communicate with other computers. Hewlett-Packard **404**

**Electron microscope.** MEM 20 multienvironment electron microscope allows the direct examination of any specimen type without the need for specimen preparation. High-resolution imaging with magnifications up to 100,000X is provided using both secondary and backscattered imaging. ElectroScan **405**

**Gas detector.** Leak detector, designed for use in hospitals, food and textile plants, and in the agricultural industry, can detect < 1 ppm ethylene oxide. The sensor is unaffected by moisture, temperature change, or poisons. CEA Instruments **406**

**FT-IR.** Three sampling accessories for quality control applications are the CIRCLE cell, for analysis of all types of liquid samples; QC Contact Sampler, for viscous liquids, powders, pastes,

semisolids, and films; and COLLECTOR, for analysis of powders, crystals, fibers, foams, catalysts, and coal by DRIFT spectroscopy. Spectra-Tech **407**

**LC detector.** SP8410 fluorescence detector features split beam 90° optics, a 30-μL high-purity fused silica sample cell, 10 mV and 5 V outputs, and a drift of less than 5%/h at a range setting of 2. Spectra-Physics **408**

**Environmental analysis.** Purge and trap injector permits separations in the parts-per-trillion range and provides cold trapping to temperatures as low as -190 °C. Cold trap temperature can be regulated to within 2 °C. Chrompack **409**

**Gas analysis.** MINI-IR infrared analyzer is designed for on-line monitoring of carbon monoxide, carbon dioxide, methane, aromatics, and other hydrocarbon gases. Features include integrated zero and span controls and a digital meter readout. Teledyne Analytical Instruments **410**

**XRF.** QX series wavelength-dispersive X-ray fluorescence spectrometer can

be fitted with up to 10 monochromators for simultaneous determination of up to 10 elements ranging from sodium to uranium. The instrument is controlled by the IBM PC System 2 computer. Oxford Analytical Instruments **411**

**LC.** Jule HPLC gradient former produces linear or exponential gradients without microprocessor-controlled proportioning valves and a two-pump setup. Gradient ranges between 10 and 100 mL of increasing and decreasing concentrations are possible. Research Products International **412**

**Water analysis.** DIGI-DISC photometer contains 12 custom-designed filters mounted internally on a rotating disc. Exterior controls are protected from liquids, and a dimpled drain hole minimizes cleanup of accidental spills inside the meter. Nalco Chemical Company **413**

## Software

**Chromatography.** ACCESS\*CHROM, designed for use with the DEC Micro-VAX 2000, allows multiple users to perform chromatography data acquisition, processing, and post-run operations on the same computer while data are collected from multiple chromatographs. Nelson Analytical **415**

**Data analysis and plotting.** Graph-PAD allows users to analyze data and create publication-quality graphs with a PC and a plotter. Data can be analyzed using error bars, curve fitting, and linear and nonlinear regression. ISI **416**

## Manufacturers' Literature

**LC.** Technical bulletin describes an empirical approach for solvent optimization using a conventional automated or manually operated liquid chromatograph.

---

For more information on listed items, circle the appropriate numbers on one of our Readers' Service Cards

---

graph. Prior knowledge of the composition of the sample is not required. Perkin-Elmer 418

**Detectors.** Brochure describes the FD series fluorescence detectors, which feature microprocessor-based electronics, user-friendly touch-sensitive control panel, and xenon flash lamp technology. 6 pp. SpectroVision 419

**ICP newsletter.** *Leeman Letter*, No. 6, features articles on ICP standard solutions and on the analysis of wear metals in oil at Blackstone Labs. 6 pp. Leeman Labs 420

**Microbore LC.** Product bulletin describes the MicroGradient system, which features flow rates from 10 to 2000  $\mu\text{L}/\text{min}$  and pressures up to 5500 psi. System capabilities and specifications are discussed. Applied Biosystems 421

**Newsletter.** *Analytical Control*, Vol. 12, No. 4, contains articles on final EPA Appendix IX regulations and the use of GC and GC/MS for organic compound determination. NUS 422

**Toxic gases.** Brochure features the TLD-1 toxic gas detector, which is pre-programmed to alarm at either one or two times the threshold limit value of the gas being monitored. Detectable gases include phosphine, silane, ammonia, chlorine, and phosgene. 4 pp. MDA Scientific 423

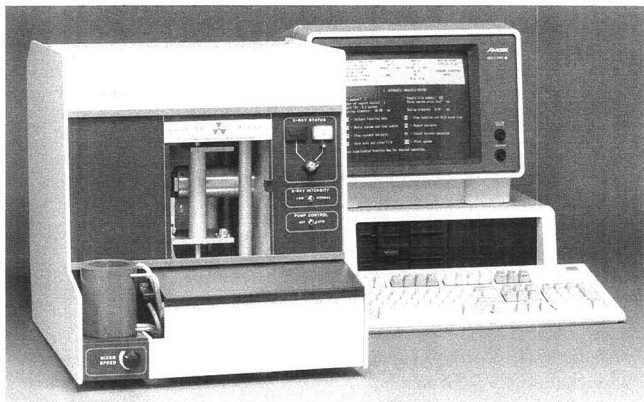
## Catalogs

**Plasticware.** Catalog includes bags, beakers, bottles, centrifuge ware, filtration equipment, flasks, funnels, and pipets. Information on the structure and properties of resins is also included. 128 pp. Cole-Parmer 425

**Amino acids.** Catalog lists amino acids and pharmaceutical intermediates produced by Diamalt AG. Empirical and structural formulae, CAS registry numbers, applications, and references are included. 72 pp. Nepera 427

**Scientific apparatus.** Catalog contains more than 23,000 laboratory apparatus items and reagents. Included is a 56-page index that lists products by trade name and manufacturer. 1984 pp. Thomas Scientific 428

**Molecular biology.** Catalog features products for DNA sequencing; molecular cloning; and nucleic acid blotting, electrophoresis, and chromatography.



**SediGraph 5100** provides particle size analysis in the range of 300–0.1  $\mu\text{m}$ . Fully automated features include baseline correction, sample cell bubble elimination, and the overlaying of up to 3 plots onto an existing plot. Micromeritics 402

Technical information and references are included. 32 pp. Bio-Rad 429

**Surface analysis.** Catalog presents ultrahigh vacuum, surface analysis, and

molecular beam epitaxy components, including products for secondary ion MS and Auger electron, photoelectron, and ion-scattering spectroscopy. 218 pp. Perkin-Elmer 426

**There are  
224 reasons why ...  
most chemists  
in the U.S. belong to the  
American Chemical Society.**

The fact is, there are more than 137,000 chemists in this vital, career-enhancing society — *the largest scientific organization in the world!* To learn those reasons, write, use coupon or CALL TOLL FREE 1-800-ACS-5558

American Chemical Society, 1155 Sixteenth St., NW, Washington, DC 20036

**Yes!**

I would like to know 224 reasons to join the American Chemical Society. Please send free brochures to:

Name \_\_\_\_\_

Address \_\_\_\_\_

City, State, ZIP \_\_\_\_\_



***For American Chemical Society Members Only:***

***1988 Member Prices Held at 1987 Levels!***

***PLUS, Multiyear Rates Are Now Available for  
the First Time on All Journals***

***This Means Big Savings in 1988 . . .***

Multiyear discounts have been combined with a price freeze to give ACS members the best subscription rates possible. Members electing to take advantage of these new rates will be paying less for an annual subscription in 1988 and 1989 than they did in 1987!

☐ **ACCOUNTS OF CHEMICAL RESEARCH**

Editor, F.W. McLafferty

Cornell University

12 issues a year. ISSN 0001-4842

Member: One year \$23 Two years \$41

☐ **ANALYTICAL CHEMISTRY**

Editor, George H. Morrison

Cornell University

24 issues a year. ISSN 0003-2700

Member: One year \$25 Two years \$42

☐ **BIOCHEMISTRY**

Editor, Hans Neurath

University of Washington

26 issues a year. ISSN 0006-2960

Member: One year \$75 Two years \$135

☐ **CHEMICAL & ENGINEERING NEWS**

Editor, Michael Heylin

51 issues a year. ISSN 0009-2347

Member: Free

☐ **CHEMICAL RESEARCH IN TOXICOLOGY**

Editor, Lawrence J. Marnett

Wayne State University

6 issues a year. ISSN 0893-228X

Member: One year \$46 Two years \$82

☐ **CHEMICAL REVIEWS**

Editor, Josef Michl

University of Texas

8 issues a year. ISSN 0009-2665

Member: One year \$22 Two years \$39

☐ **CHEMTECH**

Editor, Benjamin J. Luberoft

12 issues a year. ISSN 0009-2703

Member: One year \$34 Two years \$57

☐ **ENERGY & FUELS**

Editor, John W. Larsen

Lehigh University

6 issues a year. ISSN 0887-0624

Member: One year \$46 Two years \$82

☐ **ENVIRONMENTAL SCIENCE & TECHNOLOGY**

Editor, William H. Glaze

University of California, Los Angeles

12 issues a year. ISSN 0013-936X

Member: One year \$30 Two years \$51

☐ **INDUSTRIAL & ENGINEERING CHEMISTRY RESEARCH**

Editor, Donald R. Paul

University of Texas, Austin

12 issues a year. ISSN 0888-5885

Member: One year \$52 Two years \$93

☐ **INORGANIC CHEMISTRY**

Editor, M. Frederick Hawthorne

University of California, Los Angeles

26 issues a year. ISSN 0020-1669

Member: One year \$79 Two years \$142

☐ **JOURNAL OF AGRICULTURAL AND FOOD CHEMISTRY**

Editor, Irvin E. Liener

University of Minnesota

6 issues a year. ISSN 0021-8561

Member: One year \$24 Two years \$43

☐ **JOURNAL OF THE AMERICAN CHEMICAL SOCIETY**

Editor, Allen J. Bard

University of Texas, Austin

26 issues a year. ISSN 0002-7863

Member: One year \$70 Two years \$126

☐ **JOURNAL OF CHEMICAL AND ENGINEERING DATA**

Editor, Bruno J. Zvolinski

Call Toll Free (U.S.)

**800-227-5558**

Telex: 440159 ACSP UI or

892582 ACSPUBS

Cable Address: JIECHEM

Teletypewriter (SANYO Group 1,2,3): 202-872-4615

**American Chemical Society  
Marketing Communications  
Department  
1155 Sixteenth St., N.W.  
Washington, D.C. 20036  
U.S.A.**

Texas A&M University

4 issues a year. ISSN 0021-9568

Member: One year \$29 Two years \$52

☐ **JOURNAL OF CHEMICAL INFORMATION AND COMPUTER SCIENCES**

Editor, Thomas L. Isenhour

Utah State University

4 issues a year. ISSN 0095-2338

Member: One year \$17 Two years \$30

☐ **JOURNAL OF MEDICINAL CHEMISTRY**

Editor, Philip S. Portoghesi

University of Minnesota

12 issues a year. ISSN 0022-2623

Member: One year \$40 Two years \$72

☐ **THE JOURNAL OF ORGANIC CHEMISTRY**

Editor, Frederick D. Greene

Massachusetts Institute of Technology

26 issues a year. ISSN 0022-3263

Member: One year \$53 Two years \$95

☐ **JOURNAL OF PHYSICAL AND CHEMICAL REFERENCE DATA**

Editor, David R. Lide, Jr.

National Bureau of Standards

4 issues a year. ISSN 0047-2689

Member: One year \$60 Two years N/A

☐ **THE JOURNAL OF PHYSICAL CHEMISTRY**

Editor, Mostafa A. El-Sayed

University of California, Los Angeles

26 issues a year. ISSN 0022-3654

Member: One year \$65 Two years \$117

☐ **LANGMUIR**

Editor, Arthur W. Adamson

University of Southern California

6 issues a year. ISSN 0074-7463

Member: One year \$55 Two years \$99

☐ **MACROMOLECULES**

Editor, Field H. Winslow

AT&T Bell Laboratories

12 issues a year. ISSN 0024-9297

Member: One year \$53 Two years \$95

☐ **ORGANOMETALLICS**

Editor, Dietmar Seyferth

Massachusetts Institute of Technology

12 issues a year. ISSN 0276-7333

Member: One year \$55 Two years \$99

Rates listed are for 1988 U.S. subscriptions. For subscription rates outside the U.S., contact American Chemical Society or your subscription agency. Member rates are for personal use only. For nonmember subscriptions in Japan, write Maruzen Co., Ltd.

# Issues and Directions in Laboratory Automation

**Joseph G. Liscouski**  
Digital Equipment Corp.  
Marlboro, Mass. 01752

Previous A/C INTERFACE articles have reviewed the technologies that will help us change and improve the chemistry laboratory. Having facilities available to us is one thing; understanding how to use and manage them is quite another. New technology will have an impact on how we work, what our workplace will be like, and the work we do. This article will examine some of the current issues raised by the application of automation systems to the laboratory. Computers, robotics, and networks may or may not play a significant role in your laboratory at the moment, but there is no doubt that they will in the very near future.

## Organizational issues

The introduction of a computer system into a laboratory represents both an opportunity and an agent for change. Will the computer system become just an electronic substitute for the paper system that you are currently using, or will it be used to improve the way your organization functions? We must identify the needs and key objectives that the computer automation system is going to satisfy. To do this we must develop a corporate-wide research computing strategy (RCS). In Digital's approach to laboratory and scientific computing (Computer Integrated Research), the RCS is part of a three-part process that aids in planning and implementing lab automation projects,

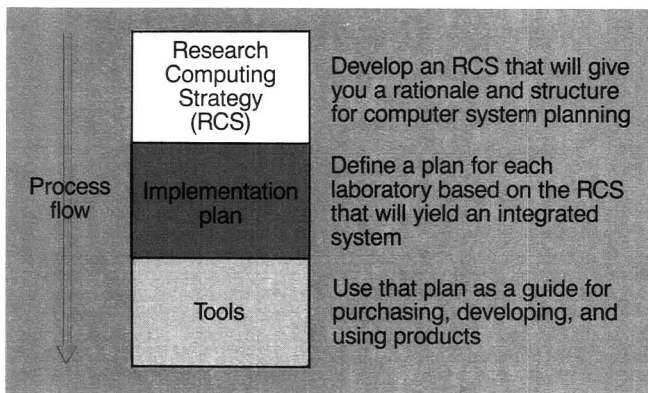


**Figure 1.** Research computing strategy for planning and implementing laboratory automation.

## A/C INTERFACE

as shown in Figure 1.

The strategy should be the same for all scientific applications and laboratories within a particular organization. Differences between lab groups (e.g., basic research vs. an analytical laboratory) are reflected in how the strategy is implemented and in the actual products or tools used (Figure 2). The primary responsibility for the formation of strategies lies with the laboratory personnel and management, but it should be done in conjunction with corporate computer groups. The coopera-

tion of the computer group is important because issues of support, maintenance, networks, system compatibility, and growth must be addressed.

The primary benefits of planning include better understanding of overall requirements, a basis for communicating and comparing approaches between scientific and corporate computing groups, the ability to show how each part of the system will contribute to the automation plan, avoidance of premature obsolescence of systems, and improved support from higher levels of management (which will make the plans easier to implement).

Setting goals to meet needs and objectives is the first stage in strategy development. Frequently the goals that first come to mind are improving productivity, providing more accurate results, and removing the tedium from routine portions of laboratory work. In addition, some other goals can be suggested, such as improving your ability to manage and work with data, information, and knowledge; providing an integrated hardware and software system within the laboratory; and improving the ability of your laboratory to

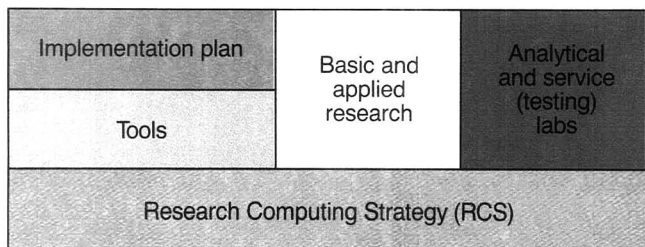


**Figure 2.** Implementation of a research computing strategy.

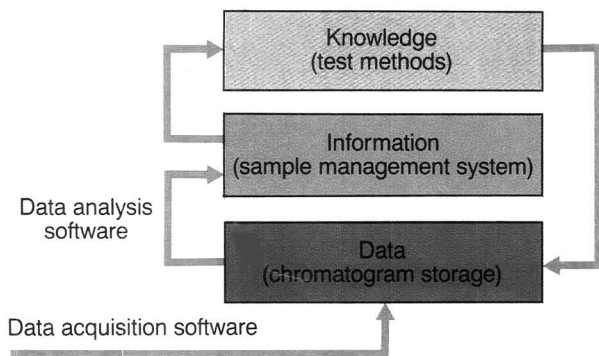


**Figure 3.** Databases and software package for collecting and analyzing chromatograms.

work with the rest of your organization.

The products of analytical laboratories are information and knowledge. These products and the data on which they are based represent a valuable asset to your group and your company and should be properly managed so that you derive the maximum benefit from them. This management should require that data be stored in a way that makes it accessible and prevents it from being lost.

Integration is a highly desirable attribute of any system. Providing for integration in a strategy designed to cover a broad range of applications can be difficult, particularly when you are working with products from a variety of sources. We can use the management of data, information, and knowledge as a means of testing for integration.

First, we need to establish some definitions. *Data* refers to the measurements we obtain from instruments, including both individual measurements (such as weights) and collections (such as spectra and chromatograms). *Information* consists of statements or conclusions based on that data, such as the amount of antioxidant in a polymer. *Knowledge* is what we use (e.g., test methods) to produce and interpret the data. Note that these definitions will change as you move from one type of laboratory or group to another; information (e.g., the amount of antioxidant) to one group may be a data point to another group (e.g., process control). Information, data, and knowledge can be viewed as separate collections or databases. Applications software provides a means of taking an element from one database, working with it, and then storing it somewhere. Although this approach may seem a bit academic, it does have some ramifications when we consider integration in a laboratory system.

Figure 3 shows the three databases and a software package for collecting and analyzing chromatograms. If the data analysis package cannot be used to insert results into the sample management system, then we do not have an integrated system. To achieve integration, additional software must be written either by the supplier or by you.

When implementing the system you might consider the following questions. Once data are collected, what tools will allow me to analyze and synthesize information? Do those tools have the ability to read the data and store the results in a sample management-tracking database? If I capture my knowledge in the form of test methods, reports, and papers, will the available tools (e.g., word processors) allow me to pull in supporting evidence and graphics? How does the system help me distribute my findings?

Automation efforts can provide a substantial benefit to a particular lab-

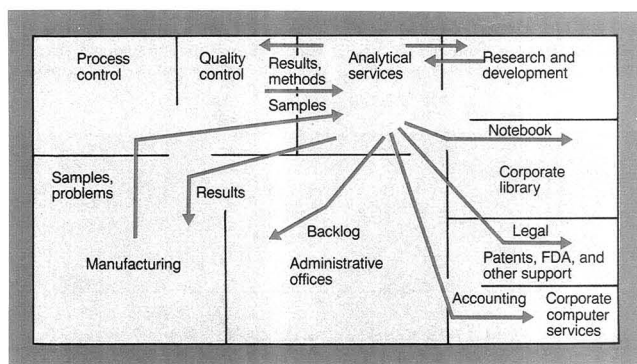
oratory. When the interactions between that lab and the groups they support or work with are taken into account, the benefits not only are greater, they are more likely to generate corporate support.

Figure 4 shows some of the interactions that can occur in an organization. Each of these interactions is an opportunity to gain additional support for, and benefit from, a full lab automation project. For example, if the sample management system can electronically send results to a process control system, integration activities can expand outside the laboratory.

Once the broad strategy has been set, the implementation plan must be developed. This is the time to establish your priorities. Few groups can afford to satisfy all their automation needs at once, and choices must be made between long- and short-term requirements. The key point to keep in mind is the ability to adapt to changes in priorities. Will the systems that satisfy your top priorities today be compatible with those installed later? Do they share a common base of communications? If you start with a smaller system for database work, can you expand to a larger one later without affecting your software system?

## Implementation

Once all of the necessary strategies and plans have been established, the next issue is the actual implementation of the system. Many chemists have become familiar with interfacing a particular instrument to a computer system, but that ability does not always translate directly into the ability to plan and implement a laboratory automation project. Even if your automation system is purchased as a turn-key system, it will still have to be maintained, have backup facilities provided, and have someone responsible for changes to the system.



**Figure 4.** Interactions within an organization.

Depending on the way in which the departments in your company work, some of this support may be provided by the computer services group. If so, this group will want to have considerable involvement in choosing the hardware and software and should fully understand and support your research computing strategy and implementation plans.

If your company is considering the implementation of numerous lab automation programs, it would be worthwhile to put together a group of people responsible for those projects. This prevents each individual lab automation project from climbing the same learning curve. Although this method may mean retraining or adding people, the payback in smooth implementations, speed, and minimized total project cost will be worth the trouble.

Knowledge and expertise in areas such as computer database design, communications networks, operating systems, languages, systems design, chemistry, laboratory instrumentation, robotics, and general systems theory, plus the ability to plan an automation project and then manage the implementation, are fundamental skills in "laboratory systems engineering." The people doing this work should evaluate the entire laboratory and plan a system that will permit growth and integration rather than provide a patchwork of incompatible solutions. These areas can be addressed by well-designed graduate programs that would substantially benefit the field.

Part of your implementation effort should concern people in the laboratory. Do they understand what is being done and why? Are they part of the process in making decisions about automation? Hardware and software choices are only part of a successful implementation. If people fail to use the equipment or use it ineffectively, you will not realize the benefits that made the project attractive. Education can go a long way in training people to help make you successful.

Although it is hard to avoid coming in contact with computers, some individuals are reluctant to work with them. Reasons for this reluctance vary. Some people may not understand the impact of the computer on their jobs; they may lack good typing skills; or they may be concerned about how to use the system, how it will fit into their routine, and what will happen if they make mistakes. Most of these concerns can be put to rest by providing a good in-house training program that familiarizes people with the technology and its impact on them. One company set up a formal training program on their sampling tracking system that allowed people to practice, learn, and make mistakes on a dummy database. This

approach built the necessary confidence and familiarity that encourage people to be successful. During these sessions, you will very likely get comments about things people like or dislike about the system, and these can be used to improve the system before it goes into production.

### Terminology

It has been said that one purpose of an undergraduate education is to teach a new language: that of the specialty. Language assumes that an agreed-upon set of terms and definitions exists. Computer science and chemistry have met that requirement for a language; lab automation has not. We speak the same words (instrument interfacing, LIMS, networks, sample tracking, etc.), but with different frames of reference, and thus we attach different meanings to the words.

Take the acronym LIMS, for laboratory information management system. What does it mean to you? I've listened to, and participated in, discussions of a LIMS system only to discover that each person had a different definition of what was meant. To some people it means a sample tracking system; to others it means everything concerning data and information handling in the laboratory, including capture, analysis, storage, management, documentation, and eventual distribution. The words sound like they should mean something, but the definition is highly subjective.

Another ambiguous term is *instrument interfacing*. Before microprocessors became part of what is being sold as an instrument today, instrument interfacing usually meant connecting an analog signal from the instrument to a computer system and digitizing it. Now that processors are being sold as part of the package, much of what comes under the heading of instrument interfacing is really a problem in communications. Instruments that provide serial ASCII, IEEE-488, or BCD (binary-coded decimal) input and output require something—usually a microprocessor—to digitize the analog signal and then format it for output.

The point of this is that you should define your interpretation of the terms before you use them and make sure that your audience (e.g., the budget review committee or the vendor) understands your requirements. The fact that you are asking for a LIMS system, and that three or four vendors have them, doesn't mean you have that many choices of comparable systems. The capabilities of various LIMS systems differ among vendors, and the list of features varies widely. Describe your needs according to the functions you want performed and the problems you want solved. Shopping for a LIMS sys-

# WHO ARE WE HOOKED ON?



**The Vector/One family of PC based computer workstations are successfully interfaced to over 200 mass spectrometers. One is right for your application.**

**TEKNAVANT**  
ADDED POTENTIAL FOR ANALYTICAL INSTRUMENTS

1684 LILBURN PARK ROAD • ST. LOUIS, MO 63146 • (314)934-0500 • (800)523-2321

**See us at PITTCON  
Booth 1245, 1247**

CIRCLE 159 ON READER SERVICE CARD

**Just published . . . latest research results from leading scientists in the hot new area of superconductivity!**

# Chemistry of HIGH-TEMPERATURE SUPERCONDUCTORS

## **Looks at current progress and understanding from the point of view of solid-state chemistry . . .**

Hot off the presses! This new book presents the most current information in developing technologies for commercial uses of high-temperature superconductivity. Although this area is multidisciplinary, chemistry plays a key role throughout . . . from materials preparation to processing for small- and large-scale operations. This book presents the chemistry necessary to further the research in this exciting area.

## **Information is presented in the following major areas:**

- Theory • Materials Preparation and Characterization • Structure-Property Relationships • Surfaces and Interfaces • Processing and Fabrication • Applications • Research Needs and Opportunities

## **The editors are . . .**

- David L. Nelson, Office of Naval Research • M. Stanley Whittingham, Schlumberger-Doll Research • Thomas F. George, State University of New York at Buffalo

## **Plus more than 100 contributors from major research groups worldwide!**

ACS Symposium Series No. 351 Approx. 400 pages (28 chapters)  
Clothbound (1987) **US & Canada \$64.95, Export \$77.95**

## **Order today . . . and put these critical new findings to work for you!**

The ACS Guarantee: If you are not satisfied with your book for any reason, return it within 15 days for a full refund or charge card credit.

**To charge your book by phone, call TOLL FREE (800) 227-5558.**

**ORDER FORM** ☐ Yes!  
Please rush me  
Chemistry of  
High-Temperature  
Superconductors!  
\$64.95 US & Can. \$77.95 Export

Qty: \_\_\_\_\_ Total: \$ \_\_\_\_\_  
☐ Payment enclosed (make checks payable to American Chemical Society).

☐ Purchase order enclosed. P.O. # \_\_\_\_\_  
Charge my ☐ MasterCard/VISA ☐ American Express  
☐ Diners Club/Carte Blanche ☐ Access/Barclaycard

Account # \_\_\_\_\_ Expires \_\_\_\_\_

Interbank # \_\_\_\_\_ Name of Cardholder \_\_\_\_\_

Signature \_\_\_\_\_

Ship books to: \_\_\_\_\_

Name \_\_\_\_\_

Address \_\_\_\_\_

City, State, Zip \_\_\_\_\_

ORDERS FROM INDIVIDUALS MUST BE PREPAID. Prepaid and credit card orders receive free postage and handling. Prices subject to change without notice. Please allow 4-6 weeks for delivery. Foreign payment must be made in US currency by international money order, UNESCO coupons, or US bank draft. Order through your local bookseller or directly from ACS.

To charge your books by phone, CALL TOLL FREE (800) 227-5558. Mail this order form with your payment or purchase order to: American Chemical Society, Distribution Office Dept. 30, P.O. Box 57136, West End Station, Washington, DC 20037.

30

tem, or something to "connect instrument to computer," presupposes that you have fully identified the solution to the problem you are trying to solve. You also bias the vendor's response in a particular direction, which may not have anything to do with the real problem. By presenting vendors with your problem rather than your perceived need, you may discover possibilities that previously had not occurred to you.

## **Communications**

Communications are essential for the proper implementation of a laboratory automation project. Of all the fundamental technical requirements, communications suffer the most from a lack of standardization. Basically, the system requires communication both from the instrument to the data system and between data systems.

Generally the producers of instrumentation for chemical analysis and data stations have adopted the RS232 serial ASCII port as a common means of transmitting data to computer systems. When you ask if a particular instrument or data system can be connected to a larger computer system, the typical response is "Sure, we have an RS232 connection." But have they really told you anything?

RS232 refers to a recommended standard (the RS part) for the transmission of characters (each having a unique 7- or 8-bit code that indicates which character is being sent) between two devices such as a computer and a terminal or printer. The recommended standard specifies the functions of wiring connections that are used to make the physical connection and the voltage levels that are used to designate the logical "0" and "1" that represent character code.

If the recommended standard is followed, you can be reasonably assured that a character sent from one device will be received by a second device, that is, unless an error occurs on the way. Error handling is the beginning of the problem, and it is not addressed by the RS232 specification.

Let us look at the problem we are really trying to solve. We have two devices. Assume that one is an instrument system with a microprocessor in it that will take the digitized values from the experiment, analyze them, and cause them and the results to be sent to a computer via the RS232 port. The second device is the computer system, which can be programmed to accept the data. The data and the result need to be transmitted. Together they constitute a message that in turn is made up of individual characters. If the message is to be sent and received correctly, several things must happen.

First, we have to understand the for-



mat of the message—which characters are the data and which constitute the result—so that the message can be interpreted correctly. We also have to understand how to recognize the beginning and the end of the message. Next, we must be able to determine if the message has been received correctly and what action can be taken if it has, such as letting the instrument know so that it can go on to the next task, or, if it hasn't, telling the instrument to re-send the message. These steps taken together describe the message protocol. None of this procedure is covered by the RS232 recommended standard. The implementation of all or part (or none) of this protocol is at the discretion of the vendor. There is no standard for a data transfer protocol in the field of chemical instrumentation. Each device, from each vendor, must be understood in terms of which capabilities it can or cannot support, and the computer system has to be programmed for the capabilities that are of the most interest to you.

The range of capabilities varies widely with different vendors. Some devices simply spew out the data without any protocol at all, and if an error occurs the data are lost. Presumably the error will be sufficiently drastic that you will recognize that it has occurred and not continue with faulty data. How do you know that the data you are working with accurately represent the data that were sent? Many instruments use the same port for a computer connection and a printer connection, and this frequently assumes that the receiver is always ready to take the characters as they are sent. If the computer system is busy doing something else, improperly designed software can cause the data to be lost.

What is needed is an industry-supported standard for a data transfer protocol. Serial ASCII transfer provides a low-cost approach to communications. The adoption of such a standard protocol would make the technique more effective. In addition, it would be easier and less costly to develop instrument computer systems and software because only one protocol would have to be understood, and its support could be included as part of a standard instrument software library. (This is part of the reason for the success of the IEEE-488 standard.)

#### Legal issues

Legal issues pertaining to the electronic laboratory notebook present serious obstacles to implementing computer systems in the laboratory. True electronic laboratory notebooks do not exist. The limiting factor is the ability of a computer-based system to stand up in a court of law. Although much of the technology exists to put something to-

gether that resembles a notebook, nothing to date satisfies the legal requirements (surviving a court test). We are in a Catch-22 situation: We must test the technology in court to see if it is legally acceptable, but vendors are reluctant to invest the large sums needed to fully develop a system unless they can be sure that it is marketable (which implies the survival of a court test). We need to find a way out of the bind.

The benefits of a true computer-based lab notebook are huge. Have you ever been sure that certain work has been done but that no one knew where to find the data? If the results are really important, you may find yourself redoing the work, and that doubles the money spent to get specific information and data. Lab notebooks represent a large database, assembled at a high cost, frequently with little value—if you can't find it or you don't know it exists, it has no value. A searchable database, substituting for current lab notebooks, makes that collection much more valuable, particularly if it could help support your research or if new analytical techniques become available to treat that data.

#### Conclusions

Although a number of issues must be taken into account if this technology is to be introduced and implemented successfully, the payback is clearly visible. Laboratory automation is not based on a single technology, but rather on several technologies that can be focused on different parts of a lab operation. Some of those approaches are mature, others are evolving, and others are still experimental. Thus you should not attempt to implement a system in one grand stroke, but rather consider the options and plan a stepwise implementation.



*Joseph G. Liscouski did his undergraduate work in chemistry at Montclair State College and his graduate work in computer science at Farleigh Dickinson University. He is a marketing consultant with Digital Equipment Corp., where he developed the Integrated Laboratory Automation program and the ILA Standards program and is responsible for the Computer Integrated Research program. He is one of the founders of the Lab Automation subdivision of the ACS Division of Computers in Chemistry.*

**NEW!**

**The Metal-Free  
Ion Chromatography  
System from Wescan**

**Representing State-of-the-Art  
Performance in Single  
Column Ion Chromatography**

**INERT  
RELIABLE  
COMPLETE  
VERSATILE  
SENSITIVE  
AFFORDABLE**

**Inquire for free  
technical literature!**

**WESCAN INSTRUMENTS  
2051 Waukegan Road  
Deerfield, IL 60015  
(312) 392-2670**

CIRCLE 175 ON READER SERVICE CARD

# LABORATORY SERVICE CENTER

4-Aminoantipyrine • Cesium Chloride • 3,4-Dihydroxybenzoic Acid  
p-Dimethoxybenzene • Dimethyl Adipate • p-Dimethylaminobenzaldehyde  
Dimethylchloroacetal • 3,5-Dinitrobenzoic Acid • Diphenylcarbazide  
a-Furildioxime • 4-Heptanone • 2-Hydroxy-iso-butyric Acid • INT  
pH Indicators • Levulinic Acid • Magnesium Disodium EDTA • Maltose  
Melibiose • Methyl Acetate • Neocuproine & HCl • Orcinol • Oxamide  
Pyruvic Acid & Na Salt • Succinic Acid & DiNa Salt • Syringic Acid  
p-Toluenesulfonic Acid • o-Vanillin • Veratraldehyde • Veratrole

Write for our Products List of over 3,000 chemicals

Tel: 516-273-0900 • TOLL FREE: 800-645-5566 • Telefax: 516-273-0858 • Telex: 497-4275

**EASTERN CHEMICAL**  
A Division of UNITED-GUARDIAN, INC.

P. O. Box 2500  
DEPT AC  
SMITHTOWN, N. Y. 11787

**Laboratory Service Center** (Equipment, Materials, Services, Instruments for Leasing). Maximum space — 4 inches per advertisement. Column width, 2-3/16"; two column width, 4-9/16". Artwork accepted. No combination of directory rates with ROP advertising. Rates based on number of inches used within 12 months from first date of first insertion. Per inch: 1" — \$148; 12" — \$146; 24" — \$143; 36" — \$138; 48" — \$134.

CALL OR WRITE JANE GATENBY

**ANALYTICAL CHEMISTRY**  
500 Post Road East  
P.O. Box 231  
Westport, CT 06880  
203-226-7131

# CLASSIFIED HELP WANTED

Chemist, to determine needs for specialized printing inks involving polymers and develop formulae for such inks. Test various ink properties. Develop acrylic polymers for high-speed lithographic printing inks and determine both the physical and chemical characteristics of polymers required for these inks. M.Sc. in Chemistry required. Education must include at least 6 credit hours in research involving the synthesis of acrylic and methacrylic copolymers and their evaluation in IPN systems. Salary \$26,000.00 per year, 40-hr. week. Send resumes and transcripts to 7310 Woodward Avenue, Room 415, Detroit, Michigan 48202. Ref. No. 71887. This ad paid by employer.

## FREE DATA, FAST

To quickly amass data on all of the products you need, consult the Lab Data Service section on our *Analytical Chemistry* reader reply card insert.

## Light-Activated Pesticides

The pressures on world agricultural productivity caused by pests is reaching a critical stage. At the same time, there is an increasing concern about pesticide use.

Researchers are hard pressed to meet the future demand for safe, effective pesticides. A promising area of pesticide research is in the catalytic action of light on certain chemicals in biological systems. This book explores the rapid exploitation of this mechanism over the past two decades and charts the possible courses this research will take in the future. Primary consideration has been given to insecticides, followed by herbicides and fungicides. This volume focuses on four main areas of research and development • development of light as part of the toxicological action of pesticides • development of the various classes of light activated pesticides • underlying mechanisms of light activation • specific studies of applied areas of light activation. This work serves as a single source for anyone interested in obtaining current knowledge of light-activated pesticides. Specialists in the fields of photochemistry, photobiology, agriculture, chemical ecology, or plant pathology will find this book a valuable addition to the literature.

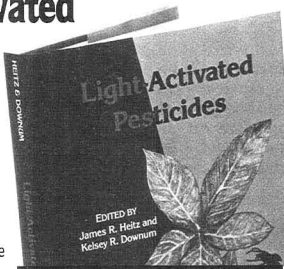
James R. Heitz, Kelsey R. Downum *Editors*.

ACS Symposium Series No. 339  
LC 87-1342 ISBN 0-8412-1026-8

355 pages (1987) Clothbound  
US & Canada \$69.95 Export \$83.95

Order from: American Chemical Society, Distribution Office Dept. 56  
1155 Sixteenth St., N.W., Washington, DC 20036

or CALL TOLL FREE **800-227-5558** and use your credit card!



## Solving Hazardous Waste Problems

Society's concern about pollutants in the environment requires pollution control and cleanup of hazardous waste sites.

This book publicizes recent advances in the methodology of cleanup of sites contaminated with polychlorinated dibenzodioxins (PCDDs). The multidisciplinary nature of this work covers the detection of the contaminant in the environment, its toxicology to living organisms, risk assessment through exposure routes, and elements in management of risk. The editors have divided the 31 chapters into four major categories • Distribution and Toxicology • Risk Assessment: Exposure • Risk Assessment: Evaluation • Risk Assessment: Technology. This book serves to define a very complex problem from many points of view. The examples of dioxin cleanup issues and procedures will provide chemists, engineers, health scientists, regulators, lawyers, business people, and other concerned individuals with a methodology applicable to many hazardous chemicals.

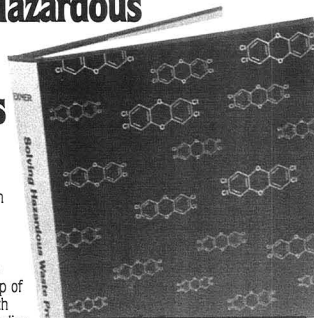
Jurgen H. Exner, *Editor*

ACS Symposium Series No. 338  
LC 87-1389 ISBN 0-8412-1025-X

405 pages (1987) Clothbound  
US & Canada \$79.95 Export \$95.95

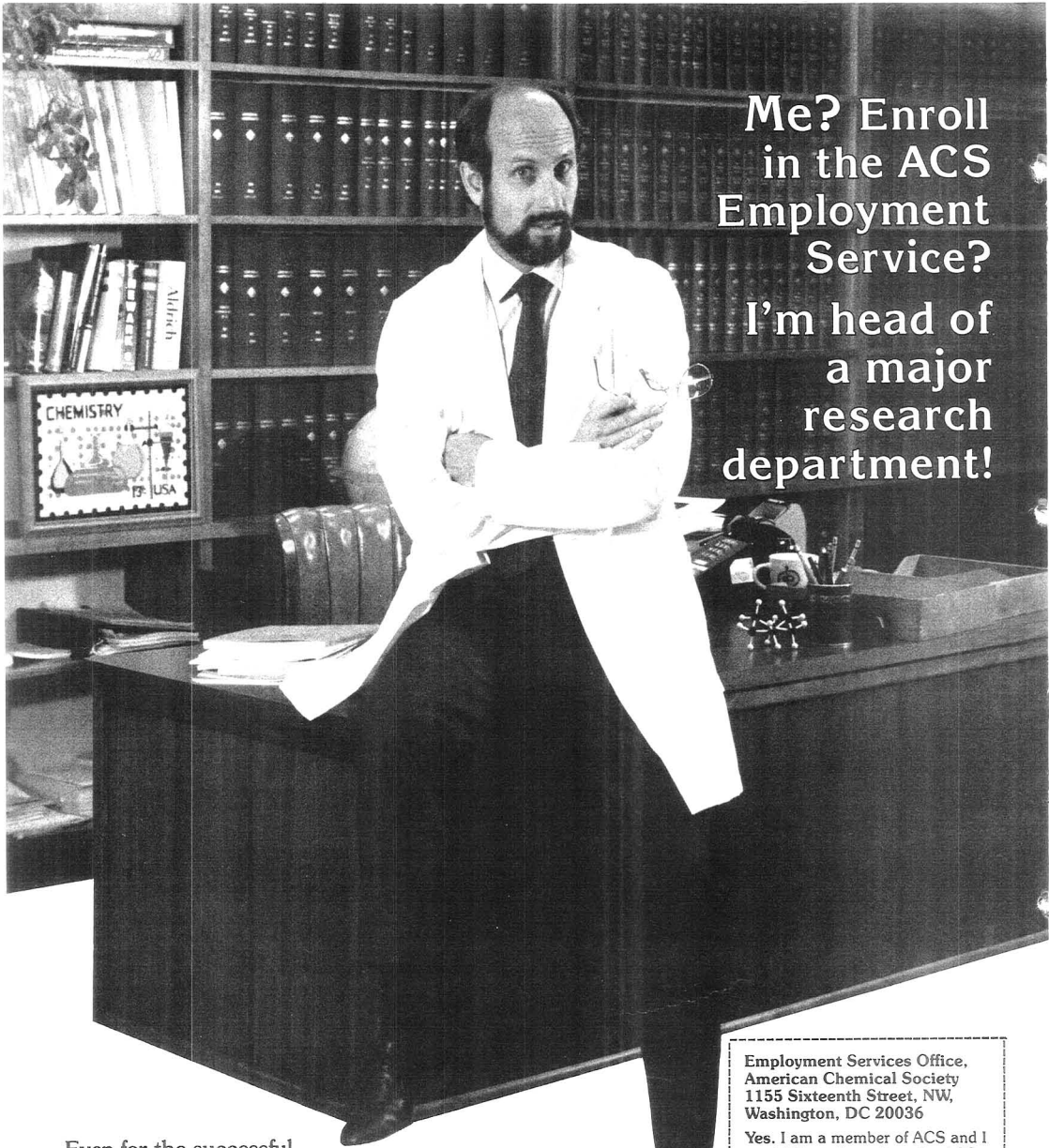
Order from: American Chemical Society Distribution Office Dept. 55  
1155 Sixteenth St., N.W., Washington, DC 20036

or CALL TOLL FREE **800-227-5558** and use your credit card!



# INDEX TO ADVERTISERS IN THIS ISSUE

CIRCLE INQUIRY NO.	ADVERTISERS	PAGE NO.	CIRCLE INQUIRY NO.	ADVERTISERS	PAGE NO.
18	Baird Corporation Design 2 Inc.	81A	177	*Wheaton Instruments The Wheaton Agency	80A
20	*Brinkmann Instruments, Inc. Lavey/Wolff/Swift Inc.	62A	<p>Directory section, see page 100A. Classified advertising section, see page 100A. * See ad in ACS Laboratory Guide. Advertising Management for the American Chemical Society Publications</p>		
50, 51	Finnigan MAT Corporation Lena Chow, Inc.	89A	<p><b>CENTCOM, LTD</b> President Thomas N. J. Koerwer</p> <p>Executive Vice President Senior Vice President James A. Byrne Benjamin W. Jones</p> <p>Clay S. Holden, Vice President Robert L. Voepel, Vice President Joseph P. Stenza, Production Director</p> <p>500 Post Road East P.O. Box 231 Westport, Connecticut 06880 (Area Code 203) 226-7131 Telex No. 643310</p>		
64	*Hewlett-Packard Company Pinné, Garvin, Herbers & Hock, Inc.	OBC	<p>ADVERTISING SALES MANAGER <b>Bruce E. Poorman</b></p>		
75	*Instruments SA, Inc. Kathy Wyatt & Associates	65A	<p>ADVERTISING PRODUCTION MANAGER Jane F. Gatenby</p>		
96	*Matheson Gas Products Kenyon Hoag Associates	69A	<p>SALES REPRESENTATIVES</p> <p>Philadelphia, PA... Patricia O'Donnell, CENTCOM, LTD., GSB Building, Suite 725, 1 Belmont Avenue, Bala Cynwyd, Pa. 19004. Telephone: 215-667-9666</p> <p>New York, NY... Dean A. Baldwin, CENTCOM, LTD., 60 East 42nd St., New York, N.Y. 10165. Telephone: 212-972-9660</p> <p>Westport, CT... Edward M. Black, CENTCOM, LTD., 500 Post Road East, P.O. Box 231, Westport, Ct. 06880. Telephone: 203-226-7131, Telex 643310</p> <p>Cleveland, OH... Bruce E. Poorman, John C. Guyot, CENTCOM, LTD., 325 Front St., Suite 2, Berea, Ohio 44017. Telephone: 216-234-1333</p> <p>Chicago, IL... Michael J. Pak, CENTCOM, LTD., 540 Frontage Rd., North- field, Ill. 60093. Telephone: 312-441-6383</p> <p>Houston, TX... Michael J. Pak, CENTCOM, LTD., Telephone: 312-441-6383</p> <p>San Francisco, CA... Paul M. Butts, CENTCOM, LTD., Suite 1070, 2672 Bayshore Frontage Road, Mountain View, CA 94043. Telephone: 415- 969-4604</p> <p>Los Angeles, CA... Clay S. Holden, CENTCOM, LTD., Newton Pacific Center, 3142 Pacific Coast Highway, Suite 200, Torrance, CA 90505. Telephone: 213-325-1903</p> <p>Boston, MA... Edward M. Black, CENTCOM, LTD., Telephone: 203-226- 7131</p> <p>Atlanta, GA... Edward M. Black, CENTCOM, LTD., Telephone: 203-226- 7131</p> <p>Denver, CO... Paul M. Butts, CENTCOM, LTD., Telephone: 415-969-4604</p> <p>United Kingdom Reading, England... Malcolm Thiele, Technomedia Ltd., Wood Cottage, Shurlock Row, Reading RG10 0QE, Berkshire, England. Telephone: 073-434-3302, Telex #648800</p> <p>Lancashire, England... Technomedia Ltd., c/o Meconomics Ltd., Me- conomics House, 31 Old Street, Ashton Under Lyne, Lancashire, En- gland. Telephone: 061-308-3025</p> <p>Continental Europe... Andre Jamar, International Communications, Inc., Rue Mallard 1, 4800 Verviers, Belgium. Telephone: (087) 22-53-85, Telex #49263</p> <p>Tokyo, Japan... Naoko Hatakeyama, International Media Representatives Ltd., 2-29 Toranomon, 1-Chome Minato-ku Tokyo 105 Japan. Tele- phone: 502-0656, Telex #22633</p>		
94	*Mettler Instrument Corporation McKinney, Inc.	IFC			
120, 121	*Ohaus Scale Corporation Techmarketing, Inc.	67A			
123	*O.I. Corporation	72A			
127	Pharmacia LKB Biotechnology AB Media Services	74A			
125	The Pittsburgh Conference	71A			
152, 153	*Shimadzu Scientific Instruments, Inc. Techmarketing, Inc.	77A			
150	*Swagelok Company Falls Advertising Company	70A			
159	*Teknivent	97A			
156	Thermo Jarrell Ash Corporation Noon, Inc.	61A			
170	*Varian Instrument Group Moran, Lanig & Duncan Advertising	79A			
175	*Wescan Instruments Chromad	99A			



**Me? Enroll  
in the ACS  
Employment  
Service?  
I'm head of  
a major  
research  
department!**

Even for the successful chemist or scientist in an allied field, sometimes the best way to get ahead is to make a change.

The ACS Employment Service offers the opportunity to investigate the possibilities discreetly—and at very low cost.

Our Employment Service is free to all ACS members. If you request confidentiality from current employers or other designated organizations there is a nominal charge.

For more information write, use coupon, or CALL TOLL FREE 800-227-5558

Employment Services Office,  
American Chemical Society  
1155 Sixteenth Street, NW,  
Washington, DC 20036

Yes, I am a member of ACS and I  
would like to learn how the ACS  
Employment Service can help me  
advance my career.

Name (please print) \_\_\_\_\_

Membership # \_\_\_\_\_

Address \_\_\_\_\_  
\_\_\_\_\_

City \_\_\_\_\_

State \_\_\_\_\_

ZIP \_\_\_\_\_

EDITOR: GEORGE H. MORRISON

ASSOCIATE EDITORS: Klaus Blemann,  
Georges Guiochon, Fred E. Lytle,  
Robert A. Osteryoung, John A. Smith,  
Edward S. Yeung

**Editorial Headquarters**

1155 Sixteenth St., N.W.  
Washington, D.C. 20036  
Phone: 202-872-4570  
Teletype: 710-8220 151

*Managing Editor:* Sharon G. Boots

*Associate Editors:* Donald W. Cunningham,  
Rani A. George, Louise Voress

*Assistant Editors:* Grace K. Lee,  
Mary D. Warner

*Production Manager:* Leroy L. Corcoran

*Art Director:* Alan Kahan

*Staff Artist:* Amy A. Meyer

*Production Editor:* Elizabeth E. Wood

*Circulation:* Cynthia G. Smith

*Editorial Assistant, LabGuide:* Joanne Mullican

**Journals Dept., Columbus, Ohio**

*Associate Head:* Marianne Brogan

*Assistant Manager:* Joseph E. Yurvati

*Associate Editor:* Rodney L. Temos

**Advisory Board:** Harry V. Drushel, Michael S.  
Epstein, Larry P. Faulkner, Peter R. Griffiths,  
Nobuhiko Ishibashi, Peter C. Jurs, Mary A. Kai-  
ser, David L. Nelson, Lawrence A. Pachla, Erno  
Pungor, Dennis Schuetzle, Ralph E. Sturgeon,  
Nicholas Winograd, Mary A. Wirth,  
Andrew T. Zander

**Instrumentation Advisory Panel:** Howard G.  
Barth, Richard F. Browner, James B. Callis,  
Bruce Chase, L. J. Cline Love, Joel M. Harris,  
Ronald E. Majors, Linda B. McGown, R. Mark  
Wightman

**The Analytical Approach Advisory Panel:** Ed-  
ward C. Dunlop, Robert A. Hofstadter, Wilbur D.  
Shults

*Published by the*  
**AMERICAN CHEMICAL SOCIETY**  
1155 16th Street, N.W.  
Washington, D.C. 20036

**Books and Journals Division**

*Director:* D. H. Michael Bowen

*Journals:* Charles R. Bertsch

*Production:* C. Michael Phillippe

*Research and Development:* Lorrin R. Garson

Manuscript requirements are published in the  
January 1, 1988 issue, page 91. Manuscripts  
for publication (4 copies) should be submitted  
to ANALYTICAL CHEMISTRY at the ACS Washing-  
ton address.

The American Chemical Society and its editors  
assume no responsibility for the statements  
and opinions advanced by contributors. Views  
expressed in the editorials are those of the  
editors and do not necessarily represent the  
official position of the American Chemical  
Society.

Anderson, J. L., 156, 163  
Ashmore, R. W., 115

Baer, C. D., 188  
Baldwin, R. P., 151  
Bellama, J. M., 142  
Bidlemyer, B. A., 192  
Breninkmeijer, C. A. M., 191

Cantwell, F. F., 181  
Chaniotakis, N. A., 185  
Chasser, A. M., 185  
Corso, N. P., 173

Djordjevic, N. M., 124  
Durst, R. A., 142

Fabre, H., 136  
Fosdick, L. E., 156, 163  
Freiser, H., 180

Goyal, S. S., 175  
Groves, J. T., 185

Halverson, J. M., 115  
Huffaker, R. C., 175

Kallury, K. M. R., 169  
Kamikado, H., 147  
Kannuck, R. M., 142  
Kearle, P., 98  
Kenndler, E., 120  
Kok, W. T., 136  
Krull, U. J., 169  
Kryger, L., 151

Laub, R. J., 124

Lawrence, A. H., 104  
Lin, A. J., 115  
Linton, R. W., 110  
Liu, T.-Y., 173

Matsubara, H., 147  
Matsumoto, K., 147  
Meyerhoff, M. E., 185  
Morales, A., 98  
Musselman, I. H., 110

Neudorfl, P., 104

Osajima, Y., 147  
Osteryoung, J., 131

Rains, D. W., 175  
Reich, G., 120  
Ridder, W. E., 115  
Robbat, A., Jr., 173

Santasia, C. T., 192  
Simons, D. S., 110  
Smyth, M. H., 115  
Stojek, Z., 131  
Stone, N. J., 188  
Sunder, J., 98  
Sweigart, D. A., 188

Theoharides, A. D., 115  
Thompson, M., 169  
Thomsen, K. N., 151  
Tran, C. D., 182

Warren, F. V., Jr., 192

Zhou, Z. M., 115

# Kinetic Modeling of Fast Atom Bombardment Spectra of Glycerol-Diethanolamine Mixtures

Jan Sunner,<sup>1</sup> Angelina Morales, and Paul Kebarle\*

Department of Chemistry, University of Alberta, Edmonton, Alberta, Canada T6G 2G2

The intensities of molecular ions, fragment ions, and cluster ions in fast atom bombardment (FAB) mass spectra of diethanolamine (DEA) solutions in glycerol were measured at different DEA concentrations, from neat glycerol to neat DEA. The decays of the intensities of protonated glycerol, of glycerol fragment ions, and of the larger glycerol cluster ions were nearly exponential with increasing DEA concentration. However, the decay was slowest for the fragment ions and fastest for the glycerol cluster ions. Other patterns were observed for the DEA ions and for the mixed cluster ions. A gas-phase kinetic scheme based on the "gas collision model" (GCM) was shown to successfully reproduce the experimental results. A distribution of residence times for the ions in the "gas" is derived. Highly excited molecular ions spend a shorter time in the high density "gas" than do less excited ions. The origin of "noise" ions is discussed.

Whereas the initial collision cascade, through momentum transfer, likely is the main direct cause of ion desorption in atomic secondary ion mass spectrometry (SIMS) (1), other processes are believed to play a major role in determining the desorption spectrum in molecular SIMS and in particular in liquid SIMS or fast atom bombardment (FAB) (2). Many of these processes are thought to occur in a surface environment which is highly disturbed by the collision cascade. This surface state has frequently been referred to as the "selvedge" (2, 3). The physical picture of this surface state or selvedge has, however, remained obscure (2, 4).

The idea that the intermediate surface state in SIMS may be best described as a gas dates back to 1978 (3, 5). Rabalais et al. (6) studied SIMS spectra of molecular solids like water ice and frozen benzene. In the water ice spectra, they found very extensive clustering of water molecules around hydronium ions. They described the SIMS process as "... a transient thermal activation of a localized site ... followed by irreversible expansion to relieve the nonequilibrium situation." (5). Their idea of the "selvedge" was clearly rather close to that of a gas. For example, they suggested that frequent collisions and clustering reactions occur in the selvedge (5).

Michl et al. have investigated SIMS of frozen gases, like N<sub>2</sub>, NO, and O<sub>2</sub>. They have forwarded a "gas flow model" (7, 8). Within this model, Michl has given explanations for cluster formation (8) and the origin of ionization (7). In contrast to the view of Rabalais et al., Michl et al. do not consider (8) that three-body association reactions in the gas jet are responsible for the clustering that is observed.

Recently, Cooks et al. also explicitly described the selvedge in terms of a gas (2). They recognize cationization/anionization and electron transfer in the selvedge as sources of ions in addition to direct desorption of ions already present in the liquid (preformed ions).

In previous publications from this laboratory, we have shown that many spectral features of FAB can be explained on the basis of well-known gas phase ionic processes and their

energetics. The overriding importance of proton transfer reactions and relative gas phase basicities (GB) for the formation of protonated molecular ions in FAB was demonstrated by showing that it is the gas-phase basicity and not the liquid phase basicity that determines the direction of the proton transfer (9, 10). The fact that the total ion current did not increase with electrolyte (preformed ions) concentration (11) led to the conclusion that either extensive charge recombination precedes the ion/molecule chemistry or desorption of preformed ions is inefficient relative to desorption of ions formed in the collision cascade. Though possibly these observations may be given alternative interpretations, we have explained them by using a "gas collision model" (GCM) (11).

In the present paper, we present FAB spectra of solutions of diethanolamine (DEA) in glycerol, with compositions ranging from neat glycerol to neat DEA. In a kinetic study of the reaction mechanism in FAB, one has to vary the concentrations as it is not possible to vary the residence time independently. The results are modeled by using a kinetic scheme based on the GCM model. This model is briefly described. The relation between the present results and the idea that the FAB matrix undergoes a "phase explosion" into a gaseous state from deep into the metastable liquid region close to the "limit of absolute stability" or "spinodal" is also discussed. This "phase explosion" model of desorption is presented in a separate paper (12).

## EXPERIMENTAL SECTION

The FAB spectra were obtained on an MS9 equipped with a saddle field atom gun (13). The gun was operating with Xe gas, a discharge current of 1.0 mA, and a voltage of 8 kV. The angle between the atom beam and the ion exit path was 90°. The incidence angle on the Cu-tip FAB probe was 20°.

The chemicals were obtained commercially. Two microliters of the liquid solutions was applied to the probe tip with a syringe.

The kinetic calculations were performed on an IBM-PC using numerical integration of the rate equations.

## RESULTS AND DISCUSSION

(a) FAB Spectra of DEA/Glycerol Solutions Ranging from Neat Glycerol to Neat DEA. FAB spectra were recorded for diethanolamine (DEA) solutions in glycerol (GI) with 17 different concentrations of DEA. The main results are given in Figures 1-4. In part a of this section the experimental results will be briefly described, and in the next part (b) a more complete discussion of the GCM model will be given together with the results from the kinetic modeling of the FAB spectra. Part c deals with fragment and "noise" ions in FAB spectra, and part d has a short discussion of ions in solution.

In the concentration range below 10 mol %, the effect of DEA in glycerol on FAB spectra is similar to that of many other analytes with high gas-phase basicity (GB) (9). However, DEA was chosen for the present measurements because glycerol and DEA are completely miscible and both are used as FAB matrices. Thus, FAB spectra could be obtained over the whole concentration range up to the neat analyte. In the text below, "matrix" refers to glycerol and "analyte" refers to DEA.

Figure 1 shows the intensities of the molecular and major cluster ions in the DEA/glycerol spectra as a function of DEA

<sup>1</sup>Present address: Department of Chemistry, Montana State University, Bozeman, MT 59717.



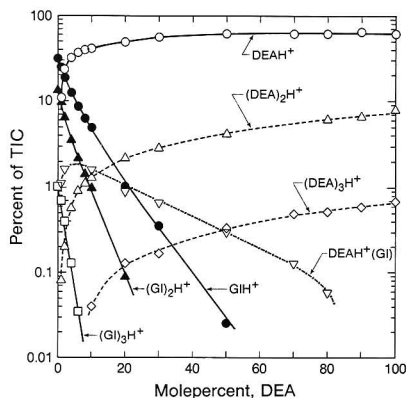


**Figure 1.** Intensities in percent of total ion current (TIC) of molecular ions and of cluster ions in FAB spectra of solutions of diethanolamine (DEA) in glycerol (GI). The intensities are plotted against the mole percent concentration of DEA.

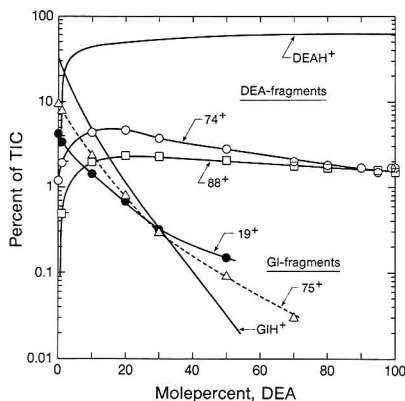


**Figure 2.** Intensities in percent of total ion current (TIC) of molecular ions and of four major fragment ions in FAB spectra of solutions of diethanolamine (DEA) in glycerol. The intensities are plotted against the mole percent concentration of analyte, DEA. (Small contributions from DEA to the intensities of the "glycerol fragments" 19<sup>+</sup> and 75<sup>+</sup> were estimated and subtracted prior to plotting the data.)

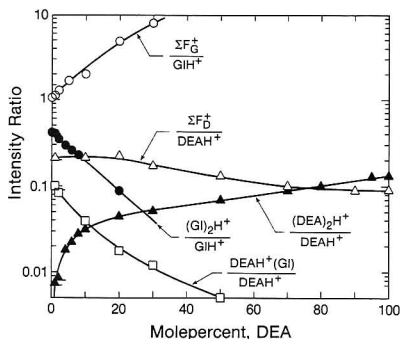


**Figure 3.** Figure shows fragment ratios, eq 3, for glycerol ( $F_0^+/GIH^+$ ) and for DEA ( $F_0^+/DEAH^+$ ) and dimer ratios, eq 2, for glycerol ( $(GI)_2H^+/GIH^+$ ) and for DEA ( $(DEA)_2H^+/DEAH^+$ ) and the  $DEAH^+(GI)/DEAH^+$  ratio for the mixed cluster vs mole percent DEA.

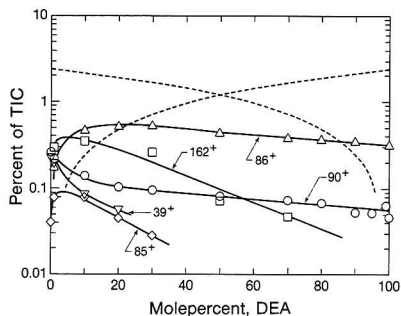


**Figure 4.** Intensities in percent of total ion current (TIC) of representative "chemical noise" ions in FAB spectra of solutions of diethanolamine (DEA) in glycerol. The intensities are plotted against the mole percent concentration of DEA. The intensity/concentration profiles for the noise ions give information on the "kinetic history" of the ions. Dashed lines show the linear dependence of intensity on analyte and matrix concentration, respectively, that is expected in a direct desorption mechanism without ion/molecule reactions.

concentration. It is seen that the concentration dependence is quite regular. The DEA peaks increase very rapidly as the DEA concentration increases from zero whereas the glycerol peaks decrease. Thus, already at ca. 2 mol %, the analyte peaks are about as intense as the matrix peaks. This observation is in accordance with the high preference observed earlier (9) for high GB analytes ( $GB(DEA) = 220$  kcal/mol) over a matrix with a lower GB ( $GB(GI) = 196$  kcal/mol). This preference for the high GB analyte was explained (9) as due to proton transfer mainly from protonated glycerol, reaction 1. The ions in eq 1 may be bare or they may be solvated by one or more matrix molecules.



In the semilogarithmic plot in Figure 1, the intensities of the  $(GI)_nH^+$  clusters and the  $GIH^+$  ion are seen to closely follow straight lines. This means that their decays are approximately exponential. It is also seen in the figure that the intensity of the dimer,  $(GI)_2H^+$ , decreases more rapidly than the intensity of the matrix molecular ion,  $GIH^+$ . The decrease is even more rapid for the trimer,  $(GI)_3H^+$ . The more rapid attenuation of the intensity of the dimer than of the molecular matrix ion was observed earlier also when electrolytes were added to the matrix (11).

The dimer (to monomer) ratios

$$\text{dimer ratio} = \frac{\text{intensity of dimer ion}}{\text{intensity of molecular ion}} \quad (2)$$

for the matrix and for the analyte ions are plotted in Figure 3 as a function of analyte concentration. It is striking that the dimer ratios of the matrix and of the analyte behave so very differently. The dimer ratio for the matrix decays exponentially whereas the  $(DEA)_2H^+/DEAH^+$  ratio for the analyte increases with increasing analyte concentration! Finally, it can be seen in Figure 3 that the ratio for the mixed cluster  $DEAH^+(GI)/DEAH^+$  also decreases exponentially.

In addition to the molecular and the cluster ions, the FAB spectra also contain fragment ions. The intensities of two of the matrix fragment ions and of two of the analyte fragment ions are plotted in Figure 2. The molecular ions (see Figure 1) are also plotted in the figure for comparison purposes. It is seen that the intensities of the matrix fragments (19<sup>+</sup> and 75<sup>+</sup>) decrease nearly exponentially, but not quite as rapidly as the matrix molecular ion ( $GIH^+$ ). Thus, the exponential decay rate of the glycerol ions gradually increases in the

following order: fragments  $F_G^+ < GIH^+ < (GI)_2H^+ < (GI)_3H^+$ .

As a result of the slower decay of the  $F_G^+$ , the intensity of  $F_G^+$  increases relative to the intensity of  $GIH^+$  as the concentration of the analyte is increased; i.e. the fragment ratio given in eq 3 increases. See Figure 3. It can also be observed that the glycerol fragment 19+ decreases more slowly than the fragment 75+.

$$\text{fragment ratio} = \frac{\text{sum of intensities of main fragments}}{\text{intensity of molecular ion}} \quad (3)$$

We have assumed above that the ion 19+ ( $H_3O^+$ ) is due to glycerol and not to traces of water that could be present in the (hygroscopic) glycerol. The neglect of  $H_2O$  as a precursor to the observed  $H_3O^+$  is justified by our previous observations that the protonated molecular ions of analytes present in trace amounts (water in the present case) in a matrix of higher gas-phase basicity (glycerol) are completely suppressed (9, 10).

The analytical fragment ions 74+ and 88+ are seen to decrease relative to the analyte molecular ion,  $DEAH^+$ , in Figure 2. Thus, for the analyte, the fragment ratio given by eq 3 decreases; see Figure 3. This behavior contrasts with the increase observed above for the fragment ratio of the matrix ions; see Figure 3.

Most of the trends outlined above can be explained to be consequences of the ion/molecule chemistry and of the desorption process as discussed in part b of this section.

**(b) Kinetic Model Calculation of the FAB Spectra of DEA/Gl Solutions Based on the GCM Model.** In this section we will show how it is possible to reproduce many of the observations described in the previous section, using a kinetic scheme based on the gas collision model, GCM. Although the model has been described previously (11), a brief outline concentrating on those features that are of importance for the present work will be given here.

The fast bombarding atom causes a collision cascade (1) which ends with a thermal spike. Ions are formed out of neutral molecules in the energetic collisions in the cascade (7). Neutral radicals and energetic fragments are also formed in these collisions.

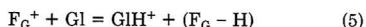
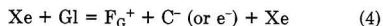
The central idea in the GCM model is that extensive ion/molecule chemistry occurs (9) during the FAB desorption process in what is best described as a gas (10). There are indeed both experimental and theoretical justifications for assuming that a FAB matrix undergoes a "phase explosion" to a gaseous state as a result of the thermal spike. This occurs when the liquid penetrates so deeply into the metastable region that the "limit of absolute stability" or the "spinodal" is approached. The idea of a "phase explosion" and its implications for FAB and the other desorption ionization techniques is presented in a separate publication (12). In this paper, the term "phase explosion" will refer to this very rapid transition of the matrix from a "liquid" to a "gas". We will in most cases keep the quotation marks around the word "gas" since it is not clear at what stage in the expansion process the majority of the various ion/molecule processes occur.

The exploding "gas" contains ions formed in the collision cascade. It may also contain ions that were already present in the liquid prior to the bombardment—Preformed ions. However, positive-negative ion recombination is very fast and extensive (11). As a result, only a small fraction, maybe 1 in 100 of the ions originally present in the liquid, survive the phase explosion and survive into the vacuum. Recombination of charges results in ion pairs, neutral molecules, or molecular fragments, depending on the nature of the ions that recombine.

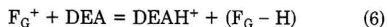
As the matrix gas escapes into the vacuum and while recombination still occurs, the ions undergo a number of collisions with different neutral molecules (9). These collisions

lead to ion/molecule reactions, most significantly proton transfer. Thus, ion/molecule reactions change the nature of the ions whereas recombination attenuates the total ion current. Those preformed ions that are unreactive in the "gas" and that survive the extensive recombination will be expressed in the FAB mass spectra. Desorption of ions preformed in the liquid is often referred to as the mechanism of "precursor ion formation".

The reactions leading to the protonated molecular ions in the glycerol matrix may be represented by the following simplified reaction sequence:



where Xe is the bombarding atom, Gl is glycerol,  $F_G^+$  is a glycerol fragment ion produced in the collision cascade,  $e^-$  is an electron, and  $C^-$  a negative ion produced in the collision cascade. The analyte is protonated by  $GIH^+$  (reaction 1) or by  $F_G^+$



The proton transfer reaction (eq 1) is fast only if the gas phase basicity (GB) of the analyte is higher than that of the matrix (9).

A consideration of the negative ions  $C^-$  or  $e^-$ , see eq 4, and their changing chemical nature with changing composition of the Gl-DEA solutions, will not be given. As a first approximation we assume that the positive-negative ion recombination coefficient is independent of the nature of the ions. This means that the changing nature of the negative ions will not have a direct effect on the positive ion abundances in the FAB spectra.

When modeling the ion/molecule reactions occurring during the desorption in FAB, one may for simplicity think of the FAB "gas" as being initially in a closed box at a given gas pressure. At time  $t = 0$  a number of ions  $A^+$  are produced. These react with neutral molecules B



with a rate constant  $k_7$ . The initial concentrations are  $[A^+] = [A^+]_0$  and  $[B] = [B]_0$ , respectively. The rate equation is

$$-d[A^+]/dt = k_7[A^+][B] \quad (8)$$

Since  $[B]_0 \gg [A^+]_0$  the reaction is pseudo first order. Integration of eq 8 at constant  $[B]$  gives the concentration of  $A^+$  as a function of time

$$[A^+] = [A^+]_0 \exp(-k_7 t [B]) \quad (9)$$

Assuming for the present that the ions in the box are sampled at a single (residence) time  $t = t_r$ , the observed current of  $A^+$ ,  $I(A^+)$ , is given by

$$I(A^+) = c[A^+]_{t=t_r} \quad (10)$$

where  $c$  is a constant connected to the sampling efficiency. It is seen from eq 9 that at a constant  $t$ ,  $[A^+]$  decreases exponentially with increasing concentration of B and thus due to eq 10 also  $I(A^+)$  will decrease exponentially with increasing  $[B]$ . In the present experiments,  $A^+$  is identified with the total glycerol-derived ions,  $\Sigma GIH^+$  (major fragments, molecular ions and clusters), and B with the DEA analyte molecules. The decay of the total glycerol-derived ions is due to the general reaction



The experimentally observed dependence of the total glycerol-derived ions ( $\Sigma GIH^+$ ) on the concentration of DEA is shown in Figure 5. The observed decay in the semilogarithmic

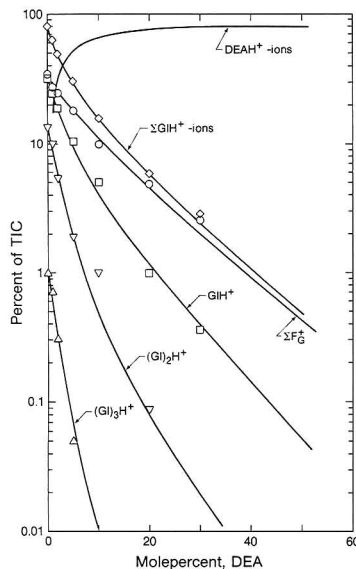


**Figure 5.** Result of kinetic model calculation on FAB spectra of solutions of DEA/glycerol solutions:  $\diamond$ , total glycerol ion intensities ( $\Sigma \text{GIH}^+$ );  $\circ$ , total intensity of major glycerol fragment ions ( $75^+$ ,  $57^+$ ,  $45^+$ ,  $31^+$ ,  $29^+$ , and  $19^+$ );  $\square$ , glycerol molecular ions;  $\nabla$ , glycerol dimer ions;  $\Delta$ , glycerol trimer ions. Intensities are given in percent of total ion current. Calculated intensities are shown by solid lines.

plot deviates from a straight line as the curvature is quite significant. This shows that the assumption of a single residence time for all ions ( $\Sigma \text{GIH}^+$ ) is unrealistic. We will instead assume that the ions have a residence time distribution,  $f(t)$

$$\int_{t=0}^{\infty} f(t) dt = 1 \quad (12)$$

The resulting current of  $\text{A}^+$ ,  $I(\text{A}^+)$ , is obtained from eq 8 by integrating over the time distribution, eq 12, and combining with eq 10, as shown in eq 13. The functional form of  $f(t)$

$$I(\text{A}^+) = c \int_{t=0}^{\infty} \{f(t)[\text{A}]_0 \exp(-k_7 t[\text{B}])\} dt \quad (13)$$

can be determined by comparing  $I(\text{A}^+)$  predicted by eq 13 to the experimentally observed decay of  $\Sigma \text{GIH}^+$  with  $[\text{DEA}]$ ; see Figure 5. The rate constant,  $k_7$  ( $=k_{11}$ ), was set to a typical diffusion-limited rate constant,  $k_{11} = 10 \times 10^9 \text{ M}^{-1} \text{ s}^{-1}$ , since a gas-phase ion/molecule rate constant is hardly applicable at molecular densities close to that of a liquid. The rate constant  $k_{11}$  can be expected to be a function both of density and of temperature. This had to be ignored in the present kinetic model. Different functional forms of  $f(t)$  were substituted into eq 13 in order to obtain a good fit to the experimental decay. An exponential time distribution did not give enough curvature of the  $\Sigma \text{GIH}^+$  curve in Figure 5. An inverse function of  $t$ , eq 14, was found to give the best fit. This distribution function  $f(t)$ , shown in Figure 6a, leads to the calculated result for the total glycerol ion current,  $\Sigma \text{GIH}^+$ , in Figure 5. The fit to the experimental points is seen to be very good.

$$f(t) = \frac{1}{at + b} \quad (14)$$

The exact functional form of  $f(t)$  can of course not be deduced from a fitting procedure like the one used here, in

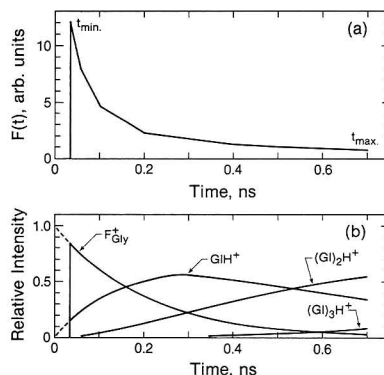


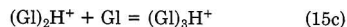
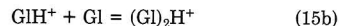
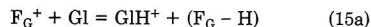
**Figure 6.** (a) Distribution of (effective) residence times for ions in FAB desorption on DEA/glycerol solutions obtained by modeling the intensity of the total glycerol ions ( $\text{GIH}^+$ ) in Figure 5. The segmented curve approximates  $f(t) = 1/(at + b)$ ;  $a = 1.818 \times 10^9 \text{ s}^{-1}$ ;  $b = 0.001818$ . (b) Time dependence of the FAB spectrum of neat glycerol, based on reactions 15.

particular considering the simplicity of the model. With this caution in mind, it is still of interest to discuss the  $f(t)$  curve. Equation 14 has the same form as the integrated rate law of a second-order reaction like the ion-ion recombination reaction. This is a very suggestive result since it is conceivable that  $f(t)$  is determined more by ion-ion recombination loss than by the time dependence for escape from the reaction region, i.e. the time dependence of the desorption process. This would mean that the residence time distribution for the neutrals decreases much more slowly with time than that for the ions. If this result is correct, it would justify the use of a constant concentration  $[\text{B}]$  in the integration of eq 8 to obtain eq 9.

When eq 14 is interpreted as an integrated rate law, the constant  $b$  equals  $1/[\text{A}^+]_0$ . At the scale of Figure 6a,  $[\text{A}^+]_0 = 45$ . The attenuation of the original ion concentration by a factor of ca. 20 (at the time of maximum intensity of protonated matrix) is reasonably close to an earlier estimate (11).

The minimum cutoff time ( $t_{\min}$ ) used in the time distribution function (Figure 6a), may be interpreted as related to the minimum time required for the gas expansion to occur. However, it should be observed that 19% of the total ion current, mostly low intensity "noise" ions (see part c of this section), was not included in the calculation. Presumably, the inclusion of such ions would extend the  $f(t)$  curve toward shorter times. The physical significance, if any, of the maximum cutoff time ( $t_{\max}$ ) is not clear.

The  $\Sigma \text{GIH}^+$  ions in eq 11 are detected as fragments, molecular ions, or cluster ions. It was seen in part a of this section (Figure 5) that the decay of the glycerol fragment ions was slower than the decay of the molecular ion and that the decays of the cluster ions were progressively faster. This behavior can be modeled. Two alternatives will be considered in the modeling. In the first model it is assumed that the reaction sequence



occurs in the "gas". This model may be called the "clustering model". The rate constants  $k_{15}$  used in this model were obtained from the condition that reactions 15, in the absence of analyte, should lead to the product distribution observed

**Table I. Reactions and Rate Constants Used in "Full" Kinetic Model for Glycerol/DEA Mixtures**

no. and reaction	$K/10^9$ $M^{-1} s^{-1}$
4a $Xe + Gl = F_G^+ + C^-$ (or $e^-$ ) + $Xe$	
4b $Xe + DEA = F_D^+ + C^-$ (or $e^-$ ) + $Xe$	
15a $F_G^+ + Gl = GIH^+ + (F_G - H)$	0.42
15b $GIH^+ + Gl = (GI)_2H^+$	0.175
15c $(GI)_2H^+ + Gl = (GI)_3H^+$	0.035
11a $\{F_G^+, GIH^+, (GI)_2H^+\} + DEA = F_D^+ + N_i$	1.3
11b $\{F_G^+, GIH^+, (GI)_2H^+\} + DEA = DEAH^+ + N_i$	8.7
27a $F_D^+ + DEA = DEAH^+ + N_i$	1.95
27b $DEAH^+ + DEA = (DEA)_2H^+$	0.054
27c $(DEA)_2H^+ + DEA = (DEA)_3H^+$	0.039
28 $DEAH^+ + Gl = DEAH^+(Gl)$	0.025
29 $DEAH^+(Gl) + Gl = DEAH^+(Gl)_2$	0.020
30 $DEAH^+(Gl) + DEA = (DEA)_2H^+ + Gl$	3.0
31 $DEAH^+(Gl)_n + DEA = DEAH^+(DEA)(Gl)_{n-1} + Gl$	3.0

in the FAB spectrum of neat glycerol. With the time distribution curve in Figure 6 the neat glycerol spectrum was reproduced with the following values of the (second order) rate constants (in  $10^9 M^{-1} s^{-1}$ ):  $k_{15a} = 0.42$ ,  $k_{15b} = 0.175$ , and  $k_{15c} = 0.035$ . (The values of these fitted rate constants depend on the value chosen for the rate constant for reaction 11.) The kinetic scheme, eq 15, predicts a time-dependent glycerol ion distribution in neat glycerol. This distribution is shown in Figure 6b.

In the presence of DEA, each of the ions in eq 15 also protonates DEA; see eq 11. The product distribution induced by this additional reaction was modeled by combining eq 11 with eq 15. Using the rate constants  $k_{15a}$  to  $k_{15c}$  obtained above from the neat glycerol spectrum and the residence time distribution of Figure 6a, one obtains by calculation the dependence on [DEA] of the intensities of the glycerol fragment, molecular, and cluster ions. These results are shown in Figure 5 together with the experimental points. It is seen that the calculation is very close to the experimental result.

The behavior of the curves for the DEA ions and for the mixed clusters (Figures 1 and 2) was studied with an expanded kinetic scheme. The residence time distribution of Figure 6a was again used. The chemical reactions and the rate constants used are given in Table I. The collision cascade was assumed to form fragment ions of both glycerol,  $F_G^+$ , and of DEA,  $F_D^+$  (fragments containing a nitrogen atom), with relative intensities given by the mole fractions of glycerol and DEA, respectively (eq 4a and 4b, Table I).

The glycerol spectrum was modeled as before, eq 15. Proton transfer from glycerol to DEA (eq 11a–b, Table I) was assumed to result in DEA fragment and DEA molecular ions. A sequence of reactions used for DEA (eq 27a–c, Table I) parallels those for glycerol (eq 15). The rate constants for eq 27 were obtained from the FAB spectrum of neat DEA in the same way as described above for glycerol. The formation of mixed clusters was also modeled (eq 28 and 29 in Table I). The reason that the rates for formation of mixed clusters are lower than for the corresponding reactions for DEA (eq 27a–c, Table I) can be sought in the lower bond energies in the mixed clusters; see below. The rate constant for ligand exchange (eq 30 and 31 in Table I) is determined by the decay of these clusters with increasing analyte concentration, Figure 1.

The results of the full kinetic scheme are shown in Figure 7. The main features of the experimental curves, shown in Figures 1 and 2, are reproduced quite well. Thus, the reaction scheme summarized in Table I, together with the time distribution in Figure 6b, leads to a satisfactory modeling of the complete experimental observations.

It should be noted that the ion/molecule reactions in Table I also would be observed in glycerol/DEA gas mixtures where

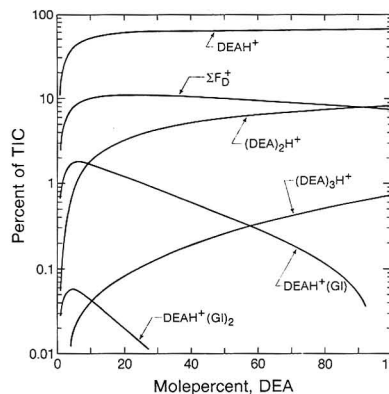
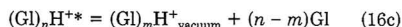
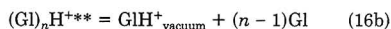
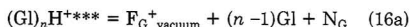


**Figure 7.** Intensities in percent of total ion current, TIC, of diethanolamine (DEA) molecular, fragment, and cluster ions in FAB spectra of solutions of DEA in glycerol (Gl), calculated using the "clustering" kinetic model in Table I. The intensities are plotted against the mole percent concentration of DEA; D = DEA.

the initial ions were produced by a pulse of high-energy electrons. This means that the chosen scheme is based on experience with measurements of ion/molecule reactions with the pulsed high-pressure mass spectrometer (14). Of course, the conditions in the FAB event are very different. However, the model would seem to be applicable if the "primary ions" ( $F_G^+$ ,  $F_D^+$ ) were produced slightly ahead in time in the center of the collision cascade cavity and subsequently mixed in with the expanding monomeric-like neutral matrix and analyte phase. Such a picture is not implausible. The production of monomeric matrix molecules by the "phase explosion" is examined in ref 12.

A different model that corresponds to a very different physical picture can also be used to fit the experimental results. This "declustering" model is described below.

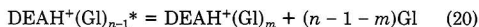
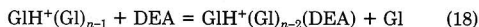
Instead of assuming that the ions of the type  $(GI)_nH^+$  are formed by a gas-phase-like clustering sequence (eq 15), one may consider that cluster ions  $(GI)_nH^+$ , where  $n$  is considerably larger than 1, are initially produced in the very first stage of the rapid phase explosion. It is further assumed that these cluster ions have different internal excitation energies. The ions with high internal excitation,  $(GI)_nH^{+***}$ , decompose to glycerol fragments before mass analysis. Those with lesser excitation only decluster, and the extent of declustering decreases with decreasing excitation. These processes are shown in eq 16a–c. It is further assumed that the excitation of the



$(GI)_nH^+$  cluster decreases with increasing residence time  $t$ . This situation can be expected to lead to spectra of the same appearance as those in Figures 1–5. The glycerol clusters proton transfer to the DEA analyte in the "gas"



The DEA/glycerol clusters formed in reaction 17 subsequently dissociate unimolecularly in the vacuum in reactions analogous to reactions 16. Glycerol clusters that do not proton transfer to the analyte dissociate as described by reaction 16. Reaction 17 can also be described as a ligand exchange reaction followed by proton transfer within the cluster



Additional ligand exchange reactions



followed by unimolecular declustering in the vacuum



can result in the formation of DEA cluster ions. Reaction 21 is expected to be exothermic, since the bond strength for the  $\text{NH}^+-\text{N}$  bond is ca. 21 kcal/mol, whereas the  $\text{NH}^+-\text{O}$  bond is ca. 15 kcal/mol (15).

At high analyte concentrations only those glycerol ions that have short residence times will "escape" the proton transfer to DEA, reaction 17, and "survive". These will be the ions with high internal excitation and short residence time that decompose in vacuum to  $\text{F}_G^+$  by eq 16a. This explains the increasing ratio of  $\text{F}_G^+$  to  $\text{GIH}^+$ , see eq 3, with increasing analyte concentration observed in the experiments, Figure 3. The increasing ratio  $\text{GIH}^+ / (\text{GI})_2\text{H}^+$  with increasing [DEA] is similarly explained.

The operation of the "declustering" model described by eq 16 will lead to a residence time dependent FAB spectrum in neat glycerol whose features are similar to the spectrum (Figure 6b) predicted with the consecutive "clustering" model, eq 15. However, with the declustering model, eq 16, there is no simple way of predicting the time-dependent spectrum.

The clustering and the declustering model have in common that short residence times (few reactive ion/molecule reactions) correspond to low mass ions (fragments) and conversely long residence times (extensive ion/molecule chemistry) correspond to extensive clustering of the observed ions. It is this correlation that explains many of the spectral features of FAB spectra. This relation between the excitation energy of the ions and the extent of ion/molecule chemistry can be understood to be a result of the phase explosion (12) since a hotter liquid will "explode" more violently, with less time for ion/molecule reactions. This also results in ions with higher excitation energies. In this picture, it is the temperature of the liquid just prior to the "phase explosion" that determines both the extent of ion/molecule reactions and the final excitation energy of the ejected ions.

#### (c) Fragment Ions and "Noise" Ions in FAB Spectra.

Much interest has been focused on the question whether fragment ions in FAB spectra are formed prior to desorption or as a result of unimolecular dissociation in the vacuum (2). In part b of this section it was seen that the kinetic modeling could not distinguish between the clustering model, where the ionic fragments are the precursors of all the molecular ions, and the declustering model, where the ionic fragments are all formed as a result of unimolecular dissociation of molecular ions in the vacuum.

A particularly striking experimental observation is that there is a decrease in the fragmentation of  $\text{DEAH}^+$  with increasing DEA concentration (Figures 2 and 3). In the clustering model, this feature is reproduced. This can be seen in Figure 7 where there is a decrease in the calculated intensity of the DEA fragment ions and at the same time an increase in the intensity of the DEA molecular ion as [DEA] increases. The reason for this behavior (according to the model) is that the DEA fragment ions whether formed by the collision cascade or by protonation of DEA neutral fragments are unreactive toward glycerol (matrix). At a low DEA concentration they have therefore an increased chance of entering the vacuum. At a high DEA concentration, on the other hand,

most of these ions react by eq 27a (Table I). This behavior is well illustrated by the concentration profile of the 74+ DEA fragment in Figure 2 which has a pronounced maximum at intermediate DEA concentrations.

The simple declustering model does not explain the decrease in the fragmentation of  $\text{DEAH}^+$  with increasing DEA concentration. However, a more realistic declustering model would consider the effects of  $\text{DEAH}^+$  forming a stronger bond with DEA than with GI. For this reason,  $\text{DEAH}^+$  ions that are formed by unimolecular desolvation of a  $\text{DEAH}^+(\text{DEA})$  cluster will have a lower excitation energy than those formed by desolvation of  $\text{DEAH}^+(\text{GI})$  as the energy for the dissociation is taken from the internal excitation energy of the cluster. Thus, a decrease in the average excitation energy of the desorbed  $\text{DEAH}^+$  ions may be expected as the molecular environment changes from glycerol to DEA. This would result in decreased fragmentation of  $\text{DEAH}^+$  as is experimentally observed, Figure 3.

The presence of a large number of small peaks at almost every mass, the "background" or "chemical noise", is typical of FAB spectra. It has been suggested that the noise originates from the high-energy region of the surface cascade (16), where molecules fragment as a result of energetic collisions. Williams (17) suggested that the ions came from "hot spots" in the bombarded region where extensive radiation damage occurs. A wide range of ions would result from free radical reactions in the matrix (18).

The intensities of a few representative "noises" peaks in the DEA/GI spectra are plotted in Figure 4. In part a of this section it was seen that ions with different "kinetic history" have qualitatively different behavior in the intensity vs analyte concentration curves (Figures 1 and 2). The main categories of ions, i.e. molecular, fragment, and cluster ions of matrix and analyte, respectively, as well as mixed clusters, can easily be distinguished. The concentration dependence for the noise peaks in Figure 4 parallels the behavior of these ion "categories". Thus,  $m/e$  39 behaves like a glycerol fragment,  $m/e$  86 like a fragment of DEA, and  $m/e$  90 like a glycerol fragment at low concentration of DEA and like a DEA fragment at higher concentration. The ions  $m/e$  162 and 85 behave like mixed clusters, i.e. like  $\text{DEAH}^+(\text{GI})$ .

Results like those shown in Figure 4 indicate that many of the background ions probably have a chemical history that is similar to that of the major fragment and cluster ions. If ionic fragments of matrix and analyte molecules were formed on the surface, for example by direct hits in the collision cascade, and subsequently directly ejected into the vacuum, the intensity of such fragments would be expected to be proportional to the concentration of matrix and analyte, respectively. Such behavior is shown by the dashed lines in Figure 4. Clearly, these dashed curves are very different from the experimental ones.

It is concluded from the discussion above that at the most a small fraction of the "chemical noise" ions are formed in "hotspots" with no subsequent ionic reactions.

(d) Ions in Solution and FAB Ions. It was shown above that the observed FAB spectra can be consistently modeled on the basis of gas collision mechanisms. On the other hand, a simple consideration shows that the FAB observed ion ratios bear no relationship to the ion ratios present in the liquid solution. In connection with earlier work (10) the  $pK_a = 8.5$  of DEA in glycerol was determined. This value predicts the ratio in the glycerol solution:  $[\text{GIH}^+]/[\text{DEAH}^+] = 3 \times 10^{-8}/[\text{DEA}]$ . This means that even in as dilute a solution as  $10^{-8}$  M of DEA, the  $[\text{GIH}^+]/[\text{DEAH}^+]$  ratio will be  $3 \times 10^{-6}$ ; i.e.  $[\text{DEAH}^+]$  will completely dominate. The observed FAB ion ratio is vastly different; i.e. at such concentrations the  $\text{GIH}^+$  ions dominate. Thus, a direct desorption of preformed

ions from the present solutions is not supported by the FAB spectra.

### ACKNOWLEDGMENT

We wish to thank Alan Hogg and his co-workers for the use of and help with the MS9 instrument.

### APPENDIX

In the kinetic modeling described in this paper, the actual expansion process is ignored; i.e.  $[B]$  was assumed to be constant. In reality the gas expands and, therefore, the "effective" residence time depends on the characteristics of the gas expansion. This can be illustrated with an exponential gas expansion, described by

$$[B] = [B]_0 \exp(-bt) \quad (23)$$

where  $[B]_0$  is the concentration of B in the liquid. Equation 23 may be substituted into eq 8. By solving the linear first-order differential equation, we find

$$[A^+] = [A^+]_0 \exp(-k_7[B]_0/b) \exp(-k_7[B]_0 \exp(-bt)/b) \quad (24)$$

which in the limit of large  $t$  simplifies to

$$[A^+] = [A^+]_0 \exp(-k_7[B]_0/b) \quad (25)$$

By comparison with eq 9 it is seen that, in this case, the "effective residence time" is given by

$$t = 1/b \quad (26)$$

In general, we expect to find that the largest contribution to the effective residence time is the time that the ions spend in a "gas" with a density quite close to that of the liquid. If this is correct, most of the ion/molecule chemistry takes place during the initial stage of the phase explosion when the density

of the "gas" is still 1/3 to 1/10 of that of the liquid.

Registry No. GI, 56-81-5; DEA, 111-42-2.

### LITERATURE CITED

- (1) Sigmund, P. in *Sputtering by Particle Bombardment-I*, Topics in Applied Physics; Benninghoven, A. Ed.; Springer-Verlag: Berlin, 1981; pp 9-71.
- (2) Pachuta, S. J.; Cooks, R. G. in *Desorption Mass Spectrometry: Are SIMS and FAB the Same?*; American Chemical Society: Washington DC, 1985; p 1.
- (3) Honda, F.; Lancaster, G. M.; Fukuda, Y.; Rabalais, J. W. *J. Chem. Phys.* **1978**, *69*, 4931.
- (4) Cooks, R. G.; Busch, K. L. *Int. J. Mass Spectrom. Ion Phys.* **1983**, *53*, 111-124.
- (5) Murray, P. T.; Rabalais, J. W. *J. Am. Chem. Soc.* **1981**, *103*, 1007.
- (6) Lancaster, G. M.; Honda, F.; Fukuda, Y.; Rabalais, J. W. *J. Am. Chem. Soc.* **1979**, *101*, 1951.
- (7) Michl, J. *Int. J. Mass Spectrom. Ion Phys.* **1983**, *53*, 255.
- (8) David, D. E.; Magnera, T. F.; Tian, R.; Stulik, D.; Michl, J. *Nucl. Instrum. Methods Phys. Res., Sect. B* **1986**, *B14*, 378-391.
- (9) Sunner, J. A.; Kulatunga, R.; Kebarle, P. *Anal. Chem.* **1986**, *58*, 1312.
- (10) Sunner, J.; Morales, A.; Kebarle, P. *Anal. Chem.* **1987**, *59*, 1378.
- (11) Sunner, J. A.; Kulatunga, R.; Kebarle, P. *Anal. Chem.* **1986**, *58*, 2009.
- (12) Sunner, J.; Ikononou, M.; Kebarle, P. *Int. J. Mass Spectrom. Ion Processes*, in press.
- (13) Hogg, A. M. *Int. J. Mass Spectrom. Ion Phys.* **1983**, *49*, 25.
- (14) Kebarle, P. in *Techniques for the Study of Gas-Phase Ion-Molecule Reactions*; Saunders, W. H., Farrar, J. M., Eds.; Wiley: New York; 1988.
- (15) Davidson, W. R.; Sunner, J.; Kebarle, P. *J. Am. Chem. Soc.* **1979**, *101*, 1675.
- (16) Benninghoven, A. *Int. J. Mass Spectrom. Ion Phys.* **1983**, *46*, 459-462.
- (17) Williams, D. H.; Bradley, C.; Bojesen, G.; Santikarn, S.; Taylor, L. C. E. *J. Am. Chem. Soc.* **1981**, *103*, 5700-5704.
- (18) Field, F. H. *J. Phys. Chem.* **1982**, *86*, 5115-5123.

RECEIVED for review May 6, 1987. Accepted September 28, 1987. The work was supported by a grant from the Canadian Natural Sciences and Engineering Research Council.

## Detection of Ethylene Glycol Dinitrate Vapors by Ion Mobility Spectrometry Using Chloride Reagent Ions

A. H. Lawrence\* and Pavel Neudorff

Unsteady Aerodynamics Laboratory, National Aeronautical Establishment, National Research Council, Ottawa, Ontario K1A 0R6, Canada

**The detection of ethylene glycol dinitrate (EGDN) vapors by ion mobility spectrometry (IMS) using chloride reagent ions is discussed. The addition of dichloromethane to the carrier stream leads to increased specificity of ionization and to the formation of EGDN-Cl<sup>-</sup> ions. Two sampling and sample introduction methodologies are described. The effect of sample concentration, temperature, and matrix composition on the sensitivity of response of IMS/Cl<sup>-</sup> chemistry to EGDN vapors is presented.**

One of the most effective methods for detecting hidden bombs in either civilian or military situations is through trace analysis of ambient air for characteristic telltale vapors emanating from the explosive material (1, 2). The same approach can sometimes be useful in postexplosion investigations to identify the type of explosive that has been used in a bombing incident.

Ethylene glycol dinitrate (EGDN) is the most volatile effluent in dynamite formulations and is also present as a vapor impurity in many explosive products that do not contain it as an ingredient (3). Accordingly, the detection of hidden explosives by using analytical instrumentation is often based on the analysis of ambient air for the presence of traces of EGDN vapors (2). A number of analytical techniques have been employed in recent years including gas chromatography with an electron capture detector (GC-ECD) (2), gas chromatography-mass spectrometry (GC-MS) (4), atmospheric pressure chemical ionization mass spectrometry (APCIMS) (5), and ion mobility spectrometry (IMS) (6-8).

IMS, also known as plasma chromatography, is an atmospheric-pressure-based technique that resolves ionic species on the basis of the differences in their mobilities through a gas under an applied electrostatic field (9). Drift time (milliseconds) or ion mobility reduced to standard temperature and pressure  $K_0$  ( $\text{cm}^2 \text{V}^{-1} \text{s}^{-1}$ ), much as retention time in GC, can be used to identify the trace molecules originating a peak



in IMS. Because of its sub-part-per-billion detection capability, fast response time (0.1–10 s), and ease of operation, IMS is rapidly gaining acceptance as a chemical sensor for the detection of trace compounds in the ambient environment. The apparatus has been designed as a compact hand-held (10) and man-portable (11) detector.

In IMS, the sample, in vapor form, is introduced into a reaction chamber by means of a carrier gas ( $N_2$ , air). Ionization of reactive trace impurities in the carrier gas, such as  $H_2O$  and  $NH_3$ , is generally brought about by energetic electrons released from a  $^{63}Ni$  radioactive source with the formation of a number of positive and negative reactant ions, e.g.,  $(H_2O)_nH^+$  and  $(H_2O)_nO_2^-$ ; the value of  $n$  depends on the concentration of the water vapor. These ions undergo a complex series of ion/molecule reactions with the analyte, and product ions are produced. Compounds with high proton affinity form positive product ions through proton ( $or NH_4^+$  and  $NO^+$ ) exchanges, and those containing atoms with high electron affinity, such as halogen, oxygen, and nitrogen, form negative product ions through electron attachment and other mechanisms (11).

Organonitrates such as EGDN and nitroglycerin (NG) are electronegative in character, and due to the large cross section offered by these compounds to charge transfer and ion/molecule reactions, negative IMS is particularly suited for their detection and analysis. However, EGDN and NG undergo dissociative electron capture and do not produce molecular anions in the IMS, but instead produce an ion peak with a reduced mobility of  $2.46\text{--}2.48\text{ cm}^2\text{ V}^{-1}\text{ s}^{-1}$  corresponding to the fragment  $NO_3^-$  ion (6–8). This peak overlaps significantly with the peak associated with the reactant ions when air or nitrogen is used as the carrier gas, thus restricting its usefulness as an IMS marker for identification purposes.

It is well-established that the selectivity of ionization in atmospheric pressure chemical ionization as well as in conventional chemical ionization mass spectrometry is dependent upon the makeup of the reagent gas. Different ionization characteristics may be obtained by adding trace amounts of various reagent gases. Jennings et al. (12) have examined the negative chemical ionization mass spectrometry (NCIMS) of EGDN and other organonitrates by using various reagent ions including the chloride ion ( $Cl^-$ ). They showed that  $Cl^-$  attachment to EGDN parent molecule occurs readily with the formation of a new abundant ion ( $EGDN\text{-}Cl^-$ ) of mass  $m/z$  187.

The IMS behavior of EGDN with reagent ions such as  $Cl^-$  and  $Br^-$  has been reported by Todd and Proctor (13). They showed that the addition of  $Cl^-$  to the carrier stream led to greater selectivity of ionization and better resolution in the mobility spectrum; at a drift tube temperature of  $50^\circ\text{C}$  and EGDN concentration of  $\sim 100$  ppb, all sample ionization resulted in one ionic species,  $EGDN\text{-}Cl^-$ . In an independent investigation, using negative IMS and an inlet temperature of  $227^\circ\text{C}$ , Spangler et al. (14) demonstrated that the  $NO_3^-$  peak form EGDN can be resolved from the peak associated with the reactant ions when chloride ions are added to the system.

This paper presents the results of an assessment of the sensitivity of  $IMS/Cl^-$  ion chemistry to EGDN vapors. The limit of detection and the effect of temperature on the formation of the  $EGDN\text{-}Cl^-$  ion cluster have been characterized. Effective sampling and sample introduction methodologies have been developed. The prospective values of  $IMS/Cl^-$  ion chemistry in the detection of EGDN vapors in a preconcentrated ambient air sample have also been investigated.

## EXPERIMENTAL SECTION

**Reagents and Chemicals.** EGDN was synthesized in this laboratory according to a procedure involving nitration of ethylene

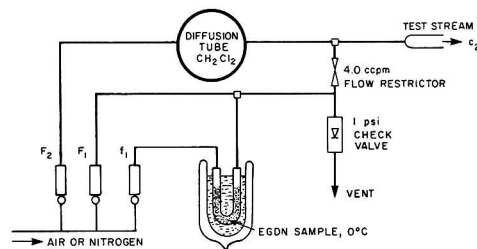


Figure 1. Double-dilution vapor source.

glycol with an acid mixture [ $HNO_3/H_2SO_4$  (7:3)]. Standard EGDN solutions were prepared as  $4 \times 10^{-11}\text{ g}/\mu\text{L}$  in hexane. Forcite 40, a commercial dynamite containing EGDN and NG, was obtained from Canadian Industries, Ltd. (CIL), Montreal, Quebec. Chromosorb 750 with 3% OV-17 (80–100 mesh) was obtained from Chromatographic Specialties (Brockville, Ontario). Linde ultrahigh-purity nitrogen was dried by Linde molecular sieve 13X and used for both carrier and drift gases. Dichloromethane and *n*-hexane were distilled-in-glass grade (Caledon, Georgetown, Ontario).

**Adsorption Tubes.** The adsorption tubes used in this study were constructed of nickel tubing, 10-cm length  $\times$  0.3-cm o.d.  $\times$  0.22-cm i.d., and contained about 30 mg of sorbent material (3% OV-17 on Chromosorb 750) held in place with two fine-mesh platinum disks. The tubes were conditioned for several minutes at  $150^\circ\text{C}$  in a nitrogen stream at a flow rate of 200 mL/min. Before use an IMS trace was recorded to check the cleanliness of the adsorbent.

**Vapor Source.** A dynamic gas blending system was used to generate known and controllable concentrations of EGDN vapor in purified air or nitrogen. The double-dilution vapor source used in this study was an upgraded version of the single-stage device reported previously from this laboratory (15, 16) and is shown schematically in Figure 1. A small stream of air ( $f_1$ ) was saturated with EGDN vapor by passing it through a sample of EGDN in a glass tube thermostated at  $0^\circ\text{C}$ ; the carrier stream was then diluted in two stages by large air streams to produce any EGDN concentration within the range  $0.5\text{--}1000$  ppb (parts in  $10^{12}$ ) as required. The vapor source can deliver anywhere from 1 to 20 L/min. The actual EGDN concentration in the air stream was confirmed by GC-ECD analysis of air samples collected in adsorber tubes and based on calibration with standard solutions of EGDN (2). Reproducibility of EGDN concentrations from the vapor source was within  $\pm 10\%$ . The measured values were in close agreement with the vapor pressure data of EGDN at  $0^\circ\text{C}$  published by the National Bureau of Standards (17). In one set of experiments involving chloride ion chemistry (see below), nitrogen was used as the diluent and carrier streams, and dichloromethane was added in trace amounts to the diluting stream ( $F_2$ ) by means of a diffusion tube and an independently controlled flow (Figure 1), thus allowing the concentration of EGDN and that of  $CH_2Cl_2$  to be varied separately.

**Instrumentation.** The IMS data presented in this paper were obtained with a PheMo-Chem 100 ion mobility spectrometer (PCP, Inc., West Palm Beach, FL). The instrument has a membraneless inlet and has been recently described (18). The signal from the IMS was averaged with a Nicolet 1170 signal averager and the spectra were recorded with a Hewlett-Packard 7010B X-Y recorder. The analog-to-digital converter (ADC) resolution used with the signal averager was always 12 bits and the full-scale volt setting was kept at  $\pm 4\text{ V}$ . The ion peak amplitude was used as a quantitative measure of specific ions. Mass identification of ions giving particular mobility peaks was obtained with a PheMo-Chem MMS-160 ion mobility spectrometer/mass spectrometer (IMS/MS) (19). The experimental parameters used to operate the IMS and the IMS/MS are presented in Table I.

**Sample Introduction Techniques.** Two sampling procedures were used in this study. In one series of experiments, the IMS was operated as a "Sniffer" and was allowed to sample a continuous nitrogen stream containing known concentrations of

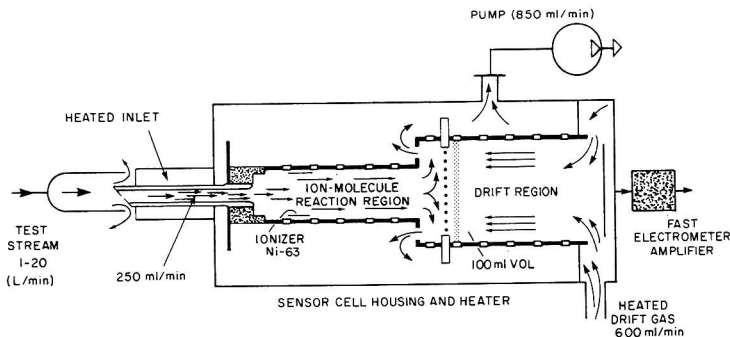


Figure 2. Continuous detection of EGDN.

Table I. Instrument Parameters

parameter	value
Ion Mobility Spectrometer (Phemto-Chem 100)	
drift length	8 cm
drift voltage	-3000 V
carrier gas (purified nitrogen spiked with dichloromethane)	250 mL/min
drift gas (purified nitrogen)	600 mL/min
inlet and drift temperature	75 °C
pressure	atmosphere
dwell time	20 $\mu$ s/channel
gate width	0.2 ms
delay time <sup>a</sup>	6 ms
Ion Mobility Spectrometer-Mass Spectrometer (Phemto-Chem MMS-160) <sup>b</sup>	
drift length (between grid G <sub>1</sub> and IMS collector)	10 cm
drift voltage	-3214 V
carrier gas (purified air spiked with dichloromethane)	200 mL/min
drift gas (purified air)	600 mL/min
inlet and drift temperature	75 °C
gate width	0.2 ms
dwell time	25 $\mu$ s/channel
delay time	6.4 ms
mass spectrometer pressure	$4 \times 10^{-5}$ Torr
scanning speed	1000 amu/s

<sup>a</sup>The time between gate opening and start of data collection.<sup>b</sup>IMS-MS experiments were conducted at PCP Laboratories.

EGDN. A diaphragm pump (Fisher Scientific Instruments) was connected to the gas exhaust port of the instrument and suction was applied at the rate of 850 mL/min. The drift gas ( $N_2$ ) was supplied at the rate of 600 mL/min. When the vapor source was placed in front of the inlet of the IMS (Figure 2), 250 mL/min was drawn in the instrument and the excess spilled out to the atmosphere. In a second set of experiments, purified air was used as the carrier and diluent streams in the vapor source and sampling was performed by means of a suction probe (20) remote from the IMS unit. Samples were collected from the vapor source at a sampling flow rate of 200 mL/min and the sampling time was varied over 1-4.5 min to collect various amounts of EGDN on the traps. The collector probe was subsequently inserted in the heated inlet of the IMS, which, unless indicated otherwise, was kept at 75 °C; EGDN evaporated immediately and was flushed with the carrier gas stream (nitrogen spiked with dichloromethane) to the ion reaction chamber of the instrument (Figure 3).

**Gas Chromatography.** Gas chromatographic experiments were performed with a portable microprocessor-controlled GC which was designed and constructed in-house. The instrument is equipped with an electron capture detector, a six-port switching valve, and a two-stage thermal desorption system. The general description and operation of the GC have been described elsewhere (2).

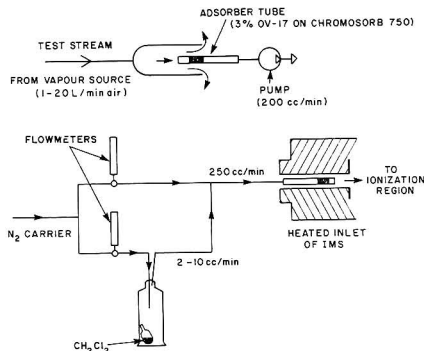


Figure 3. Collection of EGDN vapors in adsorbent tubes.

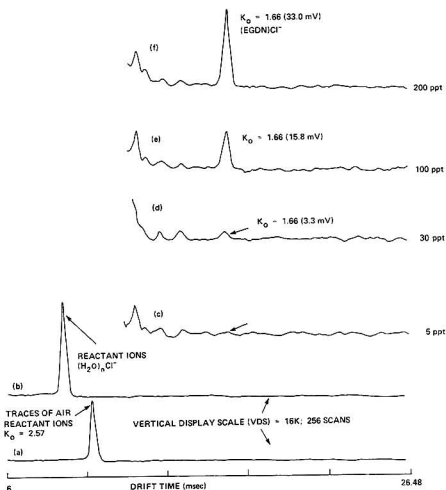


Figure 4. Effect of EGDN concentration on IMS signal amplitude: (trace a) system blank, carrier gas  $N_2$ , 256 scans, vertical display scale (VDS) = 16K; (trace b) system blank, carrier gas  $N_2 + CH_2Cl_2$ , 256 scans, VDS = 16K; (traces c-f): carrier gas  $N_2 + CH_2Cl_2$ , 512 scans, VDS = 4096.

**Continuous-Action Preconcentrator.** The continuous-action preconcentrator (CAP) was developed in this laboratory (21) and is used to enhance the concentration of gases and vapors present

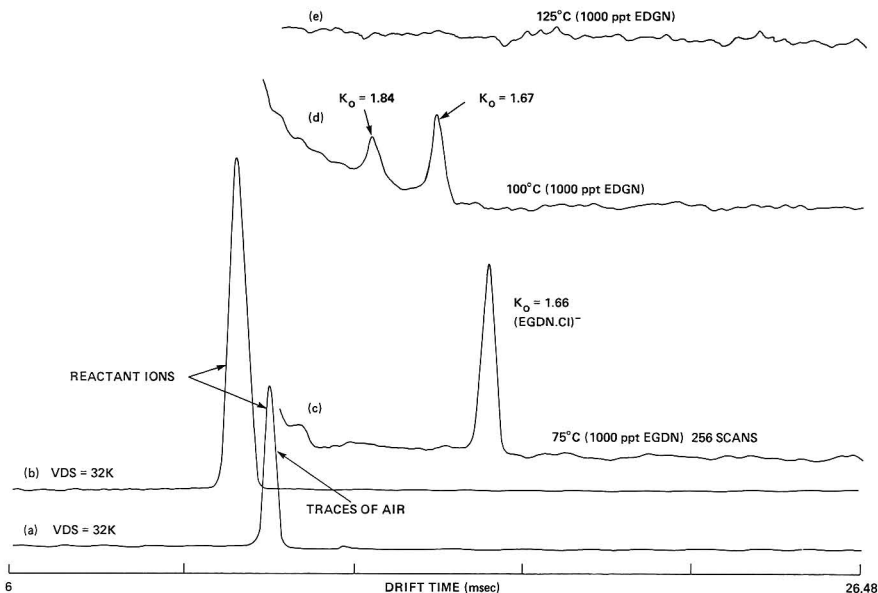


Figure 5. Effect of temperature on the stability of  $(\text{EGDN-Cl})^-$  ion cluster. IMS parameters: 512 scans; VDS = 4096.

in trace quantities in the atmosphere (or some other gaseous medium) to such level that they may be more readily analyzed by appropriate analytical instrumentation. The CAP is based on an adsorption-thermal desorption technique, a proven pre-concentration method in trace vapor analysis. The novel feature of this device is that where, conventionally, discrete volumes of air are scrubbed of the target vapors by a stationary bed of adsorbent material, so that the process is discontinuous and time-consuming, the CAP achieves a similar concentrating effect on a continuous and nearly real-time basis; a vapor enrichment factor greater than  $10^3$  was obtained in less than 5 s when traces of EGDN vapor were presented at the inlet of the instrument (2, 21).

## RESULTS AND DISCUSSION

**Continuous Detection of EGDN.** In this series of experiments, the IMS was operated as a sniffer and was allowed to sample a continuous stream of purified nitrogen spiked with EGDN; i.e., sensitivity tests in this mode of operation were limited to vapor source sampling only, since in the absence of a membrane inlet the water vapor in an ambient air sample causes the reactant ion peak  $[(\text{H}_2\text{O})_n\text{Cl}]^-$  to vary erratically. Furthermore, in all experiments involving chloride ion chemistry, the concentration of  $\text{CH}_2\text{Cl}_2$  was increased gradually until the peak for free electrons (usually observed in negative IMS when nitrogen is used as a carrier gas) was no longer observable and only the peak corresponding to  $(\text{H}_2\text{O})_n\text{Cl}^-$  ions could be detected. Under these optimal conditions, the minimum detectable concentration at a signal amplitude of 3 times the  $1\sigma$  noise was 30 ppb, corresponding to a mass flow of EGDN of  $4.7 \times 10^{-11}$  g/min. The negative IMS spectrum exhibited a well-resolved major ion peak at a reduced mobility  $K_0$  of  $1.66 \text{ cm}^2 \text{ V}^{-1} \text{ s}^{-1}$  with a peak width at half height of 0.4 ms, corresponding to  $\text{EGDN-Cl}^-$  of mass  $m/z$  187 (see below). As the concentration of EGDN in the test stream was increased, the amplitude of the peak corresponding to  $\text{EGDN-Cl}^-$  increased proportionally (Figure 4). No attempt was made to determine the linear working range.

**Effect of Temperature.** Figure 5 illustrates the effect of temperature on the sensitivity of response of the  $\text{IMS/Cl}^-$

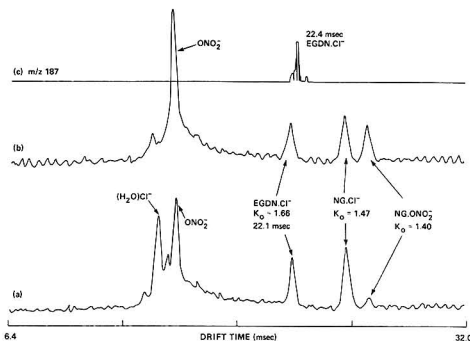
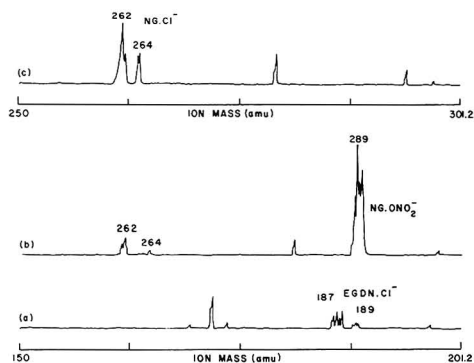


Figure 6. Negative ion mobility spectra and mass-identified ion mobility spectral data for dynamite.

chemistry to EGDN vapors. In this experiment, the vapor source was set to deliver 1000 ppb of EGDN in nitrogen (Figure 1), and ion mobility spectra were recorded as a function of temperature over the range 50–125 °C. The spectra were acquired only after the signal became stable, and 512 scans were averaged for each spectrum. At a frequency of 41 Hz, signal averaging lasted about 10 s while the sample was introduced continuously into the IMS. As expected, increasing the temperature has the effect of increasing the mobility of the ions through the drift gas. The drift time of the  $\text{EGDN-Cl}^-$  ion cluster decreases, whereas the value of  $K_0$  remains constant; however, there is a significant decrease in sensitivity, e.g., at 125 °C, no peak corresponding to  $\text{EGDN-Cl}^-$  is observed at an input concentration of EGDN equivalent to 1000 ppb. This could be due to the decomposition of the sample in the inlet of the IMS or to fragmentation of the  $\text{EGDN-Cl}^-$  cluster ion.

**IMS-MS Experiments.** In this series of experiments, the headspace vapors from a commercial dynamite sample were



**Figure 7.** Mass spectral data of a dynamite sample collected at small chloride ion concentrations (traces a and b) and large chloride ion concentrations (trace c).

collected on a stainless steel wire, which was subsequently inserted in the heated inlet of the instrument. One to two microliters of dichloromethane was injected directly with a syringe, which produced a strong and persistent chloride ion peak. Figure 6a illustrates the total negative IMS spectrum of a dynamite sample in the presence of chloride ions. In addition to  $(\text{H}_2\text{O})\text{Cl}^-$  ( $m/z$  53, 55) and  $(\text{H}_2\text{O})_n\text{NO}_3^-$  ( $m/z$  62, 80), two intense well-resolved peaks are observed at  $K_0$  1.66 and 1.47 and correspond to  $\text{EGDN-Cl}^-$  ( $m/z$  187, 189; ratio 3:1) and  $\text{NG-Cl}^-$  ( $m/z$  262, 264; ratio 3:1), respectively. The ion of  $m/z$  289 ( $\text{NG-NO}_3^-$ ) is responsible for the small peak at  $K_0 = 1.40$ , the  $\text{NO}_3^-$  ions being formed by dissociative electron capture from the organonitrate molecules. As the concentration of the chloride ions in the system decreases, the intensity of the  $\text{NG-NO}_3^-$  peak increases (Figures 6b and 7b). Reintroducing dichloromethane in the system has the effect of reducing the intensity of the  $\text{NG-NO}_3^-$  ion while enhancing

the intensity of the peaks corresponding to the chloride ion adducts (Figure 7c).

The mass identified mobility data shown in Figure 6c clearly demonstrates that the major ion contributing to the IMS peak at  $K_0 = 1.66 \text{ cm}^2 \text{ V}^{-1} \text{ s}^{-1}$  is  $m/z$  187 corresponding to  $\text{EGDN-Cl}^-$ . In this mode of operation, the MS can filter a single mass while the drift time of the corresponding ion is measured. Since the detector sees only one ionic species, the mobility spectrum consists of only that peak corresponding to the ion (19).

**Remote Vapor Collection.** In order to test the efficacy of the system in "real" air, different vapor collection and sample introduction techniques were used. "Real air" in this context was ambient air of the workplace environment with no EGDN vapor. In this mode of operation, EGDN vapors were collected from the vapor source by means of a suction probe containing an adsorbent material. Following sampling, the probe is inserted in the heated inlet of the IMS. The adsorbed chemicals are removed by heating and flushed with the carrier gas stream (nitrogen spiked with dichloromethane) to the ion reaction chamber of the instrument (Figure 3). The desorption temperature,  $75^\circ\text{C}$ , was low enough to prevent decomposition of EGDN while providing a desorption time that was sufficiently short to allow for 10–20 s response time. When the above vapor collection and sample introduction techniques are used, the minimum detectable quantity at a signal amplitude of 3 times the  $1\sigma$  noise was 30 pg; however, superimposing a 30-pg sample of EGDN from the vapor source (source strength, 5 ppt; sampling rate, 200 mL/min; sampling time, 4.5 min) on an equivalent room air sample, or vice versa, has the effect of degrading the signal to noise ratio.

In the absence of chloride ions in the IMS, autoionization and dissociative electron capture of EGDN occur and result in the formation of  $\text{NO}_2^-$  and  $\text{NO}_3^-$ , which then act as reagent ions and attach to the parent molecule to give  $(\text{EGDN-NO}_2)^-$  and  $(\text{EGDN-NO}_3)^-$  (13). With the use of the remote sampling method and the sample introduction technique described above, the minimum detectable quantity of EGDN determined

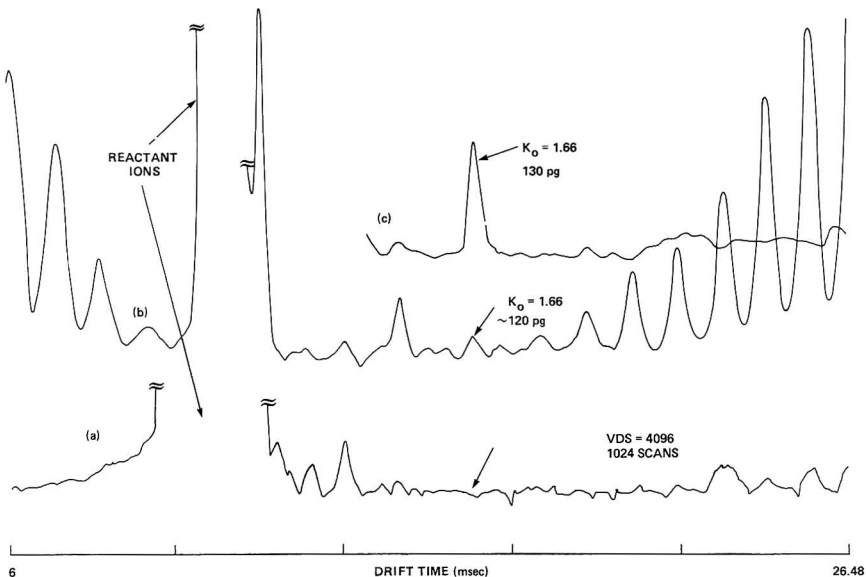


**Figure 8.** Detection of EGDN in a complex gaseous matrix: (a) test of adsorbent cleanliness; (b) detection of 120 pg of EGDN from the CAP; (c) detection of 130 pg of EGDN from a purified air stream. IMS parameters: carrier gas  $\text{N}_2 + \text{CH}_2\text{Cl}_2$ ; inlet temperatures  $75^\circ\text{C}$ .

as (EGDN-NO<sub>3</sub>)<sup>-</sup> ( $K_o = 1.60 \text{ cm}^2 \text{ V}^{-1} \text{ s}^{-1}$ ) was found to be 500 pg, as compared to 30 pg for the IMS/Cl<sup>-</sup> chemistry.

The procedure involving vapor sampling by adsorption followed by thermal desorption directly in the IMS offers numerous advantages, such as elimination of the requirements for a membrane inlet thus preventing the continuous suction of unwanted chemicals into the system, higher sensitivity compared to IMS equipped with a membrane inlet (a 10<sup>2</sup>–10<sup>4</sup> loss of vapor concentration through membrane systems has been reported (22)), and cleardown from overloading can be as low as 30 s. Furthermore, vapor collection by means of a detachable sampler remote from the analyzer has proven to be more useful in an actual search for hidden bombs (2).

**Interferences in Atmospheric Detection.** A series of experiments were designed and aimed at investigating the effect of matrix composition and sample size on the response of IMS/Cl<sup>-</sup> chemistry to EGDN vapors. With the adsorbent tubes described above, a 10-mL sample was collected from the continuous action preconcentrator (CAP) and subsequently analyzed by IMS and chloride reagent ions. In these experiments, the CAP input was a 60 L/min ambient air stream spiked with 5 ppb EGDN. The CAP output was a 30 mL/min nitrogen stream with an EGDN concentration of 1700 ppb as established by GC-ECD. Figure 8b is a representative total ion mobility trace and shows a complex spectrum with a large number of broad and unresolved peaks. More importantly, the response to the ion of interest—EGDN-Cl<sup>-</sup>—was erratic and, in some cases, was eliminated entirely. This is probably due to competitive formation of chloride addition product ions by reaction of the chloride ions with interfering compounds present in the complex gaseous matrix of the CAP.

The IMS/Cl<sup>-</sup> chemistry has been shown to be a specific, rapid, and sensitive technique for detection of EGDN vapors in a purified air sample. However, the system is very sensitive to matrix composition, and efforts are currently being made to improve the interfacing of the continuous action preconcentrator to the IMS.

#### ACKNOWLEDGMENT

We thank Robert M. Stimac of PCP, Inc., West Palm Beach, FL, for assistance in obtaining IMS-MS data, and Dr.

L. Elias for helpful discussions throughout the study.

**Registry No.** EGDN, 628-96-6; CH<sub>2</sub>Cl<sub>2</sub>, 75-09-2.

#### LITERATURE CITED

- (1) Elias, L. "Development of a Portable Gas Chromatograph Explosives Detector"; LTR-UA-57, National Research Council Canada, Jan 1981.
- (2) Neudorff, P.; Elias, L. J. *Energ. Mater.* **1986**, *4*, 415.
- (3) Cartright, N. S., personal communication.
- (4) Drew, P. C.; Stevens, C. M. "A Man Portable GC-MS for Explosives Detection"; Proceedings of the International Symposium on the Analysis and Detection of Explosives, Quantico, VA, March 29–31, 1983; p 419.
- (5) Davidson, W. R.; Fulford, J. E. "The Instantaneous Detection of Explosives by Tandem Mass Spectrometry"; Proceedings of the International Symposium on the Analysis and Detection of Explosives, Quantico, VA, March 29–31, 1983; p 409.
- (6) Asselin, M. "Detection of Dynamite with a Plasma Chromatograph"; Proceedings—New Concepts Symposium and Workshop on Detection and Identification of Explosives, Reston, VA, Oct 20–Nov 1, 1978; p 177.
- (7) Wernlund, R. F.; Cohen, M. J.; Kindel, R. C. "The Ion Mobility Spectrometer as an Explosive or Taggant Vapor Detector"; Proceedings—New Concepts Symposium and Workshop on Detection and Identification of Explosives, Reston, VA, Oct 20–Nov 1, 1978; p 185.
- (8) Spangler, G. E.; Carrico, J. P.; Kim S. H. "Analysis of Explosives Residues with Ion Mobility Spectrometry"; Proceedings of the International Symposium on the Analysis and Detection of Explosives, Quantico, VA, March 29–31, 1983; p 267.
- (9) *Plasma Chromatography*; Carr, T. W., Ed.; Plenum: New York, 1984.
- (10) Blyth, D. A. Proceedings of the International Symposium on Protection Against Chemical Warfare Agents, Stockholm, Sweden, June 6–9, 1983; p 65.
- (11) Carrico, J. P.; Davis, A. W.; Campbell, D. N.; Roehl, J. E.; Sima, G. R.; Spangler, G. E.; Vora, K. N.; White, R. J. *Am. Lab. (Fairfield, Conn.)* **1986**, *18*, 152.
- (12) Bouma, W. J.; Jennings, K. R. *Org. Mass. Spectrom.* **1981**, *16*(8), 331.
- (13) Proctor, C. J.; Todd, J. F. *J. Anal. Chem.* **1984**, *56*, 1794.
- (14) Spangler, G. E.; Carrico, J. P.; Campbell, D. N. *J. Test. Eval.* **1985**, *13*(3), 234.
- (15) Krzymien, M.; Elias, L. J. *Phys. E* **1976**, *9*, 584.
- (16) Elias, L., unpublished results.
- (17) Pella, P. A. *Anal. Chem.* **1976**, *48*, 1632.
- (18) Rokushika, S.; Hatano, H.; Hill, H. H., Jr. *Anal. Chem.* **1986**, *58*, 361.
- (19) Lawrence, A. H. *Anal. Chem.* **1986**, *58*, 1269.
- (20) Lawrence, A. H. *Forensic. Sci. Int.* **1987**, *34*, 73.
- (21) Elias, L. U.S. Patent Application No. 850 524, Nov 4, 1986.
- (22) Spangler, G. E. "Membrane Technology in Trace Gas Detection" Report 2083, U.S. Army Mobility Equipment Research and Development Center, Fort Belvoir, VA, 1973.

RECEIVED for review July 20, 1987. Accepted September 25, 1987. This paper was presented at the 69th Canadian Chemical Conference, Saskatoon, Saskatchewan, Canada, June 1–4, 1986.



# Cluster Ion Formation under Laser Bombardment. Studies of Recombination Using Isotope Labeling

Inga H. Musselman,<sup>1,2</sup> Richard W. Linton,<sup>1\*</sup> and David S. Simons<sup>2</sup>

Department of Chemistry, University of North Carolina, Chapel Hill, North Carolina 27514, and Center for Analytical Chemistry, National Bureau of Standards, Gaithersburg, Maryland 20899

The analysis of natural abundance NIS particles mounted on an isotopically enriched  $^{34}\text{S}$  film using a transmission geometry laser microprobe mass spectrometer provides a means for observing recombination reactions in the laser-induced plasma. Sulfur-34 from the isotopically enriched thin film is extensively combining in the plasma with nickel from the NIS particle. The data suggest that this recombination phenomenon occurs to a similar extent for the three cluster ions  $\text{NiS}^+$ ,  $\text{NiS}_2^+$ , and  $\text{Ni}_2\text{S}^+$ . One exception for the  $\text{NiS}_2^+$  case is the  $^{58}\text{Ni}^{34}\text{S}^{34}\text{S}^+$  ion, which has a much larger contribution to recombination by the  $^{34}\text{S}$  film. This probably reflects Ni attachment to  $^{34}\text{S}^{34}\text{S}$  dimers which are formed almost exclusively by contributions from the  $^{34}\text{S}$  film.

The investigation of cluster ions is a current area of interest in laser microprobe mass spectrometry (LAMMS) research. A better understanding of ion formation mechanisms will improve the ability to interpret the laser mass spectra of solids with respect to chemical speciation and structure. A review of the applications to solids of the laser ion source in mass spectrometry by Conzemius and Capellen (1) and a bibliography of laser mass spectrometry of solids by Conzemius et al. (2) provide background to this research problem. Processes including volatilization, ionization, and cluster ion formation by pulsed lasers occurring at various places and times in the plasma surrounding the point of sample-laser interaction have been discussed (3-7). Throughout this paper, the term plasma will be used to describe the high energy vapor formed by the high power density laser ablation process even though the charge densities in these experiments are unknown.

Several research groups have used LAMMS specifically to study cluster ion formation in inorganic and organic compounds. The LAMMS studies have included experiments concerned with polyatomic ions generated from silica particles (8), thin carbon foils (9), thin foils of various metals and semiconductors (10), binary oxide particles (11), and substituted pyridines (12). Cluster ions, formed by the laser ionization process, also have been used empirically to differentiate among closely related compounds including inorganic perhenates (13), titanium oxides (14), inorganic sodium sulfoxo salts (15, 16), and calcium oxide and calcium salts (17).

Cluster ion formation in laser ionization mass spectrometry may occur either by direct ionization of the sample by the pulsed laser beam or by a recombination of ions and neutral atoms or molecules in the laser-induced plasma formed above the sample surface. For example, cluster ions of  $\text{Ag}_n\text{Cu}_m^+$ , formed by recombination in the plasma, were observed by Wurster et al. in laser mass spectra obtained from physically separated Cu/Ag sandwich foils (18). Recombination ions of  $\text{Ag}_n\text{Au}_m^+$  were present along with cationized species in positive ion spectra collected by Benninghoven and Anders when in-

ducing Ag cationization of leucine on Au-Ag sandwich substrates (19). Recently, Bruynseels and Van Grieken studied recombination reactions occurring in elemental  $^{12}\text{C}/^{13}\text{C}$  bilayers (20).

The experiments reported here evolved from a cooperative project with the Environmental Protection Agency (EPA)/Environmental Monitoring Systems Laboratory, Research Triangle Park, NC, to study new methods for nickel speciation in airborne particles produced by stationary sources. The development of new techniques to provide speciation information about elements present in trace quantities within complex and highly heterogeneous samples is a challenging area of analytical chemistry. Microscopic analysis techniques, such as LAMMS, which combine the advantages of high spatial resolution and high sensitivity, are being developed to provide information about chemical species and their distribution among, or within, individual particles.

Model nickel species ( $\text{Ni}$ ,  $\text{NiO}$ ,  $\text{NiSO}_4$ ,  $\text{NiS}$ , and  $\text{Ni}_3\text{S}_2$ ) and pollution source samples were examined in prior analytical technique development projects. These nickel species were analyzed, and in many cases differentiated, by LAMMS using characteristic cluster ion fingerprint mass spectra (21-23). The production of these unique cluster ion spectra sparked a more fundamental interest in ion formation mechanisms of nickel/sulfur compounds. In this study, a unique approach was developed to study ion formation permitting the recombination process to be observed directly in the production of cluster ions from nickel sulfide particles deposited on an isotopically enriched sulfur thin film.

## EXPERIMENTAL SECTION

The LAMMS measurements were made with a laser microprobe mass analyzer, LAMMA-500 (Leybold Heraeus) (24-26). A frequency-quadrupled Nd-YAG laser ( $\lambda = 266 \text{ nm}$ ,  $\tau = 15 \text{ ns}$ , average energy per pulse =  $0.28 \mu\text{J}$ , average laser power density =  $2.8 \times 10^9 \text{ W/cm}^2$ ) was focused on the sample with the aid of a He-Ne pilot laser. The energy of each laser pulse was monitored by an energy meter. The ions, generated by the laser pulse, were extracted at  $180^\circ$  relative to the incident laser (transmission geometry) by an immersion lens, focused by an ion lens ( $\sim 1050 \text{ V}$ ), analyzed by a time-of-flight (TOF) mass spectrometer, and detected by a secondary electron multiplier. The amplified analog signal was digitized by two Biomation Model 8100 transient recorders and transferred in digital form to a computer for storage and further processing. Integral areas were obtained from the peaks of interest for use in isotope ratio calculations.

Twenty positive ion mass spectra were obtained from nickel(II) sulfide particles (Alfa Division, 99.99% pure) deposited on a Formvar-coated (Ernest F. Fullam, Inc., 0.25% Formvar in ethylene dichloride) 200-mesh Cu transmission electron microscope grid, and from NIS particles mounted on an isotopically enriched  $^{34}\text{S}$  sputtered thin film deposited on a Formvar-coated TEM grid (Figure 1). The sulfur film, approximately 150 nm thick as estimated by optical interference microscopy, was made by sputter-depositing 93 atom %  $^{34}\text{S}$  from a powder (Monsanto Research Corp., Mound Facility) target onto a Formvar-coated TEM grid via argon bombardment using a Gatan Dual Ion Mill, Model 600. The typical particle sizes analyzed were 1 or 2  $\mu\text{m}$ . The natural isotopic abundances of sulfur and nickel are as follows:  $^{32}\text{S}$ , (95.0%);  $^{33}\text{S}$ , 0.8%;  $^{34}\text{S}$ , 4.2%;  $^{58}\text{Ni}$ , 0.02%;  $^{59}\text{Ni}$ , 68.3%;  $^{60}\text{Ni}$ ,

<sup>1</sup> University of North Carolina.

<sup>2</sup> National Bureau of Standards.

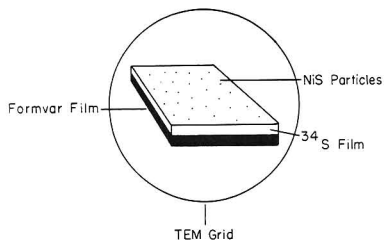


Figure 1. NIS particles mounted on an isotopically enriched  $^{34}\text{S}$  sputtered thin film deposited on a Formvar-coated TEM grid.

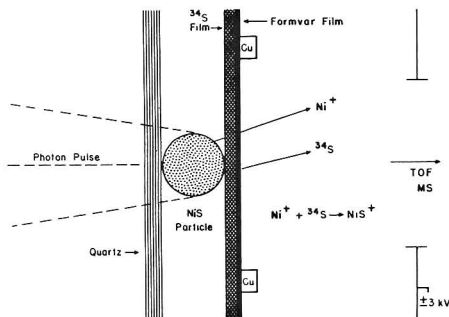


Figure 2. Transmission geometry of laser microprobe with schematic illustration of recombination reaction which may occur in the laser-induced plasma. NIS particle contains 4.2%  $^{34}\text{S}$ . Enriched  $^{34}\text{S}$  film contains 93%  $^{34}\text{S}$ .

26.1%;  $^{61}\text{Ni}$ , 1.1%;  $^{62}\text{Ni}$ , 3.6%;  $^{64}\text{Ni}$ , 0.9% (27).

The laser conditions were not typical of laser desorption but rather allowed for complete ablation of the sample. These conditions were chosen to maximize the production and detection of cluster ions (28–30). The samples were first mounted in the sample holder so that the Formvar film faced the extraction optics. The experiment was repeated with the sample in the other orientation, i.e. with the NIS particles facing the ion extraction optics, to determine whether sample orientation had a major influence on the spectra.

The transmission geometry of the laser microprobe requires that the laser perforates the sample so that the ions may be extracted from the back side of the sample into the TOF mass spectrometer. This geometry, shown in Figure 2, ensures that both the NIS particles and the isotopically enriched  $^{34}\text{S}$  film, which are physically separate for NIS on  $^{34}\text{S}$ , are vaporized in a single laser shot. By comparison of the isotope ratios from the spectra collected from NIS and from NIS on  $^{34}\text{S}$ , it is possible to determine whether recombination reactions in the laser-induced plasma between the nickel from the NIS particle and the sulfur from the isotopically enriched  $^{34}\text{S}$  film produce clusters, an example of which is schematically illustrated in Figure 2.

## RESULTS AND DISCUSSION

The following data are from the experiment in which the Formvar film faced the extraction optics. Representative positive ion laser mass spectra obtained from NIS and from NIS on  $^{34}\text{S}$  are presented in Figure 3. The cluster ions  $\text{NiS}^+$ ,  $\text{NiS}_2^+$ , and  $\text{Ni}_2\text{S}^+$ , found in both spectra, may be formed by direct ionization of the sample by the laser and/or by recombination reactions in the laser-induced plasma. There are, however, some obvious differences between the two spectra. In the spectrum of NIS on  $^{34}\text{S}$ , the larger peaks at  $^{34}\text{S}^+$  and  $^{34}\text{S}_2^+$  ( $m/z$  68) are evident. In addition, the ratios of the peaks reflecting various combinations of nickel and sulfur isotopes within each of the clusters,  $\text{NiS}^+$ ,  $\text{NiS}_2^+$ , and  $\text{Ni}_2\text{S}^+$ , differ significantly between the two spectra. A more detailed ex-

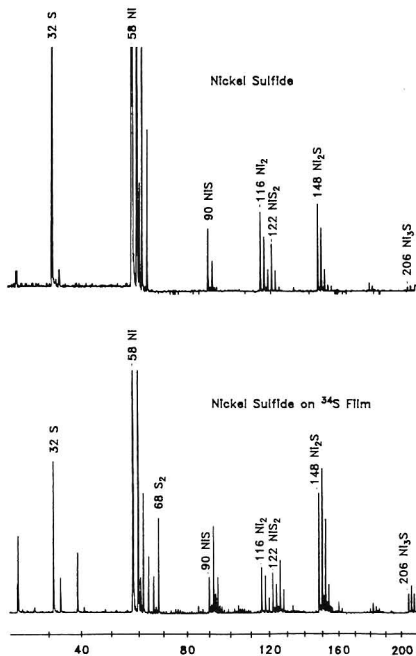


Figure 3. Representative positive ion laser mass spectra obtained from NIS and from NIS on  $^{34}\text{S}$ . Due to limited dynamic range of transient recorder, atomic nickel isotopes are saturated to bring cluster ions on scale. Peaks at low mass reflect ubiquitous  $\text{Na}^+$  and  $\text{K}^+$  contaminants.

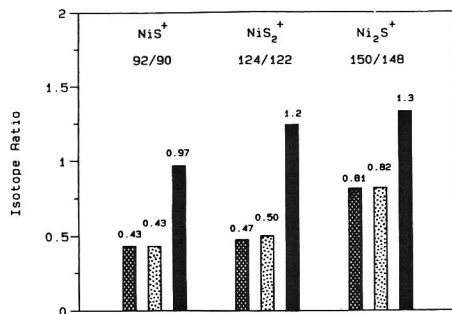


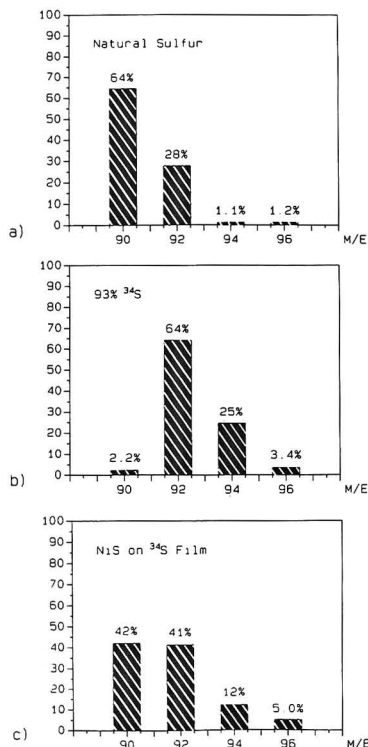
Figure 4. Isotope ratios for cluster ions  $\text{NiS}^+$ ,  $\text{NiS}_2^+$ , and  $\text{Ni}_2\text{S}^+$  from NIS (dotted bar, 19 spectra) and NIS on  $^{34}\text{S}$  (solid bar, 20 spectra) compared with predicted values based on natural nickel and sulfur abundances (hatched bar). Standard deviations of the mean,  $s/\sqrt{n}$ , where  $n$  is the number of spectra averaged, are as follows: for  $\text{NiS}^+$ , NIS 0.016, NIS on  $^{34}\text{S}$  0.072; for  $\text{NiS}_2^+$ , NIS 0.030, NIS on  $^{34}\text{S}$  0.12; for  $\text{Ni}_2\text{S}^+$ , NIS 0.022, NIS on  $^{34}\text{S}$  0.061.

amination of these differences follows.

Isotope ratios from the spectra obtained from each sample were calculated for the  $\text{NiS}^+$  (92, 90),  $\text{NiS}_2^+$  (124, 122), and  $\text{Ni}_2\text{S}^+$  (150, 148) cluster ions. The peak areas for the cluster ion  $\text{NiS}_2^+$  were corrected for the isobaric interference  $\text{Ni}_2^+$ . The average isotope ratios are compared in Figure 4 with the predicted values based on the natural isotopic abundances. The isotope combinations which contribute to the peaks of interest are presented in Table I. For NIS, the average experimental isotope ratios are within 6% of the predicted natural abundance values and therefore provide an estimate

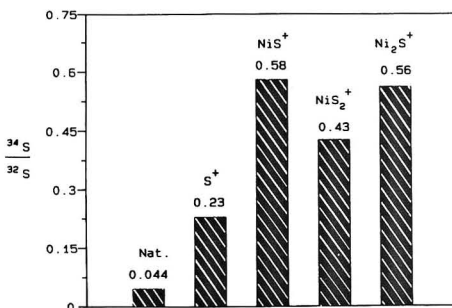
**Table I. Nickel and Sulfur Isotope Combinations Which Contribute to the Cluster Ion Peaks of Interest**

$\text{NiS}^+$	mass 90	$^{58}\text{Ni}^{32}\text{S}$
	mass 92	$^{58}\text{Ni}^{34}\text{S}$ , $^{60}\text{Ni}^{32}\text{S}$
$\text{NiS}_2^+$	mass 122	$^{58}\text{Ni}^{32}\text{S}_2$
	mass 124	$^{58}\text{Ni}^{32}\text{S}_2$ , $^{58}\text{Ni}^{33}\text{S}_2$ , $^{60}\text{Ni}^{32}\text{S}_2$
$\text{Ni}_2\text{S}^+$	mass 148	$^{58}\text{Ni}^{58}\text{Ni}^{32}\text{S}$
	mass 150	$^{58}\text{Ni}^{58}\text{Ni}^{34}\text{S}$ , $^{58}\text{Ni}^{60}\text{Ni}^{32}\text{S}$

**Figure 5.** Relative peak intensities for the  $\text{NiS}^+$  cluster ion: (a) nickel and sulfur present in their natural abundances; (b) sulfur present as 93%  $^{34}\text{S}$ ; (c) experimental intensities,  $\text{NiS}$  on  $^{34}\text{S}$ , average of 19 spectra. Isotopic contributions are as follows:  $m/z$  90 ( $^{58}\text{Ni}^{32}\text{S}$ ),  $m/z$  92 ( $^{58}\text{Ni}^{34}\text{S}$ ,  $^{60}\text{Ni}^{32}\text{S}$ ),  $m/z$  94 ( $^{60}\text{Ni}^{34}\text{S}$ ,  $^{58}\text{Ni}^{32}\text{S}_2$ ),  $m/z$  96 ( $^{60}\text{Ni}^{34}\text{S}$ ,  $^{58}\text{Ni}^{32}\text{S}_2$ ).

of the measurement error for comparison of the data from  $\text{NiS}$  on  $^{34}\text{S}$ . For  $\text{NiS}$  on  $^{34}\text{S}$ , these same ratios deviate positively by more than 60% from the predicted natural abundance values. This clearly demonstrates the presence of excess  $^{34}\text{S}$  in the cluster ion peak integrals.

Figure 5 summarizes data from  $\text{NiS}$  on  $^{34}\text{S}$  using the  $\text{NiS}^+$  cluster ion as an example. Figure 5a illustrates the relative peak intensities for  $\text{NiS}^+$  at  $m/z$  90, 92, 94, and 96 provided that nickel and sulfur are present in their natural abundances. At the other extreme, Figure 5b shows the relative peak intensities for these same masses under the assumption that the  $\text{NiS}^+$  cluster ion contains 93%  $^{34}\text{S}$ , i.e., essentially all of the  $\text{NiS}^+$  forms via contributions from the  $^{34}\text{S}$  film. The relative intensities obtained from the average of the 19 spectra from  $\text{NiS}$  on  $^{34}\text{S}$  are presented in Figure 5c. The intensities in Figure 5c lie between the extremes of parts a and b of Figure 5 suggesting that  $^{34}\text{S}$  from the isotopically enriched  $^{34}\text{S}$  film

**Figure 6.** Sulfur ratios calculated from atomic and cluster ion peak areas obtained from  $\text{NiS}$  on  $^{34}\text{S}$  film, average of 19 spectra. Standard deviations of the mean,  $s/\sqrt{n}$ , where  $n$  is the number of spectra averaged, are as follows:  $\text{S}^+$ , 0.042;  $\text{NiS}^+$ , 0.072;  $\text{NiS}_2^+$ , 0.060;  $\text{Ni}_2\text{S}^+$ , 0.061.

is recombining with nickel from the  $\text{NiS}$  particle, to a significant extent in the laser-induced plasma, to form the  $\text{NiS}^+$  ion. The fact that the experimental intensity at  $m/z$  96 (Figure 5c) does not lie between the values of natural sulfur and 93%  $^{34}\text{S}$  is attributed to the inherent measurement error of the instrument as described earlier.

From this experiment, it is difficult to exclude solid-state diffusion as a mixing mechanism; data are not available for elemental sulfur diffusing into  $\text{NiS}$ . Significant diffusion is unlikely to have occurred at room temperature during the short time that the sample was stored prior to analysis. In addition, the extent of diffusion during the  $\leq 15$ -ns laser pulse event is difficult to assess because the temperature that the sample achieved prior to ablation is unknown. The observation of  $\text{Ni}_2\text{S}_2$  cluster ion formation by recombination, however, has also been observed from laser ablation of a sandwich sample in which elemental sulfur and nickel layers were separated by a film of elemental gold (31).

Ratios of  $^{34}\text{S}/^{32}\text{S}$  for the atomic sulfur ion (34, 32) and the cluster ions  $\text{NiS}^+$  (92, 90),  $\text{NiS}_2^+$  (124, 122), and  $\text{Ni}_2\text{S}^+$  (150, 148), from the spectra of  $\text{NiS}$  on  $^{34}\text{S}$  are reported in Figure 6 and each may be compared with the natural  $^{34}\text{S}/^{32}\text{S}$  ratio of 0.044. The  $^{34}\text{S}$  is highly enhanced in both the atomic and cluster ions relative to the natural abundance value but is significantly more enriched in the various cluster ion peaks. There is no reason to assume, however, that the ratio of  $\text{S}^0/\text{S}^+$  is the same for ion formation out of  $\text{NiS}$  as compared with the enriched  $^{34}\text{S}$  film. The ratio of  $^{34}\text{S}/^{32}\text{S}$  may therefore not necessarily be reflected in the corresponding isotope ratio of each of the cluster ions. This difference may also suggest that more  $^{34}\text{S}$  from the film is present in the periphery of the plasma where gas-phase reactions to form clusters are more favored than in the more energetic plasma center where atomic ions are preferentially formed (3-5). It is consistent with the fact that the laser perforation usually encompasses a greater area (2-3  $\mu\text{m}$  diameter) than a typical  $\text{NiS}$  particle occupies (1  $\mu\text{m}$  diameter). Thus, the edges of the vaporized sample area would contain almost exclusively  $^{34}\text{S}$ . The lower laser power density at the periphery of the perforation should contribute to a greater production of neutral, relative to charged,  $^{34}\text{S}$  atoms as well as to a greater probability of direct emission of  $^{34}\text{S}_2$  clusters. On the basis of differences in ionization potential, it is likely that a major contribution to recombination ions is the cationization of neutral  $^{34}\text{S}$ -containing species from the film by  $\text{Ni}^+$  produced from the particles. The  $^{34}\text{S}/^{32}\text{S}$  ratio from the three cluster ions varies by much less than a factor of 2 (Figure 6) suggesting that the recombination process occurs to a similar extent in the for-

Table II. Ratios of  $^{34}\text{S}/^{32}\text{S}$  for Ions Obtained in Two Sample Orientations

ratio	$^{34}\text{S}$ film facing optics	NiS particle facing optics
$\text{NiS}^+/\text{S}^+$	2.52	3.43
$\text{NiS}_2^+/\text{S}^+$	1.87	1.83
$\text{Ni}_2\text{S}^+/\text{S}^+$	2.43	3.28

Table III. Ratio of Sulfur Isotopes Compared with Analogous Ratios Containing One  $^{58}\text{Ni}$  Atom

ratio	experiment (expt)	natural abundance (nat)	expt/nat
1. $^{34}\text{S}/^{32}\text{S}$	$x = 0.228$ $s/\sqrt{16} = 0.0418^a$	0.0444	5.14
$^{58}\text{Ni}^{34}\text{S}/^{58}\text{Ni}^{32}\text{S}^b$	$x = 0.580$ $s/\sqrt{19} = 0.0718$	0.0444	13.1
2. $^{32}\text{S}^{34}\text{S}/^{32}\text{S}^{32}\text{S}^c$	$x = 0.700$ $s/\sqrt{15} = 0.132$	0.0888	7.88
$^{58}\text{Ni}^{32}\text{S}^{34}\text{S}/^{58}\text{Ni}^{32}\text{S}^{32}\text{S}^d$	$x = 0.851$ $s/\sqrt{19} = 0.120$	0.0888	9.58
3. $^{34}\text{S}^{34}\text{S}/^{32}\text{S}^{32}\text{S}^e$	$x = 0.902$ $s/\sqrt{14} = 0.219$	0.00197	458
$^{58}\text{Ni}^{34}\text{S}^{34}\text{S}/^{58}\text{Ni}^{32}\text{S}^{32}\text{S}^f$	$x = 1.05$ $s/\sqrt{19} = 0.162$	0.00197	533

<sup>a</sup> Standard deviation of the mean,  $s/\sqrt{n}$ , where  $n$  is the number of spectra averaged. <sup>b</sup>  $m/z$  92 corrected for  $^{60}\text{Ni}^{32}\text{S}$ . <sup>c</sup>  $m/z$  64 corrected for  $^{60}\text{Ni}$ . <sup>d</sup>  $m/z$  122, 124 corrected for  $\text{Ni}_2$ ,  $m/z$  124 corrected for  $^{60}\text{Ni}^{32}\text{S}$ . <sup>e</sup>  $m/z$  64 corrected for  $^{60}\text{Ni}$ . <sup>f</sup>  $m/z$  122 corrected for  $\text{Ni}_2$ ,  $\text{Ni}_2$  contribution at  $m/z$  126 is negligible,  $m/z$  126 corrected for  $^{60}\text{Ni}^{32}\text{S}^{34}\text{S}$  and  $^{62}\text{Ni}^{32}\text{S}$ .

mation of the three cluster ions  $\text{NiS}^+$  (92, 90),  $\text{NiS}_2^+$  (124, 122), and  $\text{Ni}_2\text{S}^+$  (150, 148). In the case of  $\text{NiS}_2^+$ , this refers to the inclusion of one  $^{34}\text{S}$  atom in the cluster, i.e.  $^{58}\text{Ni}^{32}\text{S}^{34}\text{S}$ .

The variation in the concentration or charge state of various  $^{34}\text{S}$ -containing species in the laser-induced plasma may also reflect a gradation of laser power density with depth into the sample as a result of positional differences of the NiS particle and the  $^{34}\text{S}$  film with respect to laser focus. If such were the case, data obtained with the sample in the alternative orientation should indicate that difference. The same calculations as above were performed on the data set from a second experiment in which 20 spectra were obtained from NiS and from NiS on  $^{34}\text{S}$  with the samples mounted in the alternative orientation, i.e. the NiS particles faced the extraction optics. The  $^{34}\text{S}$  component to the cluster ions is a factor of 2 higher in this orientation which could imply that the  $^{34}\text{S}$  film experiences a higher laser power density. The relative abundances of the cluster ions, however, are very similar in both orientations (Table II). The variation of laser power density with depth, therefore, does not appear to be the controlling factor in cluster ion formation.

Further insight into possible formation mechanisms for the nickel/sulfur cluster ions can be gained from additional ratio calculations performed on the first data set taken from NiS on  $^{34}\text{S}$ . The average values of these ratios are compared in Tables III and IV with ratios calculated by using natural sulfur and nickel isotope abundances. Ratios of experimental to natural abundances are presented in the tables to ease the comparison. These ratios have been corrected for the presence of other combinations of isotopes at the same nominal mass as indicated in the tables.

Table III is divided into three sets of ratio pairs. Within each pair, a ratio of sulfur isotopes is compared with an analogous ratio containing one  $^{58}\text{Ni}$  atom. The ratio values within each pair differ at most by a factor of 3. This agreement indicates that the relative contributions of sulfur species

Table IV. Ratios of  $^{34}\text{S}/^{32}\text{S}$  for Ions Containing from Zero to Three  $^{58}\text{Ni}$  Atoms

ratio	experiment (expt)	natural abundance (nat)	expt/nat
1. $^{34}\text{S}/^{32}\text{S}$	$x = 0.228$ $s/\sqrt{16} = 0.0418^a$	0.0444	5.14
2. $^{58}\text{Ni}^{34}\text{S}/^{58}\text{Ni}^{32}\text{S}^b$	$x = 0.580$ $s/\sqrt{19} = 0.0718$	0.0444	13.1
3. $^{58}\text{Ni}^{58}\text{Ni}^{34}\text{S}/^{58}\text{Ni}^{58}\text{Ni}^{32}\text{S}^c$	$x = 0.561$ $s/\sqrt{19} = 0.0613$	0.0444	12.6
4. $^{58}\text{Ni}^{58}\text{Ni}^{58}\text{Ni}^{34}\text{S}/^{58}\text{Ni}^{58}\text{Ni}^{58}\text{Ni}^{32}\text{S}^d$	$x = 0.895$ $s/\sqrt{16} = 0.173$	0.0444	20.2

<sup>a</sup> Standard deviation of the mean,  $s/\sqrt{n}$ , where  $n$  is the number of spectra averaged. <sup>b</sup>  $m/z$  92 corrected for  $^{60}\text{Ni}^{32}\text{S}$ . <sup>c</sup>  $m/z$  150 corrected for  $^{58}\text{Ni}^{60}\text{Ni}^{32}\text{S}$ . <sup>d</sup>  $m/z$  208 corrected for  $^{58}\text{Ni}^{58}\text{Ni}^{60}\text{Ni}^{32}\text{S}$ .

(charged or neutral) that react with a nickel atom (charged or neutral) to form the corresponding clusters  $\text{NiS}_x^+$  ( $^{58}\text{Ni}^{32}\text{S}^+$ ,  $^{58}\text{Ni}^{34}\text{S}^+$ ,  $^{58}\text{Ni}^{32}\text{S}^{32}\text{S}^+$ ,  $^{58}\text{Ni}^{32}\text{S}^{34}\text{S}^+$ ,  $^{58}\text{Ni}^{34}\text{S}^{34}\text{S}^+$ ) reflect the respective ion intensities of  $\text{S}_x^+$  ( $^{32}\text{S}^+$ ,  $^{34}\text{S}^+$ ,  $^{32}\text{S}^{32}\text{S}^+$ ,  $^{32}\text{S}^{34}\text{S}^+$ ,  $^{34}\text{S}^{34}\text{S}^+$ ). The ratios of experimental to natural abundances for the clusters shown in Table III are all larger than one, thus offering another indication of the contribution from ion recombination. The values are similar for pairs 1 and 2, indicating comparable contributions from ion recombination reactions involving sulfur from the  $^{34}\text{S}$  film. However, the ratio of experimental to natural abundance is greatly enhanced for case 3 in Table III. This suggests that the  $^{58}\text{Ni}^{34}\text{S}^{34}\text{S}^+$  cluster has a much larger contribution from recombination reactions involving the  $^{34}\text{S}$  film, a likely consequence of  $^{34}\text{S}^{34}\text{S}$  dimer production dominated by  $^{34}\text{S}$  atoms originating from the film. Such  $^{34}\text{S}^{34}\text{S}$  species could be produced by direct emission from the film or by the recombination of two  $^{34}\text{S}$  atoms, especially in the periphery of the plasma where  $^{34}\text{S}$  species are apparently more abundant relative to  $^{32}\text{S}$  as described earlier. If the  $^{58}\text{Ni}^{34}\text{S}^{34}\text{S}^+$  ion is formed primarily by recombination in the plasma, however, one would expect the experimental to natural ratio in case 3 to equal the square of the experimental to natural ratios in cases 1 and 2 reflecting the gas-phase concentration of atomic  $^{32}\text{S}$  and  $^{34}\text{S}$ . The ratio in case 3 is far in excess of this prediction suggesting that the formation of the  $^{58}\text{Ni}^{34}\text{S}^{34}\text{S}^+$  ion depends primarily on the production of the  $^{34}\text{S}^{34}\text{S}$  dimer from the film by direct emission, followed by reaction with  $^{58}\text{Ni}$  in the laser-induced plasma. This one event recombination mechanism is also favored based on collisional probabilities. Cationization of the neutral sulfur dimer by  $\text{Ni}^+$  is an obvious mechanistic possibility.

In Table IV, the  $^{34}\text{S}/^{32}\text{S}$  ratio is compared for ions containing from zero to three  $^{58}\text{Ni}$  atoms. The experimental to natural ratios in Table IV are again greater than 1 indicating the occurrence of recombination. These ratios exhibit a relatively constant contribution of  $^{34}\text{S}$ , the ratios differing at most by a factor of 2 for the clusters, which suggests that formation of these cluster ions is controlled by reaction of  $\text{Ni}_x^+$  with a sulfur atom roughly in proportion to the gas phase concentration of the sulfur isotopes (reflected in the intensity ratio of  $^{34}\text{S}/^{32}\text{S}$ ). There is no evidence of a greater probability or direct emission of specific clusters from the particles; i.e.  $\text{NiS}^+$  has a very similar  $^{34}\text{S}$  enrichment to  $\text{Ni}_2\text{S}^+$  and  $\text{Ni}_3\text{S}^+$ .

## CONCLUSION

We have demonstrated in a previous study that particulate nickel species may be differentiated by the LAMMA using their unique cluster ion fingerprint spectra (21). This study, however, shows that ion/molecule recombination reactions do indeed occur in the laser-induced plasma in the formation of these unique cluster ions. Therefore, caution is necessary

when assigning molecular structures from particle spectra which exhibit cluster ions that may not be directly representative of the bonds which exist in the solid state. A complication of this study is that all of the cluster ions observed may have contributions from both direct emission and recombination. Additional experiments of ion formation as a function of sample geometry, laser power density, and ion lens potential have been conducted in which only recombination is possible, e.g., Ni/Au/S sandwich films for which  $\text{Ni}_2\text{S}_2^+$  reflected only recombination mechanisms in the plasma (31).

### ACKNOWLEDGMENT

We wish to thank W. R. Kelly of the National Bureau of Standards for providing the  $^{34}\text{S}$  powder used to make the sputtered thin film and Frank Butler of the U.S. Environmental Protection Agency for his support of this project.

### LITERATURE CITED

- (1) Conzemius, R. J.; Capellen, J. M. *Int. J. Mass Spectrom. Ion Processes* **1980**, *34*, 197-271.
- (2) Conzemius, R. J.; Simons, D. S.; Shankai, Z.; Byrd, G. D. In *Microbeam Analysis*; Goooley, R., Ed.; San Francisco Press: San Francisco, CA, 1983; pp 301-332.
- (3) Hercules, D. M.; Day, R. J.; Balasanmugam, K.; Dang, T. A.; Li, C. P. *Anal. Chem.* **1982**, *54*, 280A-305A.
- (4) Novak, F. P.; Balasanmugam, K.; Viswanadham, K.; Parker, C. D.; Wilk, Z. A.; Mattern, D.; Hercules, D. M. *Int. J. Mass Spectrom. Ion Phys.* **1983**, *53*, 135-149.
- (5) Hercules, D. M. *Pure Appl. Chem.* **1983**, *55*, 1869-1885.
- (6) Hillenkamp, F. In *Ion Formation from Organic Solids*; Benninghoven, A., Ed.; Springer-Verlag: Berlin, 1983; pp 190-205.
- (7) Furstenau, N. *Fresenius' Z. Anal. Chem.* **1981**, *308*, 201-205.
- (8) Michiels, E.; Celis, A.; Gijbels, R. *Int. J. Mass Spectrom. Ion Phys.* **1983**, *47*, 23-26.
- (9) Furstenau, N.; Hillenkamp, F.; Nitsche, R. *Int. J. Mass Spectrom. Ion Phys.* **1979**, *31*, 85-91.
- (10) Furstenau, N.; Hillenkamp, F. *Int. J. Mass Spectrom. Ion Phys.* **1981**, *37*, 135-151.
- (11) Michiels, E.; Gijbels, R. *Anal. Chem.* **1984**, *56*, 1115-1121.
- (12) Dang, T. A.; Day R. J.; Hercules, D. M. *Anal. Chim. Acta* **1984**, *158*, 235-246.
- (13) Salvati, L., Jr.; Hercules, D. M. *Spectrosc. Lett.* **1980**, *13*, 243-251.
- (14) Michiels, E.; Gijbels, R. *Spectrochim. Acta, Part B* **1983**, *38B*, 1347-1354.
- (15) Bruynseels, F. J.; Van Grieken, R. E. *Anal. Chem.* **1984**, *56*, 871-873.
- (16) Marien, J.; De Pauw, E. *Anal. Chem.* **1985**, *57*, 361-362.
- (17) Bruynseels, F. J.; Van Grieken, R. E. *Spectrochim. Acta, Part B* **1983**, *38B*, 853-858.
- (18) Wurster, R.; Haas, U.; Wieser, P. *Fresenius' Z. Anal. Chem.* **1981**, *308*, 206-211.
- (19) Benninghoven, A.; Anders, V. The Ionization of Organic Molecules in LAMMA and SIMS, A Comparison. LAMMA Workshop, Forschungsinstitut Borstel, Sept 1-2, 1983, Leybold-Heraeus GMBH.
- (20) Bruynseels, F. J.; Van Grieken, R. E. *Int. J. Mass Spectrom. Ion Processes* **1986**, *74*, 161-177.
- (21) Musselman, I. H.; Linton, R. W.; Simons, D. S. In *Microbeam Analysis*; Armstrong, J. T., Ed.; San Francisco Press: San Francisco, CA, 1985; pp 337-341.
- (22) Musselman, I. H.; Rickman, J. T.; Linton, R. W. In *Microbeam Analysis*; Geiss, R. H., Ed.; San Francisco Press: San Francisco, CA, 1987; pp 361-364.
- (23) Musselman, I. H.; Rickman, J. T.; Linton, R. W.; Butler, F. E., to be submitted for publication in *Environ. Sci. Technol.*
- (24) Vogt, H.; Heinen, H. J.; Meier, S.; Wechsung, R. *Fresenius' Z. Anal. Chem.* **1981**, *308*, 195-200.
- (25) Denoyer, E.; Van Grieken, R.; Adams, F.; Natusch, D. F. S. *Anal. Chem.* **1982**, *54*, 26A-32A.
- (26) Kaufmann, R.; Wieser, P. In *Particle Characterization in Technology*; Beddow, J., Ed.; CRC Press: Boca Raton, FL; 1984, pp 21-57.
- (27) Holden, N. E.; Martin, R. L.; Barnes, I. L. *Pure Appl. Chem.* **1984**, *56*, 675-694.
- (28) Mauney, T.; Adams, F. *Int. J. Mass Spectrom. Ion Processes* **1984**, *59*, 103-119.
- (29) Michiels, E.; Mauney, T.; Adams, F.; Gijbels, R. *Int. J. Mass Spectrom. Ion Processes* **1984**, *61*, 231-246.
- (30) Michiels, E.; De Wolf, M.; Gijbels, R. *Scanning Electron Microsc.* **1985**, *III*, 847-958.
- (31) Linton, R. W.; Musselman, I. H.; Bruynseels, F.; Simons, D. S. In *Microbeam Analysis*; Geiss, R. H., Ed.; San Francisco Press: San Francisco, CA, 1987; pp 365-368.

RECEIVED for review April 6, 1987. Accepted September 9, 1987. Support of this research under U.S. Environmental Protection Agency (EPA) Cooperative Agreement CR-812908-01-1 is gratefully acknowledged. Although the research described in this article has been funded in part by the EPA, it has not been subjected to agency review. Therefore, it does not necessarily reflect the views of the agency and no official endorsement should be inferred. Certain commercial equipment, instruments, or materials are identified in this paper. Such identification does not imply recommendation or endorsement by the National Bureau of Standards, nor does it imply that the materials or equipment are necessarily the best available for the purpose. Portions of this work were presented at the 1987 Pittsburgh Conference and Exposition on Analytical Chemistry and Applied Spectroscopy, Atlantic City, NJ.



# Determination of Dihydroqinghaosu in Blood by Pyrolysis Gas Chromatography/Mass Spectrometry

Anthony D. Theoharides,\* Michael H. Smyth, Robert W. Ashmore, James M. Halverson, Zhong Ming Zhou,<sup>1</sup> William E. Ridder, and Ai Jeng Lin

Department of Pharmacology, Division of Experimental Therapeutics, Walter Reed Army Institute of Research, Washington, D.C. 20307-5100

**A sensitive and specific method using packed or capillary column gas chromatography/mass spectrometry (GC/MS) has been developed for the quantitation of the major active metabolite dihydroqinghaosu (DQHS) of the antimalarial drug artesunic acid in blood. Quantification is achieved with an internal standard method, petroleum ether or *n*-butyl chloride extraction of blood and gas chromatography/mass spectrometry analysis of the extract with selected ion monitoring. Since DQHS is thermally unstable, the method is based on the observations that at high injector temperature and specific GC conditions, DQHS is pyrolyzed to (2*S*,3*R*,6*R*)-2-(3-oxobutyl)-3-methyl-6-[(*R*)-2-propanal]cyclohexanone. Quantitation of this cyclohexanone pyrolysis product by GC/MS with selected ion monitoring precisely and accurately reflects DQHS blood levels and calibration curves are linear in the range of 10–1000 ng/mL. The method is currently being used for pharmacokinetic and metabolism studies in animals.**

Over the last 12 years, the active antimalarial principal of the Chinese herb qinghao (*Artemisia annua* L.) has been isolated and chemically characterized (1–4). This compound, a unique 15-carbon sesquiterpene lactone endoperoxide (Figure 1) named qinghaosu (QHS) or artemisinin, and its synthetic derivatives have been shown to be more effective than chloroquine against the erythrocytic stages of plasmodia; their parasitocidal action is faster, and they are equally effective against chloroquine-resistant strains of parasites (5). In recent years, over 2000 cases of vivax or falciparum malaria have been treated with QHS or its derivatives in China with excellent results (6). No toxic side effects were observed in these studies (6), and it has been reported that QHS and its derivatives are superior to chloroquine in chemotherapeutic index, margin of safety, and side effects (7). Furthermore, it has been shown that QHS and its derivatives are extremely effective in the treatment of cerebral malaria (8). A comprehensive review on the chemistry and some of the pharmacological properties of artemisinin and its analogues was recently published by Klayman (9).

Previous studies on the pharmacokinetics of artesunic acid (ARTA) (Figure 1) after intravenous administration of the sodium salt suggested that ARTA is rapidly hydrolyzed to dihydroqinghaosu (DQHS) in rats (10), therefore, DQHS was measured rather than ARTA. DQHS was measured by thin-layer chromatography (TLC), staining with *p*-(dimethylamino)benzaldehyde. The sensitivity of the method was reported to be 0.5 µg (10). Considering the low dose of ARTA administered to humans, the poor sensitivity and lack of specificity of the TLC method, and the fact that little is known about the pharmacokinetics of ARTA and DQHS in

the therapeutic range, our laboratory sought to develop new specific and sensitive methodologies to accurately measure DQHS in blood in the nanogram per milliliter range. Since ARTA and DQHS have no UV-vis or fluorescence properties, our efforts were focused on developing suitable gas chromatography/mass spectrometry (GC/MS) techniques for the quantitation of DQHS in blood. Initial experiments demonstrated that DQHS is thermally unstable and is degraded to two major and a number of minor compounds during GC/MS. The structural identification of these two major pyrolysis products has been determined (11) (see Figure 2). Other experiments also showed that the relative formation of these two major pyrolysis products is dependent on the conditions of chromatography and that suitable chromatographic conditions can be utilized such that only one major pyrolysis product of DQHS is formed during GC/MS (>90%). In this paper, the results on the development and validation of packed and capillary column gas chromatographic methodologies are described in which DQHS is pyrolyzed in the GC injector to one major degradation product such that accurate and precise quantitation of DQHS in blood can be achieved in the low nanogram per milliliter range. We also demonstrate the utility of the developed methods in measuring blood levels of DQHS after *in vivo* administration of ARTA to rabbits and dogs.

## EXPERIMENTAL SECTION

**Chemicals and Supplies.** Artesunic acid and dihydroqinghaosu were provided by the Institute of Chinese Materia Medica, Academy of Traditional Chinese Medicine, Beijing, China. Cedrol and triphenylmethanol (internal standards) were obtained from Aldrich Chemical Co. (Milwaukee, WI) and Eastman Organic Chemicals (Rochester, NY), respectively. Petroleum ether was purchased from Mallinckrodt, Inc. (Paris, KY), and ethyl acetate, *n*-butyl chloride, and methyl *tert*-butyl ether were purchased from Burdick and Jackson (Muskegon, MI). Fused silica capillary columns (15-m SPB-1 and 15-m SPB-5, 0.25-mm film thickness, 0.25 mm i.d.) and 3% OV-3, 3% OV-17, or 3% SP-2100 on 100/120 Supelcoport for packed column studies were purchased from Supelco, Inc. (Bellafonte, PA). The dry solids injector used for capillary column studies was purchased from Allen Scientific (Boulder, CO).

**Gas Chromatography/Mass Spectrometry.** GC/MS was performed with a Varian Vista gas chromatograph (GC) (Palo Alto, CA) interfaced to a Nermag R10-10C quadrupole mass spectrometer (Delsi Nermag, Fairfield, NJ). The mass spectrometer was interfaced to an INCOS data system (Finnigan Corp., Sunnyvale, CA). Packed column GC was performed with 6 ft × 2 mm i.d. silanized glass columns using either helium or methane as carrier gas at a flow rate of 20 mL/min (measured at atmospheric pressure at column outlet). A 1000 L/s diffusion pump on the source region of this instrument permits packed column GC without carrier gas splitting; therefore, the effluent from the GC was plumbed directly to the ion source with a 2 ft length of fused silica tubing. For capillary column GC, split/splitless, on-column, or dry solids injection techniques were utilized with helium as carrier gas at a flow rate of 40 cm/s. The outlet of the capillary column was plumbed directly to the ion source. EI or CI mass spectrometry was performed at 70 and 90 eV, respectively, and 130 °C source temperature. Methane or isobutane were used

<sup>1</sup> Permanent address: Department of Pharmacology, Institute of Chinese Materia Medica, Academy of Traditional Chinese Medicine, Beijing, China 100700.

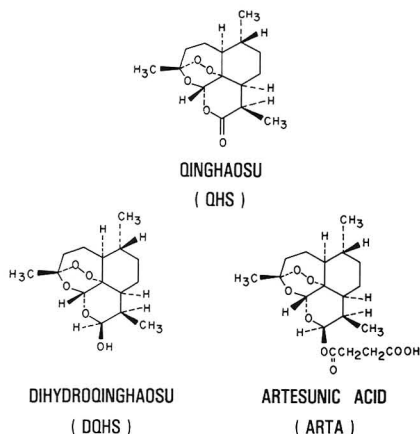


**Figure 1.** Structures of qinghaosu (QHS), dihydroqinghaosu (DQHS), and artesunic acid (ARTA).

as reagent gases for CI at a source pressure of 0.25 Torr for capillary and 0.4 Torr for packed column gas chromatography.

**Quantitation of DQHS by GC/MS with Selected Ion Monitoring.** Detection and quantitation of DQHS and internal standard were achieved by monitoring the intensity of  $m/z$  221.3  $\pm$  0.5 amu under methane CI conditions for method 1 or 221.3  $\pm$  0.5, 239.3  $\pm$  0.5, and 243.3  $\pm$  0.5 amu for method 2. Packed column GC was performed with a 6 ft  $\times$  2 mm i.d. silanized glass column packed with 3% OV-3 on 100/120 Supelcoport (Supelco). Conditions of GC were as follows: injector, 320  $^{\circ}$ C; interface, 240  $^{\circ}$ C; carrier gas,  $\text{CH}_4$  (20 mL/min). A temperature gradient run from 160 to 240  $^{\circ}$ C at 10  $^{\circ}$ C/min was utilized to elute internal standard (cedrol, method 1) (retention time, 3.2 min) and the cyclohexanone pyrolysis product of DQHS (retention time 5.5 min). Capillary column GC was performed with a 15-m SPB-5 fused silica column connected to a dry solids falling needle injector. Conditions of GC were as follows: injector, 320  $^{\circ}$ C; carrier gas, He (40 cm/s); interface, 240  $^{\circ}$ C; system was run from 100 to 200  $^{\circ}$ C at 10  $^{\circ}$ C/min to elute compounds of interest.

Quantitation of DQHS in blood was achieved by using peak height ratios of the cyclohexanone pyrolysis product of DQHS to internal standard (cedrol or triphenylmethanol). For each analysis, a standard curve was generated by adding known and varying amounts of DQHS and a constant amount of the internal standard (500 or 1000 ng for high range and 100 ng for low range, method 1; 20 ng, method 2). Spiked samples were treated as unknowns to evaluate the precision and accuracy of the methods.

**Standard Solutions.** All standard stock solutions of DQHS (10 ng/ $\mu\text{L}$ , 1 ng/ $\mu\text{L}$ , 100 pg/ $\mu\text{L}$ ) and internal standard, cedrol or triphenylmethanol (10, 1, 0.1 ng/ $\mu\text{L}$ ), were prepared fresh daily and dissolved in HPLC grade methyl *tert*-butyl ether or ethyl acetate.

**Extraction Procedure for DQHS. Method 1.** To disposable glass extraction tubes (16  $\times$  125 mm) previously washed with 3 mL of methyl *tert*-butyl ether, were added various amounts of DQHS and cedrol. Solvent was evaporated with a Buchler vortex evaporator and then 1 mL of heparinized (10 IU/mL) human blood was added to each sample. Samples were vortexed and then kept at room temperature for 15–20 min. Four milliliters of petroleum ether was added to each sample; samples were then vortexed for 30 s each and centrifuged at 2500g for 5 min. The upper organic phase was removed and transferred to clean extraction tubes. An additional 4 mL of petroleum ether was added to the aqueous sample, and the above procedure was repeated. The petroleum ether extracts were combined and evaporated to dryness at room temperature with a Buchler vortex evaporator. The dry residues were reconstituted in 100  $\mu\text{L}$  of ethyl acetate for GC/MS analysis with selected ion monitoring (GC/SIM). By use of external standards, extraction recoveries of DQHS and cedrol were 20–60% and 60–80%, respectively.

The pronounced variability in the extraction efficiency of DQHS was due to decreased recovery at low blood levels of DQHS (less than 50 ng/mL), whereas recoveries in the 100–1000 ng/mL range were 55–65%. This dependence of the extraction efficiency on the amount of DQHS present in blood was always consistent and was corrected for by the internal standards ratio method. As shown in Tables I and II, standard curves with this method showed good correlation to a linear equation.

During the development of the extraction methodologies, many different types of solvents (*tert*-butyl ether, diethyl ether, methylene chloride, ethyl acetate, hexane) and mixtures of these solvents were tested in an attempt to improve the extraction efficiency of the method. Initial experiments showed that these solvents were found to be unsatisfactory because of poor recovery or because the extracts were heavily contaminated with endogenous blood constituents. Additional experiments designed to study the utility of protein precipitation followed by liquid-liquid or liquid-solid extraction also failed for the same reasons.

Although the extraction efficiency with petroleum ether is poor, we chose to validate the method using this solvent for extraction, in order to initiate animal pharmacokinetic studies and, at the same time, continue studies to improve the specificity and recovery of the initial extraction step.

Additional detailed observations of the characteristics of the method and performance of the procedures by different analysts demonstrated that the internal standard, cedrol, slowly sublimed from the dry solids injector needle (60% in 30 min) and that linear standard curves and reproducible results with this internal standard could only be obtained if the sample was injected shortly after solvent evaporation from the needle (less than 2 min).

**Method 2.** This extraction procedure is identical with that described in method 1 except that triphenylmethanol was used as the internal standard, and the extraction was performed with *n*-butyl chloride rather than petroleum ether. Recoveries for DQHS and triphenylmethanol were 76  $\pm$  12% and 100  $\pm$  15%, respectively, with this method.

Since a major pyrolysis product of ARTA on GC is the same cyclohexanone pyrolysis product formed from DQHS, some experiments were performed in which blood was spiked with ARTA (1  $\mu\text{g/mL}$ ) and cedrol or ARTA and triphenylmethanol, and then samples were extracted with petroleum ether or *n*-butyl chloride and analyzed as described above. The results demonstrated that less than 0.1% of the spiked ARTA was extracted and measured as the cyclohexanone pyrolysis product. These results prove that the presence of ARTA in blood does not affect the quantitation of DQHS, since ARTA is not extracted from blood with petroleum ether or *n*-butyl chloride under these conditions.

**In Vivo Infusion and Sampling Methodologies.** All animal studies were conducted by using approved protocols in compliance with all DoD regulations and the NIH Publication, 85-23, *Guide for the Care and Use of Laboratory Animals*. Animals were housed in standard cages and given food (Rabbit Chow, Dog Lab Diet, Ralston Purina, St. Louis, MO) and tap water ad libitum. All animals were in a fed state at the time of study. Initial experiments to determine the feasibility and utility of the developed methodologies were with New Zealand white rabbits, male, weighing 2–3 kg. Each animal was restrained in a nalgene restraint cage during the 2-h study period. Repeated blood sampling was accomplished by using the medial artery of one ear by the method of Paulsen and Valentine (12). Drug at a dose of 5 mg/kg was administered as a bolus injection into the marginal ear vein of the opposite ear. The drug, the sodium salt of ARTA, was prepared by dissolving ARTA in sterile 3.5% sodium bicarbonate (Gibco Laboratories, Grand Island, NY) at a concentration of 200 mg/mL. Healthy, manually restrained, and awake male beagle dogs (9.3 and 10.4 kg) were also used to study DQHS pharmacokinetics after intravenous administration of ARTA. An indwelling pediatric, disposable intravenous catheter with a 23-gauge needle was aseptically placed into the cephalic vein of one of the forelegs for blood sampling. Patency of this catheter was maintained by instilling a volume of saline containing 30 units/mL of heparin.

Blood samples were drawn into heparinized-rinsed (30 units/mL of saline) 3-cm<sup>3</sup> syringes after withdrawing the heparinized saline and approximately a half milliliter of blood into a separate syringe. The cephalic vein of the opposite leg was used to ad-

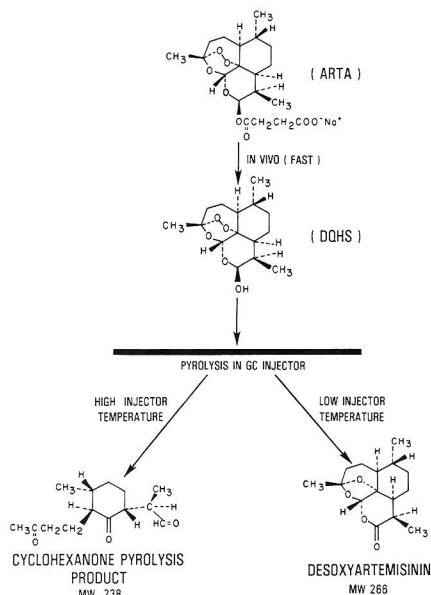


**Figure 2.** Reaction scheme of in vivo hydrolysis of sodium artesunate to dihydroqinghaosu and pyrolysis reactions in GC. Low injector temperature (180 °C) causes primarily desoxyartemisinin formation whereas high injector temperature (320–350 °C) causes cyclohexanone pyrolysis product formation.

minister the drug at a dose of 5 mg/kg. The sodium salt of ARTA was prepared as described above in the rabbit studies; however this solution was then diluted with 5% glucose solution such that the final solution was isotonic. This solution was administered as a bolus injection into the opposite leg as previously mentioned.

Heparinized blood samples were frozen immediately after sampling with a dry ice-acetone bath and kept at -70 °C for the duration of the experiment. Samples were then thawed at room temperature and extracted as described above. Blood concentration time data were analyzed by using model equations with an iterative nonlinear curve fitting computer program with a nonweighted least-squares criterion of fit (13).

## RESULTS AND DISCUSSION

Previous reports have suggested (10) and information obtained in this laboratory with HPLC methodologies using reductive electrochemical detection (14) have demonstrated that ARTA is rapidly hydrolyzed to DQHS in vivo as depicted in Figure 2. DQHS is considered to be the active antimalarial compound (15, 16), and ARTA is utilized only for purposes of water solubility and intravenous administration and should be considered as a prodrug of DQHS. Because of this, we focused on developing accurate and precise methodologies to quantitate DQHS in blood. However, DQHS is thermally unstable and degrades to two major pyrolysis products during GC. Figure 2 shows the structures of these two compounds (cyclohexanone pyrolysis product (2*S*,3*R*,6*R*)-2-(3-oxobutyl)-3-methyl-6-[(*R*)-2-propanol]cyclohexanone and desoxyartemisinin) which were recently characterized structurally as a result of these observations (11). Early studies also showed that the pyrolysis products formed and the ratios were quite variable, and dependent on injector type, injector temperature, column packing, and duration of run. More specifically, the use of an on-column injector (50–160 °C at 10 °C/min) with a 6-meter SPB-1 fused silica column 50–160 °C ballistically, then 10 °C/min to 180 °C) caused primarily

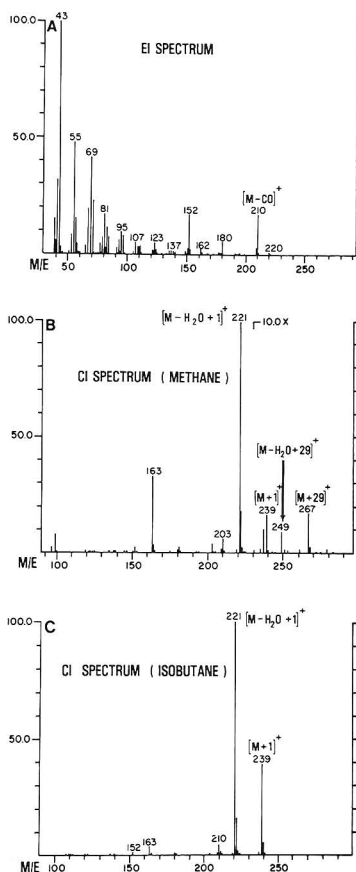


**Figure 3.** EI and CI mass spectra of the cyclohexanone pyrolysis product of DQHS. Spectra were obtained by injecting DQHS on a 15-m SPB-5 capillary column with the dry solids injector: injector, 320 °C; (A) EI spectrum, (B) CI spectrum, methane, (C) CI spectrum, isobutane.

desoxyartemisinin formation (80%) and only 20% of the cyclohexanone pyrolysis product. Furthermore, it was observed that the cyclohexanone pyrolysis product formation could not be eliminated even under very mild conditions. However, extremely high injector temperature (300–400 °C) completely eliminates the formation of desoxyartemisinin on 3% SP2100, 3% OV-3 or 3% OV-17. The same findings were obtained by capillary column GC; however elimination of desoxyartemisinin formation (<2.5%) was obtained only when the dry solids injector was used. These results suggested that quantitation of DQHS in blood by GC/MS is feasible if DQHS is first pyrolyzed in the GC injector to the cyclohexanone pyrolysis product and quantitation is performed on this compound.

Figure 3 shows the EI and CI mass spectra of the cyclohexanone pyrolysis product obtained from injection of DQHS and some structural assignments of major ions. No molecular weight information is obtained from the EI spectrum; however some structural information is present. The methane CI spectrum shows an additional methane adduct ion at  $m/z$  249 and is probably due to dehydration before chemical ionization ( $[M - H_2O + C_2H_5]^+$ ); i.e., the cyclohexanone pyrolysis product

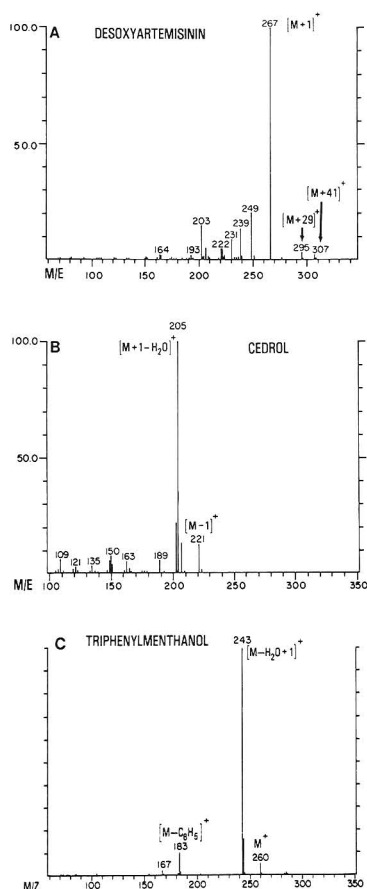


**Figure 4.** CI mass spectra of desoxyartemisinin (methane), and internal standards cedrol (methane) and triphenylmethanol (isobutane). (A) Desoxyartemisinin, obtained by injecting DQHS on a 15-m SPB-5 capillary column; injector, 180 °C. (B) Cedrol, obtained by using identical conditions as described in Figure 3. (C) Triphenylmethanol.

and a dehydrated cyclohexanone pyrolysis product are present in the ion source at the same time. These results demonstrated that methane or isobutane CI and selected ion monitoring of  $m/z$  221 could be used to quantitate the cyclohexanone pyrolysis product of DQHS.

Figure 4 shows the methane CI spectra of desoxyartemisinin, cedrol, and triphenylmethanol. The methane CI spectrum of cedrol is shown in Figure 4B, with base peak at  $m/z$  205 due to dehydration of the tertiary alcohol of the molecule. Pseudo molecular ion at  $m/z$  221  $[M-1]^+$  is also present. Since this ion ( $m/z$  221) is also the base peak ion of the cyclohexanone pyrolysis product spectrum, it appeared that quantitation of both cedrol and the cyclohexanone pyrolysis product of DQHS could be performed by GC/SIM by monitoring  $m/z$  221 (method 1). Figure 5 shows chromatograms of the intensity at  $m/z$  221, 239, and 243 of extracts of blood spiked with 20, 50, and 0 ng/mL of DQHS, respectively, with sample cleanup performed as described for method 2. One percent of the total extract was injected on column, representing approximately 150 and 375 pg on column for DQHS and 200 pg for triphenylmethanol. Samples in which

**Table I. Precision and Accuracy Data for Analysis of DQHS in Human Blood by Packed Column GC/SIM<sup>a</sup>**

amt added, ng/mL	amt measd (ng/mL $\pm$ std dev)	rel std dev, %	accuracy (% error)	<i>n</i>
100	106 $\pm$ 10	9.4	+6	20
400	411 $\pm$ 38	9.1	+3	20

<sup>a</sup>Data represent a compilation of five separate experiments using method 1. Samples for standard curves contained 500 ng of cedrol (internal standard) and 0, 100, 200, 300, 500, 750, or 1000 ng of DQHS. Mean correlation coefficients ( $r^2$ ) for five standard curves were  $0.992 \pm 0.005$ . Intraday coefficients of variation ranged from 2 to 12% and 2 to 7% for 100 and 400 ng/mL, respectively. 5% of the total extract was injected on column for both standards and samples.

**Table II. Precision and Accuracy Data for Analysis of DQHS in Human Blood by Capillary Column GC/SIM<sup>a</sup>**

amt added, ng/mL	amt measd (ng/mL $\pm$ std dev)	rel std dev, %	accuracy (% error)	<i>n</i>
20 <sup>b</sup>	22.6 $\pm$ 1.4	6.2	+13	16
50 <sup>b</sup>	49.1 $\pm$ 5.4	11.0	-1.9	16
100 <sup>c</sup>	99.4 $\pm$ 4.2	4.2	-0.6	20
400 <sup>c</sup>	386 $\pm$ 29	7.5	-3.6	20

<sup>a</sup>Data represent a compilation of ten separate experiments using method 1 with  $n = 4$  for each experiment. 5% of the total extract was injected on column for both standards and samples. <sup>b</sup>Samples for standard curves contained 100 ng of cedrol and 0, 10, 20, 30, 50, or 100 ng of DQHS. Mean correlation coefficients ( $r^2$ ) for four standard curves were  $0.980 \pm 0.016$ . Intraday coefficients of variation ranged from 9 to 18% and 2 to 13% for 20 and 50 ng/mL, respectively. <sup>c</sup>Samples for standard curves contained 1000 ng of cedrol and 0, 50, 100, 200, 300, 500, or 750 ng of DQHS. Mean correlation coefficients ( $r^2$ ) for five standard curves were  $0.976 \pm 0.020$ . Intraday coefficients of variation ranged from 4 to 10% and 4 to 12% for 100 and 400 ng/mL, respectively.

**Table III. Precision and Accuracy Data for Analysis of DQHS in Human Blood by Capillary Column GC/SIM<sup>a,b</sup>**

amt added, ng/mL	amt measd (ng/mL $\pm$ std dev)	rel std dev, %	accuracy (% error)	<i>n</i>
20	19.8 $\pm$ 0.9	4.8	1.2	16
50	49.8 $\pm$ 3.6	7.2	0.3	16

<sup>a</sup>Data represent a compilation of four separate experiments using method 2 with  $n = 4$  for each experiment. 1% of the total extract was injected on column for both standards and samples. <sup>b</sup>Samples for standard curves contained 20 ng of triphenylmethanol and 0, 10, 20, 30, 50, 100, and 500 ng of DQHS. Mean correlation coefficients were  $0.980 \pm 0.012$ . Intraday coefficients of variation ranged from 5 to 20% and 2 to 13% for 20 and 50 ng/mL, respectively.

DQHS, triphenylmethanol, or both compounds were omitted, demonstrated that no detectable interferences eluting in the regions of interest were present using either the capillary or packed column method (Figure 5C).

Results from the validation studies of the method for both packed and capillary column procedures are shown in Tables I-III. By use of the packed column procedure, excellent results (less than 10% relative standard deviation and less than 10% error in accuracy) were achieved at 100 and 400 ng/mL (Table I). Validation of the capillary column procedure at 20, 50, 100, and 400 ng/mL was also achieved with good results (Table II) by using method 1. Validation studies using method 2 with the capillary column procedure are shown in Table III. Excellent precision and accuracy data were obtained by using this method as well. Furthermore, much less contamination was present using *n*-butyl chloride for extraction than with petroleum ether extraction. Since ex-

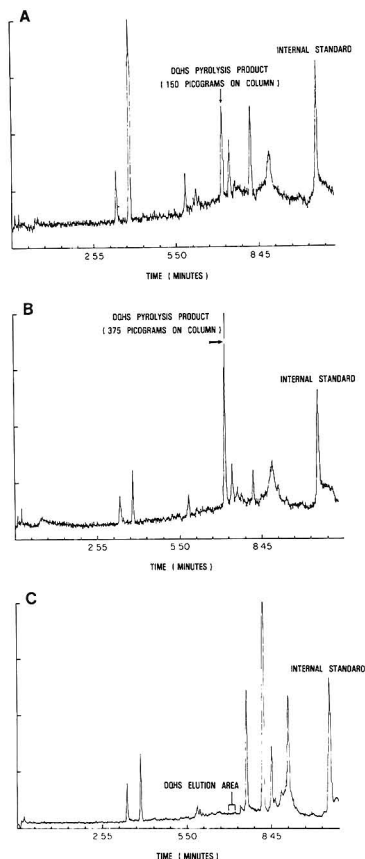


**Figure 5.** Selected ion chromatograms of human blood spiked with DQHS and internal standard, triphenylmethanol: (A) 20 ng/mL, 1% of the total extract; (B) 50 ng/mL, 1% of the total extract; (C) blank, 5% of the total extract.

traction efficiencies were higher with *n*-butyl chloride extraction, only 1% of the total extract on column was required for an adequate signal-to-noise ratio at 10 ng/mL. This also resulted in a much longer column lifetime.

Figure 6A shows the blood levels of DQHS measured using method 1 after intravenous administration of 5 mg/kg of the sodium salt of ARTA to a rabbit, and a plot of the computerized nonlinear regression best fit of the data. Blood levels ranged from approximately 400 ng/mL at 8 min postdosing and decreased to 8 ng/mL at 110 min. Excellent fits of the data were obtained with a two-compartment open model consisting of the sum of two exponential terms (13). Ninety-nine percent of the total area under the curve (346 ng·mL<sup>-1</sup>·h (0–110 min vs 0 to ∞ [trapezoidal rule]) was characterized during the sampling period with a terminal elimination half-life of 17.7 min. In a second identical experiment in the same rabbit (not shown), total area under the curve was 483 ng·mL<sup>-1</sup>·h with a terminal elimination half-life of 19.1 min. Figure 6B shows blood levels of DQHS measured using method 2 after intravenous administration of 5 mg/kg of the sodium salt of ARTA of two beagle dogs and a plot of the computerized nonlinear regression fit of the data. Area under the curve and terminal elimination half-life were calculated

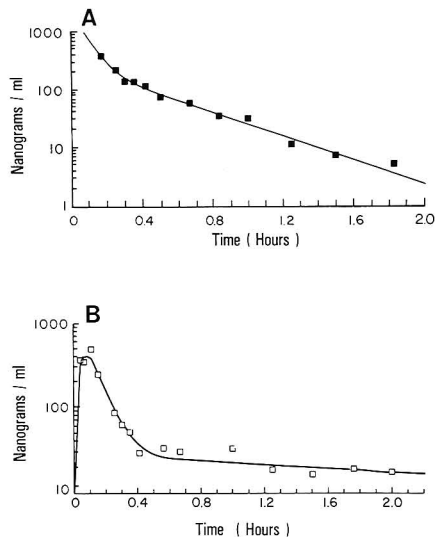


**Figure 6.** Blood concentration/time data for DQHS after intravenous administration (5 mg/kg) of the sodium salt of ARTA in a rabbit (A) and a dog (B). Points represent measured blood levels and line represents best fit line determined by nonlinear regression analysis.

to be 150 ng·mL<sup>-1</sup>·h and 2.4 h, respectively. In a second identical experiment in the dog, essentially identical blood levels were measured, and the area under the curve was calculated to be 175 ng·mL<sup>-1</sup>·h with a 2.7-h terminal elimination half-life.

It is important to point out that the cyclohexanone pyrolysis product of DQHS is not formed when authentic desoxyartemisinin is chromatographed under identical conditions for quantitation of DQHS. These results suggest that the mechanisms for the formation of the cyclohexanone pyrolysis product and desoxyartemisinin are unrelated, i.e., desoxyartemisinin is not a precursor of the cyclohexanone pyrolysis product, and also indicate that the presence of desoxyartemisinin in blood would not interfere with DQHS quantitation. Furthermore, desoxyartemisinin is thermally stable under mild GC conditions (injector, 180 °C; 15 M SPB-5; 100–200 °C at 10 °C/min) and can be detected and quantitated in blood under identical conditions of extraction as described above for DQHS. The presence of desoxyartemisinin in human blood samples after treatment with derivatives of QHS is anticipated, since this compound has been reported to be a metabolite of QHS in man (10).

Although there is not close structural similarity between the internal standards cedrol or triphenylmethanol and DQHS, the results reported in this study demonstrate that quantitation of DQHS in blood using this method is accurate and reproducible in the low to high nanogram per milliliter range and also show that this method can be utilized for pharmacokinetic studies at therapeutic doses in animals and man. Furthermore, much better accuracy, precision, and sensitivity should be obtained with a deuterated internal standard; however synthesis of DQHS is currently extremely difficult due to the complex stereochemistry of the molecule. The method as described above currently has detection limit of 2 ng/mL with 5% of the *n*-butyl chloride extract on column. Since extraction of blood with *n*-butyl chloride results in much cleaner extracts and much higher recovery of DQHS even in the 2–20 ng/mL range, this change in the method results in lower detection limits, less interfering peaks, and longer

column lifetime. As shown in Figure 6 and also in animal pharmacokinetic studies currently in progress, this methodology is proving to be quite useful and will be utilized for pharmacokinetic studies in the clinic and aid in the development of this potent class of compounds for treatment of malaria in man.

The analysis of this class of compounds in biological fluids in the low nanogram per milliliter range is a significant challenge in which little progress has been made in the past. The studies reported in this paper were initiated when it was observed that adequate sensitivity could not be obtained by HPLC with reductive electrochemical detection (14). Unlike the HPLC method in which qinghaosu and any derivatives with the peroxide moiety can be detected and quantitated, this method was specifically designed for the analysis of DQHS after administration of ARTA, or other DQHS derivatives with a carboxyl moiety. Since ARTA and other ester or ether derivatives of DQHS also pyrolyze to the cyclohexane pyrolysis product, a carboxyl moiety permits separation of DQHS from the parent compound by liquid-liquid extraction. Therefore, this method is not useful for the analysis of DQHS formed from artemether or arteether (methyl or ethyl ethers of DQHS). This difficulty represents the major limitation in the general utility of the method for the analysis of DQHS; however, as shown in this paper, the method is useful for the quantitation of DQHS after administration of ARTA. Other studies to find a generally applicable method are in progress in this laboratory. In the interim, this method is now being used to study the pharmacokinetics of DQHS formation and elimination in various animal models.

Registry No. DQHS, 71939-50-9.

## LITERATURE CITED

- (1) Fourth Meeting of the Scientific Working Group on the Chemotherapy of Malaria, Beijing, People's Republic of China; WHO Report TDR/CHE-MAL-SWG(4)/QHS/81, 1981.
- (2) Qinghaosu Research Group, *Sci. Sin. (Engl. Transl.)* **1980**, *23*, 380.
- (3) Liu, J.; Ni, M.; Fan, J.; Tu, Y.; Wu, Z.; Qu, Y.; Chou, W. *Acta Chim. Sin.* **1979**, *37*, 129.
- (4) China Cooperative Research Group on Qinghaosu and Its Derivatives as Antimalarials *J. Tradit. Chin. Med.* **1982**, *2*, 3.
- (5) China Cooperative Research Group on Qinghaosu and Its Derivatives as Antimalarials *J. Tradit. Chin. Med.* **1982**, *2*, 17.
- (6) China Cooperative Research Group on Qinghaosu and Its Derivatives as Antimalarials *J. Tradit. Chin. Med.* **1982**, *2*, 45.
- (7) China Cooperative Research Group on Qinghaosu and Its Derivatives as Antimalarials *J. Tradit. Chin. Med.* **1982**, *2*, 31.
- (8) China Cooperative Research Group on Qinghaosu and Its Derivatives as Antimalarials *J. Tradit. Chin. Med.* **1982**, *2*, 125.
- (9) Klayman, D. L. *Science* **1985**, *228*, 1049.
- (10) China Cooperative Research Group on Qinghaosu and its Derivatives as Antimalarials, *J. Tradit. Chin. Med.* **1982**, *2*, 25.
- (11) Lin, A. J.; Theoharides, A. D.; Klayman, D. L. *Tetrahedron* **1986**, *42*, 2181.
- (12) Paulsen, R.; Valentine, J. L. *Lab. Anim.* **1984**, *13*, 34.
- (13) Desjardins, R. E.; Pamplin, C. L.; von Bredow, J.; Barry, K. G.; Canfield, C. J. *Clin. Pharmacol. Ther. (St. Louis)* **1979**, *26*, 372.
- (14) Zhou, Z. M.; Anders, J. C.; Chung, H.; Theoharides, A. D. *J. Chromatogr. Biomed. Appl.* **1987**, *414*, 77.
- (15) Qichao, Y.; Weizhi, S.; Lei, L.; Jun, G., *J. Tradit. Chin. Med.* **1982**, *2*, 99.
- (16) Li, Z.; Qu, H.; Warhurst, D.; Peters, W. R. *Soc. Trop. Med. Hyg.* **1983**, *77*, 522.

RECEIVED for review May 29, 1987. Accepted September 21, 1987. Zhong Ming Zhou was a visiting scientist sponsored by the UNDP/World Bank/WHO Special Programme for Research and Training in Tropical Diseases.

# Characterization and Selection of Electrolyte Systems for Isotachopheresis of Anions by Cluster Analysis

Ernst Kennndler\* and Gregor Reich

Institute for Analytical Chemistry, University of Vienna, Waehringerstrasse 38, A-1090 Vienna, Austria

A rational strategy based on cluster analysis is proposed for the selection of leading electrolytes in the identification of anions by isotachopheresis in aqueous solutions. The calculations were carried out by using ionic mobilities or not linearly transformable relative step heights as properties. Linear correlation coefficients and Euclidian distances were used as similarity measures. The data for the computation were taken from a library consisting of the values for 263 anionic compounds in eight electrolyte systems with integer pH values ranging from 3 to 10. The sequence of the similarities of the systems is nearly unaffected by the choice of the properties or that of the measure of resemblance. The results of a hierarchical and a nonhierarchical clustering procedure were used to select combinations of electrolytes, which yield maximum identification power. For binary combinations, a system with pH 3 and one with pH ranging from 6 to 10 were found to be most favorable. For ternary combinations, pH 3, 4, and one from 6 to 10 or 3, 5, and one from 6 to 10 were selected. Additional systems do not essentially increase the identification power.

The selection of an electrolyte system is one of the most important steps in developing a method for the separation or identification of ions by electrophoresis. Until now all

strategies proposed for isotachopheresis were applicable only for a restricted range of separation problems (1-12). They allowed a selection of an electrolyte system for the separation of a known pair of ions: starting from their known ionic mobilities and  $pK_a$  values it was possible to calculate whether the considered pair of ions could be separated under the given conditions. This method fails, however, even for the simple case to select electrolyte systems for the identification of analytes from a known large set of substances. In practice this problem was solved by informed trial and error, starting from a first scouting experiment.

On the other hand, chemometric methods (13) were already applied to solve similar problems for other separation techniques like thin-layer chromatography or gas chromatography, where phase systems were characterized and their optimal combinations were selected by cluster analysis (or numerical taxonomy) (14-24). In a previous paper (25), we compared the similarities of aqueous and mixed aqueous-organic electrolyte systems in isotachopheresis by this technique. In the present paper, cluster analysis is used to characterize aqueous buffering electrolytes with different pH values, described for the isotachopheresis of anions, and a rational strategy for the combination of electrolytes is proposed. Furthermore, the effect of the choice of different analyte characters on the result of the clustering procedure is briefly discussed, when the different properties are not linearly transformable.



**Table I. Buffering Counterions of the Leading Electrolytes with Different pH Values<sup>a</sup>**

pH of the leading electrolyte	counterion
3.0	$\beta$ -alanine
4.0	$\beta$ -alanine
5.0	creatinine
6.0	histidine
7.0	imidazole
8.0	tris(hydroxymethyl)aminomethane
9.0	2-amino-2-methyl-1,3-propanediol (ammediol)
10.0	ethanolamine

<sup>a</sup> The leading ion was chloride in all systems**EXPERIMENTAL SECTION**

Relative step heights ( $R_E$  values) and ionic mobilities of 263 anions in eight electrolyte systems with different pH values of the leading electrolyte were used for cluster analysis. The solutes were selected from the library published by Hirokawa et al. (26) as described in a previous paper (27). The (calculated)  $R_E$  values are related to chloride as the leading ion. The buffering counterions of the different leading electrolytes are presented in Table I. The ionic mobilities were calculated from the  $R_E$  values by assuming a mobility of  $74.6 \times 10^{-5} \text{ cm}^2 \text{ V}^{-1} \text{ s}^{-1}$  for chloride. The Euclidian distances were calculated from the scaled values of mobilities and  $R_E$  values. The computer program used for the cluster analysis was ARTHUR (28).

**RESULTS AND DISCUSSION**

**Taxonomic Units and Properties.** Eight leading electrolyte systems with (integer) pH values from 3.0 to 10.0 are chosen as taxonomic units. These systems are symbolized by the numbers corresponding to the particular pH values. The solutes are characterized as usual in isotachopheresis by relative step heights like  $R_E$  values or  $h^{\text{rel}}$  values, defined by

$$R_{E,i} = m_L/m_i \quad (1)$$

and

$$h^{\text{rel}} = (m_L/m_i - 1)/(m_L/m_R - 1) = (R_{E,i} - 1)/(R_{E,R} - 1) \quad (2)$$

where  $m_L$ ,  $m_R$ , and  $m_i$  are the ionic mobilities of the leading ion, L, the reference ion, R, and the analyte ion, i, respectively. It can be seen from the equations given above that  $R_E$  values can be linearly transformed into  $h^{\text{rel}}$  and vice versa. This means, that both properties are totally correlated, and the results of cluster analysis based on these characters will be redundant. In contrast, the ionic mobility, which is the most important property in electrophoresis, is not linearly transformable into either the  $h^{\text{rel}}$  or the  $R_E$  values. We have therefore selected the ionic mobilities and the  $R_E$  values as properties for the cluster analysis.

**Measures of Resemblance.** The similarity of the electrolyte systems was expressed as in previous papers (25, 27) by the linear correlation coefficient,  $r$ , and the Euclidian distance,  $d_{kl}$ . The latter is the distance between two points, representing two electrolyte systems, k and l, in an  $n$ -dimensional pattern space.  $n$  is the number of characters in the particular systems. In the present work, each electrolyte system is therefore represented by one point in a 263-dimensional space.

When the linear correlation coefficient was used as a measure of resemblance and the ionic mobilities were taken as properties, systems 8 and 9 have the highest and 3 and 10 have the lowest similarity, as can be seen from Table II. Although mobilities are not linearly transformable into  $R_E$  values, nearly the same sequence of the similarity parameters is found with the  $R_E$  values as properties (27). However, the absolute values of the correlation coefficients differ: it is

**Table II. Similarity Matrix of the Electrolyte Systems, Given by the Linear Correlation Coefficients<sup>a</sup>**

system	correlation coefficient $r$							
	3	4	5	6	7	8	9	10
3	1.000							
4	0.976	1.000						
5	0.882	0.950	1.000					
6	0.801	0.875	0.975	1.000				
7	0.779	0.845	0.944	0.987	1.000			
8	0.777	0.837	0.928	0.972	0.996	1.000		
9	0.772	0.831	0.921	0.964	0.991	0.998	1.000	
10	0.759	0.819	0.910	0.954	0.982	0.990	0.996	1.000

<sup>a</sup> The ionic mobilities of the solutes in the different electrolyte systems were used as the properties.**Table III. Similarity Matrix of the Electrolyte Systems, Given by the Euclidian Distances<sup>a</sup>**

system	Euclidian distance, $d_{kl} \times 10$							
	3	4	5	6	7	8	9	10
3	0							
4	2.03	0						
5	7.34	5.54	0					
6	9.66	8.12	3.19	0				
7	9.85	8.49	4.30	1.96	0			
8	9.82	8.55	4.76	2.83	0.97	0		
9	9.87	8.62	4.93	3.12	1.43	0.71	0	
10	9.97	8.74	5.16	3.45	2.02	1.52	0.88	0

<sup>a</sup> The scaled  $R_E$  values of the solutes were used as the properties.**Table IV. Similarity Matrix of the Electrolyte Systems, Given by the Euclidian Distances**

system	Euclidian distance, $d_{kl} \times 10$							
	3	4	5	6	7	8	9	10
3	0							
4	2.20	0						
5	4.85	3.17	0					
6	6.30	4.99	2.25	0				
7	6.65	5.56	3.35	1.60	0			
8	6.68	5.71	3.80	2.38	0.94	0		
9	6.76	5.81	3.99	2.68	1.37	0.63	0	
10	6.95	6.02	4.25	3.03	1.91	1.39	0.84	0

<sup>a</sup> The distances are based on the scaled values of the ionic mobilities of the solutes.

found, that the mobilities show a higher linear correlation than the  $R_E$  values in most cases.

In Tables III and IV, the similarities of the electrolyte systems are expressed by their Euclidian distances, based on  $R_E$  values and on ionic mobilities. It follows, that the results are in agreement with those obtained by the correlation coefficient: the smallest distances are found for systems 8 and 9, and the largest distances for 3 and 10.

It can be seen that the sequence of the similarity of the systems under consideration is not sensitive to the choice of the taxonomic properties or to the choice of the measure of resemblance.

**Clustering Procedure.** The electrolyte systems are classified by the aid of two clustering methods: a hierarchical and a nonhierarchical procedure. For both, the Euclidian distances were used as similarity parameters.

The results of the hierarchical clustering procedure are shown in Figure 1. The dendrograms were obtained by an unweighted, average linkage method, using the normalized distances,  $\Delta$ , calculated from the values in Tables III and IV. It can be seen from both dendrograms, that two main clusters are formed, one consisting of systems 3 and 4 and the other

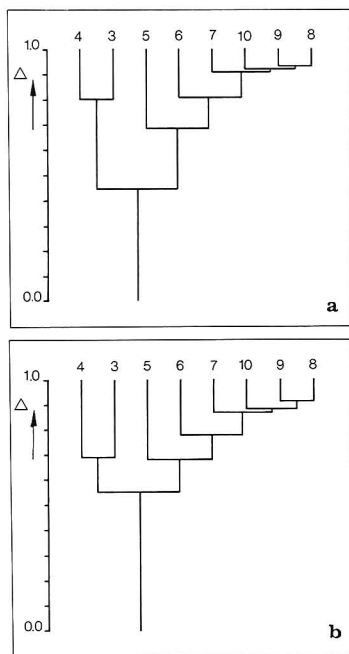


**Figure 1.** Dendrograms as the results of the hierarchical clustering procedures, based on the data of the Euclidian distances, given in Tables III and IV. The properties used were (a)  $R_E$  values and (b) ionic mobilities of the solutes in the different electrolyte systems.  $\Delta$  = normalized distances.

consisting of the remaining systems with pH values from 5 to 10.

As a second clustering algorithm, the nonhierarchical method of the minimum spanning tree was used. The nonlinear mapping (29) projects multidimensional data to the two-dimensional space, preserving the interpoint distances as correct as possible. The axes of the plots have no known relationship to the data values.

The results of this classification method are presented in Figure 2. In both graphs, the two subgroups separated by the longest branch consist of the same electrolyte systems as found in the dendrograms.

**Selection of Leading Electrolyte Systems.** The result of the clustering procedures can serve as a tool to select combinations of electrolyte systems that yield maximum identification power. By the aid of the dendrograms shown in Figure 1, two systems will be selected from each of the two main clusters in a first step. As an aid for the selection, the information content (23) calculated from the same isotachophoretic data as applied in the present work can be used. The information content, expressed in bits, is an appropriate measure of the identification power of electrolyte systems. It was found (27), that system 3 has the highest information content of all single systems (about 5.7 bits), and the combination of systems 3 and 10 has the highest information content of all binary combinations (ca. 8.6 bits). These systems are found in the two separated main clusters and are therefore selected as a first choice. The differences in similarities are found to be small for all systems with pH values from 6 to 10. Thus, instead of system 10, another system from this group can be selected without substantial loss of information, which is in agreement with previous results (27). In a second

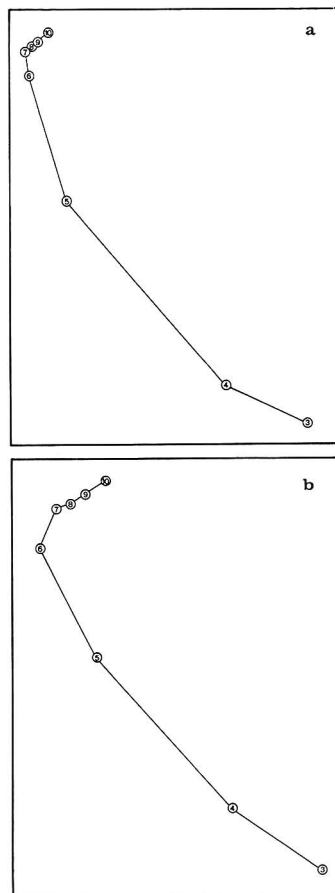


**Figure 2.** Nonlinear mapping of the data connected by the minimum spanning trees, based on the Euclidian distances given in Tables III and IV. The properties used were (a)  $R_E$  values and (b) ionic mobilities of the solutes in the different electrolyte systems.

step, an additional, third system with pH of 4 (or 5) is chosen according to the dendrograms. The application of further systems should not lead to a significant increase of identification power, due to the high similarity of these systems with those already combined.

The selection strategy by the minimum spanning tree, presented in Figure 2, consists of successively breaking the longest branches between the points, by which the systems are represented. This leads to the same two groups of systems as found with the hierarchical method. On the basis of the information content of the different pairs of systems, 3 and 10 are selected too. The high resemblance of systems 6, 7, 8, 9, and 10 clearly can be seen from the structure of the tree. These systems are therefore interchangeable in the combinations without significant loss of information. From the remaining clusters, the longest branch is found between systems 5 and 6. This leads to the selection of three systems: 3, 5, and one from 6 to 10. Again, only short distances between the latter systems are found, indicating only small increase of identification power for additional electrolyte systems. Thus, different types of cluster analysis lead to the same

**Table V. Number of Pairs of Ions of the Data Library, Remaining Undifferentiated in the Single Electrolyte Systems and their Binary Combinations<sup>a</sup>**

electrolyte system	3	4	5	6	7	8	9	10
3	873	249	148	128	125	120	126	123
4		1322	306	229	216	206	211	208
5			2199	778	675	655	636	633
6				2337	1739	1620	1546	1547
7					2344	2057	1976	1980
8						2199	2032	2019
9							2212	2072
10								2157

<sup>a</sup> For details, see text.

conclusions. The following leading electrolyte systems are selected as yielding favorable results in the following situations: for binary combinations, 3 and one from 6 to 10; for ternary combinations, 3 and 5 or 3 and 4 and one from 6 to 10.

#### Evaluation of the Results of the Selection Procedure.

The identification power of the particular leading electrolyte systems and their combinations as discussed above is verified by another approach. It is based on the number of analytes, which can be discriminated in an isotachopherogram under realistic conditions with an universal detector like a potential gradient or electric conductivity detector. This number either can be derived theoretically (27) or can be calculated by using the data of the library mentioned above. For the latter calculation, two analytes are considered to be differentiated when their ionic mobilities differ more than 3% in at least one of the electrolyte systems. The lack in identification power is related to the number of pairs of analytes remaining nondifferentiated, given by the number of pairs with ratios  $m_i/m_j$  smaller than 1.03. From the data of the library, matrices of  $263 \times 263$  elements are constructed, formed by the ratios of the mobilities,  $m_i/m_j$ , for each possible pair of analytes,  $i$  and  $j$ , in the particular electrolyte system, with  $m_i > m_j$ . The number of pairs of analytes that have ratios smaller than 1.03 in all considered systems is determined. The resulting numbers of nondifferentiated pairs are given in Table V for the single systems and their binary combinations. One can see for the single systems (represented by the diagonal), that system 3 has the lowest number of nondiscriminated pairs of analytes, followed by system 4. All other single systems from 5 to 10 show about the same number of undifferentiated pairs. This result is in agreement with the results obtained with information theory (27).

The selection of system 3 in combination with a second system in the range from 6 to 10, as predicted by cluster analysis, is in accordance with the values of Table V: the number of pairs is reduced to about 120–128. All other combinations of two electrolyte systems lead to a significantly higher number of undifferentiated pairs of analytes.

The calculation for three electrolyte systems, which include system 3, leads to numbers of pairs ranging from 120 (systems 3, 5, 6 and 3, 9, 10) to 112 (3, 4, 8 and 3, 5, 8). The only exception is the combination of 3, 4, and 5, with 138 undiscriminated pairs of analytes.

All other combinations of three systems, not containing system 3, show essentially larger numbers of nondifferentiated pairs of analytes: about 200 pairs for all ternary combinations with system 4, about 600 to 700 for all combinations including system 5 (but without 3 and 4), and between 1600 and 2000 pairs for the remaining ternary combinations (without systems 3, 4, and 5).

However, the minimum number of 112 pairs, obtained for the combination of the three most favorable systems, as mentioned above, is very close to the number of 109 pairs, found as the minimum number of pairs of analytes, when all the eight electrolyte systems under consideration are com-

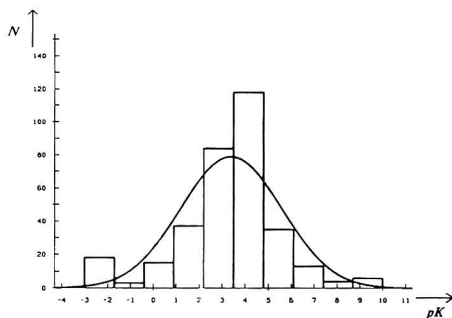


**Figure 3.** Distribution of the  $pK_a$  values of the solutes. Both the histogram and the fitted Gaussian curve are presented.  $N$  = number of analytes in the particular class of the histogram.

bined. This number of pairs is almost reached by the combination of the four most favorable systems: with 3, 4, 8, 9 and 3, 5, 8, 9 only 110 pairs of analytes remain undiscriminated, and with the combinations of 3, 4, 5, 8, 3, 4, 6, 8, 3, 4, 8, 10; and 3, 5, 8, 10 only 111 pairs remain.

The minimum value of 109 is already reached by the combination of five instead of eight electrolyte systems, namely with 3, 4, 5, 8, 9 and 3, 4, 6, 8, 9. It can be seen, that, compared with the combination of only two or three favorable systems, the increase in identification power is poor.

In addition it can be seen that the results of the cluster analysis are in agreement with the evaluation given above. It follows that the gain in identification power of isotachopheresis in aqueous solutions obtained by combining different leading electrolyte systems is limited: after the combination of only a few systems, no further substantial information is gained.

The results of the cluster analysis are very plausible, when the distribution of the  $pK_a$  values of the analytes is considered. The effect of the pH of the leading electrolyte and that of the sample zone, respectively, on the mobilities is most pronounced in the pH range near the  $pK_a$  value, due to the strong change of the degree of dissociation. It can be seen from the distribution of the  $pK_a$  values presented in Figure 3 that the maximum number of analytes is found at  $pK_a$  range of about 3 to 4. The largest effects on the effective mobilities therefore can be expected at the corresponding pH range of the leading electrolyte. This is in fact the result of both approaches, the cluster analytical one as well as the information theoretical one. It can be seen from Figure 3, that the standard deviation of the Gaussian distribution, fitted to the distribution of the  $pK_a$  values, is about 2  $pK$  units. The less pronounced variation of the effective mobilities is expected therefore with electrolyte systems with pH values larger than 6. In fact, the electrolyte systems with pH 6 and higher are found in clusters with high similarity values. Therefore, the results of the cluster analysis to characterize and select leading electrolyte systems are

plausible with regard to the physicochemical behavior of the analytes in the electrolyte systems.

### LITERATURE CITED

- (1) Everaerts, F. M.; Routs, R. J. *J. Chromatogr.* **1971**, *59*, 181.
- (2) Beckers, J. L.; Everaerts, F. M. *J. Chromatogr.* **1972**, *68*, 207.
- (3) Everaerts, F. M.; Beckers, J. L.; Verheggen, Th. P. E. M. *Isotachopheresis: Theory, Instrumentation and Applications*; Elsevier, Amsterdam, 1976.
- (4) Mikkers, F. E. P.; Everaerts, F. M.; Peek, J. A. F. *J. Chromatogr.* **1979**, *168*, 293.
- (5) Mikkers, F. E. P.; Everaerts, F. M.; Peek, J. A. F. *J. Chromatogr.* **1979**, *168*, 317.
- (6) Bocek, P.; Lekova, K.; Deml, M.; Janak, J. *J. Chromatogr.* **1976**, *117*, 97.
- (7) Gebauer, P.; Bocek, P. *J. Chromatogr.* **1983**, *267*, 49.
- (8) Bocek, P.; Gebauer, P. *Electrophoresis (Weinheim, Fed. Repub. Ger.)* **1984**, *5*, 338.
- (9) Gebauer, P.; Bocek, P. *J. Chromatogr.* **1985**, *320*, 49.
- (10) Krivankova, L.; Foret, F.; Gebauer, P.; Bocek, P. *J. Chromatogr.* **1987**, *390*, 3.
- (11) Kasicka, V.; Vacik, J.; Prusik, Z. *J. Chromatogr.* **1985**, *320*, 33.
- (12) Mosset, D.; Gareil, P.; Desbarres, J.; Rosset, R. *J. Chromatogr.* **1987**, *390*, 69.
- (13) Kaufman, L.; Massart, D. L. In *Chemometrics, Mathematics and Statistics in Chemistry*; Kowalski, B. R., Ed.; Reidel: Dordrecht, Netherlands, 1984; pp 393-402.
- (14) De Clercq, H.; Massart, D. L. *J. Chromatogr.* **1975**, *115*, 1.
- (15) Massart, D. L.; De Clercq, H. *Anal. Chem.* **1974**, *46*, 1988.
- (16) De Clercq, H.; Massart, D. L.; Dryon, L. *J. Pharmac. Sci.* **1977**, *66*, 1269.
- (17) Leary, J. J.; Justice, J. B.; Tsuge, S.; Lowry, S. R.; Isenhour, T. L. *J. Chromatogr. Sci.* **1973**, *11*, 201.
- (18) Lowry, S. R.; Tsuge, S.; Leary, J. J.; Isenhour, T. L. *J. Chromatogr. Sci.* **1974**, *12*, 124.
- (19) Haken, J. K.; Wainwright, M. S.; Do Phuong, N. *J. Chromatogr.* **1976**, *117*, 23.
- (20) Eskes, A.; Dupuis, F.; Dijkstra, A.; De Clercq, H.; Massart, D. L. *Anal. Chem.* **1975**, *47*, 2168.
- (21) De Beer, J. O.; Heyndrickx, A. M. *J. Chromatogr.* **1982**, *235*, 337.
- (22) Lowry, S. R.; Ritter, G. L.; Woodruff, H. B.; Isenhour, T. L. *J. Chromatogr. Sci.* **1976**, *14*, 126.
- (23) Massart, D. L.; De Clercq, H.; In *Advances of Chromatography*; Giddings, J. C., Keller, R. A., Eds.; Marcel Dekker: New York, 1978; Vol. 16.
- (24) Huber, J. F. K.; Reich, G. *J. Chromatogr.* **1984**, *294*, 15.
- (25) Kennler, E.; Jenner, P. *J. Chromatogr.* **1987**, *390*, 169.
- (26) Hirokawa, T.; Nishino, M.; Aoki, N.; Kiso, Y. *J. Chromatogr.* **1983**, *271*, D1.
- (27) Kennler, E. *Anal. Chim. Acta* **1985**, *173*, 239.
- (28) Duewer, D. L.; Harper, A. M.; Koskinen, A. M.; Fasching, J. L.; Kowalski, B. R. *ARTIFUR, Version Infomatrix: Infomatrix: Seattle, WA*.
- (29) Kowalski, B. R.; Bender, C. F. *J. Am. Chem. Soc.* **1973**, *95*, 686.

RECEIVED for review May 26, 1987. Accepted September 14, 1987.

## Effects of Dilution of Poly(ethylvinylbenzene-divinylbenzene) Adsorbent on the Adsorption of Aliphatic, Alicyclic, and Aromatic Hydrocarbon Adsorbates from Effective Zero to Finite Surface Coverage

N. M. Djordjevic and R. J. Laub\*

Department of Chemistry, San Diego State University, San Diego, California 92182

The chromatographic measurement and systematic interpretation of the solid/gas partition coefficients  $K_s$  and related thermodynamic properties of a number of hydrocarbon adsorbates (*n*-pentane through *n*-octane, cyclohexane, methylcyclohexane, benzene, dichloromethane, chloroform, carbon tetrachloride, tetrahydrofuran, thiophene, and acetone) at effective zero surface coverage with a 1:10 admixture of the title adsorbent-inert diluent from 393 to 443 K are reported. Despite a difference of an order of magnitude in the surface areas of bulk and admixed packings, the adsorbate relative retentions were in good agreement with those found in previous work with neat Porapak Q. The heats of adsorption also coincided to within an experimental error of ca.  $\pm 5\%$ . The GSC technique of elution by characteristic point was then used to derive the finite-concentration adsorption isotherms and isosteric heats of adsorption of *n*-hexane, cyclohexane, benzene, carbon tetrachloride, and acetone adsorbates with "diluted" Porapak Q over the temperature range 393-433 K. All exhibited BET Type IV isotherms, as well as changes in the respective isotherm temperature coefficients. The latter is said to be a consequence of the microporous substructure of this adsorbent.

(i.e., GLC), since conventional solid inorganic adsorbents (e.g., silica, alumina) generally give rise to retentions that, relatively speaking, are inordinately long. Also, because of the slow kinetics of mass transfer in gas-solid chromatography (GSC), adsorbate peaks often exhibit considerable band broadening (poor column efficiency). In addition, isotherm curvature even at very low adsorbate surface coverage can result in peak asymmetry, which reduces even further the column efficiency as well as rendering retentions dependent upon the amount of material injected.

Attempts at overcoming some of the drawbacks to analytical GSC have historically included the fabrication of "porous-layer" open-tubular (PLOT) columns, wherein either the column wall is activated or where finely divided adsorbent particles are deposited and made to adhere to it (ref 1 and 2 and references therein). The advantage in either case is said to be improvement in the mass-transfer characteristics of adsorbate/stationary-phase interactions, resulting in turn in higher chromatographic efficiency. However, there is considerable practical skill involved in the fabrication of columns of these types. Moreover, despite recent and considerable progress (3), the number of commercially available PLOT systems comprised of varieties of adsorbents is as yet somewhat limited.

As one alternative to PLOT technology, packed-column GSC efficiency can be improved somewhat, e.g. by using columns of reduced internal diameter. The system efficiency can also be enhanced by dilution by mechanical admixture

The preponderance of packed-column gas chromatographic separations is carried out today with a liquid stationary phase

of adsorbents with inert support materials. Further, there are significant advantages to packing dilution that cannot be realized simply by reducing the column diameter or length. First, in terms of the kinetics of mass transport, and considering that any streaming or mobile-phase contributions are minor, the van Deemter relation reduces approximately to  $H \approx B/\bar{u}$  when  $C_S$  (i.e., the amount of "active" phase) approaches zero, as was implied in the work, first, of Bombaugh (4), and as demonstrated more recently in the comprehensive studies by Al-Thamir, Purnell, and Laub (1, 2) of the dilution of alumina by diatomaceous earth and glass beads. ( $H$  is the height equivalent to a theoretical plate,  $B$  is the abbreviated longitudinal diffusional term,  $C_S$  represents stationary-phase mass-transfer nonequilibrium, and  $\bar{u}$  is the carrier average linear velocity.) The immediate practical consequence of this form of plate-height dependency is that  $H$  decreases (i.e., the column efficiency increases) as the flow rate is increased. In practice, of course, this is never fully realized since there must be present at least some stationary phase in order to effect separations, that is, some mass-transfer nonequilibrium is inevitable. Even so, band broadening can be reduced to the point that packed-column GSC systems of conventional dimensions can be made to exhibit efficiencies that approach 2000 effective theoretical plates/m, i.e., comparable with what can be achieved with open-tubular columns.

An additional advantage to packing dilution over the use of short and/or narrow-bore packed columns is *quantitative* control over the time of analysis, as embodied in the well-established relation (1, 2, 4)

$$k'_{(M)} = w_B k'_{(B)} + w_C k'_{(C)} \quad (1)$$

where  $k'_{(i)}$  are the solute capacity factors with the indicated adsorbents B, C, or M ( $=B + C$ ) and where, for  $k'_{(B)} = 0$

$$k'_{(M)} \Rightarrow w_C k'_{(C)} \quad (2)$$

This is, raw retention times can be adjusted simply by modifying the extent of dilution of the adsorbent. (The associated reduction in sample capacity is of little concern in view of the extreme sensitivity of modern GC detectors.) Further, if the capacity factor of the least-retained adsorbate is maintained greater than 10, the overall analysis time can be decreased with little or no loss in resolution. Indeed, as pointed out above, since the column efficiency will be enhanced as the extent of dilution is increased, resolution can actually be made to improve as the retentions are diminished.

Equations 1 and 2 of course apply as well to open-tubular columns, as do the considerations regarding system efficiency. Dilution of adsorbent wall coatings with granulated inert diluent materials would therefore also appear to offer measurable benefits to PLOT technology. Moreover, the above principles have been shown by Laub and Madden (5) to apply equally to packed-column liquid chromatography, where the interesting situation was presented that a  $C_{18}$  (ODS) "reverse-phase" packing was the active adsorbent (methanol-water mobile phase) and where silica, deactivated as a result of the high water content of the carrier, served as the inert diluent medium.

Diluted packings also find utility in physicochemical studies of adsorbent properties, especially in GSC work with catalysts that promote on-column reactions (1). In addition, the determination of finite-concentration adsorption isotherms (e.g., ref 6) generally involves the injection of large volumes of vapor, which can result in the so-called "sorption" effect wherein the viscosity of the adsorbate-carrier mixture differs substantially from that of the carrier alone (7, 8). The column flow rate thereby changes as the adsorbate pulse proceeds down the system; i.e., the measured flow rate (carrier sans adsorbate) differs substantially from the actual flow rate (carrier + adsorbate). Dilution of the column packing eludes this drawback

insofar as the amount of adsorbate necessary to achieve a high adsorbent surface coverage is diminished; that is, only small quantities of the compounds of interest need be injected.

However, despite the studies cited above, and in the absence of any relevant quantitative data of appropriate form, there might well remain some doubt as to whether, in fact, diluted packings give retentions that reflect those observed with bulk materials. Therefore, in order to explore further the several apparent advantages of the packing dilution technique in analytical separations as well as in physicochemical studies, and in view of the importance of understanding of the underlying fundamental aspects of adsorption, we undertook in the present work to contrast the properties of bulk vs "diluted" adsorbent GSC stationary phases in terms of adsorbate retentions. We recently completed a comprehensive study of bulk Porapak Q adsorbent (6), and so, we employed it in this work also in order to facilitate comparisons of data sets.

## EXPERIMENTAL SECTION

**Apparatus and Equipment.** The laboratory-constructed high-precision gas chromatograph (thermal conductivity detection; helium carrier) has been described in detail elsewhere (9), and its precision, accuracy, and potential sources of error have been discussed at length (6, 10).

**Materials and Supplies.** Porapak Q, batch No. 030 (60–80 mesh; specific surface area  $S$  of  $524 \text{ m}^2 \text{ g}^{-1}$ ) was obtained from Waters Associates, Milford, MA. Chromosorb G (60–80 mesh; AW, DMCS treated;  $0.5 \text{ m}^2 \text{ g}^{-1}$ ) was from Alltech Associates. The specific surface areas of 10:1 dilutions of the adsorbent were determined with a Stroheilm areameter using the single-point nitrogen method and were found on average to be  $39.5 \text{ m}^2 \text{ g}^{-1}$ .

**Procedures.** Prior to rapid displacement by suction into  $1/4$ -in. nickel or stainless steel GC columns (thereby preventing particle segregation), sieved packings were conditioned overnight in a vacuum oven at  $395 \text{ K}$  and  $2 \times 10^5 \text{ Pa}$ . Data acquisition and reduction were then carried out as described by us in detail elsewhere (6) and as briefly recounted below.

**Adsorbate Retentions at Zero Surface Coverage.** For zero surface coverage experiments, the smallest detectable amounts of gases or adsorbate vapors were injected with a Hamilton 10-mm<sup>3</sup> syringe. The raw retentions  $t_R$  were measured with a stopwatch and cross-checked against tracings on a strip-chart recorder, the average of at least three runs being taken. All peaks exhibited acceptable symmetry, and the retentions were independent of the (Henry's law) amounts of highly diluted vapors that were introduced into the columns.

Adsorbate net retention volumes were calculated from the expression

$$V_N = j(t_R - t_A)F_c \quad (3)$$

where  $j$  is the James-Martin carrier compressibility correction factor,  $F_c$  is the carrier corrected flow rate, and  $t_A$  is the retention time of a nonretained compound (e.g., air).  $F_c$  was calculated in the usual way from the observed flow rate  $F_{tm}$ , the latter measured with a soap-bubble flowmeter at temperature  $T_{tm}$

$$F_c = F_{tm}(T_c/T_{tm})/[(p_o - p_w)/p_o] \quad (4)$$

where  $T_c$  is the column temperature,  $p_o$  is the column outlet pressure (taken as barometric), and  $p_w$  is the vapor pressure of water at  $T_{tm}$ . Surface partition coefficients  $K_S$ , precise to no worse than  $\pm 5\%$  (6), were then calculated from the relation

$$K_S = V_N/A_S \quad (5)$$

where the surface area  $A_S$  is the product of the specific area  $S/\text{m}^2 \text{ g}^{-1}$  and the total weight of column packing  $w_S/\text{g}$ .

Thermodynamic data describing the adsorption process were derived from the temperature dependence of the partition coefficients. Thus, the standard-state free energy of adsorption  $\Delta G_S^\circ$  was calculated from the relation (11, 12)

$$\Delta G_S^\circ = -RT \ln (K_S p_A^\circ / \pi_S) \quad (6)$$

where  $R$  is the gas constant,  $p_A^\circ$  is the adsorbate bulk vapor pressure, and  $\pi_S$  is the two-dimensional (surface) standard-state spreading pressure of the adsorbed gas. The values of the ref-

**Table I. Adsorbate Boiling Points  $T_b$ /K, Molar Refractions  $R_m$ /dm<sup>3</sup> mol<sup>-1</sup>, van der Waals Volumes  $b$ /dm<sup>3</sup> mol<sup>-1</sup> (14), and Absolute  $K_s$ /cm<sup>3</sup> m<sup>-2</sup> and Relative Partition Coefficients  $\alpha_i/c_{\text{ref}}$  at Zero Effective Surface Coverage on Porapak Q Adsorbent at Indicated Temperatures  $T$ /K**

adsorbate	$T_b$ /K	$b$ /dm <sup>3</sup> mol <sup>-1</sup>	$R_m$ /dm <sup>3</sup> mol <sup>-1</sup>	$K_s$ /cm <sup>3</sup> m <sup>-2</sup>				$\alpha_i/c_{\text{ref}}$	
				393 K	413 K	433 K	443 K	this work	ref 6
<i>n</i> -pentane	309.4	0.1460	25.27	0.221	0.124	0.072	0.055	0.37	0.40
<i>n</i> -hexane	342.2	0.1735	29.91	0.677	0.333	0.169	0.130	(1.00)	(1.00)
<i>n</i> -heptane	371.6	0.2065	34.55	1.662	0.747	0.360	0.272	2.24	2.48
<i>n</i> -octane	399.0	0.2368	39.19				0.721		6.62
cyclohexane	354.6	0.1424	27.71	0.854	0.392	0.215	0.164	1.18	1.19
methylcyclohexane	373.5		32.50	1.751	0.846	0.413	0.313	2.54	2.54
benzene	353.3	0.1154	26.18	0.822	0.392	0.209	0.150	1.18	1.13
dichloromethane	313.3		16.36	0.183	0.102	0.060	0.047	0.31	0.29
chloroform	334.5	0.1022	21.46	0.487	0.248	0.138	0.104	0.75	0.69
carbon tetrachloride	350.1	0.1383	26.44	0.758	0.387	0.200	0.159	1.16	
tetrahydrofuran	337.2			0.611	0.293	0.158	0.113	0.88	0.77
thiophene	357.3	0.1270	24.37	0.740	0.405	0.200	0.151	1.22	
acetone	329.3	0.0994	16.18	0.164	0.088	0.048	0.037	0.26	

\*Relative to *n*-hexane at 413 K.

erence states were taken (11, 12) to be 101 kN m<sup>-2</sup> for  $p_A^\circ$  and 0.338 mN m<sup>-1</sup> for  $\pi_s$ . The differential heats of adsorption of the adsorbates at zero surface coverage, i.e., the standard-state enthalpies of adsorption  $-\Delta H_s^\circ$ , were obtained from the relation

$$d(\ln K_s)/d(1/T_s) = -\Delta H_s^\circ/R \quad (7)$$

The corresponding standard-state entropies of adsorption  $\Delta S_s^\circ$  were then calculated from

$$\Delta S_s^\circ = (\Delta H_s^\circ - \Delta G_s^\circ)/T_c \quad (8)$$

**Adsorbate Retentions at Finite Surface Coverage.** The GC method used in this work to determine finite surface coverage adsorption isotherms was essentially that derived initially by Cremer and Huber (ref 13; see also ref 6), which is commonly referred to as the technique of "elution by characteristic point" (ECP). Briefly, it is possible to show from simplified mass-balance considerations that

$$dq/dc = V_N/w_s \quad (9)$$

where  $q$ /mol g<sup>-1</sup> is the amount of adsorbate that has been adsorbed per gram of adsorbent,  $V_N$ /cm<sup>3</sup> is the adsorbate net retention volume, and  $c$ /mol cm<sup>-3</sup> ( $=p/RT$ , ignoring virial effects) is the adsorbate concentration in the gas phase. Equation 9 thus provides the means of calculating  $q$  as a function of  $p$ , i.e., the adsorption isotherm  $q = f(p)$ , via  $V_N$ .

In practice, the amount  $q_A$  of adsorbed material A corresponding to a particular partial pressure  $p_A$  is given by

$$q_A = (n_A S_A)/w_s S_t \quad (10)$$

where  $n_A$  is the number of moles of adsorbate injected, which can be calculated from the (syringe) volume of liquid and its density and molecular weight,  $S_A$  is the chart area bounded by the diffuse profile of the chromatogram, the carrier gas front (as measured from a nonretained compound), and the peak height  $h$ , and  $S_t$  is the chart area bounded only by the peak trace. The recorder pen displacement  $h$  is then related to the partial pressure of the adsorbate in the gas phase via the relation

$$p_A = (n_A s h R T_c)/S_t F_c \quad (11)$$

where  $s$  is the recorder chart speed.

## RESULTS AND DISCUSSION

**Adsorbate Retentions at Zero Surface Coverage.** Table I presents the partition coefficients  $K_s$ /cm<sup>3</sup> m<sup>-2</sup> of the adsorbates at from 393 to 443 K with Porapak Q diluted 10:1 with Chromosorb G, together with the compound boiling points  $T_b$ /K, molar refractions  $R_m$ /dm<sup>3</sup> mol<sup>-1</sup>, and van der Waals volumes  $b$ /dm<sup>3</sup> mol<sup>-1</sup>. Also provided is a comparison of the adsorbate retentions relative to *n*-hexane,  $\alpha_i/c_{\text{ref}}$ , with those found previously with a different batch of Porapak Q adsorbent at 413 K (6). Table II then gives the heats, entropies, and Gibbs free energies of the adsorbates with diluted

**Table II. Heats  $-\Delta H_s^\circ$ /kJ mol<sup>-1</sup>, Entropies  $-\Delta S_s^\circ$ /J mol<sup>-1</sup> K<sup>-1</sup>, and Free Energies of Adsorption  $-\Delta G_s^\circ$ /kJ mol<sup>-1</sup> for Indicated Adsorbates with Porapak Q Adsorbent at 443 K**

adsorbate	$-\Delta H_s^\circ$ /kJ mol <sup>-1</sup>		$-\Delta S_s^\circ$ /J mol <sup>-1</sup> K <sup>-1</sup>	$-\Delta G_s^\circ$ /kJ mol <sup>-1</sup>
	this work	ref 6		
<i>n</i> -pentane	40.2 ± 2.0	45.3 ± 2.8	68.2	10.3
<i>n</i> -hexane	48.2 ± 2.4	52.5 ± 3.7	80.1	13.5
<i>n</i> -heptane	52.8 ± 2.6	59.8 ± 1.8	84.4	16.2
<i>n</i> -octane		67.6 ± 5.0		19.8
cyclohexane	47.6 ± 2.4	50.7 ± 3.7	76.8	14.3
methylcyclohexane	50.3 ± 2.5	56.1 ± 2.5	77.5	16.7
benzene	48.8 ± 2.4	48.3 ± 2.5	80.4	14.0
dichloromethane	39.3 ± 2.0	43.1 ± 3.0	68.3	9.73
chloroform	44.6 ± 2.2	42.6 ± 3.8	73.6	12.7
carbon tetrachloride	45.8 ± 2.3		72.9	14.2
tetrahydrofuran	48.4 ± 2.4	49.1 ± 2.7	81.7	13.0
thiophene	46.6 ± 2.3	50.2 ± 0.9	75.1	14.0
acetone	43.3 ± 2.2		79.5	8.85

Porapak Q at 443 K, as well as the  $\Delta H_s^\circ$  found previously with the bulk adsorbent (6). The precision of the absolute retentions was on average ca. ±2–3%, roughly in accord with what we found in previous studies of separate lots of this material.

**Comparison of Relative Retentions with Bulk vs "Diluted" Adsorbent.** The adsorbate relative retentions, columns 9 and 10 of Table I, were in gratifyingly good agreement, ca. ±0.05, considering the lack of correlation between adsorbent surface area and adsorbate absolute retentions found previously (cf. Table I of ref 6; the surface area of the batch of 60–80 mesh material used in this work was 524 m<sup>2</sup> g<sup>-1</sup> whereas that employed previously was 516 m<sup>2</sup> g<sup>-1</sup>). That is, despite a difference of an order of magnitude between the surface areas of bulk and admixed packings, the relative retentions were approximately invariant with packing surface area as well as extent of dilution. The data thereby establish that the "diluent" packing, Chromosorb G, is in fact very nearly inert as a GSC substrate for the compounds studied. Moreover, the heats of adsorption, columns 2 and 3 of Table II, agreed to within an experimental error of ca. ±5%, albeit the majority of those obtained with the diluted packing were marginally less negative than those found with the bulk material.

**Batchwise Imprecision of Absolute Retentions.** The imprecision of absolute retentions with various batches of a given Porapak has been regarded over the years as due largely to what amount to vagaries in the manufacturing process (15–19), the reproducibility of which continues to pose difficulties (20). However, it is certain that discrepant retentions are only partly a result of adsorbent batchwise variations. For example,



Johnson and Barrell (16) were led to postulate that the distribution and size of micropores may be as important in determining the GSC characteristics (21, 22) of porous polymer adsorbents as are their physical properties, such as rigidity, surface area, and surface activity (23), as well as the effects of various surface pretreatments (24). In addition, in work forming part of an extensive review of polymeric GSC stationary phases, Hollis (25) reported that the elution order of  $C_2$  hydrocarbons can vary quite substantially depending not only on the type of Porapak used but the column temperature as well. It was also found that the adjusted retention times  $t_R'$  of adsorbates changed with column temperature in different ways from one Porapak to another. Thus, various compounds exhibited near-identical  $t_R'$  over a particular temperature range (i.e., no separation), while below or above this there were considerable differences in elution order. [As one consequence of this, thermal effects alone can be used for window-diagram optimization (26) of adsorbate separations, as described and discussed first by Laub and Purnell (27) in their studies of the temperature-based enhancement of resolution in both gas and liquid chromatography].

An investigation of the potential influence of thermal modification of various porous polymers has also been reported by Coppi, Betti, Blo, and Bighi (27), who studied the retentions of a range of adsorbates spanning Kiselev's classifications (29). The results pertinent to this work were that adsorbate retentions with Porapak Q increased as the conditioning temperature was increased from 423 to 473 K, ketones and alcohols being the most severely affected. Moreover, when the conditioning temperature was increased beyond 473 K, a further increase in the retention volumes of benzene and *n*-hexane was observed, while those for acetone and 2-propanol decreased.

In related investigations of the oxidative degradation of Porapak Q at elevated temperatures resulting from traces of oxygen in carrier gases (the pyrolysis of Porapak Q at 523 K also produces *m*- and *p*-ethylvinylbenzene), Neumann and Morales (30) carried out infrared spectroscopic studies of Chromosorb 102 and Porapak Q packings that had been exposed to nitrogen that contained small amounts of oxygen. They found that each of these polymers can react with adsorbed oxygen to form surface carbonyl compounds that can then induce oxidative depolymerization. Presumably, the reaction is initiated by the adsorption of oxygen onto a surface vinyl group, followed by oxidation of the carbon atom nearest an aromatic ring. Trowell (31) has also shown that trace amounts of  $NO_2$  in carrier gases can result in the formation of nitric oxide, water, and nitration of the aromatic rings of Porapak Q. In addition, competitive adsorption even of unreactive carrier gases can affect adsorbate retentions with Porapak stationary phases, as pointed out by Rabbani, Rusek, and Janak (32); although the effects of gas-phase virial interactions (33, 34) coupled with deactivation of the adsorbent by the mobile phase have only recently been treated in any quantitative detail (35, 36).

**Multiplicity of Mechanisms of Retention.** In view of the above-mentioned sources of uncertainty regarding the properties of porous polymer packings, it is hardly surprising that attempts at speciating the mechanism(s) of adsorbate retentions with such materials have in the past been the source of some controversy. Moreover, it is fair to say even today that the matter has not by any account been fully resolved. For example, Zado and Fabecic (37) reported that porous polymer packings appear to act both as gas-solid and gas-liquid chromatographic stationary phases and that adsorption, diffusion, and partitioning (cf. ref 6) all contribute to the selectivity of the materials. Hollis (38) has also suggested that the "solubility" of compounds in such polymers is the most

important factor in determining the elution order of adsorbates [we have referred elsewhere to this process as imbibition (39)], and that their boiling points and/or vapor pressures are of little consequence. Conversely, Smith and Waddington (40) reported that log (retention times) were linear with adsorbate boiling point with Porapak Q within classes of compounds. Sakodinskii (41) also found that log  $V_R'$  regressed linearly with the total polarizability and molecular weight of members of homologous series of adsorbates with this adsorbent.

The results of this work indicate that, in fact, adsorbate retentions at effective zero surface coverage are due to a complex combination of factors, the most important of which are point-contact and sieving effects. In addition, adsorbates are retained subject to electrostatic-induced polarization. Since these factor bear on the analytical as well as physicochemical properties of Porapak Q, each is considered in turn below.

**Homologous-Series Behavior.** We determined, first, that plots of log  $K_S$  as a function of *n*-alkane carbon number routinely yielded straight lines with linear regression correlation coefficients *r* on the order of 0.999. Log  $K_S$  was also linear in the number of chlorine atoms in the haloalkane adsorbates at each experimental temperature. Thus, homologous-series behavior, e.g., homologue-unit incremental increases in the enthalpy of adsorption, can be assumed to apply both in the former case (representative of nonspecific interactions) as well as with the latter class of adsorbates that, presumably, give rise to specific interactions with Porapak Q.

**Point-Contact and Sieving Effects.** In an attempt to determine the relative contributions of point-contact and molecular sieving effects to retentions (the latter due to the microporous structure of Porapak Q), we next examined the dependence of the adsorbate  $-\Delta G_S^\circ$ , Table II, on factors such as van der Waals volumes *b* and molecular geometry.

Broadly speaking, cycloalkanes are retained more strongly than the corresponding *n*-alkanes of the same carbon number in GSC, that is, *n*-hexane is expected to elute before cyclohexane, followed by *n*-heptane and then methylcyclohexane. This is also the order that would be predicted on the basis of boiling points  $T_b$ , i.e., as if the adsorbate-adsorbent interactions were completely nonspecific. On the other hand, if the retentions were to correspond solely to decreasing molecular volumes *b*, that is, be governed by a kind of molecular sieving mechanism, then the least-retained adsorbate would be *n*-heptane, followed in turn by cyclohexane and then *n*-hexane.

The former order of elution was in fact observed experimentally, that is, the free energies of adsorption for cyclohexane and methylcyclohexane were uniformly more negative than the respective values for *n*-hexane and *n*-heptane. These findings suggest that molecular geometry most likely plays a smaller role in governing the adsorbate retentions with Porapak Q than has heretofore been supposed. For example, in the case of *n*-hexane, all six carbon atoms can approach a plane simultaneously, whereas, depending on the steric form that cyclohexane may take, only three or four of its atoms can interact with a given surface at the same time. Yet cyclohexane elutes well after *n*-hexane. Also, while the heat of adsorption of *n*-heptane was found to be greater than that of methylcyclohexane, the former was observed to elute well prior to the latter, a consequence of the greater entropy change for *n*-heptane on passing from the vapor to the adsorbed state (see also below).

We also observed that while the regression of  $-\Delta G_S^\circ$  with  $b^{-1}$  was linear for the *n*-alkanes, there was no such correlation for the remaining adsorbates. Nevertheless, we cannot entirely dismiss the effects of molecular volume, particularly as regards

sieving. For example, Dressler, Duha, and Janak (42) observed several anomalies in the retentions as well as peak shapes of branched alkanes and cycloalkanes with Porapak P (a copolymer of styrene and divinylbenzene), e.g., the higher the degree of branching of the adsorbate the lower was its retention time and the broader its peak width. This suggests that the retentions were due at least in part to some or other manner of molecular exclusion, for which adsorbate band broadening in excess of that due to adsorption can be attributed to partial penetration of the adsorbent matrix. In addition, silylation of the Porapaks (Porapak PS, etc.) had no effect on the anomalous retention behavior. The elution order of the adsorbates hence cannot be claimed to be due solely to variations in the energetics of the adsorbent surface, that is, residual functionality, but must also involve its topology, i.e., pores and fissures. Porous polymer packings such as Porapaks P and Q are also comprised of substantial interstitial free space in addition to that associated with irregularly shaped cracks and crevices, the accessibility to which is enhanced at higher temperatures. (It is noteworthy in this regard that as Porapak P was coated with increasing amounts of a stationary liquid, adsorbate band broadening decreased substantially.)

**Surface Heterogeneity.** It is a virtual certainty that energetically distinguishable sites of adsorption are present on the surfaces of virtually all solids. An alternative view of the retention data with supposed nonspecific adsorbents such as Porapak Q is, therefore, that surface heterogeneities are responsible for anomalies in elution behavior such as those mentioned above. That is, adsorbates can be adsorbed onto different sites in different ways. For example, it is conceivable that high-field sites are associated with high energies of activation and so, predominate the adsorption process at high temperatures. In contrast, since these sites are not active at lower temperatures, less-energetic sites govern the retentions. (The extent to which an adsorbent appears to be energetically heterogeneous depends in part on the size of the adsorbate molecule. For example, if high-energy sites were to extend over small regions of space, they would affect only small molecules to any appreciable extent. The surface would otherwise appear to larger molecules to be energetically uniform due to the fewer contacts made over the greater surface area.)

In contrast, if the adsorption process were based entirely on nonpolar van der Waals forces, the magnitude of the heat of adsorption would be a function almost entirely of the number of adsorbate atoms that can come into simultaneous contact with an adsorbent surface. However, as pointed out earlier for *n*-hexane and cyclohexane adsorbates with Porapak Q, this is not so (the latter elutes after the former). Nevertheless, the majority of treatments of adsorption in GSC attribute gas-solid interactions largely to nonpolar van der Waals forces. That is, the assumption is made that the same forces that produce condensation are responsible for the adsorption of adsorbate molecules onto a surface. There is undoubtedly some degree of truth in this insofar as adsorbed layers of solutes do in fact behave in many respects like two-dimensional liquids. Also, physisorption, like condensation, is a phenomenon that virtually all compounds can undergo with any solid at appropriate temperature and pressure. Further, since physisorption is undoubtedly related to the pressure of liquefaction, multilayer adsorption of adsorbates usually occurs to an appreciable extent at pressures and temperatures close to those required for liquefaction. In addition, the heat of physisorption is of the same order of magnitude as that of condensation.

**Electrostatic Effects.** According to the electrostatic model of adsorption developed by King and Benson (43, 44), gases

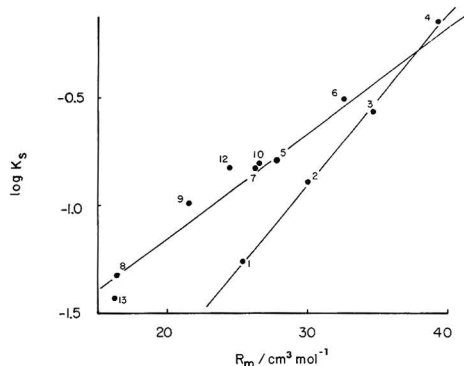


**Figure 1.** Regression of  $\log K_s$  at 443 K against molar refraction  $R_m/\text{dm}^3 \text{mol}^{-1}$  for the adsorbates (1) *n*-pentane, (2) *n*-hexane, (3) *n*-heptane, (4) *n*-octane, (5) cyclohexane, (6) methylcyclohexane, (7) benzene, (8) dichloromethane, (9) chloroform, (10) carbon tetrachloride, (11) tetrahydrofuran, (12) thiophene, and (13) acetone.

are polarized by uncompensated charges on the surface of the adsorbent, the energy of attraction being

$$\sigma_{\text{att}} = -\alpha C_{\text{eff}}/2z^2 \quad (12a)$$

or, alternatively

$$\sigma_{\text{att}} = -\alpha Ez^2/2 \quad (12b)$$

where  $C_{\text{eff}}$  is an effective surface charge,  $z$  is the distance of separation of charges, which is usually replaced by  $(r - r')$  where  $r$  is the distance between the adsorbate and the adsorbent surface and  $r'$  is the radius of the adsorbed molecule,  $\alpha$  is the polarizability of the adsorbed molecule, and  $E$  is the electric field intensity normal to the surface. Molecules adsorbed in a monolayer are assumed in this model to be mobile in any direction coplanar with the adsorbent surface and, moreover, to be unaffected by the surface-parallel component of the electric field. Also, the perpendicular component of the electric field is said to cause adsorbate orientation in the direction of greatest polarizability, which for diatomic as well as chainlike species lies along the internuclear backbone.

In consideration of the practical consequences of electrostatic effects in GSC, it is useful to relate the electronic polarizability of an adsorbate  $\alpha_e$  to its molar refraction  $R_m$

$$R_m = [(\eta^2 - 1)/(\eta^2 + 2)] M/N\rho = 4\pi\alpha_e/3 \quad (13)$$

where  $\eta$  is the refractive index of an adsorbate of molecular weight  $M$  and density  $\rho$ , and where  $N$  is Avogadro's number. Thus, retentions should exhibit some or other dependence upon  $R_m$ .

Plots of  $\log$  (adsorbate partition coefficient) against molar refraction are shown in Figure 1; the *n*-alkanes form a single straight line, while all other adsorbates roughly correspond to a second straight line of shallower slope. In addition, there was a good correlation of  $\Delta H_s^\circ$  with  $R_m$  and, hence,  $\alpha_e$  as well (cf. Figure 2 of ref 6). There can therefore be little question that polarization effects also play a substantial role in governing adsorbate retentions at zero surface coverage with Porapak Q. Little else can be said at this time, however, without further and comprehensive study (the results of which we hope soon to report).

**Adsorbate Retentions at Finite Surface Coverage.** The adsorption isotherms for *n*-hexane, cyclohexane, benzene, carbon tetrachloride, and acetone at 443, 433, 413, and 393 K were all represented by the function  $q_A = f(p_A/p_A^\circ)$ , where  $p_A^\circ$  is the bulk adsorbate vapor pressure; an example of the

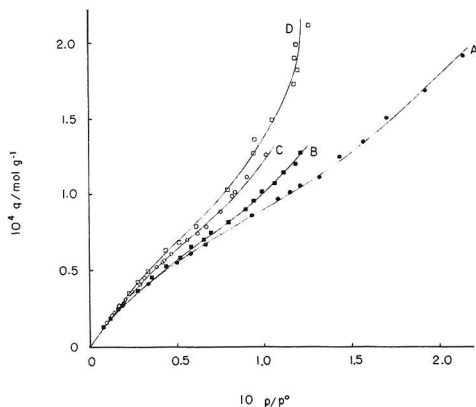


**Figure 2.** Adsorption isotherms (uptake vs relative pressure) for acetone adsorbate with "diluted" Porapak Q adsorbent at 443 K (A), 433 K (B), 413 K (C), and 393 K (D).

results is provided in Figure 2 (acetone adsorbate). All isotherms were of BET Type IV (45), which indicates the presence of mesopores in addition to micropores. (In consideration of the surface properties of solids having a large specific surface, it is convenient to define micropores as less than 2 nm in width; mesopores are said to be between 2 and 50 nm wide; and macropores are all those greater than 50 nm in diameter. It is also useful to distinguish between external and internal surfaces, where the latter consists of the walls of all cracks, pores, and cavities that are deeper than they are wide, while the former is taken to include all prominences and all cracks that are wider than they are deep.)

Figure 3 shows the lower region of the adsorption isotherm for *n*-hexane at 413 K, which was obtained at various flow rates and which is representative of all of those measured in this work. Plots of these kinds established that the flow rate had little or no effect on adsorbate partitioning between the adsorbent and the carrier (all points lay on the same isotherm), that is, equilibrium partitioning was extant throughout chromatographic migration of the adsorbate bands.

**Temperature Coefficient of Adsorption.** The adsorption of gases is invariably an exothermic process so that, provided equilibrium has been established, the amount adsorbed at a given relative pressure must diminish as the temperature is increased. It is not infrequently observed, however, that an isotherm at a given temperature actually lies above its counterpart at a lower temperature. Anomalous behavior of this kind is characteristic of a system for which the combined effects of temperature on the position of equilibrium as well as on the rate of approach to it are important. It therefore points to a process that is "activated" in a true kinetic sense, that is, which occurs more rapidly as the temperature is increased. We believe that this "activated" process in fact corresponds to the diffusion of adsorbate molecules through very narrow constrictions into cavities that lie beyond (46, 47). Further, when the width of a constriction is very close to the diameter of an adsorbate, the molecule will encounter an energy barrier to its passage through the opening such that the rate of entry into the cavity will have a positive temperature coefficient (i.e., the higher the temperature the greater the rate of passage). If adsorption were to occur on surfaces both internal and external to such pores, there should then exist a temperature at which the sign of the adsorption coefficient would change. The reversal would correspond to an initial decrease in uptake because of minimal pore "activation" at lower temperatures, followed by an increase

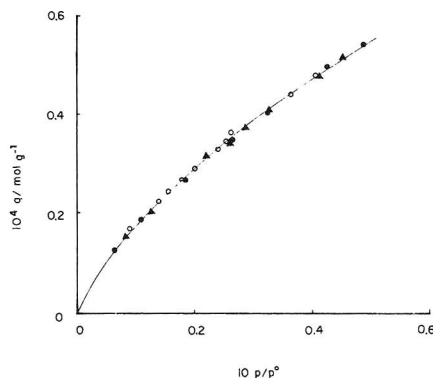


**Figure 3.** Adsorption isotherm for *n*-hexane with "diluted" Porapak Q at 413 K and at various carrier flow rates: filled circles, 42.6 cm<sup>3</sup> min<sup>-1</sup>; open circles, 27.4 cm<sup>3</sup> min<sup>-1</sup>; and triangles, 18.1 cm<sup>3</sup> min<sup>-1</sup>.

due to penetration of cavities as the temperature increased. However, the effect is easily masked by the adsorption that takes place on external surfaces. Thus, a change in the adsorption temperature coefficient was observed in our previous study (6) only for acetone at 493 K (Figure 10 of that work). In contrast, in the present instance, we found a positive adsorption coefficient for acetone adsorbate with diluted Porapak Q at temperatures of as low as 393 K, Figure 2. That is, dilution of the adsorbent has the effect of lowering the total surface area available for adsorption, which in turn results in a lowering of the positive adsorption temperature coefficient. [The effect was also observed in the isotherms for cyclohexane and benzene, those at 443 K lying above those at 433, 393, and 413 K. In addition, the isotherms of *n*-hexane at 443 K lay above those at 433, 413, and 393 K. In contrast, the positive and negative adsorption temperature coefficients for carbon tetrachloride adsorbate were of the same order of magnitude, that is, there was only a small change in uptake with temperature when compared with that observed for the same adsorbate with bulk Porapak Q (6).]

**Isosteric Heats of Adsorption.** Application of the Clausius-Clapeyron equation to the adsorption isotherms yielded the isosteric (i.e., constant surface coverage) heats of adsorption,  $q_{st}$

$$-q_{st}/R = [\partial \ln p / \partial (1/T_c)]_q \quad (14)$$

A representative example of the results, plotted as a function of surface coverage, is shown for carbon tetrachloride adsorbate in Figure 4. At low surface coverage the data tend toward the heat of liquefaction  $\Delta H_L$  because of the increasing importance of adsorbate-adsorbate interactions as well as the decreasing influence of the adsorbent as  $p/p^0$  is increased. Also, because of the small quantity of adsorbent in the diluted packing,  $q_{st}$  was observed in this work to fall below  $\Delta H_L$  for some adsorbates (*n*-hexane, benzene) even at very low  $p/p^0$ . That is, trace quantities of adsorbates were sufficient to give relatively high surface coverage of the meager amount of adsorbent present in the column.

**Capillary Condensation.** Values of  $q_{st}$  that fall below  $\Delta H_L$  at high surface coverage are a result of capillary condensation, the driving force of adsorption in these instances being the pressure difference across an interface. The onset of this phenomenon generally coincides with an inflection in the isotherm, e.g., BET Type IV, several explanations for which have been offered over the years (48). For example, it has been suggested that there is a buildup of multilayers during adsorption onto capillary walls, but that a complete meniscus

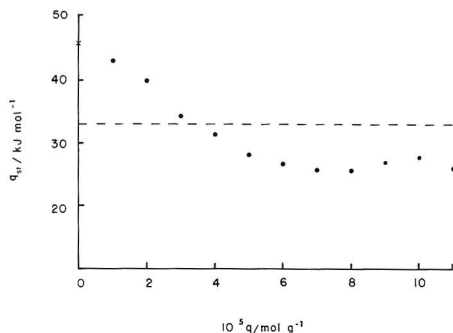


**Figure 4.** Plots of isosteric heats of adsorption against surface coverage for carbon tetrachloride adsorbate with "diluted" Porapak Q: cross,  $\Delta H_s$  from measurements at zero surface coverage; horizontal dashed line, molar heat of liquefaction  $\Delta H_L$ .

is not formed until saturation is achieved (i.e., when all pores have been filled). The relationship between pressure and concentration along the adsorption branch of the isotherm will then be governed by an appropriate multilayer isotherm in accordance with the BET equation. However, once the saturation limit for capillaries of a particular size has been reached, desorption will occur from a curved meniscus and the equilibrium pressure hence will be governed by the Kelvin equation

$$\ln(p/p^0) = -2\gamma\bar{V} \cos \phi / rRT \quad (15)$$

where  $\gamma$  is the surface tension of the condensate,  $\phi$  is the contact angle,  $r$  is the radius of a cylindrical pore,  $p$  is the equilibrium vapor pressure under which a liquid is evaporating from the pore and condensing onto a plane surface over which the vapor pressure is  $p^0$  (the saturation vapor pressure of the pure liquid at the same temperature  $T$ ), and  $\bar{V}$  is the molar volume of the adsorbate. However, the liquid film formed during adsorption is in a metastable state, the true equilibrium state being represented by liquid condensed in the capillary. The stability of such multilayer films would therefore depend upon the absence of nucleating agents that could give rise to bulk-liquid condensation. In contrast, it might be thought that capillary effects would be extant along both the adsorption and desorption branches of isotherms, differences between the two being due to the difference in meniscus shape. (During adsorption pores fill radially, which results in cylindrical menisci.) However, the data of the present work are insufficient to distinguish between these effects; supplemental studies of capillary condensation as related to finite-concentration adsorption isotherms are therefore called for.

**Registry No.** Porapak Q, 9043-77-0; *n*-pentane, 109-66-0; *n*-hexane, 110-54-3; *n*-heptane, 142-82-5; *n*-octane, 111-65-9; cyclohexane, 110-82-7; methylcyclohexane, 108-87-2; benzene, 71-43-2; dichloromethane, 75-09-2; chloroform, 67-66-3; carbon tetrachloride, 56-23-5; tetrahydrofuran, 109-99-9; thiophene, 110-02-1; acetone, 67-64-1.

## LITERATURE CITED

- (1) Al-Thamir, W. K.; Purnell, J. H.; Laub, R. J. *J. Chromatogr.* **1979**, *176*, 232-236.
- (2) Al-Thamir, W. K.; Purnell, J. H.; Laub, R. J. *J. Chromatogr.* **1980**, *188*, 79-88.
- (3) De Zeeuw, J.; De Nijs, R. C. M.; Henrich, L. T. *J. Chromatogr. Sci.* **1987**, *25*, 71-83.
- (4) Bombaugh, K. J. *Nature (London)* **1963**, *197*, 1102-1103.
- (5) Laub, R. J.; Madden, S. J. *J. Liq. Chromatogr.* **1985**, *8*, 271-280.
- (6) Djordjevic, N. M.; Kopećni, M. M.; Laub, R. J.; Milonjic, S. *Anal. Chem.* **1986**, *58*, 1395-1404.
- (7) Laub, R. J.; Pecsok, R. L. *Physicochemical Applications of Gas Chromatography*; Wiley-Interscience: New York, 1978; Chapter 7.
- (8) Conder, J. R.; Young, C. L. *Physicochemical Measurement by Gas Chromatography*; Wiley: Chichester, England, 1979; Chapter 9.
- (9) Chien, C.-F.; Kopećni, M. M.; Laub, R. J.; Smith, C. A. *J. Phys. Chem.* **1981**, *85*, 1864-1871.
- (10) Laub, R. J.; Purnell, J. H.; Williams, P. S.; Harbison, M. W. P.; Martire, D. E. *J. Chromatogr.* **1978**, *155*, 233-240.
- (11) Katz, S.; Gray, D. G. *J. Colloid Interface Sci.* **1981**, *82*, 326-338.
- (12) de Boer, J. H. *The Dynamical Character of Adsorption*; Clarendon: Oxford, 1953; p 49.
- (13) Cremer, E.; Huber, H. F. *Angew. Chem.* **1961**, *73*, 461-465.
- (14) *CRC Handbook of Chemistry and Physics*, 64th ed.; 1983-1984; p 191.
- (15) Hollis, O. L. *Anal. Chem.* **1966**, *38*, 309-316.
- (16) Johnson, J. F.; Barrall, E. M., II. *J. Chromatogr.* **1967**, *31*, 547-549.
- (17) Dressler, M.; Vespaic, R.; Janak, J. *J. Chromatogr.* **1971**, *59*, 423-428.
- (18) Fuller, E. N. *Anal. Chem.* **1972**, *44*, 1747-1753.
- (19) Gough, T. A.; Simpson, C. F. *J. Chromatogr.* **1972**, *68*, 31-45.
- (20) Pollock, G. E.; O'Hara, D.; Hollis, O. L. *J. Chromatogr. Sci.* **1984**, *22*, 343-347.
- (21) Castello, G.; d'Amato, G. *J. Chromatogr.* **1983**, *254*, 69-82.
- (22) Castello, G.; d'Amato, G. *J. Chromatogr.* **1983**, *269*, 153-160.
- (23) Dave, S. B. *J. Chromatogr. Sci.* **1969**, *7*, 389-399.
- (24) Hertl, W.; Neumann, M. G. *J. Chromatogr.* **1971**, *60*, 319-327.
- (25) Hollis, O. L. *J. Chromatogr. Sci.* **1973**, *11*, 335-342.
- (26) Laub, R. J.; Purnell, J. H. *J. Chromatogr.* **1975**, *112*, 71-79.
- (27) Laub, R. J.; Purnell, J. H. *J. Chromatogr.* **1978**, *161*, 49-57.
- (28) Coppi, S.; Betti, A.; Blo, G.; Bighi, C. *J. Chromatogr.* **1983**, *267*, 91-99.
- (29) Kiselev, A. V.; Yashin, Ya. I. *Gas-Adsorption Chromatography*; Bradley, J. E. S., Translator; Plenum: New York, 1969; Chapter IV.
- (30) Neumann, M. G.; Morales, S. T. *J. Chromatogr.* **1972**, *74*, 332-334.
- (31) Trowell, J. M. *J. Chromatogr. Sci.* **1971**, *9*, 253-254.
- (32) Rabbani, G. S. M.; Rusek, M.; Janak, J. *J. Gas Chromatogr.* **1968**, *6*, 399-400.
- (33) Laub, R. J. *Anal. Chem.* **1984**, *56*, 2110-2115.
- (34) Laub, R. J. *Anal. Chem.* **1984**, *56*, 2115-2119.
- (35) Slais, K.; Krejci, M.; Chmelikova, J.; Kourilova, D. *J. Chromatogr.* **1987**, *388*, 179-187.
- (36) Laub, R. J., unpublished work, 1987, San Diego State University.
- (37) Zado, F. M.; Fabecic, J. *J. Chromatogr.* **1970**, *51*, 37-44.
- (38) Hollis, O. L. *J. Chromatogr. Sci.* **1973**, *11*, 335-342.
- (39) Laub, R. J. *HRC CC, J. High Resolut. Chromatogr. Chromatogr. Commun.* **1987**, *10*, 565-569.
- (40) Smith, J. R. L.; Waddington, D. J. *J. Chromatogr.* **1968**, *36*, 145-151.
- (41) Sakodinskii, K. *Chromatographia* **1968**, *1*, 483-487.
- (42) Dressler, M.; Guha, O. K.; Janak, J. *J. Chromatogr.* **1972**, *65*, 261-269.
- (43) King, J., Jr.; Benson, S. W. *Anal. Chem.* **1966**, *38*, 261-265.
- (44) King, J., Jr.; Benson, S. W. *J. Chem. Phys.* **1966**, *44*, 1007-1014.
- (45) Brunauer, S.; Emmett, P. H.; Teller, E. *J. Am. Chem. Soc.* **1938**, *60*, 309-319.
- (46) Zwietering, P. W.; van Krevelin, D. W. *Fuel* **1954**, *33*, 331-337.
- (47) Maggs, F. A. P. *Research* **1953**, *6*, S13.
- (48) Young, D. M.; Crowell, A. D. *Physical Adsorption of Gases*; Butterworths: London, 1962.

RECEIVED for review June 17, 1987. Accepted September 30, 1987. Support provided for this work in part by the Department of Energy Office of Basic Energy Sciences (analytical considerations) and by the National Science Foundation (high-precision and finite-concentration work) is gratefully acknowledged.

# Anodic Characterization of Mercury Microelectrodes in Electrolytes at the Micromolar Level

Zbigniew Stojek

Department of Chemistry, Warsaw University, Pasteura 1, 02-093 Warsaw, Poland

Janet Osteryoung\*

Department of Chemistry, State University of New York at Buffalo, Buffalo, New York 14214

Mercury microelectrodes based on platinum wires of a radius of either 1 or 12.5  $\mu\text{m}$  were examined anodically in several very dilute electrolytes: NaBr, NaCl,  $\text{Na}_2\text{C}_2\text{O}_4$ , NaOH, ethylenediaminetetraacetic acid, NaSCN,  $\text{NaNO}_3$ , and thiourea. Anodic response was obtained in micromolar solutions of the electrolytes and the measured current was in most cases directly proportional to the concentration. Waves obtained with such electrodes provide fast, reliable diagnosis in cases of adsorption or precipitation at the electrode surface. Equations describing anodic waves of mercury microelectrodes are proposed.

Microvoltammetric electrodes are very small, generally with one dimension in the range of micrometers. When used for experiments with a sufficiently long time scale ( $\Lambda = r/(Dt)^{1/2} \ll 1$ , where  $r$  is the small dimension,  $D$  the diffusion coefficient, and  $t$  the characteristic time of the experiment) they display unusual voltammetric response compared with that for larger electrodes for which diffusion is mainly planar (e.g., for  $\Lambda \gg 1$ ) (1). Use of microelectrodes is increasing rapidly, and there are many reports of applications in electroanalytical chemistry (2). There is some confusion in the literature regarding the term "microelectrode". In the following we mean by "microelectrode" an electrode with  $r$  in the range of micrometers that is used under conditions where  $\Lambda \ll 1$ .

Thus far, mercury microelectrodes have been used mainly for anodic stripping voltammetry (3-7). In most cases mercury has been plated in situ on carbon fibers (3-5, 7). Wehmeyer and Wightman (6) used platinum wires as the support for mercury and prepared mercury hemispheres with radii of several micrometers in a separate cell by electroreduction of  $\text{Hg}_2^{2+}$ .

The anodization of mercury to form strong complexes of  $\text{Hg(II)}$  or insoluble compounds with  $\text{Hg(I)}$  is well-known (8, 9). Following the diffusion layer treatment of Heyrovský and Kóta (8) for complex formation, we have the Nernst equation for the oxidation of  $\text{Hg}$  to  $\text{Hg}^{2+}$ :

$$E = E^{\circ'} + (1/nf) \ln [\text{Hg}^{2+}]_s \quad (1)$$

where  $E^{\circ'}$  is the formal potential for the reaction  $\text{Hg}^{2+} + ne^- \rightleftharpoons \text{Hg}$ ,  $f = F/RT = 38.9 \text{ V}^{-1}$  at  $25^\circ\text{C}$ , and the subscript  $s$  indicates the surface concentration. In the absence of a complexing agent, at a microelectrode, this yields the current-potential response

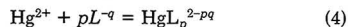
$$E = E^{\circ'} + (1/nf) \ln [i] + (1/nf) \ln [\delta/nFAD_M] \quad (2)$$

where  $\delta$  is the diffusion layer thickness,  $A$  the electrode area, and  $D_M$  the diffusion coefficient of  $\text{Hg}^{2+}$ . The value of  $n$  is expected to be two for both  $\text{Hg(II)}$  and  $\text{Hg(I)}$ . Although the physical situation corresponding to  $\Lambda \ll 1$  is not a steady state, we identify the quantity  $\delta$  with the diffusion layer thickness

appropriate to the reduction of a substance with bulk concentration  $C$  and diffusion coefficient  $D$  at a circular electrode with  $\Lambda \ll 1$ . The limiting current in that case is given by  $i_L = 4nFD_Cr$  or by the diffusion layer model as  $i_L = nFADC/\delta$ . Equating these two expressions, with  $A = \pi r^2$ , yields  $\delta = \pi r/4$  and eq 2 becomes

$$E = E^{\circ'} + (1/nf) \ln [i] - (1/nf) \ln [4nFD_Mr] \quad (3)$$

When coupled with the complex formation reaction



the oxidation of mercury to  $\text{Hg(II)}$  yields a limiting current at a microdisk electrode given by

$$i_{d,L} = 4nFD_L C_L r/p \quad (5)$$

where  $D_L$  and  $C_L$  are the diffusion coefficient and bulk concentration, respectively, of the ligand. Employing eq 1 and 4 with the same diffusion layer treatment yields the current-potential relation

$$E = E_{1/2} + (1/nf) \ln [i i_{d,L}^{p-1} 2^{1-p} / (i_{d,L} - i)^p] \quad (6)$$

$E_{1/2} =$

$$E^{\circ'} - (1/nf) \ln K + (1/nf) \ln [2^{p-1} D_L / p D_{ML} C_L^{p-1}] \quad (7)$$

where  $K$  is the equilibrium constant for reaction 4, and  $D_{ML}$  is the diffusion coefficient of the complex,  $\text{HgL}_p^{2-pq}$ . Note that eq 7 differs from that expected for planar diffusion only in that the ratio  $D_L/D_{ML}$  appears to the power one rather than one-half. Equation 5 is an approximation to the actual experimental situation, as will become clear from the details presented below.

In all cases the concentration of ligand and amount of mercury were chosen so that the change in size or shape of the electrode by anodization should be negligible, that is, the stationary electrode model is appropriate rather than the shrinking electrode model. The latter is of course equivalent to models for growth of nuclei (11, 12). Amounts of mercury large enough to approximate a stationary electrode, when deposited on a small circular substrate, may approximate the geometry of a hemisphere, or section of a sphere, more nearly than that of a disk. For hemispherical geometry the numerical coefficient of eq 5 should be replaced by  $2\pi$ . The uncertainty in specifying the exact geometry therefore probably corresponds to an inability to specify the numerical coefficient of eq 5 more exactly than the range 4-6.3. (That is,  $\pi r/4 \leq \delta \leq r$ .)

At microelectrodes diffusion of product is enhanced, so that the faradaic reaction of nondiffusing product, e.g., adsorbed or precipitated material, can be observed directly without being mixed with the faradaic reaction of diffusing material. Also studies of anodization of mercury in large concentrations of supporting electrolyte are limited by both metal ion and ligand impurities. It is possible with microelectrodes to work



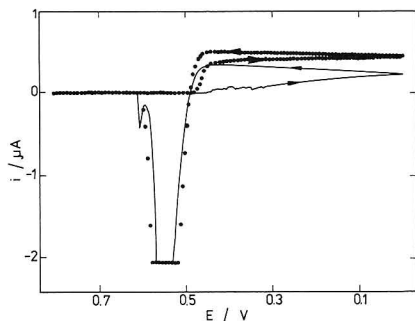


Figure 1. Cyclic staircase voltammery of 0.025 M  $\text{Hg}_2^{2+}$  in 0.125 M  $\text{HClO}_4$ .  $\Delta E_s = 5$  mV,  $\tau = 0.25$  s, 1  $\mu\text{m}$  Pt (—), 12.5  $\mu\text{m}$  Pt (●).

effectively with no deliberately added electrolyte (13, 14). Therefore, we adopted as the specific aim of this work characterization of the voltammetric response of mercury microelectrodes in dilute (micromolar) solutions of various ions in deionized water.

### EXPERIMENTAL SECTION

Cyclic voltammetric measurements were carried out by using an EG&G PARC 174A polarographic analyzer and a Houston Instruments 200 XY recorder. Staircase, square wave, and normal pulse voltammetry were done with an EG&G PARC 273 potentiostat and a Keithley 427 current amplifier, which, connected to the auxiliary input of the PARC 273, served as a current measuring device. This setup was controlled by a PDP 8/e minicomputer. Saturated calomel (SCE) and Pt wire were reference and auxiliary electrodes, respectively. Mercury electrodes were prepared by electrodepositing mercury from  $\text{Hg}_2^{2+}$  solutions onto platinum microdisk electrodes of 1 or 12.5  $\mu\text{m}$  radius. The platinum disks were made by sealing in glass under vacuum. Silver was tried as a base but abandoned despite its excellent wetting properties since it yields a formal potential that is too close to that of mercury in many electrolytes.

There is a substantial difference between certain properties of mercury electrodes on the two sizes of substrate used. The area of the mercury surface increases with deposition time much faster in the case of the platinum 1- $\mu\text{m}$  disk. The situation is illustrated in Figure 1 with two cyclic staircase curves. In the limiting current region ( $E \lesssim 0.45$  V) the current is proportional to electrode area under these conditions. For the 1- $\mu\text{m}$  disk the current at +0.4 V on the forward scan is only about 20% of that on the reverse, whereas on the 12.5- $\mu\text{m}$  disk, the corresponding value is nearly 80%. Deposition of mercury was carried out at constant potential in the range 0 to -0.4 V. In 0.025 M  $\text{Hg}_2^{2+}$  solution also 0.125 M in  $\text{HClO}_4$ , an electrolysis time of only tens of seconds was required to obtain the amount of mercury required to maintain constant area during the anodic process. Under these conditions, the chronoamperometric curve on the 1- $\mu\text{m}$  platinum substrate could be described by the equation  $i$  ( $\mu\text{A}$ ) =  $0.002 + 0.052t^{1/2}$  for  $2.5 < t/\text{s} < 40$  with correlation coefficient 0.997, which agrees with the hemispherical deposit model (11, 12). The platinum electrode of 12.5  $\mu\text{m}$  radius behaved differently, due to larger area, the current for deposition of mercury being linear with time:  $i$  ( $\mu\text{A}$ ) =  $0.264 + 0.00275t$  (s). The current-time curve was often erratic due to coalescence of small mercury drops formed in the first few seconds of plating. The amount of mercury deposited was 3.6  $\mu\text{C}$  for 1- $\mu\text{m}$  platinum and usually slightly higher for 12.5- $\mu\text{m}$  platinum (4.5–7.0  $\mu\text{C}$ ). A full hemisphere on the 12.5- $\mu\text{m}$  radius platinum disk would require 26.7  $\mu\text{C}$ . The efficiency of deposition was close to 100%. Finally, when the same amount of mercury was plated, the larger platinum disk formed the more stable electrode. The amount of mercury was always checked after the experiment by oxidizing mercury in the plating solution.

The scan rate in voltammetric experiments was chosen as 10 mV/s. Under this condition the electrode should be in the

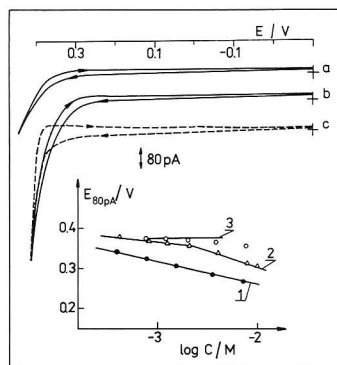


Figure 2. Cyclic voltammograms obtained in deionized water (a), 800  $\mu\text{M}$   $\text{NaNO}_3$  (b), and 800  $\mu\text{M}$  acetate buffer, pH 4.8 (c). Plot: potential at which current is 80 pA vs.  $\log C$  (●,  $\Delta$ ) (1)  $\text{NaNO}_3$ ; (2, 3) acetate buffer; (○) potential for which  $i/C$  is constant; 12.5- $\mu\text{m}$ -radius platinum covered with 92 pmol of mercury;  $v = 10$  mV/s.

steady-state regime (10). This was confirmed experimentally by constancy of the anodic wave heights of  $\text{OH}^-$  and EDTA and the cathodic wave height of  $\text{Fe(III)}$  in  $\text{Na}_2\text{C}_2\text{O}_4$  up to 50 mV/s. The largest value of  $\Delta$  at 10 mV/s is calculated to be 0.38.

All reagents were of analytical grade. Deionized water was obtained by passing distilled water through a four-cartridge Milli-Q purification system. Deionized water was also placed in the bridge to prevent any electrolyte from leaking into the cell. Estimates of junction potentials obtained by employing the Henderson equation assume the salt bridge contains 1  $\mu\text{M}$  KCl. At the outset many days of repeated soaking and rinsing were required to remove traces of adventitious electrolyte from the system. Temperature was controlled at 25  $^\circ\text{C}$ .

### RESULTS AND DISCUSSION

Figure 2 presents typical curves for oxidation of a mercury microelectrode in nominally pure water and in nitrate and acetate supporting electrolytes. Curve b for nitrate exhibits no cathodic peak, which means there is no significant accumulation of electroactive product at the electrode surface. At a concentration of 400  $\mu\text{M}$   $\text{NaNO}_3$ , the resistance between the working and counter electrodes was about 600 k $\Omega$ . To examine the predictions of eq 3 and 7 without introducing problems of  $iR$  drop, the potential at a fixed current (80 pA) was plotted vs  $\log C$ , as shown also in Figure 2. This corresponds to 0.05 mV of  $iR$  drop at the highest resistance obtaining for this plot. The slope  $\partial E_{80\text{pA}}/\partial \log C_{\text{NaNO}_3}$  is -62 mV. Similar experiments for reduction of  $\text{H}^+$  and oxidation of ferrocene in varying concentrations of  $\text{NaNO}_3$  gave slopes of -52 and -51 mV, respectively. As estimated from the Henderson equation, the change in potential due to change in liquid junction potential is ca. +10 mV/ $\log C$ . Thus for  $\text{H}^+$  and ferrocene the corrected slopes are ca. -60 mV. Furthermore, the slope  $\partial E_{80\text{pA}}/\partial \log i$  was found to range from 63 to 94 mV for the oxidation of mercury in the presence of nitrate under the conditions of Figure 2. The expected value, since the value of  $n$  is almost certainly 2, is 30 mV, according to eq 2.

Nitrate does not form stable complexes with  $\text{Hg(I)}$  or  $\text{Hg(II)}$  in homogeneous solution under these conditions (15, 16). Therefore the potential at any point on the wave should be independent of nitrate concentration, except for the change in liquid junction potential. However we definitely find a concentration dependence that exceeds that due to changes in  $iR$  drop. This and the anomalous wave shape are in accord with numerous observations in the literature concerning anomalies in the anodic oxidation of mercury in the presence of nitrate (17, 18). The anomalous response notwithstanding,



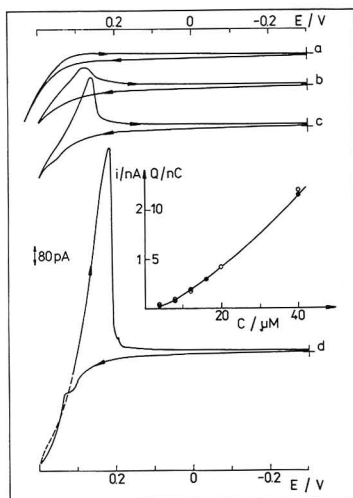


**Figure 3.** Cyclic voltammograms of bromide in deionized water obtained at a 12.5- $\mu\text{m}$ -radius platinum disk covered with 62 pmol of mercury. NaBr concentration ( $\mu\text{M}$ ): 0 (a); 4 (b); 8 (c); 20 (d). Plot: cathodic peak current ( $i$ ) and the charge under the cathodic peak vs.  $C_{\text{NaBr}}$ .

the current at +0.4 V was found to depend linearly on the concentration of  $\text{NaNO}_3$  up to 1600  $\mu\text{M}$ .

Acetate forms complexes with  $\text{Hg(II)}$  with formation constants given by  $\log \beta_i = 5.55, 9.30, 13.28, \text{ and } 17.06$  for  $i = 1-4$ , respectively (15). In addition it forms the insoluble mercurous salt  $\text{Hg}_2(\text{OAc})_2(\text{s})$  ( $\text{p}K_{\text{SO}} = 9.63$ ) (19). Using appropriate thermodynamic data (16), one can estimate  $\text{p}K = -2.27$  for the reaction  $\text{Hg}(\text{OAc})_2 + \text{Hg} = \text{Hg}_2(\text{OAc})_2(\text{s})$  and thus  $\text{Hg}_2(\text{OAc})_2(\text{s})$  should form only for  $C_{\text{OAc}} \geq 0.01 \text{ M}$ . Based on these values we except  $\text{Hg(II)}$  complexed by acetate to be the product of anodic oxidation, at least at the foot of the wave. It should be mentioned that Hepler and Olofsson are not happy with the equilibrium data for  $\text{Hg(II)}$  complexes with acetate (20).

The voltammogram of Figure 2c clearly shows a maximum cathodic current, which indicates some accumulation of product at the electrode surface. The plot of  $E_{\text{SO}}$  vs  $\log C_{\text{NaOAc}}$  exhibits two linear regions with slopes of  $-28$  and  $-75 \text{ mV}$ . The estimated change in junction potential is ca.  $-13 \text{ mV}/\log C$ , so the corrected slopes are ca.  $-15$  and  $-62 \text{ mV}$ , respectively. At the foot of the wave  $\partial E_{\text{SO}}/\partial \log i = 35 \text{ mV}$ . The open circles of Figure 2 are values of potential for which the quantity  $i/C$  is held constant. This corresponds to choosing as the reference point the potential for which  $i/i_{\text{dL}} = (i/C_L)/(p/4nFD_Lr)$  rather than  $i/i_{\text{dL}} = 1/2$ . From eq 6 and 7,  $\partial E/\partial \log C_L = -2.303(p-1)/nf$  at constant  $i/C_L$ . The measured slope is  $-17 \text{ mV}$  (line 3 is drawn with zero slope); the value corrected for change in junction potential is  $-4 \text{ mV}$ . Thus it appears that the product of the oxidation in this concentration range is  $\text{Hg}(\text{OAc})^+$ .

The oxidation of mercury in the presence of acetate occurs at potentials about 50 mV more positive than in nitrate. The junction potentials for curves b and c are ca. 29 and  $-29 \text{ mV}$ , respectively, so the oxidation in acetate actually occurs slightly negative of that in nitrate, as one would expect from the relative values of complex formation constants.

**Precipitation of Insoluble Products.** In the presence of bromide mercury is oxidized anodically to form  $\text{Hg}_2\text{Br}_2(\text{s})$ , which is almost insoluble in water ( $\text{p}K_{\text{SO}} = 21.9$  at  $25^\circ\text{C}$ ). Figure 3 shows the expected large cathodic peak for reduction

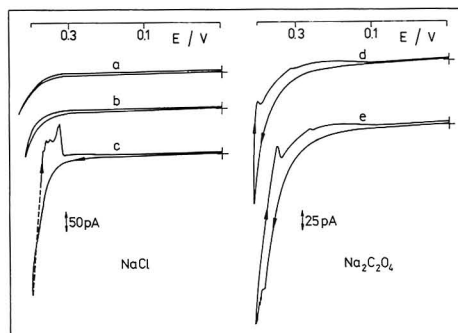


**Figure 4.** Cyclic voltammograms of chloride and oxalate in deionized water obtained at a 1  $\mu\text{m}$ -radius platinum disk covered with 37 pmol of mercury: background (a); 8  $\mu\text{M}$  NaCl (b); 80  $\mu\text{M}$  NaCl (c); 56  $\mu\text{M}$   $\text{Na}_2\text{C}_2\text{O}_4$  (d); 56  $\mu\text{M}$   $\text{Na}_2\text{C}_2\text{O}_4$  in 400  $\mu\text{M}$   $\text{NaNO}_3$  (e).

of the product, which has been deposited at the electrode surface. In 4  $\mu\text{M}$  NaBr the cathodic peak can be already seen, although the charge under the peak ( $96.9 \mu\text{C}/\text{cm}^2$ ) is smaller than expected for the monolayer charge ( $\sim 127 \mu\text{C}/\text{cm}^2$  from the bulk density of  $\text{Hg}_2\text{Br}_2$ ). The anodic current of curve b increases smoothly with  $E$ . Both facts together indicate adsorption rather than two-dimensional precipitation at the surface. For higher concentrations of bromide the cathodic peak increases in height and irregularities appear on the anodic branch of the curve. This undoubtedly reflects formation of a crystal lattice at the surface.

Both cathodic peak current and the charge under the peak increase with concentration of bromide as shown in the plot in Figure 3. Both current and charge increase faster than linearly because the efficiency of deposition also increases with increasing concentration. The efficiency of accumulation of  $\text{Hg}_2\text{Br}_2$  was easy to determine from the anodic and cathodic charge and equaled 58% and 89% for 12 and 40  $\mu\text{M}$  solution, respectively. The fact that bromides at the micromolar level can be deposited at the mercury microelectrode agrees with the cathodic stripping data of Perchard et al. (21) reported for a conventional mercury electrode.

Mercurous chloride is more soluble than  $\text{Hg}_2\text{Br}_2$  ( $\text{p}K_{\text{SO}} = 17.7$ ), so the cathodic peak cannot be seen on the reverse branch of the cyclic curve at micromolar levels of chloride (curve b in Figure 4). The peak appears for chloride concentrations higher than 20  $\mu\text{M}$ , which also agrees with data for a conventional mercury electrode (21). Curve c in Figure 4, obtained in 80  $\mu\text{M}$  NaCl solution, illustrates both formation and accumulation of  $\text{Hg}_2\text{Cl}_2(\text{s})$  at the surface.

Similarly, surface processes of oxalate could not be seen at  $\mu\text{M}$  levels. Two cathodic peaks, corresponding to bulk precipitation and the monolayer dissolution, respectively (20, 21), can be noticed on curve d in Figure 4 (56  $\mu\text{M}$   $\text{Na}_2\text{Ox}$ ). In this case the interaction of the ligand with mercury is so weak that the wave overlaps that due to the direct oxidation. The two processes are better separated when a low concentration of supporting electrolyte is added (curve e).

**Strongly Complexing Media.** Typical curves for oxidation of mercury in solutions of thiocyanate are presented in Figure 5. In each case there is a small cathodic peak attributed to adsorption of complex species  $\text{Hg}(\text{SCN})_p^{2-p}$ . Current response measured at 0.4 V was linear in  $C_{\text{SCN}}$  and after background subtraction could be described as  $i (\text{nA}) = 0.02 + 0.016C (\mu\text{M})$  with correlation coefficient 0.998. The waves are not very well defined despite the fact that logarithms of the formation constants of the complexes  $\text{Hg}(\text{SCN})_p^{2-p}$  are 17.6 ( $\beta_2$ ), 20.4 ( $\beta_3$ ), and 21.2 ( $\beta_4$ ). When the solution is made

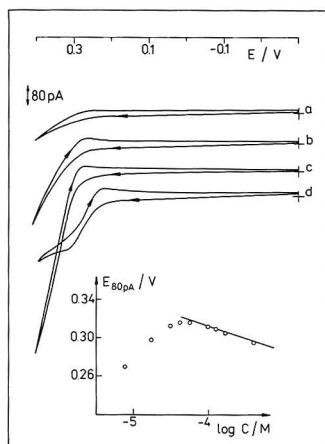


**Figure 5.** Cyclic voltammograms of thiocyanate in deionized water obtained at a 12.5- $\mu m$ -radius platinum disk covered with 50 pmol of mercury: concentration of  $NaSCN$  ( $\mu M$ ), 0 (a), 8 (b), 40 (c), 20 in 400  $\mu M$   $NaNO_3$  (d); plot, potential for which  $i/C = \text{constant}$  vs.  $\log C_{NaSCN}$ .

400  $\mu M$  in  $NaNO_3$  the wave emerges completely from the background (curve d in Figure 5). The shift in potential is ca. 50 mV whereas the change in junction potential is estimated as ca. 26 mV. Following the procedure used for acetates, the potentials of equivalent current ( $i/C_{SCN} = \text{constant}$ ) were plotted vs.  $\log C_{SCN}$  as shown in Figure 5. It is not clear why the potential increases with increasing concentration at low concentration. This may be related to adsorption of thiocyanate. The junction potentials in this range should be quite small, ca. <1 mV. The slope at higher concentrations of 30 mV, according to eq 7 indicates that  $Hg(SCN)_2$  is the species being formed. This agrees with polarographic data (22). It is possible that at lower concentrations  $Hg(SCN)^+$  is formed (slope = 0 mV).

Ethylenediaminetetraacetic acid (EDTA) is a strong, hexadentate ligand and forms 1:1 complexes with  $Hg(II)$  ( $\log K = 21.6$ ). The curve obtained in 8 mM acetate buffer of pH 4.8 and containing 4  $\mu M$  EDTA exhibits a well-defined cathodic peak and a prewave, the attributes of strong adsorption of the product ( $HgEDTA$ ). The cathodic peak increases with concentration of EDTA and for 80  $\mu M$  EDTA its area could be evaluated quantitatively, giving approximately 40  $\mu C/cm^2$ . This is a reasonable value, since detailed studies of adsorption of  $HgEDTA$  on mercury electrodes at pH 4.8 report the value of 37  $\mu C/cm^2$  (23). The half-wave potential for EDTA is practically independent of concentration, which should be expected for a 1:1 complex (eq 7). Despite strong adsorption of  $HgEDTA$ , the wave height is linear in concentration of EDTA over a wide range with or without the acetate buffer, as shown in Figure 6.

Solutions of 40  $\mu M$  EDTA in 0.1 M  $HOAc/OAc^-$  (pH 4.8) were used to examine the validity of eq 5. In this medium the diffusion coefficient of EDTA is  $5.01 \times 10^{-6} cm^2/s$  (24). The calculated value of limiting current from eq 5 for a 12.5- $\mu m$ -radius disk under these conditions is 0.19 nA, whereas for a hemisphere the value would be 0.30 nA. The reduction was carried out with differing amounts of mercury plated onto the platinum substrate, which were equivalent to spherical segments with heights 1.62, 3.05, 8.5, and 12.3  $\mu m$  (the last almost an ideal hemisphere). The corresponding wave heights were found to be 0.23, 0.26, 0.295, and 0.31 nA, respectively. Layers thinner than 1.62  $\mu m$  proved unstable, so a flat circular electrode could not be achieved exactly. However the ac-

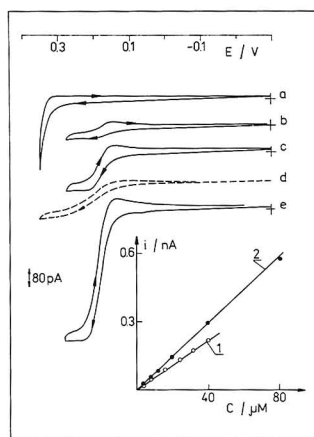


**Figure 6.** Cyclic voltammograms of EDTA in 8 mM acetate buffer, pH 4.8, obtained at a 12.5- $\mu m$ -radius platinum disk covered with 56.8 pmol of mercury: concentration of EDTA ( $\mu M$ ), 0 (a), 4 (b), 20 (c), 80 (e), 20 (no acetate buffer, equimolar mixture of  $Na_2H_2Y$  and  $Na_3HY$  (d)); plot, EDTA forward anodic wave height vs.  $C_{EDTA}$ . (1) A 12.5- $\mu m$  platinum substrate in acetate buffer; (2) a 1- $\mu m$  platinum substrate, no acetate buffer.

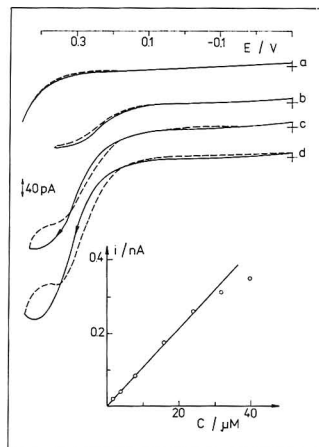


**Figure 7.** Cyclic voltammograms of thiourea in deionized water obtained at a 1- $\mu m$ -radius platinum disk as substrate for mercury: TU concentration ( $\mu M$ ), 0 (a), 8 (b), 24 (c), 40 (d); plot, TU anodic wave height vs TU concentration.

cessible experimental values agree well with the simple prediction of eq 5.

Thiourea (TU) is a neutral compound, which does not dissociate, but strongly complexes  $Hg(II)$  with  $\log \beta_1 = 22.2$ , 24.7, and 23.8 for  $i = 1-3$ . Nyman and Parry investigated its anodic wave under polarographic conditions and concluded that  $Hg(II)$  complexes with two, three, and four ligands were formed (27). The half-wave potential was independent of pH. They noticed the slope of the wave increased at higher TU concentrations.

Thiourea presents a particularly interesting case for anodic oxidation of mercury to form complexes, for the complexing agent can be added without adding ions. Typical cyclic voltammograms obtained with the mercury microelectrode

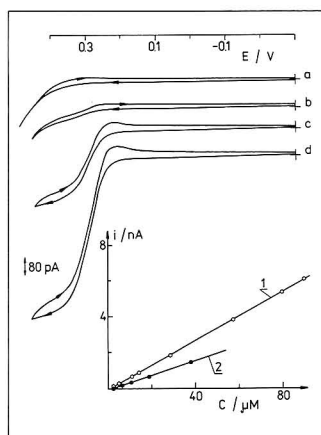


**Figure 8.** Cyclic voltammograms of hydroxide in deionized water obtained at 62 pmol of mercury on 12.5  $\mu\text{m}$ -radius platinum substrate: NaOH concentration ( $\mu\text{M}$ ), 0 (a), 1.95 (b), 5.8 (c), 11.6 (d); plot, forward wave or peak height vs  $C_{\text{NaOH}}$ . (1) linear scan voltammetry; (2) square-wave voltammetry (frequency 30 Hz; square-wave amplitude, 25 mV; step height, 5 mV).

based on the 1- $\mu\text{m}$  platinum wire are presented in Figure 7. The anodic complex formation reaction is well-behaved in 8  $\mu\text{M}$  thiourea (curve b). At higher concentrations the complicated nature of the process is revealed. The forward anodic current is depressed and at sufficiently high concentrations a peak instead of a wave is seen. A small, broad cathodic peak appears at a much more negative potential (0 to -0.1 V) with a charge of roughly  $75 \mu\text{C}/\text{cm}^2$ . This is apparently due to reduction of adsorbed complexes. This peak increases with increasing electrode area. Also, the anodic current on the reverse scan exhibits a large hysteresis.

All this suggests the formation of a compact, immobilized layer of mercury-containing species at the electrode surface. In addition, we know that thiourea itself is strongly adsorbed at the mercury surface and even can undergo phase transformations (26). Thus the plot of the wave height versus concentration of thiourea in Figure 7, and in particular its saturation at higher concentration, is not surprising. This behavior was obviously magnified by the lack of supporting electrolyte. When 4 mM acetate buffer was added to the cell, the hysteresis and the anodic peak disappeared, but a cathodic peak resembling that for EDTA (Figure 6) remained, indicating that complexes of mercury and thiourea are still adsorbed.

Electrooxidation of mercury in solutions containing hydroxide is known to produce  $\text{Hg}(\text{OH})_2$  and, at sufficiently high concentrations, insoluble compounds, which have the ability to passivate completely the electrode (9, 27). The anodic wave in NP polarography has been used for the determination of hydroxide at  $\mu\text{M}$  levels (28). The response of the mercury microelectrode to micromolar solutions of NaOH, with no deliberately added electrolyte, is presented in Figure 8. Note that a small cathodic peak can be seen on the reverse branch of the cyclic curves, which means  $\text{Hg}(\text{OH})_2$  is adsorbed at the mercury surface. The slope of  $\partial E/\partial \log C$ , measured at the foot of the wave, confirmed that two hydroxide ions participate in the process. The wave height plotted versus concentration of hydroxide gave a straight line ( $i$  (nA) =  $-0.103 + 0.0688C$  ( $\mu\text{M}$ ) with intercept 1.49  $\mu\text{M}$ ). This line marked as 1 is placed in Figure 8 together with the line 2 obtained when square-wave voltammetry was applied. The square-wave currents are smaller but peak shaped. Under these conditions, the quantity

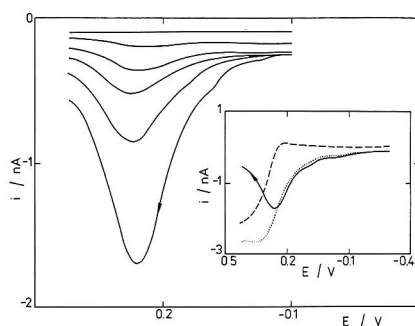


**Figure 9.** Square-wave voltammograms of hydroxide in deionized water: NaOH concentration ( $\mu\text{M}$ , from the top), 0, 3.9, 7.8, 11.7, 19.5, and 39; frequency, 30 Hz; square-wave amplitude, 25 mV; step height, 5 mV. Window: forward (---), reverse (---), and net (—) current of the 39  $\mu\text{M}$  curve.

$r(Dt)^{-1/2}$  is ca. 0.11 for the linear scan experiment and 0.95 for the square-wave experiment. In the steady-state regime the two currents would be the same (29). Details of the square-wave response are shown in Figure 9. Cathodic reverse currents become pronounced at frequencies of 100 Hz or more for which a  $r(Dt)^{-1/2} \geq 1.7$ .

Other pulse techniques were also applied in NaOH solution. The normal pulse waves were of constant height for pulse times longer than 2 s, and increased with decreasing time.

The oxidation of mercury in the presence of weak complexing agents is complicated and difficult to interpret. According to measured equilibrium data acetate should form higher complexes than found here. The data for nitrate are puzzling, but so are the contradictory results already in the literature on the electrochemistry of mercury in the presence of nitrate. The experiments done for comparison with ferrocene and hydrogen ion are consistent qualitatively with double layer effects. Without careful quantitative study, the cause for the observed shifts in potential must remain a conjecture.

The results for reactions that form solids or strong complexes agree quite well with predictions of simple theory in view of their reported properties. The absolute limiting currents depend on shape and size of the electrode as shown for EDTA. Also for EDTA the amount adsorbed measured simply from cathodic charge agrees well with previous reports. This illustrates the premise that amounts of electroactive adsorbed product can be measured directly at microelectrodes because reaction due to diffusing species is negligible. Results for bromide, chloride, and oxalate agree with previous reports on larger electrodes. Thiocyanate, EDTA, and hydroxide all give results in accord with eq 6 and 7, although thiocyanate exhibits unexpected potential-concentration behavior at lower concentrations. Therefore microelectrodes can be used to measure equilibrium constants over ranges of concentration and ionic strength not normally employed.

These results demonstrate the practicality of using voltammetric measurements to characterize the anodic reactions of mercury in dilute electrolytes. In particular they show that pulse voltammetric measurements can be used for this purpose even though the resistance is very high. From the analytical point of view these reactions could be used in a variety of applications requiring determination of anions in nominally pure water.

#### ACKNOWLEDGMENT

The authors thank the Southampton electroanalytical group for providing a 1- $\mu\text{m}$  platinum-disk microelectrode and Scott

Singleton for technical assistance.

**Registry No.** Hg, 7439-97-6; Pt, 7440-06-4; NaBr, 7647-15-6; NaCl, 7647-14-5; Na<sub>2</sub>C<sub>2</sub>O<sub>4</sub>, 62-76-0; NaOH, 1310-73-2; EDTA, 60-00-4; NaSCN, 540-72-7; NaNO<sub>3</sub>, 7631-99-4; H<sub>2</sub>NSNH<sub>2</sub>, 62-56-6; HClO<sub>4</sub>, 7601-90-3.

### LITERATURE CITED

- (1) Wightman, R. M. *Anal. Chem.* **1981**, *53*, 1125A-1130A.
- (2) Edmonds, T. E. *Anal. Chim. Acta* **1985**, *175*, 1-22.
- (3) Schulze, G.; Frenzel, W. *Anal. Chim. Acta* **1984**, *159*, 95-103.
- (4) Cushman, M. R.; Anderson, C. W. *Anal. Chim. Acta* **1981**, *130*, 323-327.
- (5) Ciszowska, M.; Stojek, Z. *J. Electroanal. Chem. Interfacial Electrochem.* **1985**, *159*, 101-110.
- (6) Wehmeyer, K. R.; Wightman, R. M. *Anal. Chem.* **1985**, *57*, 1989-1993.
- (7) Baranski, A.; Quon, H. *Anal. Chem.* **1986**, *58*, 407-412.
- (8) Heyrovský, J.; Kuta, J. *Principles of Polarography*; Academic: New York, 1966.
- (9) Wrona, P.; Galus, Z. "Mercury"; *Encyclopedia of Electrochemistry of the Elements*; Bard, A., Ed.; Marcel Dekker: New York, 1982.
- (10) Aoki, K.; Akimoto, K.; Tokuda, K.; Matsuda, H.; Osteryoung, J. J. *Electroanal. Chem. Interfacial Electrochem.* **1984**, *171*, 219-230.
- (11) Gunawardena, G. A.; Hills, G. J.; Montenegro, I. *Electrochim. Acta* **1978**, *23*, 693-697.
- (12) De Levie, R. "Electrochemical Observations of Single Molecular Events"; *Advances in Electrochemistry and Electrochemical Engineering*; Gerischer, H., Tobias, C. W., Eds.; Wiley: New York, 1984; Vol. 13.
- (13) Bond, A. M.; Fleischmann, M.; Robinson, J. J. *Electroanal. Chem. Interfacial Electrochem.* **1984**, *168*, 299-312.
- (14) Ciszowska, M.; Stojek, Z. *J. Electroanal. Chem. Interfacial Electrochem.* **1986**, *213*, 189-201.
- (15) *Stability Constants of Metal-Ion Complexes*; Special Publication No. 25; The Chemical Society: London, 1971.
- (16) Hietanen, S.; Silleń, L. G. *Ark. Kemi* **1956**, *10*, 103-125.
- (17) Kolthoff, I. M.; Miller, C. S. *J. Am. Chem. Soc.* **1941**, *63*, 2732-2734.
- (18) Golaš, J.; Osteryoung, J. *Anal. Chim. Acta* **1986**, *186*, 1-9.
- (19) *Standard Potentials in Aqueous Solution*; Bard, A. J., Parsons, R., Jordan, J., Eds.; International Union of Pure and Applied Chemistry: New York, 1985.
- (20) Hepler, L. G.; Olofsson, G. *Chem. Rev.* **1975**, *75*, 585-602.
- (21) Perchard, J. P.; Buret, M.; Molina, R. *J. Electroanal. Chem. Interfacial Electrochem.* **1967**, *14*, 57-74.
- (22) Müller, C.; Closet, J.; Sarret, H. *J. Electroanal. Chem. Interfacial Electrochem.* **1986**, *207*, 263-278.
- (23) Armstrong, R. D.; Fleischmann, M. Z. *Phys. Chem. (Munich)* **1967**, *52*, 131.
- (24) Niki, K.; Suzuki, K.; Sato, G. P.; Mori, N. *J. Electroanal. Chem. Interfacial Electrochem.* **1974**, *49*, 27.
- (25) Nyman, C. J.; Alberts, G. S. *Anal. Chem.* **1960**, *32*, 207-210.
- (26) Stojek, Z.; Ciszowska, M.; Osteryoung, J. *J. Electroanal. Chem. Interfacial Electrochem.* **1985**, *195*, 405-416.
- (27) Nyman, C. J.; Parry, E. P. *Anal. Chem.* **1958**, *30*, 1255-1257.
- (28) Hills, G. and Silva, F. *J. Electroanal. Chem. Interfacial Electrochem.* **1982**, *137*, 387-392.
- (29) Kemula, W.; Tarasewska, J. *Rev. Chim. Miner.* **1968**, *5*, 535.
- (30) Kirova-Eisner, E.; Osteryoung, J. *Anal. Chem.* **1978**, *50*, 1062-1066.
- (31) Aoki, K.; Tokuda, K.; Matsuda, H.; Osteryoung, J. *J. Electroanal. Chem. Interfacial Electrochem.* **1986**, *207*, 25-39.

RECEIVED for review May 11, 1987. Accepted September 9, 1987. This work was supported in part by the Office of Naval Research and in part by Grant 01.17.04.01 from the Polish government.

## Determination of Cephalosporins and Decomposition Products by Liquid Chromatography with Indirect Electrochemical Detection

H. Fabre<sup>1</sup> and W. Th. Kok\*

Laboratory for Analytical Chemistry, University of Amsterdam, Nieuwe Achtergracht 166, 1018 WV Amsterdam, The Netherlands

Indirect electrochemical detection, using in-line electrochemically generated bromine as oxidizing agent, has been used for the determination of cephalosporins with liquid chromatography. The method presents a general detection principle for cephalosporins since it is related to their basic structure. The detection limits obtained, which were between 0.4 and 3 ng, and the repeatability with a relative standard deviation below 1.5% comply with the requirements for drug stability studies in vitro. Application to the determination of cefotaxime and its main metabolite in serum and urine showed an improved selectivity compared to that obtained with UV detection. The method is also of interest for the detection of decomposition products resulting from the cleavage of the  $\beta$ -lactam ring, which cannot be detected by UV.

Cephalosporins are generally determined by microbiological techniques or by high-performance liquid chromatography (HPLC). As often outlined, the major drawback of micro-

biological procedures is their lack of specificity in stability studies when the decomposition products are microbiologically active (1). In that case HPLC with ultraviolet absorption detection is the method of choice, although some potential decomposition products that do not absorb UV light cannot be detected. For pharmaceutical preparations, the selectivity of reversed-phase separation and the sensitivity of UV absorption detection—due to the strong absorbance of the  $\beta$ -lactam moiety—allow the parent compound and trace levels of its main degradation products to be determined simultaneously (2). In most formulations the added ingredients do not generally interfere with the determination. In contrast, when cephalosporins have to be determined in biological samples at low levels, the interference of the matrix is a limiting factor for the detectability. The high aqueous solubility of cephalosporins does not allow their extraction with organic solvents. The difficulties that can be encountered are typically shown in the simultaneous determination of cefotaxime and its highly polar metabolite desacetylcefotaxime. Numerous extraction and HPLC procedures have been proposed to overcome the interference problems (3, 4).

In the search for sensitive and selective methods for the determination of cephalosporins (5, 6), we have investigated the possibilities of HPLC with oxidative amperometric de-

<sup>1</sup>On leave from Laboratoire de Chimie Analytique, Faculté de Pharmacie, Avenue Charles Flahaut, 34060 Montpellier Cédex, France.

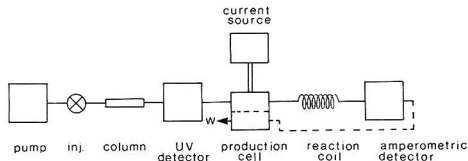


Figure 1. Scheme of the experimental setup.

tection. Despite the high detection potential that had to be used (+0.95 V vs a calomel electrode at a pH of 7.6), the detection limits obtained with standard solutions of the test compounds, cefotaxime and two of its metabolites, were about 1 ng. However, direct electrochemical detection in the oxidative mode cannot be used as a general method for cephalosporins, since the electroactivity presented by some of them is not related to the  $\beta$ -lactam structure but to the presence of an oxidizable substituent on their side-chain (6, 7). For this reason, and to avoid possible electrode passivation phenomena with biological samples, we have studied the use of indirect electrochemical detection. In this in-line coulometric titration technique, an oxidizing reagent is produced electrochemically in the column effluent from a precursor in the mobile phase. After the passage through a short reaction capillary, the excess of reagent is monitored with an amperometric detector in the reductive mode. Details on the characteristics and performance of this technique have been published (8). Indirect electrochemical detection has been shown to be advantageous in the determination of compounds with slow electrode kinetics in direct oxidation (9). Besides, electrode passivation is avoided by the moderate potential that can be applied in the reductive detection. Applications to the determination of sulfur compounds in biological samples with iodine and bromine as oxidizing reagents have been published (9, 10). Since cephalosporins react with iodine only after the opening of their  $\beta$ -lactam ring (11, 12), bromine was used as reagent in this work.

The reactivity and stoichiometry of the reaction were studied for cefotaxime (C) and five of its decomposition products: desacetylcefotaxime (D), desacetylcefotaxime lactone (L), desacetoxycefotaxime (Do), 7-aminoccephalosporanic acid (ACA), and thiazoximic acid (Th). For comparison 7-aminodesacetoxycefotaxime (ADCA) was also investigated (see Table I).

Signal-to-noise ratios were measured in order to optimize the operating conditions. The linearity range, the repeatability and the detection limits were compared to those obtained with UV detection. The applicability of the method to biological samples is shown in the simultaneous determination of cefotaxime and its active metabolite in serum and urine. The interest of the method for the monitoring of decomposition products of cephalosporins in raw materials and drugs is also shown. The extension of the method to other compounds was studied with cephalosporins (I–VIII) bearing various substituents.

## EXPERIMENTAL SECTION

**Apparatus.** The liquid chromatograph consisted of a Gynkotek (Germering, FRG) Model 300 C pump, a Rheodyne injection valve with a loop volume that was determined to be 24  $\mu$ L, a Waters Model 440 fixed-wavelength (254-nm) absorbance detector, and, in series, a production cell, reaction coil, and amperometric detector. Figure 1 shows the experimental set-up schematically. The KOBRA cell used for in-line generation of bromine (8) was obtained from the Chemistry Department Workshop of the Free University (Amsterdam, The Netherlands). The constant-current source was an Elektronika Micrometer (Amsterdam, The Netherlands). The reaction coil was a 1 m  $\times$  0.5 mm i.d. poly(tetrafluoroethylene) (PTFE) capillary with a 6.6-s hold-up time at the

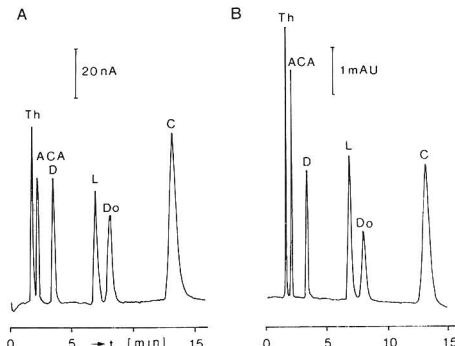


Figure 2. Separation of cefotaxime and five of its decomposition products: (A) indirect electrochemical detection,  $i_a = 25 \mu$ A; (B) UV detection. Amount injected: 92 ng of C, 25 ng of D, 47 ng of L, 24 ng of Do, 11.5 ng of Th, and 24 ng of ACA.

flow rate used. A Metrohm (Herisau, Switzerland) 656 detector cell was used with a glassy carbon working electrode at a potential of +0.4 V vs a Ag/AgCl/KCl (Saturated) reference electrode. The cell was connected to a BAS (West Lafayette, MA) potentiostat. The efficiency of the detector cell, measured as the ratio of the detector current to the generating current applied, was about 1.5%. A 200  $\times$  4.6 mm i.d. column was used, slurry packed with Hypersil ODS (5  $\mu$ m). The flow rate was 1.8 mL  $\text{min}^{-1}$ , and the pressure was about 120 bars. All experiments were conducted at ambient temperature ( $20 \pm 2^\circ\text{C}$ ).

**Chemicals and Solutions.** Cephalosporins were obtained as gifts: C, D, Do, L, ACA, and Th from Roussel UCLAF Laboratories (Romainville, France); ADCA and VI from Bristol Laboratories (Paris, France); III from Glaxo Laboratories (Greenford, UK); I from Boehringer (Mannheim, FRG); II, IV, and VII from Cassenne Takeda (Paris, France); VIII from Allard (Paris, France), and V from MSD-Chibret (Paris, France).

The compounds were used as received. Stock solutions (0.2–0.4 g  $\text{L}^{-1}$ ) were prepared daily and suitably diluted in water or the mobile phase before use. Other chemicals were of analytical grade purity. The mobile phase consisted of 0.1 M acetate buffer, pH 4.1, and methanol (83:17) with 0.01 M NaBr.

**Sample Preparation.** For recovery studies in serum, samples were spiked with 26.6  $\mu$ g  $\text{mL}^{-1}$  of C and 11.5  $\mu$ g  $\text{mL}^{-1}$  of D or with 5.3  $\mu$ g  $\text{mL}^{-1}$  of C and 2.3  $\mu$ g  $\text{mL}^{-1}$  of D, respectively. Deproteination in acidic methanol was carried out according to the procedure described by Lecaillon et al. (13). After this treatment the samples were diluted with water (1:4).

For recovery studies in urine, samples were spiked with 0.20 mg  $\text{mL}^{-1}$  of C and 0.97 mg  $\text{mL}^{-1}$  of D, and diluted with water (1:49).

## RESULTS AND DISCUSSION

**Optimization of the Experimental Parameters.** The separation was optimized both for the determination of cefotaxime and its deacetylated metabolite in biological samples and for a stability indicating assay in vitro. The mobile phase previously used (2), with a pH of 7.6, is incompatible with the electrochemical generation of bromine. Among the different mobile phases investigated in the pH range of 2–5, the best separation was obtained when using a 0.1 M acetate buffer, pH 4.1, and methanol in the ratio 83:17. A further decrease of the pH of the mobile phase resulted in an overlapping of the peaks of D and L, which are the major decomposition products of C. The values of  $k'$  of D and L were 1.1 and 3.5 at pH 4.1, while, for instance, at pH 3.5 they were 1.3 and 1.5, respectively. Chromatograms of a standard solution of cefotaxime and five of its decomposition products are shown in Figure 2. Since the electrochemical detection system was positioned in series after the UV detector, the resolution of early eluting peaks was slightly decreased. However, when

Table I

Compound

Structure

Cefotaxime ( <u>C</u> )		R <sub>2</sub> , R <sub>3</sub> = N-OCH <sub>3</sub>	R <sub>4</sub> - CH <sub>2</sub> OCOCH <sub>3</sub>	R <sub>5</sub> - H
Desacetylcefotaxime ( <u>D</u> )	id	id	- CH <sub>2</sub> OH	- H
Desacetoxycefotaxime ( <u>Do</u> )	id	id	- CH <sub>3</sub>	- H
Ceftizoxime ( <u>I</u> )	id	id	- H	- H
Cefmenoxime ( <u>II</u> )	id	id	- CH <sub>2</sub> - S -  - CH <sub>3</sub>	- H
Ceftazidime ( <u>III</u> )	id	= N-OC(CH <sub>3</sub> ) <sub>2</sub> COOH	- CH <sub>2</sub> - N <sup>+</sup> -	- H
Cefotiam ( <u>IV</u> )	id	- H, - H	- CH <sub>2</sub> - S -  - C <sub>2</sub> H <sub>4</sub> -N(CH <sub>3</sub> ) <sub>2</sub>	- H
Cefoxitin ( <u>V</u> )		- H, - H	- CH <sub>2</sub> - O-CO - NH <sub>2</sub>	- OCH <sub>3</sub>
Cefadroxil ( <u>VI</u> )		- NH <sub>2</sub> , - H	- CH <sub>3</sub>	- H
Cefsulodin ( <u>VII</u> )		- SO <sub>3</sub> H, - H	- CH <sub>2</sub> - N <sup>+</sup> -	- H
Cefazolin ( <u>VIII</u> )		- H, - H	- CH <sub>2</sub> - S -  - CH <sub>3</sub>	- H
Desacetylcefotaxime lactone ( <u>L</u> )				
Thiazoximic acid ( <u>Th</u> )				
7-aminocephalosporanic acid ( <u>ACA</u> )				
7-aminodesacetoxycephalosporanic acid ( <u>ADCA</u> )				



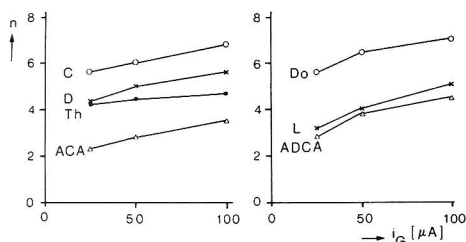


Figure 3. Dependency of the bromine consumption by cefotaxime and decomposition products on the generating current. Number  $n$  of bromine molecules consumed by one molecule of the compound.

Table II. Sensitivities and Detection Limits with UV and Electrochemical Detection

compd	UV		electrochemical	
	sensitivity, mAU ng <sup>-1</sup>	LOD, <sup>a</sup> ng	sensitivity, nA ng <sup>-1</sup>	LOD, ng
C	0.031	3.3	0.74	3.0
D	0.104	1.0	2.04	1.1
L	0.062	1.7	0.98	2.2
Do	0.056	2.0	1.50	1.4
ACA	0.192	0.5	2.12	1.0
Th	0.488	0.2	6.16	0.4

<sup>a</sup>LOD: limit of detection, signal-to-noise ratio of 2.

the column was connected directly to the reagent production cell, no significant differences in peak widths were observed compared to those observed with UV detection.

In the indirect electrochemical detection mode employed, the decrease of the reagent concentration is measured. The amount of bromine consumed by the analytes in the column effluent depends on the hold-up time in the reaction coil and the concentration of bromine produced. The latter parameter is easily controlled, since the reagent concentration is directly proportional to the generating current  $i_G$ . To investigate the rate and stoichiometry of the reactions, the compounds were injected at different generating currents. Care was taken to keep the peak concentrations of the compounds well below the reagent concentration. The number of bromine molecules reacting with one molecule of a compound was calculated from the peak areas by applying Faraday's law, taking into account the efficiency of the detector cell. Results are shown in Figure 3. A fast reaction with bromine is observed not only with the  $\beta$ -lactam moiety but also with the aminothiazole side chain in the 7-position. The amount of bromine consumed by one molecule is about equal to the sum of that of its component parts (see C vs ACA and Th or Do vs ADCA and Th). A comparison of the reactivity of C, D, and Do or of ACA and ADCA shows that the reactivity of the  $\beta$ -lactam structure is influenced by the substituent in the 3-position.

With a generating current of 25  $\mu$ A, the reaction is already almost complete for the compounds investigated. This implies that the highest signal-to-noise ratios will be obtained at low generating currents. The high number of bromine molecules consumed indicates that low detection limits can be obtained.

**Sensitivity, Linearity, and Repeatability.** The sensitivity, defined as the slope of the plot of peak height vs amount injected, increases slightly with the generating current. However, since the noise increases proportionally with it, the lowest limits of detection are obtained at a low generating current. In Table II sensitivities and detection limits at 25- $\mu$ A generating current are compared with those obtained with UV detector. With respect to detectability, the two methods give comparable results.

Table III. Recovery of C and D from Spiked Serum, Determined with UV and Electrochemical Detection

compd	concn, $\mu$ g mL <sup>-1</sup>	% recovered <sup>a</sup>	
		UV	electrochemical
C	1.8	167 $\pm$ 4	91 $\pm$ 7
	5.3	109 $\pm$ 6	102 $\pm$ 3
	26.6	107 $\pm$ 4	103 $\pm$ 4
D	2.3	106 $\pm$ 1	101 $\pm$ 3
	11.5	104 $\pm$ 5	103 $\pm$ 4

<sup>a</sup>Mean  $\pm$  SD, four separate extractions.

Since the amount of bromine available for the reaction with the analyte is limited, the upper limit of linearity increases with the generating current. Evidently, the linear range is also related to the retention time of a compound due to the peak dilution. With a generating current of 50  $\mu$ A, upper limits of 350 (C), 100 (D), 150 (L), 150 (Do), 40 (Th), and 75 ng (ACA) were found. Within the linear range, coefficients of correlation for the calibration plots were better than 0.9997 for all compounds. The upper limits of linearity obtained when using a generating current of 25  $\mu$ A were about half of those obtained at 50  $\mu$ A.

The repeatability was assessed by seven successive injections of separate solutions of each compound at  $i_G = 50$   $\mu$ A and also of C and D at  $i_G = 25$   $\mu$ A. The injected amounts were between 20 and 200 ng. The relative standard deviation of the peak height was always better than 1.5% for both detection methods, except for the lactone L for which a variation of  $\pm 4.2\%$  was observed with electrochemical detection and of  $\pm 4.7\%$  with UV detection.

**Application to Biological Samples.** For most applications to biological samples the highest sensitivity that can be obtained at low generating currents is not required. Still, to prolong the lifetime of the column we have used the 25- $\mu$ A current and diluted the samples after pretreatment to match the linear range. For serum samples a simple deproteinization procedure with acidified methanol was applied (13). Individual and pooled serum samples were investigated. In most individual serum samples less interfering peaks were found with electrochemical detection. Typical chromatograms of blank serum and serum spiked with C and D are shown in Figure 4. Table III gives the recoveries found in the simultaneous determination of C and D in spiked, pooled serum when using the two detection methods. The selectivity of the electrochemical detection is better than that of UV detection. In the blank pooled serum a compound was present that caused an interfering peak. The limit of determination (an accuracy better than  $\pm 10\%$ ) for C in serum is about 5  $\mu$ g/mL with UV detection and about 1.5  $\mu$ g/mL with indirect electrochemical detection.

For the determination of C and D in urine, the sample was diluted (1:49) with water. Typical chromatograms of blank urine and urine spiked with C and D are given in Figure 5. Recoveries were 111% (UV) or 96% (electrochemical) for D and 95% (UV) or 94% (electrochemical) for C. The superior selectivity of the electrochemical method in the determination of D is clearly seen in Figure 5. D can be determined reliably in urine at levels of 100 and 20  $\mu$ g/mL with UV and electrochemical detection, respectively.

**Stability Studies in Vitro.** As shown for cefotaxime and its decomposition products (Figure 2), indirect electrochemical detection can be an alternative method for carrying out the stability-indicating assays necessary for licensing medicinal products. The sensitivity and repeatability are comparable to those obtained with UV detection for these decomposition products. However, in addition to the products resulting from the breakdown of the side chain, a nonnegligible amount of

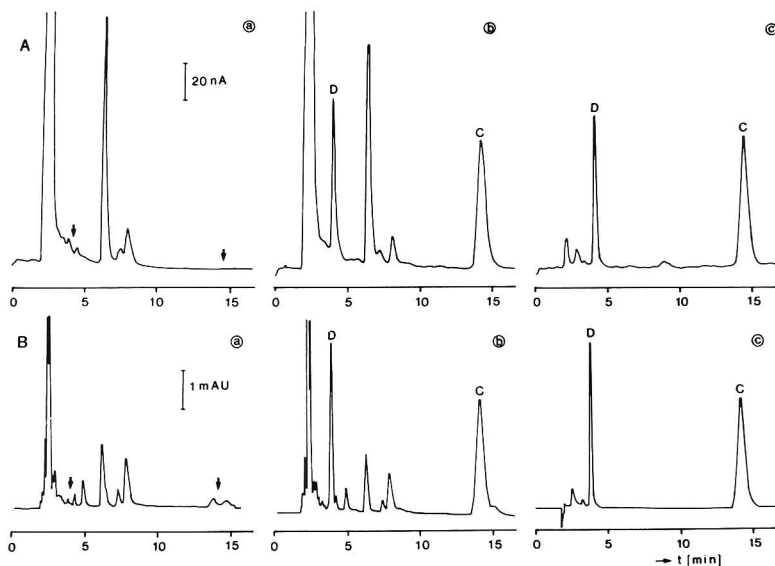


**Figure 4.** Determination of C and D in serum: (a) blank serum; (b) serum spiked with  $26.7 \mu\text{g mL}^{-1}$  C and  $11.5 \mu\text{g mL}^{-1}$  D; (c) standard solution with the same final concentrations. Samples were diluted with water (1:4) before injection. (A) Indirect electrochemical detection,  $i_G = 25 \mu\text{A}$ . (B) UV detection.

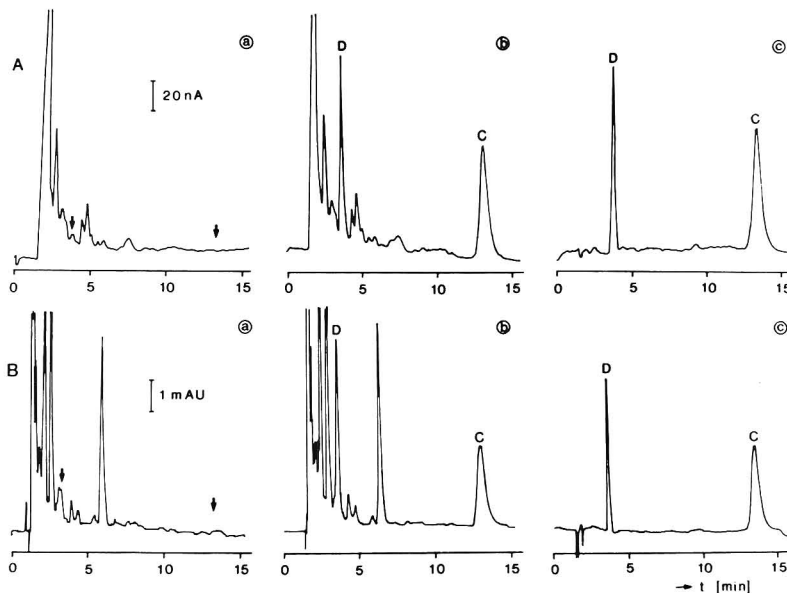


**Figure 5.** Determination of C and D in urine: (a) blank urine; (b) urine spiked with  $204 \mu\text{g mL}^{-1}$  C and  $98 \mu\text{g mL}^{-1}$  D; (c) standard solution with the same final concentrations. Samples are diluted with water (1:49) before injection. (A) Indirect electrochemical detection,  $i_G = 25 \mu\text{A}$ . (B) UV detection.

decomposition products is formed by the hydrolysis of the  $\beta$ -lactam linkage under nucleophilic attack (2). Most of these compounds cannot be detected by UV absorption since the  $\beta$ -lactam ring is responsible for the strong UV absorption of cephalosporins at 250–270 nm (14). We have investigated the

possibility of using indirect electrochemical detection as a complement to UV detection on degraded solutions of ACA. Degradation was studied on an aqueous solution of ACA ( $28 \mu\text{g mL}^{-1}$ ) stored for 7 days at  $4^\circ\text{C}$ . In order to separate polar decomposition products a mobile phase containing only 5%

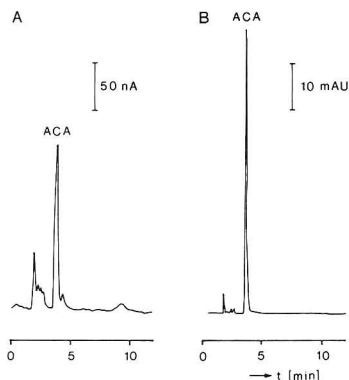


Figure 6. Chromatograms of a degraded ACA solution ( $28 \mu\text{g mL}^{-1}$ ): (A) indirect electrochemical detection,  $i_G = 25 \mu\text{A}$ ; (B) UV detection.

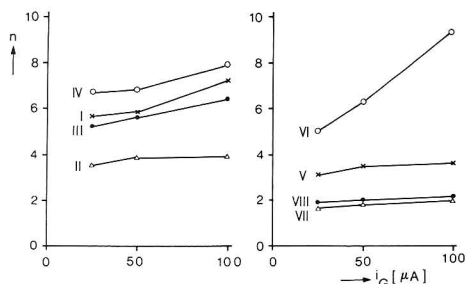


Figure 7. Dependency of the bromine consumption by various cephalosporins on the generating current.

(v/v) methanol was used. Chromatograms recorded with electrochemical detection give evidence of more products than those recorded with UV detection (Figure 6).

**Application of the Method to Other Cephalosporins.** For comparison the bromine consumption by other cephalosporins was measured under the same conditions as for C. Figure 7 gives the results. Some remarks on the observed reactivity can be made. The aminothiazole group present in I, III, and IV gives these compounds a reactivity similar to C. However, the relatively low consumption of bromine by II, which has the same substituent, is difficult to explain. The high consumption but slow rate noted for VI can be attributed to the presence of a phenolic group (8). The sulfur-containing

side chain of VIII is not oxidized by bromine under the conditions used. Although chromatographic optimization has not been carried out, it is clear from these results that indirect electrochemical detection is a promising technique for the determination of all tested cephalosporins in biological fluids.

## CONCLUSIONS

The high rate of the reaction of bromine with the basic  $\beta$ -lactam structure of cephalosporins indicates that indirect electrochemical detection can be used as a general method for cephalosporins. The ease of oxidation of the aminothiazole side chain is also of interest since this group is present in most of the cephalosporins recently synthesized.

The selectivity of indirect electrochemical detection has been shown to be superior in the analysis of biological samples in comparison to that of UV detection, even for strongly UV absorbing compounds such as cephalosporins. Therefore, it may be expected that the method is useful for other sulfur-containing compounds as well.

## ACKNOWLEDGMENT

Thanks are due to Ms. M. D. Blanchin for her participation in the experimental work.

**Registry No.** I, 68401-81-0; II, 65085-01-0; III, 72558-82-8; IV, 61622-34-2; V, 35607-66-0; VI, 50370-12-2; VII, 62587-73-9; VIII, 25953-19-9; C, 63527-52-6; D, 66340-28-1; Do, 65052-63-3; L, 66340-33-8; Th, 65872-41-5; ACA, 957-68-6; ADCA, 22252-43-3; cephalosporin, 11111-12-9.

## LITERATURE CITED

- (1) Wise, R.; Wills, P. J.; Andrews, J. M.; Bedford, K. A. *Antimicrob. Agents Chemother.* **1980**, *17*, 84.
- (2) Fabre, H.; Hussam Eddine, N.; Berge, G. J. *Pharm. Sci.* **1984**, *73*, 611.
- (3) Yost, R. L.; Derendorf, H. J. *Chromatogr.* **1985**, *341*, 131.
- (4) Jehl, F.; Birkel, P.; Montell, H. J. *Chromatogr.* **1987**, *413*, 109.
- (5) Fabre, H.; Blanchin, M. D.; Lerner, D.; Mandrou, B. *Analyst (London)* **1985**, *110*, 775.
- (6) Fabre, H.; Blanchin, M. D.; Tjaden, U. R. *Analyst (London)* **1986**, *111*, 1281.
- (7) Selavka, C. M.; Krull, I. S.; Bratin, K. J. *Pharm. Biomed. Anal.* **1986**, *4*, 83.
- (8) Kok, W. Th.; Brinkman, U. A. Th.; Frei, R. W. *Anal. Chim. Acta* **1984**, *162*, 19.
- (9) Kok, W. Th.; Halvax, J. J.; Frei, R. W. *J. Chromatogr.* **1986**, *352*, 27.
- (10) Kok, W. Th.; Halvax, J. J.; Voogt, W. H.; Brinkman, U. A. Th.; Frei, R. W. *Anal. Chem.* **1985**, *57*, 2580.
- (11) Okada, S.; Hattori, K.; Takano, T. *Bull. Chem. Soc. Jpn.* **1965**, *38*, 2168.
- (12) Frantz, B. M. J. *Pharm. Sci.* **1976**, *65*, 887.
- (13) Lecaillon, J. B.; Rouan, M. C.; Souppart, C.; Febvre, N.; Juge, F. J. *Chromatogr.* **1982**, *228*, 257.
- (14) Demarco, P. V.; Nagarajan, R. *Cephalosporins and Penicillins*; Flynn, E. H., Ed.; Academic: New York, 1972; p 313.

RECEIVED for review May 15, 1987. Accepted September 24, 1987.

# Measurement of Liposome-Released Ferrocyanide by a Dual-Function Polymer Modified Electrode

Rosanne M. Kannuck and Jon M. Bellama

Department of Chemistry and Biochemistry, University of Maryland, College Park, Maryland 20742

Richard A. Durst\*

Center for Analytical Chemistry, National Bureau of Standards, Gaithersburg, Maryland 20899

Potassium ferrocyanide is encapsulated in the aqueous cavity of spherical phospholipid bilayer vesicles (liposomes) at concentrations of approximately  $10^4$  molecules/liposome. Physical parameters and stability of these structures are determined by electrochemical and spectroscopic methods. The electroactive marker ions (ferrocyanide) are released from within the liposome by either the addition of surfactant or the complement lysis of the membrane. The classical complement pathway is an antigen/antibody-specific reaction that occurs when an antigen-sensitized liposome immunospecifically binds with a corresponding antibody in the presence of certain serum proteins (complement). The release of encapsulated ferrocyanide is monitored by differential pulse voltammetry. Preliminary investigations with an ion-exchange polymer modified electrode demonstrate the ability to preconcentrate the released marker at the electrode surface as well as the necessity of a polymer film to protect the surface from fouling during serum-mediated lysis.

The self-assembly of diacyl-chain phospholipids in aqueous solutions results in the formation of spherical bilayered structures referred to as liposomes. Unlike micelles, which form from the single acyl chain species, liposomes enclose an aqueous void volume which can be "loaded" with almost any variety of water-soluble marker molecules. Interest in the field of liposome technology has historically been as a model system for cell membrane transport studies (see for example ref 1). More recently, the application of these structures has expanded to include the use of liposomes as carriers for target-specific drug delivery systems (2). Among the features of liposomes that make this type of application possible is the fact that a variety of antigens can be incorporated into these membranes. Complexation of the antigen-sensitized liposome with its specific antibody activates a series of naturally occurring serum proteins, collectively known as complement, which ultimately form a membrane attack complex that disrupts the membrane (3). A logical extension of this reaction is the measurement of markers released from liposomes as a secondary response for monitoring antigen-antibody interactions. The advantage of this approach to immunoassays lies in the fact that each liposome can contain approximately  $10^4$  marker molecules, thereby providing an amplification of the response for each antigen-antibody interaction.

Some researchers have been able to demonstrate that electroactive species can be encapsulated in the aqueous volume trapped by bilayer membranes and detected upon lysis. D'Orazio and Rechnitz used trimethylphenylammonium ion (TPMA<sup>+</sup>)-loaded sheep red blood cell ghosts (which act in the same capacity as liposomes) to quantitate the complement enzymes present in serum samples by using a TPMA<sup>+</sup> ion selective electrode (4). They were later able to adapt this technique to indirectly detect antibodies to bovine serum albumin (5). Similarly, Shiba et al. have demonstrated the potentiometric determination of tetrapentylammonium ion

(TPA<sup>+</sup>) with a TPA<sup>+</sup> ion selective electrode upon complement disruption of the TPA<sup>+</sup>-loaded liposomes (6).

Amperometric oxygen-sensing electrodes have been used in the detection of released liposome-encapsulated glucose molecules in the presence of glucose oxidase following complement lysis of the membrane (7). Similarly, Haga et al. have encapsulated the enzyme horseradish peroxidase in the presence of its substrate (NADH) and measured the reduction of oxygen once the enzyme was released by a complement lysis (8).

One of the problems encountered with this method was that many of the electroactive species previously used partitioned through the bilayer of the liposome prior to a lysing event (4-6). Katsu et al. addressed this problem by demonstrating that potassium ions, detected by using a potassium ion selective electrode, showed less susceptibility to leakage (up to 40 days) over the other electroactive markers previously reported (9).

Although these examples have shown that certain electroactive species can be contained within the aqueous cavity of liposomes and detected upon complement lysis, no attempts have been made to characterize the system or lower the detection limits necessary for electroanalysis of clinical concentrations of antigens, antibodies, or complement components. Another serious obstacle in the development of this field has been the passivation of electrodes in serum solutions.

This study addresses some of the limitations previously encountered with electroanalysis of liposome-encapsulated species in serum solutions. We have demonstrated the feasibility of using liposomes with an inherently more sensitive electroanalytical technique, differential pulse voltammetry, to determine potassium ferrocyanide ( $K_4Fe(CN)_6$ ) after detergent lysis. The physical dimensions and stability of ferrocyanide-loaded liposomes have been investigated by photon correlation spectroscopy. The effects of lipids and detergent on voltammetric peak amplitude were determined. Finally, we discuss preliminary results, which demonstrate the necessity of modifying the electrode surface with an ion-exchange polymer for the voltammetric determination of both surfactant and complement lysis of liposomes. From this study, we can reliably use liposomes as analytical reagents and are better equipped to make meaningful interpretations of further investigations into homogeneous immunoassays based on the ferrocyanide/liposome system.

## EXPERIMENTAL SECTION

**Liposome Preparation.** Lipids used in the liposome preparations were obtained from Sigma Scientific and used without further preparation. Liposomes were prepared from a mixture of dimyristoylphosphatidylcholine (DMPC), cholesterol, and dicetyl phosphate (5:4:1 molar ratio). Stock solutions of the lipid mixture in chloroform were evaporated to dryness under argon and desiccated overnight under a vacuum. The lipid film was dissolved in dry 2-propanol and injected with a syringe (10) into a solution containing 0.5 mmol/L tris(hydroxymethyl)aminomethane (TRIS) buffer (pH 7.5), 150 mmol/L NaCl, and 50 mmol/L potassium ferrocyanide. Unencapsulated marker was

removed from the sample by size exclusion chromatography on a 5-mL Sephadex G-50 column, which had been equilibrated with the TRIS/saline buffer solution.

Total lipid concentration of the final liposome suspension was calculated as 1.87 mmol/L from a Bartlett assay of the lipid mixture (11). Octyl  $\beta$ -D-glucopyranoside (octyl glucoside) and Triton X-100 were used as surfactants in lysing of the liposomes. Octyl glucoside was made up as 250 mg/mL in water; Triton X-100 was made up as a 1:10 dilution from the concentrate. In all cases, 100–300  $\mu$ L of surfactant/mL of sample was added to induce lysis.

Dinitrophenol (DNP)-sensitized liposomes were prepared by adding 1 mol % (2,4-dinitrophenyl)amino)caproyldipalmitoylphosphatidylethanolamine (DNP-PE) (Avanti Polar Lipids) to the lipid mixture before preparation of the liposomes.

Complement lysis of the liposomes was induced by the addition of 100  $\mu$ L/mL mouse IgM anti-DNP as cell culture supernate and 500  $\mu$ L/mL serum complement (Pel-Freeze Biologicals) to 300  $\mu$ L/mL liposomes containing 50 mmol/L ferrocyanide in a total volume of 1 mL TRIS/saline buffer containing 0.5 mmol/L  $\text{CaCl}_2$  and 0.150 mmol/L  $\text{MgCl}_2$ . Incubation time of the sample for complement lysis was 30 min at 37  $^\circ\text{C}$ .

**Photon Correlation Spectroscopy.** Photon correlation spectroscopy measurements were made by using a helium–neon laser as the coherent light source at 632.8 nm. A scattering angle of 90  $^\circ$  was used for all measurements.

An apparent diffusion coefficient,  $D_T$ , can be calculated for the scattered species by using a 128-channel autocorrelator to compute the time autocorrelation function of the scattered intensities and fitting the data by a cumulants method. This diffusion coefficient can be applied to the Stokes–Einstein equation

$$D_T = kT/6\pi\eta r_h$$

where  $k$  is the Boltzmann constant,  $T$  is the absolute temperature (in kelvin), and  $\eta$  is the viscosity, to yield a hydrodynamic radius,  $r_h$ , for the scattering particles.

**Electrochemical Measurements.** Solutions were prepared in 0.10 mol/L TRIS/saline (0.150 mol/L NaCl) buffer adjusted to pH 7.5. Potassium ferrocyanide, (ferrocenylmethyl)trimethylammonium iodide, and all other reagents were used as received.

(Ferrocenylmethyl)trimethylammonium trifluoromethanesulfonate was synthesized by dropwise addition of an equimolar amount of 0.01 mol/L silver trifluoromethanesulfonate in acetone to (ferrocenylmethyl)trimethylammonium iodide while stirring. The precipitate was filtered under nitrogen and desiccated overnight under a vacuum.

All electrochemical measurements were made by using a conventional three-electrode cell and a microprocessor-controlled potentiostat. In all cases, a platinum auxiliary electrode and Ag/AgCl reference electrode were used. For all liposome lysing experiments, a background voltammogram of the liposomes prior to lysis was used to correct the peak currents obtained from the released ferrocyanide.

**Electrode Preparations.** *Poly(vinylpyridine–styrene) Electrodes.* A solution containing 5.0 g of polystyrene/10 mL of 1% poly(4-vinylpyridine) (PVP) in methanol was mixed with an equimolar amount of iodomethane. Aliquots of 20  $\mu$ L of the resulting solution were pipetted onto the surface of 0.5  $\text{cm}^2$  bright platinum disk electrodes, and the excess solvent was evaporated to dryness. The modified electrodes were heated for 2 h at 90  $^\circ\text{C}$  in a vacuum oven.

*4-[2-(Trichlorosilyl)ethyl]pyridine Electrodes.* Platinum oxide surfaces were prepared in 10% sulfuric acid by the method of Wrighton et al. (12). The potential of a clean, 0.5  $\text{cm}^2$  platinum electrode (13) was stepped to +1.9 V vs SCE for 5 min to oxidize the surface and then stepped back to +1.5 V (to form the platinum hydroxide) until current decayed to residual levels. The electrodes were placed in an oven at 90  $^\circ\text{C}$  for approximately 5 min to remove excess water, and reacted under argon with 5% 4-[2-(trichlorosilyl)ethyl]pyridine in toluene for 15 min. The modified electrodes were quaternized by refluxing for 4 h in neat iodomethane and heated for 2 h at 180  $^\circ\text{C}$  in a vacuum oven. Prior to use, the electrodes were stored in a TRIS/NaCl buffer to exchange the iodide ions for chloride.

*2-[2-(Trimethoxysilyl)ethyl]-N-methylpyridine Electrodes.* 2-[2-(Trimethoxysilyl)ethyl]-N-methylpyridinium iodide was

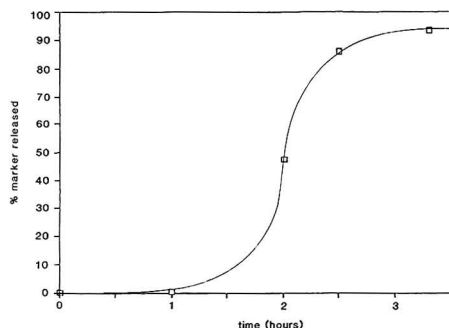


**Figure 1.** Leakage of (ferrocenylmethyl)trimethylammonium trifluoromethylsulfonate,  $\text{FcSO}_3^-$ , from the liposome cavity (300  $\mu$ L/mL sample; 50 mmol/L  $\text{Fe}(\text{CN})_6^{4-}$ ) as determined by DPV. Percentage of the marker released is calculated by comparison to the peak current obtained by surfactant lysis of the membrane.

synthesized by reacting equimolar amounts of 2-[2-(trimethoxysilyl)ethyl]-N-pyridine and iodomethane in methanol for approximately 2 h (80  $^\circ\text{C}$ ) and precipitating the compound from ethyl ether. A 2% (by weight) solution of the quaternized silane compound was prepared in a 95% ethanol/water solution adjusted to pH 4.5 with acetic acid, and this solution was reacted at room temperature for 24 h with the platinum hydroxide electrodes described above and dried for 2 h at 110  $^\circ\text{C}$ .

## RESULTS AND DISCUSSION

**Electroactive Species as Encapsulants.** One of the obstacles encountered in previous attempts to entrap electroactive markers within lipid bilayers was the nonspecific leakage of the markers prior to lysis (4–6). Therefore, finding a well-defined redox couple that remained trapped for long periods of time is imperative to the success of any liposome immunoassay scheme.

The extent to which a marker will remain entrapped within the aqueous cavity of a liposome largely depends on the solubility and charge of the marker. The stability of the lipid bilayer depends on the lipid components used in the liposome preparation. For our investigations, DMPC, a saturated lipid, was used because of its resistance to oxidation. Cholesterol has been found to associate in the hydrophobic bilayer region of DMPC thereby reducing the leakage of the contents across the bilayer structure as well as reducing the effects of temperature on the lipid physical state (14). Finally, the dicetyl phosphate provides the membrane with a net negative charge to reduce aggregation and fusion. We have designated the amount of liposomes for a given experiment in terms of microliters of liposome preparation per milliliter of reaction volume for all discussions. From light scattering determination of the liposome diameter, it was calculated that approximately  $10^{15}$  liposomes are produced per milliliter of lipid preparation.

It can be shown electrochemically that molecules containing large hydrophobic regions, which can easily partition into the lipid bilayer, leak out of the liposome over a relatively short period of time. Furthermore, some of these molecules can themselves have an autolytic ability once they are released from the membrane. For example, (ferrocenylmethyl)trimethylammonium trifluoromethylsulfonate,  $\text{FcSO}_3^-$ , was encapsulated at a concentration of 0.01 mol/L in TRIS buffer. The signal obtained by measuring the peak current from the differential pulse voltammogram showed that nearly 100% lysis of the liposomes occurred over a 3-h period (Figure 1). A much more stable encapsulant was found to be potassium ferrocyanide, the oxidation of which upon lysis could be measured at +0.200 V vs Ag/AgCl. In addition to exhibiting reversible electrochemical behavior, ferrocyanide was chosen

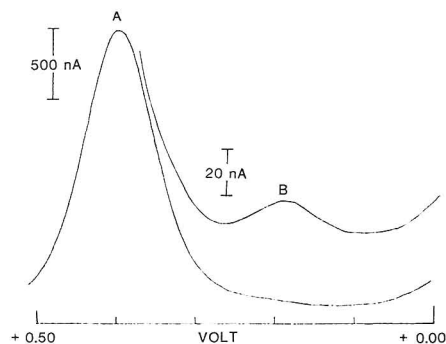


**Figure 2.** Liposome lysis induced by  $\text{FcSO}_3^-$ : (A) Differential pulse voltammogram for 1 mmol/L  $\text{FcSO}_3^-$  before addition of 300  $\mu\text{L}$  sample of liposomes containing 50 mmol/L  $\text{Fe}(\text{CN})_6^{4-}$ . (B) Oxidation of ferrocyanide observed after 2 h resulting from disruption of the membrane. Current scales have been adjusted for clarity.

because of its low oxidation potential, which minimizes interferences by other oxidizable species and eliminates the need of solution deaeration; an advantage when working under ambient conditions or with biological fluids. Unlike the ferrocene species, the ferrocyanide (encapsulated at 50 mmol/L) showed no evidence of leakage over several weeks. To verify the lysing ability of  $\text{FcSO}_3^-$ , 100  $\mu\text{L}$  of 1 mmol/L  $\text{FcSO}_3^-$  was added to 300  $\mu\text{L}$  of ferrocyanide-loaded liposomes described previously (in a 1-mL reaction volume) and shown to disrupt the membrane. After several hours, the resulting voltammogram has two peaks corresponding to the oxidations of both the ferrocyanide and ferrocene (Figure 2), clearly demonstrating the lysis of the ferrocyanide liposomes by the  $\text{FcSO}_3^-$ .

**Determination of Physical Characteristics of  $\text{Fe}(\text{CN})_6^{4-}$  Liposomes.** Variations in the intensity of 90° scattered laser light induced by any macromolecular particle can yield information about the dynamics of the scattering species (15). Koppel (16) demonstrated that the cumulants method of data analysis in photon correlation spectroscopy (PCS) permits the determination of the polydispersity in a population of scattering particles. For a solution of polydisperse particles, the distributions are described as the mean and moments about the mean. The normalized variance, or polydispersity, measures the width of the distribution. This method has been shown by Chang et al. (17) to be applicable for the determination of size and stability of unilamellar dipalmitoylphosphatidylcholine liposomes.

For the ferrocyanide liposomes prepared by the injection method described above, the diameters ranged from 0.10 to 0.15  $\mu\text{m}$  by varying the concentration of the internal marker between 25 and 75 mmol/L. Figure 3 shows a typical intensity autocorrelation function of liposomes prepared by using 50 mmol/L for ferrocyanide as the encapsulant. The polydispersity of these liposome preparations ranged from 0.30 to 0.37 for all ferrocyanide concentrations. These values for size and homogeneity remained constant over a 1-month period (stored at 4 °C under argon), which would indicate the stability of these liposomes over this time.

Among the parameters commonly used to describe the characteristics of liposomes are the capture volume and encapsulation efficiency. Capture volume describes the volume enclosed by a given amount of lipid and is usually calculated in terms of liters of entrapped species per mole of total lipid. This parameter is a function of the liposome radius; the radius in turn is a function of the technique used to form the liposomes, the lipids used, and the ionic strength of the medium.

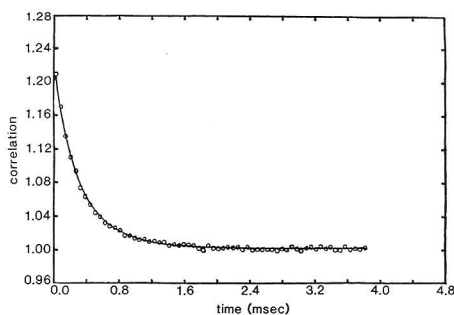


**Figure 3.** Correlation function of the intensity of scattered light induced by 50 mmol/L ferrocyanide liposomes. Cumulant analysis of the data yields an apparent diffusion coefficient of  $5.4 \times 10^{-8} \text{ cm}^2/\text{s}$  for the liposomes.

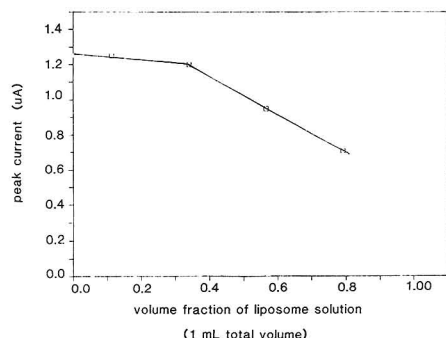


**Figure 4.** Effect of lipid concentration on differential pulse voltammograms at 0.5-cm<sup>2</sup> bright Pt electrode. Ferrocyanide concentration 1 mmol/L. Lipid was added as liposomes prepared in buffer solution alone. Voltammograms were measured after 3 min.

Encapsulation efficiency on the other hand is defined as the aqueous compartment sequestered by lipid and is proportional to the lipid concentration (18). From the PCS data, and by assuming a 40-Å bilayer thickness (19), an internal volume of approximately  $10^{-16} \text{ mL/liposome}$  can be calculated. If the liposomes are prepared in a 50 mmol/L ferrocyanide solution, more than  $10^4$  molecules are entrapped within the aqueous internal volume of each liposome.

The concentration of total lipid was determined to be 1.13 mmol/L by a Barlett phosphate analysis for a ferrocyanide/liposome sample. From these values, the capture volume was calculated to be 2.2 L/mol of lipid with an encapsulation efficiency of 0.76% for this particular liposome preparation.

**Electrochemical Detection of Released Marker.** To determine the feasibility of using liposomes with a technique such as differential pulse voltammetry, the effect of lipid on the peak shape and height was investigated at a bright Pt electrode. Increasing concentrations of the lipid mixture, in the same proportions as that of the liposome preparation, were added to solutions of potassium ferrocyanide/TRIS to yield a final ferrocyanide concentration of 1 mmol/L. The resulting voltammograms showed that there was a dramatic decrease in the peak current for solutions higher than 400  $\mu\text{L/mL}$  of the liposome solution (see Figure 4). The width at half height of the voltammetric peak remained constant (130 mV) for all lipid dilutions. Repeating this experiment, adding either octyl glucoside (as 250 mg/mL) or Triton X-100 (as a 1:10 dilution



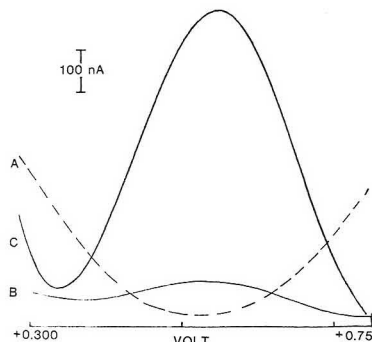
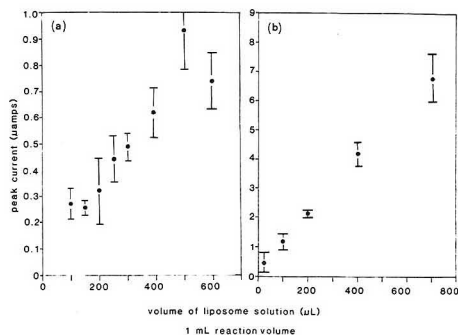


**Figure 5.** Surfactant lysis of 300  $\mu\text{L/mL}$  liposomes (0.57  $\mu\text{mol}$  of total lipid) loaded with 50 mmol/L ferrocyanide: (A) dilution of lipid to 1 mL in TRIS buffer, prior to lysis; (B) addition of 200  $\mu\text{L}$  Triton X-100, measured at bright Pt; (C) solution B after preconcentrating the analyte 5 min at a (trimethoxysilyl)pyridinium-modified electrode.

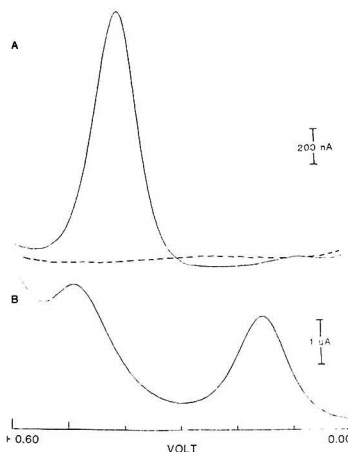
from the concentrate), showed little effect on the peak height at the concentrations necessary to induce lysis. The differential pulse voltammetric peak current,  $i_p$ , is proportional to the product of electrode area, analyte concentration, and square root of the diffusion coefficient. The decrease in peak current at high lipid concentration (500  $\mu\text{L/mL}$  of liposome preparation corresponds to 0.94  $\mu\text{mol}$  of lipid) indicates that the lipid molecules partially passivate the electrode surface by decreasing the effective area of the electrode. A reduction in the diffusion coefficient of ferrocyanide (and consequently in  $i_p$ ) due to an increase in solution viscosity with lipid concentration is a possible second-order effect and most likely negligible compared to the effect of the surface passivation by lipids. These same lysis experiments of ferrocyanide-loaded liposomes can be performed by using atomic absorption spectroscopy as the detection method for the released marker. To obtain a meaningful signal by this method, the solutions were passed through a disposable  $\text{C}_{18}$  column to remove the lipid from the sample matrix after lysis. By comparison of the resulting concentrations of released marker obtained by the spectroscopic method to those obtained electrochemically (from a standard calibration curve of ferrocyanide at a Pt electrode), it is evident that some of the analytical signal is lost due to the passivation of the electrode.

Figure 5 illustrates a typical lysis experiment. Prior to lysis, a voltammogram of ferrocyanide-loaded liposomes in buffer is stored for background correction. Addition of a surfactant, between 100 and 250  $\mu\text{L/mL}$ , induces complete lysis of the membrane, which results in the release of ferrocyanide. Calibration curves obtained from the peak heights of the voltammograms are shown in Figure 6a for an increasing volume of liposomes added to a 1-mL reaction volume. With octyl glucoside used as a lysing agent, an irreproducibility of these peak heights between samples of up to 30% relative standard deviation is obtained and total lysis is not achieved until approximately 20–30 min have passed. When Triton X-100 is used to lyse the membranes, the time necessary to obtain a maximum peak height decreases from 20–30 min to 5 min and the reproducibility of the signal is improved as indicated in Figure 6a.

**Investigation of Liposome Lysis at Modified Electrodes.** Although we have demonstrated the feasibility of using an amperometric technique such as differential pulse voltammetry to measure ferrocyanide released from liposomes, the current levels (when using a 0.5  $\text{cm}^2$  Pt electrode) are less than a microamp for 100–300  $\mu\text{L}$  of liposomes/mL samples. It is clear that further amplification of the analytical signal



**Figure 6.** Peak current response after surfactant lysis (Triton X-100) of 50 mmol/L ferrocyanide liposomes: (a) Peak current response at bright Pt. Correlation coefficient for linear range (150–400  $\mu\text{L}$  1 mL reaction volume) is 0.983. (b) Peak current response at (trimethoxysilyl)pyridinium electrode. Linear range is extended to 25–700  $\mu\text{L/mL}$  with a correlation coefficient of 0.998. Preconcentration times vary from 35 min (25- $\mu\text{L}$  samples) to 3 min (700- $\mu\text{L}$  samples).



**Figure 7.** Liposome lysis induced by  $\text{FcSO}_3^-$ : (A) Differential pulse voltammograms measured at a bright Pt electrode vs.  $\text{Ag/AgCl}$  before and after lysis. Dashed curve shows results from 300  $\mu\text{L}$  liposomes (50 mmol/L  $\text{Fe}(\text{CN})_6^{4-}$  encapsulated) in TRIS buffer. Solid curve shows results from the addition of 150  $\mu\text{L}$  (1 mmol/L) of  $\text{FcSO}_3^-$  to the sample. (B) Same solution measured by using a quaternized PVP electrode to enhance the ferrocyanide signal (cf. Figure 2).

is necessary to consider this assay scheme for clinical concentrations ( $10^{-10}$ – $10^{-12}$  mol/L) of antigens or antibodies with an immunologically sensitized membrane surface. A more serious caveat associated with this technique is that of passivation of the electrode surface when serum is used to induce complement lysis.

We have addressed both of these problems by using a dual-function polymer modified electrode. First, an anion-exchange mechanism can be used to electrostatically bind the ferrocyanide near the electrode surface (20), thereby preconcentrating it, after it has been released from the liposomes. This technique of "ion-exchange voltammetry" has been successfully demonstrated with DPV by Whiteley and Martin (21). Second, the film acts as a protective coating to prevent fouling of the electrode by proteins in serum solutions.

Early attempts involved using a quaternized poly(4-vinylpyridine) film nonspecifically adsorbed onto the platinum

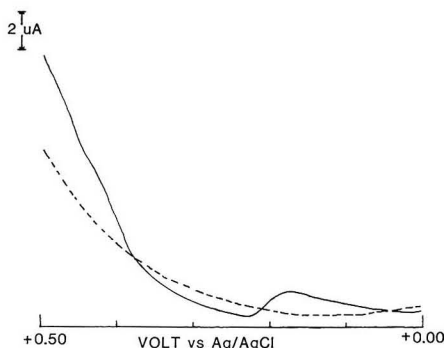


**Figure 8.** Complement induced lysis of 50 mmol/L ferrocyanide-loaded DNP-sensitized liposomes at a 5% trichlorosilylpyridinium modified electrode. Sample contained 50  $\mu\text{L/mL}$  liposomes, 100  $\mu\text{L/mL}$  anti-DNP IgM, and 750  $\mu\text{L/mL}$  rabbit complement serum. Preconcentration of marker for 20 min after lysis. Broken line: liposomes and complement serum at modified electrode. Solid line: 30 min after addition of anti-DNP cell culture supernatant.

surface by evaporation of the solvent. These films resulted in a 2–3 order of magnitude increase in peak current in a surfactant lysis of liposomes containing 50 mmol/L ferrocyanide. Investigations using this type of polymer indicate that the ion-exchange film shows preference for the tetravalent ferrocyanide over monovalent species in the sample. If the lysis experiment previously described, using  $\text{FeSO}_3$  to disrupt ferrocyanide liposomes, is repeated with this modified electrode, a 2 order of magnitude increase in the ferrocyanide oxidation peak is observed while there is little or no enhancement of the  $\text{FeSO}_3$  signal (Figure 7).

A much more durable film preparation was produced by the reaction of a solution of 5% (trichlorosilyl)ethyl-4-pyridine in toluene at a platinum oxide electrode followed by refluxing the electrodes in neat methyl iodide to quaternize the pyridine (22). By estimation of the moles of polymer from a weight difference in the electrode before and after modification and the degree of quaternization from the charge passed during the chronocoulometric oxidation of the iodide (stepping the potential to +400 mV vs. Ag/AgCl), it was determined that between 10% and 15% of the total number of pyridine sites had been methylated in the reflux reaction. This treatment

resulted in somewhat less amplification of the peak current, as well as longer equilibration times to reach the maximum peak current of the voltammogram. This type of modification, however, provided excellent protection of the surface against serum proteins. Figure 8 illustrates a typical signal obtained by using this ion-exchange polymer modified electrode in a complement mediated lysis of DNP-derivatized liposomes in the presence of  $5 \times 10^{-6}$  mol/L anti-DNP IgM and 50% complement serum.

It appears that the protection from serum proteins at the PtO-silylpyridinium electrode described here is based on a size exclusion rather than electrostatic mechanism since serum proteins have a net negative charge at physiological pH. Therefore it can be speculated that a more highly cross-linked film would be even more resistant to fouling. This, unfortunately, would be detrimental to the rate of preconcentration of the marker. Recent work in our laboratory to overcome these problems has led to the use of a (trimethoxysilyl)-ethyl-2-pyridine reagent which has been quaternized via the reaction in Figure 9 prior to deposition onto a platinum oxide surface. This provides a stable film that has nearly 100% of the pyridine sites methylated. Peak current response to a surfactant lysis of the liposomes using the modified electrodes prepared by the method described in Figure 9 results in an extension of the working range over that obtained at bare Pt from 150–400  $\mu\text{L/mL}$  to 25–700  $\mu\text{L/mL}$  with considerably improved reproducibility and linearity of the response (Figure 6b).

## CONCLUSIONS

The characterization of ferrocyanide-loaded liposomes provides information necessary for further experimentation with these structures in both homogeneous and heterogeneous immunoassay schemes. From the results of this study, we have demonstrated the feasibility of using liposomes for the selective and sensitive ( $10^{-8}$  mol/L) determination of immunoagents in serum matrices. Experiments have shown that dilute solutions of ferrocyanide require extensive equilibration times and future investigations will determine the practical detection limits for this technique. Other research in this laboratory is currently using the surfactant lysis of liposomes in a flow injection analysis scheme involving the competitive binding of these types of marker-loaded phospholipid vesicles on a packed glass bead reactor containing immobilized antibodies (23). This study will facilitate the application of an electrochemical detector for this type of immunoassay.

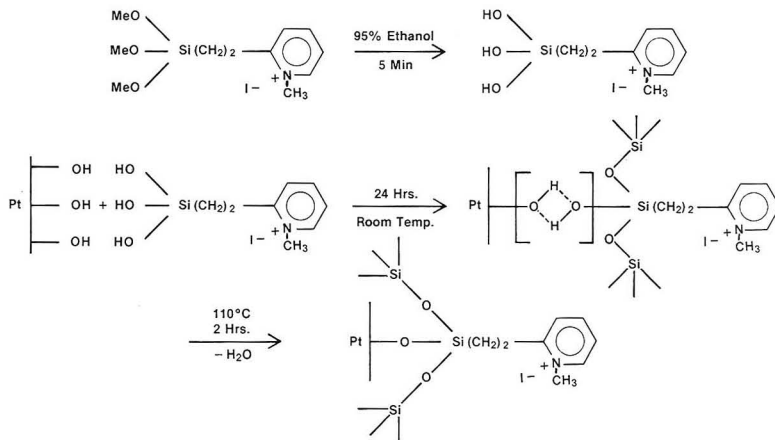


**Figure 9.** Reaction sequence for fabrication of silane-modified electrode with approximately 100% of the pyridine sites methylated.

## ACKNOWLEDGMENT

The authors thank Dr. Anne L. Plant for her assistance and helpful discussions in the preparation and characterization of the liposomes.

**Registry No.** DMPC, 18194-24-6; potassium ferrocyanide, 13943-58-3; cholesterol, 57-88-5; dicetyl phosphate, 3614-36-6; poly(PVP-styrene), 26222-40-2; 4-[2-(trichlorosilyl)ethyl]pyridine, 17082-70-1; 2-[2-(trimethoxysilyl)ethyl]-N-methylpyridinium iodide, 111160-41-9.

## LITERATURE CITED

- (1) Fendler, J. *Membrane Mimetic Chemistry*; Wiley: New York, 1982; pp 153-158.
- (2) Gregoriadis, G. *Trends Biotechnol.* **1985**, *3*, 235-241.
- (3) Rofit, I.; Brostoff, J.; Male, D. *Immunology*; Mosby: St. Louis, 1985; pp 7.2-7.13.
- (4) D'Orazio, P.; Rechnitz, G. *Anal. Chem.* **1977**, *49*, 2083-2086.
- (5) D'Orazio, P.; Rechnitz, G. *Anal. Chim. Acta* **1979**, *109*, 25-31.
- (6) Shiba, K.; Umezawa, Y.; Wanatabe, T.; Ogawa, S.; Fujiwara, S. *Anal. Chem.* **1980**, *52*, 1610-1613.
- (7) Umezawa, Y.; Sofue, S.; Takamoto, Y. *Anal. Lett.* **1982**, *15*, 135-146.
- (8) Haga, M.; Hagaki, H.; Sugawara, S.; Okano, T. *Biochem. Biophys. Res. Comm.* **1980**, *95*, 187-192.
- (9) Katsu, T.; Tanaka, A.; Fujita, Y. *Chem. Pharm. Bull.* **1982**, *30*, 1504-1507.
- (10) Batzri, S.; Korn, E. D. *Biochim. Biophys. Acta* **1973**, *289*, 1015-1019.
- (11) Bartlett, G. R. *J. Biol. Chem.* **1959**, *234*, 449-451.
- (12) Wrighton, M. S.; Palazzotto, M. C.; Bocarsly, A. B.; Bolts, J. M.; Fischer, A. B.; Nado, L. J. *Am. Chem. Soc.* **1978**, *100*, 764-767.
- (13) Conway, B. E.; Angerstein-Kozłowska, H.; Sharp, W. B. A.; Criddle, E. *E. Anal. Chem.* **1973**, *45*, 1331-1336.
- (14) Papaioannopoulos, D.; Nir, S.; Ohki, S. *Biochim. Biophys. Acta* **1971**, *266*, 561-583.
- (15) Cummings, H. *The Application of Laser Light Scattering to the Study of Biological Motion*; Earnshaw, J., Steer, M. W., Eds.; Plenum: New York, 1983; pp 171-207.
- (16) Koppel, D. J. *Chem. Phys.* **1972**, *57*, 4814-4820.
- (17) Chang, E. L.; Gaber, B. P.; Sheridan, J. J. *Biophys. Soc.* **1982**, *39*, 197-201.
- (18) *Liposomes*; Ostro, M., Ed.; Marcel Dekker: New York, 1983; pp 27-51.
- (19) Franks, N. P. J. *Mol. Biol.* **1976**, *100*, 345-358.
- (20) Guadalupe, A. R.; Weir, L. M.; Abruna, H. D. *Am. Lab. (Fairfield, Conn.)* **1986**, *18* (Aug), 102-107 and references therein.
- (21) Whiteley, L. D.; Martin, C. R. *Anal. Chem.* **1987**, *59*, 1746-1751.
- (22) Moses, P. R.; Murray, R. W. *J. Am. Chem. Soc.* **1976**, *98*, 7435-7436.
- (23) Brown, L. L.; Plant, A. L.; Durst, R. A., manuscript in preparation.

RECEIVED for review June 2, 1987. Accepted September 14, 1987. Certain commercial products are identified in order to adequately specify the experimental procedure. This does not imply endorsement or recommendation by the National Bureau of Standards. This work will be included in the dissertation of R.M.K. as partial fulfillment of PhD requirements at the University of Maryland.

## Simultaneous Determination of Glucose, Fructose, and Sucrose in Mixtures by Amperometric Flow Injection Analysis with Immobilized Enzyme Reactors

Kiyoshi Matsumoto,\* Hideaki Kamikado,<sup>1</sup> Hiroaki Matsubara, and Yutaka Osajima

Department of Food Science and Technology, Faculty of Agriculture, Kyushu University 46-09, Hakozaki, Higashi-ku, Fukuoka 812, Japan

Glucose, fructose, and sucrose were determined in a flow injection system by using parallel configurations of enzyme immobilized reactors. Hydrogen peroxide produced (for glucose and sucrose) and hexacyanoferrate(II) (for fructose) were monitored amperometrically. Sucrose determination was performed with a glucose-eliminating reactor which was set just before the sucrose reactor. Interference of ascorbic acid was completely eliminated by using an ascorbate-eliminating reactor which was set before the sample injection valve. The responses of the sensors were linear between  $2 \times 10^{-5}$  and  $1 \times 10^{-3}$  M, and the precision (coefficient of variation) was better than 1.8% (glucose), 1.8% (fructose), and 1.6% (sucrose) at the 1 mM level by 10 successive injections. Application of the system to some foods (especially fruits) is also described.

Recently much attention has been devoted to the determination of biologically important substances and food components using biospecific sensors or analyzers based on mini-reactors (1, 2). For the determination of sugars, a large

number of sensing systems have been developed that use various kinds of membranes and sensor arrangements, such as glucose (3-10), fructose (11,12), galactose (6, 13-15), sucrose (5, 7, 9, 14, 16-21), lactose (14-16, 22), and maltose (5, 14, 16, 23).

Flow injection analysis (FIA) is a dynamic process that produces a well-defined and highly reproducible concentration transient at the detector site. A number of immobilized enzymes, then, have been used in the flow-injection methodology (6, 8-11, 13, 21, 22). In many food processes, combinations of sugar, especially glucose, fructose, and sucrose, are particularly important, and measurements of these species are necessary for effective process and product control. Approaches for the measurements of glucose and disaccharide are mainly classified into three types. The first type was the subtraction methodology by two differently constituted enzyme electrodes. For example, one is for glucose only and another is for glucose and maltose, which gives the sum of two species (5). The second type was applied to the successive measurements of glucose and sucrose, which was achieved by using a measuring cell reactor containing a glucose oxidase membrane electrode and inverting sucrose in the measurement cell by means of immobilized invertase (7). The third type used the glucose eliminating methodology, which was achieved by using a glucose oxidase and catalase bienzyme system (20, 21).

<sup>1</sup>Present address: Meiji Milk Products Co., Ltd., Kyobashi, Chuo-ku, Tokyo 104, Japan.

Simultaneous determination of sucrose and glucose in mixtures has been achieved by using the appropriate immobilized enzymes in packed columns with a single detector (9). Recently, Morishita et al. (24) described the simultaneous determination of glucose, lactate, and glycerol by an FIA method with enzyme immobilized open-tubular reactors. But no papers have described the simultaneous determination of three sugar species including a glucose-eliminating system.

In an earlier paper (11), fructose was determined by flow injection analysis with immobilized fructose 5-dehydrogenase. The redox acceptor used was hexacyanoferrate(III) and the reduced acceptor was detected electrochemically by a platinum flow-through cell. This paper describes the simultaneous determination of glucose, fructose, and sucrose by an FIA method including parallel configuration of enzyme immobilized reactors with a multichannel amperometric detector and a glucose-eliminating reactor.

## EXPERIMENTAL SECTION

**Apparatus.** Amperometric measurements were made with a laboratory-made multichannel potentiostat which had three independent channels to impose different potentials and to measure the current from each channel. The potentiostat could change the imposed potential from -2.0 to +2.0 V and could measure the current from 10 nA to 100  $\mu$ A full scale.

**Reagents.** Glucose oxidase (GOD, EC 1.1.3.4, ex. *Aspergillus niger*, 303 U/mg), invertase (EC 3.2.1.26, ex. Baker's yeast, 329 U/mg), mutarotase (EC 5.1.3.3, ex. pig liver, 5000 U/mg), and catalase (EC 1.11.1.6, ex. bovine liver, 65000 U/mg) were obtained from Boehringer Mannheim GmbH. Ascorbate oxidase (EC 1.10.3.3, ex. cucumber, 150 U/mg) was purchased from Oriental Yeast Co. (Tokyo, Japan). Fructose 5-dehydrogenase (FDH, EC 1.1.99.11) was extracted from *Gluconobacter industrius* and purified as described earlier (11). The specific activity of the final preparation was about 30 U/mg of protein. Amino-Cellulofine and CNBr-activated Sepharose 4B were purchased from Seikagaku Kogyo Co. (Tokyo, Japan) and Pharmacia Fine Chemicals (Uppsala, Sweden), respectively. Fine porous glass (FPG-100M) was purchased from Wako Pure Chemical Industries, Ltd. (Osaka, Japan). The pore size and particle size were 100 Å and 120–200 mesh, respectively. (3-Aminopropyl)triethoxysilane (98%) was purchased from Aldrich Chemical Co. (Milwaukee, WI). Sodium cyanoborohydride and glutaraldehyde (25%) were obtained from Nakarai Chemical Co. (Kyoto, Japan). All other chemicals were of reagent grade and were used without further purification.

**Glucose Reactor.** Amino-Cellulofine (wet weight 0.3 g, dry weight 0.03 g) was washed thoroughly with distilled water and 0.2 M carbonate buffer (pH 10.0) on a sintered glass filter (G-3). The support was mixed with 0.2 M carbonate buffer (pH 10.0) containing 5% glutaraldehyde for 2 h at 20 °C while shaking. The resulting support was separated from the solution by filtration (sintered glass filter, G-3) and washed thoroughly with distilled water and 0.1 M phosphate buffer (pH 6.0). As the result, aldehyde functionalities were introduced at the terminal  $\text{NH}_2$  groups of the support. The resulting support was put into 2 mL of 0.1 M phosphate buffer containing glucose oxidase (100 U) and then reacted for 30 min at 5 °C while shaking. The reacted support was reduced by about 2 mg of sodium cyanoborohydride for 2 h at 5 °C and then washed thoroughly with distilled water and 0.1 M phosphate buffer containing 0.5 M NaCl (washing buffer). The unreacted functionalities on the immobilized Cellulofine were then blocked by 2 mL of 15 mg/mL glycine solution for 2 h at 20 °C and separated by filtration and the support was washed with washing buffer. The prepared Cellulofine support was packed in a glass tube (2 mm i.d.  $\times$  10 cm) and the reactor was stored at 5 °C filled with phosphate buffer.

**Sucrose Reactor.** The same procedures described above were performed except for the amount of invertase, mutarotase, and glucose oxidase and the reducing time with sodium cyanoborohydride. The prepared Cellulofine support was packed in a glass tube (2 mm i.d.  $\times$  10 cm) and the reactor was stored at 5 °C filled with phosphate buffer. Hydrogen peroxide finally produced in the enzyme reactor was monitored amperometrically.

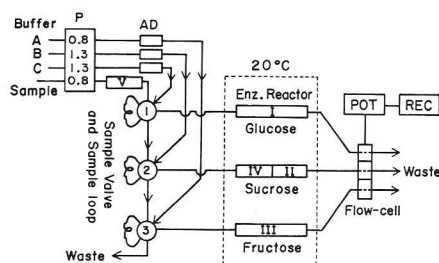


**Figure 1.** Schematic diagram of multichannel flow injection analytical system; P, microtube pump; AD, air damper; POT, multichannel potentiostat; REC, multiten recorder; I, glucose reactor; II, sucrose reactor; III, fructose reactor; IV, glucose-eliminating reactor; V, ascorbate-eliminating reactor; A, McIlvaine buffer (containing 6 mM  $\text{K}_3[\text{Fe}(\text{CN})_6]$ , pH 5.0); B, phosphate buffer (pH 7.0); C, phosphate buffer (pH 6.0).

**Fructose Reactor.** FDH was immobilized on Amino-Cellulofine as reported earlier (11) and the material was packed into a glass tube (2 mm i.d.  $\times$  6 cm). The reduced acceptor (hexacyanoferrate(II)) produced in the enzyme reactor was monitored amperometrically.

**Glucose-Eliminating Reactor.** CNBr-Activated Sepharose (0.2 g dry weight) was swollen with 1 mM HCl for 10 min and washed with 0.1 M phosphate buffer (pH 6.0) on a sintered glass filter (G-3). The gel was allowed to react at 5 °C with 1 mL of 0.1 M phosphate buffer (pH 6.0) containing mutarotase ( $2.5 \times 10^3$  U), glucose oxidase ( $6.06 \times 10^3$  U), and catalase ( $5.2 \times 10^5$  U) overnight, and then washed thoroughly with 0.5 M NaCl and deionized water. The unreacted functionalities were then blocked by 1 mL of 15 mg/mL glycine solution for 2 h at 20 °C and separated by filtration and the support was washed with 0.1 M phosphate buffer (pH 6.0) containing 0.5 M NaCl. The prepared Sepharose support was packed in a glass tube (2 mm i.d.  $\times$  10 cm) and the reactor was stored at 5 °C.

**Ascorbate-Eliminating Reactor.** Ascorbate oxidase was immobilized on CNBr-Activated Sepharose as reported earlier (11) and the material was packed into a glass tube (2 mm i.d.  $\times$  6 cm).

**Enzyme Immobilization on FPG.** Fine porous glass (3.0 g) was boiled and refluxed in 6 N HCl for 4 h, filtered on a sintered glass filter (G-3), and washed with distilled water until the washed solution reached neutral. The support was dried at 60 °C for 4 h under reduced pressure. The dried support, then, was silanized with 10% (3-aminopropyl)triethoxysilane in toluene for 2 days under shaking and shielding of the container. After the treatment, the support was filtered on a sintered glass filter (G-3), washed successively with toluene and ethanol, air-dried overnight and, finally, dried at 60 °C for 4 h under reduced pressure. The alkylaminated glass was treated with 5% glutaraldehyde in 0.2 M carbonate buffer (pH 10.0) at 20 °C for 2 h, filtered, and washed with distilled water. The formulated glass (0.35 g, wet weight) was coupled with enzymes (for instance, glucose oxidase, invertase, and mutarotase) for 30 min at 5 °C while shaking. The later procedures were the same as immobilization on Amino-Cellulofine.

**Flow System.** A schematic diagram of the flow system is shown in Figure 1. The working buffer for the glucose and sucrose reactor and for the fructose reactor consisted of 0.1 M phosphate buffer (pH 6.0 for glucose, pH 7.0 for sucrose) and McIlvaine buffer (pH 5.0, containing 6 mM  $\text{K}_3[\text{Fe}(\text{CN})_6]$  and 0.1% Triton X-100), respectively. Each working buffer (carrier solution) in the reservoir was carried by a microtube pump (Tokyo Rikakikai Co., Ltd.) through an air-damper, a sample injection valve (six-way switching valve), and an immobilized enzyme reactor and then was transported to an multichannel flow-through cell and finally to a waste tank (main flowing line). The flow rates are indicated (in mL/min) in Figure 1. The sample flow system consisted of another microtube pump connected to a sample injection valve equipped with a sample loop. The sample loops were connected in series and were set to be 240  $\mu$ L each. When elimination of ascorbate was required, the ascorbate-eliminating reactor was set in the

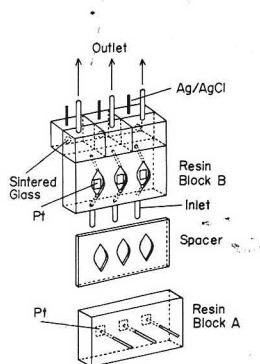


Figure 2. Schematic diagram of flow-through cell. For details, see the text.

sampling line between the pump and the first injection valve as shown in Figure 1. The glucose-eliminating reactor was set just before the sucrose reactor. The sample was injected into each carrier stream by switching (simultaneous or independent) of the valves. All enzyme reactors except the ascorbate-eliminating reactor were thermostatically controlled at 20 °C (Cotrola Cryothermostat WK-5).

**Multichannel Flow-Through Cell.** The flow-through cell was composed of three independent compartments (Figure 2). Each compartment had Pt electrodes (working and counter) and a reference electrode (Ag/AgCl). The working and counter electrodes (both 4 mm × 4 mm Pt plate, welded on the back side to a perpendicular copper wire) were bonded separately into acrylic resin blocks (resin blocks A and B) with epoxy bond. Surfaces of both of the Pt plates were polished flat and bright. A resin plate (1 mm thick), which had an oval hole (area 0.42 cm<sup>2</sup>) at the position of the Pt plate in the resin block (B), was bonded to the inside surfaces of this counter electrode block (B). The resin block (B) also had inlet and outlet holes drilled through the block above and below the Pt plate and was connected electrically to the reference electrode (Ag/AgCl) through sintered glass. The resin blocks (A and B) were joined face to face, but separated by a rubber sheet (0.6 mm thick), which functioned as a spacer and gasket. The rubber sheet spacer had the same size oval hole at the Pt-plate position, and this sandwich assembly consisting of block-spacer-block was joined securely together by tightened bolts and nuts. The volume of each cell was, consequently, about 0.067 cm<sup>3</sup>. The potentials of the working electrode in the three-electrode system were set to be +0.65 V and +0.385 V vs. Ag/AgCl for the glucose and sucrose determination and for the fructose determination, respectively.

**Measurement Procedures.** The following procedures were performed when three sugars in ternary standard mixture or in fruits samples were measured. Each working buffer was transported through the main flowing line. Each potential was imposed on platinum electrodes of each compartment of flow-through cell. When background currents decreased to small values and base lines were stabilized (about 10 min), sample solution was transported to fill all the valves through an ascorbate-eliminating reactor. About 1.6 mL (2 min) of sample solution was needed to fill all the valves. Then, the sample solution was injected to each main flowing line by switching the valves. Switching of valves was operated manually and simultaneously (at one time). The signal currents detected by the multichannel potentiostat were simultaneously recorded by a multipen recorder (Type R-50, Rikadenki Kogyo Co., Ltd., Tokyo, Japan). The cleaning of the sample line was performed by 0.1 M phosphate buffer (pH 7.0) for 3 min (about 2.4 mL) and new sample solution was transported to fill the valves. The sampling frequency, then, was about 12 h<sup>-1</sup>.

**F-Kit Method.** F-kit (sucrose/D-glucose/D-fructose, No. 716260) was purchased from Boehringer Mannheim GmbH. The F-kit method is an enzymatic, spectrophotometric method using hexokinase, phosphoglucose isomerase, glucose-6-phosphate dehydrogenase, and invertase in free state with ATP and NADP

Table I. Effect of Preparative Condition on the Sucrose Response

code	enzyme amount (×10 <sup>3</sup> U/g of wet AC) <sup>a</sup>			reduction time, h	response, <sup>c</sup> μA
	invertase	mutarotase	GOD		
C-1	9.53	0.83	0.33	2	0.043
C-2	9.53	8.33	0.33	2	0.048
C-3	14.30	8.33	0.33	2	0.062
C-4	14.30	8.33	10.10	2	0.582
C-5	16.45	8.33	10.10	2	0.589
C-6	16.45	8.33	10.10	4	0.756
C-7	16.45	8.33	10.10	18	1.204
C-8	21.00	8.33	10.10	18	1.210

<sup>a</sup> Enzyme amounts were converted to the value per g of wet Amino-Cellulofine. <sup>b</sup> Reduction was performed in 0.1 M phosphate buffer (pH 6.0). <sup>c</sup> The response was expressed when 1 mM sucrose was injected.

Table II. Effectiveness of Glucose-Eliminating Reactor

glucose, mM	sucrose, mM	sucrose response, nA
0.1	0.1	132
0.1	0.5	624
0.1	1.0	1208
0.5	0.1	132
0.5	0.5	620
0.5	1.0	1196

as cofactors. The analytic procedures were performed according to the manual from the manufacturer.

## RESULTS AND DISCUSSION

**Sucrose Reactor.** Enzymatic determination of sucrose is commonly done by a sequence of reactions in which sucrose is first hydrolyzed to α-D-glucose and D-fructose by invertase and, second, the produced α-D-glucose is converted to β-D-glucose by mutarotase and, finally, β-D-glucose is oxidized to D-glucono-δ-lactone and hydrogen peroxide by glucose oxidase. The coimmobilization of the three enzymes necessary for sucrose determination has been studied in detail previously (25, 26). From the preliminary experiment, immobilization efficiencies on three kinds of supports were as follows: CNBr-Activated Sepharose (100), Amino-Cellulofine (90), and fine porous glass (30) when sucrose response immobilized on CNBr-Activated Sepharose was regarded as 100. The flowing properties, however, were the reverse order. Glutaraldehyde treatment on Amino-Cellulofine was selected for this work considering its good flowing property and relatively high immobilization efficiency. The effects of variations of the amounts of enzymes and reducing time by sodium cyanoborohydride on the sucrose responses are shown in Table I. From C-5 to C-7, longer reducing time (18 h) produced a larger response for sucrose, so, consequently, the reducing time was decided to be 18 h. The response for sucrose was increased with the increasing amounts of enzymes. Although larger enzyme composition than that of C-8 will produce a larger response, the C-8 composition was used as the standard in consideration of economy.

**Glucose-Eliminating Reactor.** Various kinds of disaccharide sensors based on glucose oxidase have been developed (14, 16–19). In such sensors, each disaccharide can be determined only when glucose is not contained in the sample, because of the production of hydrogen peroxide by the enzyme action of glucose oxidase. Common food samples, especially fruits, contain glucose, consequently, it interferes with sucrose determination as predicted by the principle. In this work, glucose was decomposed initially to hydrogen peroxide and finally to oxygen and water by a reactor containing coimmobilized glucose oxidase, mutarotase, and cat-

Table III. Simultaneous Determination of Glucose, Sucrose, and Fructose in Ternary Standard Mixtures

glucose, mM			sucrose, mM			fructose, mM		
taken (A)	found (B)	bias (B - A)	taken (A)	found (B)	bias (B - A)	taken (A)	found (B)	bias (B - A)
0.100	0.101	0.001	0.100	0.097	-0.003	0.100	0.095	-0.005
0.100	0.100	0.000	0.100	0.097	-0.003	1.000	1.057	0.058
0.100	0.099	-0.001	0.500	0.499	-0.001	0.100	0.099	-0.001
0.100	0.101	0.001	0.500	0.514	0.014	1.000	1.016	0.016
0.100	0.102	0.002	1.000	0.988	-0.012	0.100	0.102	0.002
0.100	0.100	0.000	1.000	0.988	-0.012	1.000	0.972	-0.028
0.500	0.500	0.000	0.100	0.094	-0.006	0.100	0.115	0.015
0.500	0.504	0.004	0.100	0.097	-0.003	1.000	0.974	-0.026
0.500	0.510	0.010	0.500	0.521	0.021	0.100	0.098	-0.002
0.500	0.502	0.002	0.500	0.516	0.016	1.000	0.996	-0.004
0.500	0.499	-0.001	1.000	0.980	-0.020	0.100	0.103	0.003
0.500	0.504	0.004	1.000	0.995	-0.005	1.000	1.002	0.002

Table IV. Comparison of the Present Method (FIA) with F-Kit (Enzymatic) Method

sample	glucose, %			sucrose, %			fructose, %		
	FIA (A)	F-kit (B)	bias (A - B)	FIA (A)	F-kit (B)	bias (A - B)	FIA (A)	F-kit (B)	bias (A - B)
Coca-Cola	3.88	3.84	0.04	1.76	1.87	-0.11	4.50	4.97	-0.47
kiwi	4.00	3.82	0.12	2.20	2.13	0.07	4.52	4.54	-0.02
banana	2.12	1.94	0.18	12.59	12.50	0.09	3.44	3.56	-0.12
mandarin	2.61	2.54	0.07	4.47	4.33	0.14	2.50	2.43	0.07
apple	1.37	1.30	0.07	2.34	2.30	0.04	6.00	6.13	-0.13

alase. The eliminating reactor was effective up to the 1 mM glucose level. Table II shows the results of sucrose determination at the 0.1–1.0 mM range in the presence of glucose (0.1 and 0.5 mM). No interference was observed on the sucrose determination in the presence of glucose (0.1 and 0.5 mM) when the glucose-eliminating reactor was set just before the sucrose reactor as shown in Figure 1. Long-term stability of the eliminating reactor was also investigated at the 1 mM glucose level. No remarkable decrease of eliminating power was observed during 30 days (only 5% decrease at 30 days), and it will be safe to eliminate to the 0.5 mM glucose level for 30 days.

**Other Reactors.** Glucose reactor constructed as above had high response ability toward glucose. The property of the fructose reactor and the ability of the ascorbate-eliminating reactor were reported earlier (11).

**Typical Response Curves and Calibration.** Typical response curves for three sugars under the optimum conditions of the flow system are shown in Figure 3. The current from each channel increased rapidly just after injection of sample and returned to base line within 2 min. The relative standard deviations for ten duplicated injections at the 1 mM level were 1.8%, 1.8%, and 1.6% for glucose, fructose, and sucrose, respectively. Linear relations between sensor responses and sugar concentrations were observed over the range 0.02–1.0 mM with correlation coefficients larger than 0.999 for each sugar species.

**Long-Term Stability of Reactors.** The glucose reactor maintained its activity for over 30 days without any decrease. The sucrose signal decreased rapidly to about 60% of the initial value during 4 days and then maintained about 50% of the initial value during 15 days and gradually decreased to 25% after 30 days. The stability of fructose reactor was reported previously (11).

**Simultaneous Determination of Three Sugars in a Ternary Standard Mixture.** Ternary standard mixtures were analyzed for the simultaneous determination of glucose, fructose, and sucrose, in order to elucidate the accuracy of this FIA system. Standard samples were prepared in the various concentration ratios over the ranges of 0.1–0.5 mM (glucose), 0.1–1.0 mM (fructose), and 0.1–1.0 mM (sucrose) as shown in Table III. The bias shows the difference between theo-

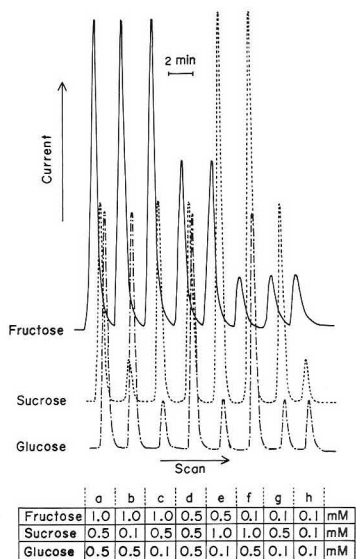


Figure 3. Typical FIA responses for glucose, fructose, and sucrose: solid line, fructose; dotted line, sucrose; dot-dash line, glucose; (a–h) sugar compositions.

retical value (taken) and the found one (found). The results are accurate and the method is very simple and reliable.

**Application and Comparison.** Table IV shows the results for simultaneous determination of three sugars in food samples by use of this system. These results are compared to those obtained by the F-kit method. Ascorbic acid naturally occurs in many fruits and has a relatively low redox potential. The potentials imposed were +0.65 and +0.385 V vs. Ag/AgCl for the detection of hydrogen peroxide and hexacyanoferrate(II), respectively, so ascorbate interfered with both detection systems. Because samples were pretreated through the as-



corbate-eliminating reactor before entering the sample loops, no interference by ascorbate was observed in this system, as described previously (11). The determinations using the present system compare relatively well with the F-kit method overall.

The system described above offers a useful continuous method for the determination of many substrates. Because the system includes parallel configuration of many reactors and a multichannel flow-cell having independent compartments, this not only allows each reactor to set up for an optimum condition but also permits application of the system to different groups of substrates, such as sugars, organic acids, alcohols, nucleic acid derivatives, etc.

**Registry No.** GOD, 9001-37-0; FDH, 37250-85-4; invertase, 9001-57-4; mutarotase, 9031-76-9; ascorbate oxidase, 9029-44-1; glucose, 50-99-7; sucrose, 57-50-1; fructose, 57-48-7; ascorbate, 50-81-7.

### LITERATURE CITED

- (1) Karube, I.; Suzuki, S. *Ion-Sel. Electrode Rev.* **1984**, *6*, 15-58.
- (2) Lowe, C. R. *Sensors* **1985**, *1*, 3-16.
- (3) Guilbault, G. G.; Lubrano, G. J. *Anal. Chim. Acta* **1973**, *64*, 439-455.
- (4) Tévenot, D. R.; Sternberg, R.; Coulet, P. R.; Laurent J.; Gautheron, D. C. *Anal. Chim. Acta* **1979**, *51*, 96-100.
- (5) Pfeiffer, D.; Scheller, F.; Janchen, M.; Berterman, K.; Weise, H. *Anal. Lett.* **1980**, *13B*, 1179-1200.
- (6) Yao, T.; Kobayashi, Y. *Bunseki Kagaku* **1983**, *32*, 253-258.
- (7) Scheller, F.; Karsten, Ch. *Anal. Chim. Acta* **1983**, *155*, 29-36.
- (8) Masoom, M.; Townshend, A. *Anal. Chim. Acta* **1984**, *166*, 111-118.
- (9) Masoom, M.; Townshend, A. *Anal. Chim. Acta* **1985**, *171*, 185-194.
- (10) Olsson, Bo.; Lundbäck, H.; Johansson, G.; Scheller, F.; Nentwig, J. *Anal. Chim. Acta* **1986**, *58*, 1046-1052.
- (11) Matsumoto, K.; Hamada, O.; Ukeda, H.; Osajima, Y. *Anal. Chim. Acta* **1986**, *58*, 2732-2734.
- (12) Schubert, F.; Kirstein, D.; Scheller, F. *Anal. Lett.* **1986**, *19*, 2155-2167.
- (13) Olsson, Bo.; Lundbäck, H.; Johansson, G. *Anal. Chim. Acta* **1985**, *167*, 123-136.
- (14) Bertrand, C.; Coulet, P. R.; Gautheron, D. C. *Anal. Chim. Acta* **1981**, *126*, 23-34.
- (15) Dahodwala, S. K.; Weibel, M. K.; Humphrey, A. E. *Biotechnol. Bioeng.* **1976**, *18*, 1679-1694.
- (16) Cordonnier, M.; Lawny, F.; Chapot, D.; Thomas, D. *FEBS Lett.* **1975**, *59*, 263-267.
- (17) Satoh, I.; Karube, I.; Suzuki, S. *Biotechnol. Bioeng.* **1976**, *18*, 269-272.
- (18) Kuly, J. J. *Anal. Lett.* **1981**, *14B*, 377-397.
- (19) Macholán, L.; Konečná, H. *Collect. Czech. Chem. Commun.* **1983**, *48*, 798-804.
- (20) Scheller, F.; Renneberg, R. *Anal. Chim. Acta* **1983**, *152*, 265-269.
- (21) Olsson, Bo.; Stålham, B.; Johansson, G. *Anal. Chim. Acta* **1986**, *179*, 203-208.
- (22) Matsumoto, K.; Hamada, O.; Ukeda, H.; Osajima, Y. *Agric. Biol. Chem.* **1985**, *49*, 2131-2135.
- (23) Coulet, P. R.; Bertrand, C. *Anal. Lett.* **1979**, *12B*, 581-587.
- (24) Morishita, F.; Nishikawa, Y.; Kojima, T. *Anal. Sci.* **1986**, *2*, 411-415.
- (25) Morkyavichene, M. V.; Dikchuyevne, A. A.; Paulyukonis, A. B.; Kazlavskas, D. A. *Appl. Biochem. Microbiol.* **1982**, *18*, 557-563.
- (26) Morkyavichene, M. V.; Dikchuyevne, A. A.; Paulyukonis, A. B.; Kazlavskas, D. A. *Appl. Biochem. Microbiol.* **1984**, *20*, 60-63.

RECEIVED for review July 13, 1987. Accepted September 22, 1987.

## Voltammetric Determination of Traces of Nickel(II) with a Medium Exchange Flow System and a Chemically Modified Carbon Paste Electrode Containing Dimethylglyoxime

Karsten N. Thomsen and Lars Kryger\*

Department of Chemistry, Aarhus University, Langelandsgade 140, 8000 Aarhus C, Denmark

Richard P. Baldwin

Department of Chemistry, University of Louisville, Louisville, Kentucky 40292

A chemically modified electrode (CME) for nickel determination was incorporated as part of a computerized flow system with facilities for automatic medium exchange. The CME, which had previously been used in a batch procedure, was based on dimethylglyoxime-containing carbon paste. Nickel(II) was chemically accumulated on the CME and quantitated voltammetrically in a separate medium. The CME surface was regenerated by a brief exposure to dilute  $\text{HNO}_3$ . The tubing of the flow system was permeable to oxygen, but the addition of 2 M  $\text{CaCl}_2$  to all media removed more than 90% of their natural oxygen content. In flow operation the CME was highly stable and showed no signs of fatigue after more than 4 h of continuous operation. The analytical characteristics observed in batch operation were conserved. The flow approach afforded quantitation of nickel in NBS fly ash.

While a number of chemically modified electrodes (CMEs) (1) have proved suitable as sensors in voltammetric determinations of trace metals (2-16), their utility in practical

analysis is largely unexplored. In our laboratories we are currently investigating the potentialities of CME-based procedures in such situations and have recently constructed CMEs with specific chemical reactivity toward nickel(II) (14) and copper(I) (15). In this paper we report on the results obtained by improvements of a crude but promising CME technique for quantitation of nickel(II). As previously described (14), the nickel(II)-sensitive CME was based on a dimethylglyoxime-containing carbon paste and was used in a batch procedure which included first a selective chemical deposition of the analyte from a slightly alkaline solution, then a transfer of the CME to a separate medium followed by a voltammetric quantitation of the  $\text{Ni}(\text{DMG})_2$  (DMG = dimethylglyoxime) deposit, and finally a brief exposure of the CME to dilute nitric acid, which efficiently regenerated its surface. Transfers between the media were carried out manually. But, in spite of the simplicity of the procedure and of CME itself, a few  $\mu\text{g/L}$  of the analyte were readily detected following a 240-s chemical deposition. Most notably the CME approach allowed an accurate quantitation of nickel(II) in test solutions prepared by decomposition of highly composite NBS

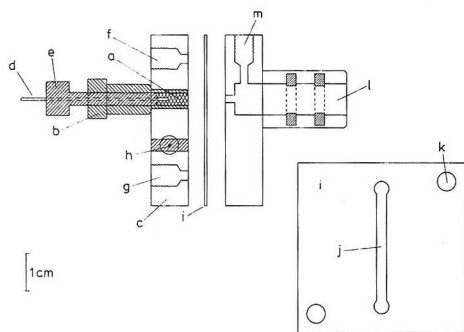


Figure 1. Flow cell.

reference materials (coals, sediments, and fly ash). The stability of the CME, however, was less favorable. A conditioned CME surface would often exhibit a constant collection efficiency for 10 cycles of chemical deposition, voltage scanning, and acid regeneration. Thus standard addition quantitation was possible. However, on continued use the CME clearly suffered from a gradual deterioration, and after 3 h only a minor fraction of its initial efficiency was retained. The present study was prompted by these findings and by the suspicion that the CME degradation could be attributed to the crudity of the manual procedure—in particular its inherent brief CME exposures to atmospheric oxygen and to the potential precipitation of products other than  $\text{Ni}(\text{DMG})_2$ , which might be generated as a result of oxygen reduction. Consequently, in order to take a step further toward its practical applications, the CME was incorporated in a computerized flow analyzer with facilities for automatic medium exchange. This modification afforded an enhanced reproducibility, both of the timing of the procedure and of the chemical and hydrodynamic environment surrounding the CME. Further, the flow system facilitated the testing of the acid regeneration procedure. Most importantly it afforded a closed CME environment, and although its tubing was permeable to oxygen, experiments revealed that calcium chloride added to the media was an efficient agent for oxygen expulsion. In fact, when 2 M of this electrolyte was added to all media, their oxygen content was nearly eliminated and the analytical CME characteristics were equivalent to those observed for batch operation. In addition the CME stability was such that an individual surface retained its performance for more than 4 h of continuous usage.

## EXPERIMENTAL SECTION

**Chemicals, Solutions, and Sample Pretreatment.** Most details have previously been reported (14). The "test" solution was prepared by spiking the ammonia buffer with 1  $\mu\text{M}$  nickel(II) and 1 mM disodium tartrate. The calcium chloride used for solution deoxygenation was of analytical grade.

**Apparatus.** The CME matrices were carbon pastes, which contained 50% (w/w) DMG, coated onto the graphite particles. Five types of paste were studied. The first was analogous to that previously described (14). The four others were prepared in a similar fashion, except that the 3 mL of Nujol oil, originally added to 5 g of modified graphite powder, was replaced by an equal volume of silicone oil. Four types of oil, article 7742, article 12525 (type 3), article 12526 (type 350), and article 9762 (type 550) (Merck) were tested. The flow cell used is shown in Figure 1. The CME paste (a) was kept in a tubular body (b) (3.3 mm i.d.), fabricated from POM (polyacetal) and mounted on the bottom Perspex piece (c) of the flow cell. Electrical contact to the CME was established via a thin platinum wire (d) protruding from the threaded piston (e). For preparation of a fresh CME surface, the electrode holder was dismounted from the flow cell and the piston

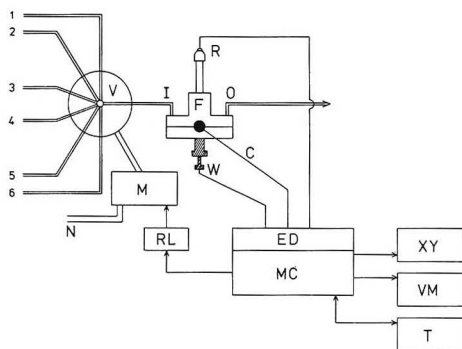


Figure 2. Computerized flow analysis system with medium exchange capability.

lowered about half a notch, such that the old surface could be scraped off. The fresh surface, thus exposed, was subsequently polished on a solid, smooth support until it had a shiny appearance. The bottom piece of the flow cell also accommodated the solution inlet (f), the solution outlet (g), the glassy carbon counter electrode, and its platinum lead (h). The cell was completed by a poly(tetrafluoroethylene) (PTFE) spacer (i)—with a flow channel (j) and holes for dowels (k)—and a Perspex top piece, containing a chamber (l) for the saturated calomel electrode (Radiometer K401) and an inlet (m), through which a flow of saturated potassium chloride could enter the flow cell. This latter facility was useful in establishing a reliable contact between the flow channel and the calomel electrode. The dimensions of the flow channel could easily be adjusted by exchange of spacer. The channel used in this study was 3.5 cm long and 0.4 cm wide. The depth (0.05 cm) allowed for a slight swelling of the CME matrix, which accompanied the electrode-conditioning procedure.

The flow system is shown in Figure 2. The central parts were the flow cell (F), with the inlet (I) and waste outlet (O) ports, and the working (W), reference (R), and counter (C) electrodes. Exchange of samples and media in the flow cell was carried out via a six-way valve (Rheodyne 5111 P) (V) with inlets (1 through 6); there was a distance of 170 mm to the inlet of the flow cell. The valve was activated pneumatically by high-pressure nitrogen (inlet N) and controlled via a magnetic valve (Humphrey, MINI-MYTE 41E1) (M) and a relay (RL). PTFE tubing (0.80 mm i.d., 1.59 mm o.d., Omnit) was used throughout the flow system. Gravitational solution flow was obtained by placing the sample and reagent reservoirs 55 cm above the flow cell.

The computerized electroanalytical device (ED), the microcomputer (MC), and its peripherals—terminal (T), video monitor (VM), and XY recorder (XY)—also displayed in Figure 2 have been described elsewhere (17). The computer program, previously used for voltammetric studies of the CME, was extended with subroutines for control of the six-way valve.

**Flow-Analytical Procedure.** Analytical responses were obtained by a "blank subtraction" approach (14), in which the net analytical signal was taken as the difference between the primary voltammetric response, obtained after chemical deposition of nickel(II), and the blank (background) response recorded with a bare (acid renewed) CME surface. The various phases of the flow analytical procedure, designed for the measurement of these signals, are summarized in Table I, together with details on the various media employed and on the timing of changes in applied potential and valve position. The sample solution (inlet 2) was kept in a reservoir with a volume of 20 or 50 mL. In standard addition experiments, four to five solutions were typically analyzed. These included the unspiked sample solution and solutions obtained by addition of known concentrations of nickel(II) to the sample.

Chemical accumulation was carried out with an applied potential of  $-420$  mV vs. SCE, where neither nickel(II), DMG, nor  $\text{Ni}(\text{DMG})_2$  are electroactive. The voltammetric quantitation step was carried out in such a way that a thin deposit of Ni-

Table I. Summary of the Optimized Analytical Procedure

phase	action performed	inlet no.	solution admitted <sup>a</sup>	potential applied, mV vs. SCE	time used, s	comment
1	flushing of cell	1	blank buffer	-420	30	v <sup>b</sup>
2	recording of background signal	1	blank buffer	sc <sup>c</sup>	25	
3	plot of background signal printout of integral	1	blank buffer	-420	33	
4	chemical deposition	2	sample/buffer	-420	30-240	v
5	idle	3	blank buffer	-420	10	v, wait for complete flushing of cell
6	recording of primary signal	3	blank buffer	sc	25	
7	acid renewal of CME surface	4	0.1 M HNO <sub>3</sub>	-420	10	v
8	flushing of cell	5	water	-420	30	v
9	plot of primary signal printout of integral and of corrected analytical response	5	water	-420	33	
10	idle	6	water	-420	10	v

<sup>a</sup> All solutions contained 2 M calcium chloride. <sup>b</sup> v = phase commences with a change in valve position. <sup>c</sup> sc = potential scan from -420 to -1206 mV.

(DMG)<sub>2</sub>—typically obtained after 60-s deposition from 1  $\mu$ M nickel(II)—was exhaustively reduced to elementary nickel during the reductive scan and such that potentials sufficient to reduce DMG were never experienced. The voltage excitation was carried out under conditions similar to those which had previously been shown to yield the highest possible signal-to-noise ratio without producing any deterioration of selectivity (14). The fundamental excitation waveform used was a cyclic staircase with  $2 \times 128$  steps, each of which lasted for 93 ms and changed the cell potential by 6.14 mV (i.e. the average scan rate was 66 mV/s). The base and switching potentials of the cyclic staircase were -420 and -1206 mV, respectively. Each potential step was succeeded by a pulse, 10.2 mV high and 42 ms long, superimposed on the staircase and applied 1 ms after the step. Cell responses were monitored by a differential pulse approach, in which the response at any particular staircase potential was taken as the difference of two sums—each obtained by addition of 40 samples of the cell current acquired with constant time intervals. One sum was recorded during the final 40 ms of the pulse, the other during the final 40 ms before application of the subsequent potential step. The primary nickel response and the background response were obtained by integration of the cathodic branches of the voltammograms recorded in phases 6 and 2 of the analytical procedure. Integrations were extended from -1000 to -1150 mV. The net analytical signal, used for quantitation of nickel, was computed as the difference between the integrated primary and background responses.

## RESULTS AND DISCUSSION

The suitability of the five carbon pastes was studied by using the batch approach (14) and 60-s depositions from the test solution. All carbon pastes were usable, and the peak currents of the net analytical signals were all of the order of 10  $\mu$ A. However, since the paste containing the most viscous silicone oil (type 550) produced the lowest background current (about 8  $\mu$ A), this particular paste was chosen for the remaining part of the study.

Subsequently the use of calcium chloride for oxygen expulsion in the flow system (18) was investigated. Previous experiments with the batch approach had revealed that the CME exposure to oxygen-containing solutions, in particular during voltage scanning, was fatal for its performance. In the flow approach, since oxygen diffuses readily through PTFE tubing, solution deaeration via conventional flushing with inert gas was not attempted. Initial observations showed that the flow procedure carried out with nondeaerated solutions suffered from problems analogous to those observed in batch analysis where deaeration had intentionally been omitted. On repeated cycling, with 60-s depositions from the test solution, an increase in background current and a decrease in sensitivity—each of about 5%—were typically suffered in each

cycle. These problems, however, were virtually eliminated by the addition of a suitable concentration of calcium chloride to the media. Solutions, saturated with calcium chloride, were too viscous for practical use in the present flow system. But media, 2 M with respect to this electrolyte, afforded a viable compromise between easy-flowing and highly deoxygenated solutions. Its addition to the media caused the gravitational flow rate to decrease from 3.0 to 2.2 mL/min. However, the degree of deoxygenation simultaneously attained was such that the oxygen reduction waves observed in separate batch voltammetric analyses of the media were decreased by 90% or more following the calcium chloride addition. Moreover, when all media contained 2 M calcium chloride, the sensitivity of the flow approach and the background current levels were stable (vide infra).

Clearly, since voltage scanning (Table I, phases 2 and 6) was always carried out with ammonia buffer surrounding the CME surface, deoxygenation of this medium was most important. Indeed, experiments revealed that stable responses could be obtained following a chemical deposition from a nondeoxygenated solution. However, in these cases to avoid instability, it was always necessary to flush the cell extensively with 2 M calcium chloride prior to voltage scanning. The remaining part of the study was carried out with 2 M calcium chloride added to all media. This precaution was taken since acid regeneration or flushing with oxygen-containing media was frequently associated with a gradual revival of the stability problems—presumably due to carry over effects.

Four variations of the acid regeneration procedure (Table I, phase 7) were attempted. These included exposure to 0.1 M nitric acid for 10 and 30 s, respectively, and 10-s exposures to a 1 M solution, of nitric acid and of citric acid, respectively. The four procedures were largely equally efficient in removing the analyte deposit from the CME, such that only a weak bump on the background voltammogram (cf. Figure 3) revealed that the CME had previously been exposed to 60-s depositions from the test solution. The 10-s exposure to 1.0 M nitric acid, however, quickly gave rise to poor reproducibility. Therefore one of the mildest cleaning procedures, 10 s in 0.1 M nitric acid, was chosen for the remaining experiments.

Under the experimental conditions thus established (Table I), a procedure including six cycles with 60-s depositions from the test solution was normally sufficient for conditioning a freshly polished CME surface such that it responded linearly to significant variations in analyte concentration and in deposition time and such that its memory of previous cycles was nearly eliminated. An example of the effects of variations in

Table II. Linear Range of the CME Flow System

CME surface no.	$n_{\text{obsd}}^a$	chemical deposition times, s	$\mu\text{M Ni(II)}$ added before breakpoint <sup>b</sup>	sensitivity: signal (arbitrary units) per $\mu\text{M Ni(II)}$ <sup>c</sup>	corr coeff	estd blank Ni(II) concn $\mu\text{M}$
1	15	60	8.0	1753 (42)	0.996	0.66
2	23	120	2.0	3644 (62)	0.997	0.22
3	29	120	2.5	3161 (92)	0.989	0.19

<sup>a</sup> Number of independent measurements, used in linear regression analysis. <sup>b</sup> The data, pertinent to the number quoted, were included in the regression analysis. <sup>c</sup> The uncertainty, quoted in parentheses, is the standard deviation of the sensitivity, as estimated by linear regression ( $n_{\text{obsd}}$  measurements) of the signal vs. concentration data.

Table III. Analysis of NBS Reference Material 1633a (Coal Fly Ash)

expt no.	quantitation approach	chemical deposition time, s	sensitivity <sup>a</sup>	corr coeff	concn found, <sup>b</sup> $\mu\text{M}$	blank, $\mu\text{M}$	blank corrected result, <sup>c</sup> $\mu\text{M}$
1	calibration	90	1669 (27)	0.998	1.18 (0.03)	0.22 (0.07)	$0.96 \pm 0.15$
2	calibration	90	2376 (34)	0.998	1.13 (0.03)	0.07 (0.06)	$1.06 \pm 0.14$
3	standard addition	60	1024 (20)	0.998	0.90 (0.07)	0.07 (0.06)	$0.83 \pm 0.19$
4	standard addition	60	1534 (33)	0.997	1.31 (0.12)	0.07 (0.06)	$1.24 \pm 0.28$
5	standard addition	60 (30, 20)	1869 (44) <sup>d</sup>	0.996	1.47 (0.14)	0.07 (0.06)	$1.40 \pm 0.32$
quantitation approach		av results $\mu\text{g}$ of Ni/g of ash			certified content $\mu\text{g}$ of Ni/g of ash		
calibration		148			127 $\pm$ 4		
standard addition		168			127 $\pm$ 4		

<sup>a</sup> Signal in arbitrary units per micromol nickel(II). The standard deviations, quoted in parentheses, pertain to the slopes of the regression lines. <sup>b</sup> Formulae, given by Davies and Goldsmith (19) were used for computation of the standard deviations, quoted in parentheses. <sup>c</sup> Uncertainties stated as 95% confidence limits. <sup>d</sup> Sensitivities normalized to 60-s chemical deposition.

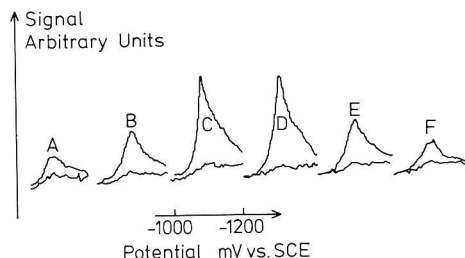


Figure 3. Variation in the responses of a conditioned CME, resulting from variation in chemical deposition time: deposition from 1  $\mu\text{M}$  nickel(II) for (A) 60, (B) 120, (C) 240, (D) 240, (E) 120, and (F) 60 s; upper traces, primary nickel responses; lower traces, background responses.

deposition time is given in Figure 3, which shows the primary and background signals recorded in six consecutive cycles where chemical deposition at a conditioned CME was carried out from the test solution for (A) 60, (B) 120, (C) 240, (D) 240, (E) 120, and (F) 60 s.

In many respects the CME behavior in the flow system compared well with that reported for batch operation (14). For instance nine consecutive cycles with 30-s depositions from the test solution resulted in analytical responses (40 samples average) with a mean of 4.82  $\mu\text{A}$  and a standard deviation of 0.60  $\mu\text{A}$ , thus indicating that submicromolar concentrations of the analyte could be detected. Because of the extensive use of calcium chloride in the present study, all solutions contained a blank concentration of the analyte, which was never below the 0.10  $\mu\text{M}$  level. Thus the CME performance near the detection limit for the batch approach (0.05  $\mu\text{M}$  following a 240 s deposition) was not investigated.

The linearity of the approach was studied via three standard addition experiments with three different CME surfaces. Chemical depositions were carried out from an ammonia

buffer, which was gradually spiked with nickel(II) such that its concentration increased in steps of 0.5 or 1.0  $\mu\text{M}$ . All experiments were continued until the signal vs. concentration plot became markedly curved as a result of CME saturation. This situation always occurred abruptly with a visually obvious negative deviation from linear behavior resulting from a single 0.5  $\mu\text{M}$  addition of the nickel(II) standard. The results (Table II) obtained with CME with surfaces 2 and 3 reflect the surface to surface variability of about 20% (14) in the CME sensitivity. Further, a comparison of these results with that for surface 1 reveals that the linear range, as expected, was longer for shorter deposition times. Clearly the linear range of the present approach was modest as compared to that observed with many electrochemical techniques—amalgam voltammetry of cadmium and lead, for instance. But the computerized instrumentation facilitated the reproduction of short deposition times such that sensitivity could be fine tuned to each particular CME surface and sample. Furthermore, since the CME approach was highly selective toward nickel(II) (14), it appeared that a direct calibration against nickel(II) standard solutions would be a legal route to quantification in a variety of applications thus rendering the linearity requirement superfluous. The suitability of these approaches was further elucidated in the study of the decomposed fly ash (Table III), in which five different CME surfaces were used, and quantitation was done both by standard addition and by direct calibration. Initially a chemical deposition time of 60 s was used in all standard addition experiments (3, 4, and 5), and additions, each corresponding to a 1  $\mu\text{M}$  increase in analyte concentration, were continued until the net analytical signal was about 3 times its initial value. In experiments 3 and 4 this situation was encountered after three additions. However, the CME surface exposed in experiment 5 was extraordinarily efficient, such that CME saturation was observed after two additions. Consequently, the experiment was repeated with 30- and 20-s depositions for the two highest analyte concentrations. Subsequently the analytical signals were normalized to 60-s deposition time by assuming strict linearity. The

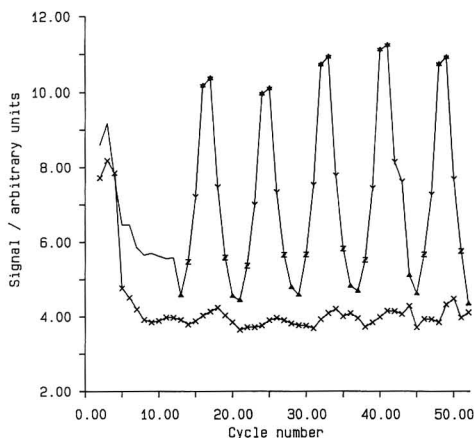


Figure 4. Long-term behavior of the CME, chemical deposition from 1  $\mu$ M nickel(II) for 30 (▲), 60 (Z), 120 (Y), and 240 s (\*). Background response indicated by X.

validity of this approach was supported by the high value of the correlation coefficient obtained. In general the observations made in the fly ash study were analogous to those previously reported with no evidence that species other than nickel(II) were collected by the CME. The dispersion of results, in particular those obtained with standard addition, was relatively large. However, part of the uncertainty could be attributed to random variations of the blank level of nickel. More importantly, the results obtained by direct calibration (experiments 1 and 2) were consistent with both the certified concentrations and those obtained by standard addition. Since the NBS fly ash is highly composite material, this latter observation was taken as additional evidence of the CME selectivity previously claimed (14).

Although the CME behavior, previously reported (14), was largely confirmed in the present investigation, the long-term stability of the CME matrix was significantly improved by introduction of the flow system instead of the beaker/stir-bar procedure. When used in the batch approach, the CME would mostly retain some ability to accumulate nickel(II) for more than 3 h. However, during this period a significant deterioration in deposition efficiency was always suffered. In the present flow system, once oxygen had been expelled, a single conditioned CME surface could always be used for hours with no signs of fatigue. Figure 4 illustrates the long-term behavior of the primary and background signals observed for a single CME surface over several analytical cycles with chemical depositions from the test solution. In order to demonstrate the instability observed with oxygen-rich solutions, the cycling (60-s depositions) was first carried out with media that did

not contain calcium chloride. Following cycle 2, 2 M calcium chloride was added to all media and when the CME had been conditioned—as reflected by a stable background (cycle 13)—cycling was continued with a deposition time which was first increased (30, 60, 120, and 240 s) and then decreased in reversed order. This sequence was repeated until, after 50 cycles, the supply of sample in reservoir 2 was exhausted. The background trace revealed that the CME “memorized” about 10% of the thickest deposit generated during 240-s depositions but also that this memory faded away after a few additional cycles with shorter depositions. Most important, once conditioned, the CME maintained its full accumulation efficiency for more than 4 h of constant usage. Furthermore, since the relative standard deviation of the net analytical signals obtained with the 60-, 120-, and 240-s depositions, respectively (9, 11, and 10 measurements), were all 6–7%, the analytical procedure clearly retained its ability to discriminate between the various amounts of NiA<sub>2</sub> deposit generated as a result of variations in deposition time.

#### ACKNOWLEDGMENT

The authors are grateful to Palle Christensen for his construction of the flow cell and to Joan Kai Christensen for her skilled assistance with CME preparation.

#### LITERATURE CITED

- (1) Murray, R. W. In *Electroanalytical Chemistry*; Bard, A. J., Ed.; Marcel Dekker: New York, 1984; Vol. 13, pp 191–368.
- (2) Cheek, G. T.; Nelson, R. F. *Anal. Lett.* **1978**, *11*, 393–402.
- (3) Cox, J. A.; Majda, M. *Anal. Chem.* **1980**, *52*, 861–864.
- (4) Price, J. F.; Baldwin, R. P. *Anal. Chem.* **1980**, *52*, 1940–1944.
- (5) Lubert, K.-H.; Schnurrbusch, M.; Thomas, A. *Anal. Chim. Acta* **1982**, *144*, 123–136.
- (6) Izutsu, K.; Nakamura, T.; Takizawa, R.; Hanawa, H. *Anal. Chim. Acta* **1983**, *149*, 147–155.
- (7) Cox, J. A.; Kulesza, P. J. *Anal. Chim. Acta* **1983**, *154*, 71–78.
- (8) Wang, J.; Greene, B.; Morgan, C. *Anal. Chim. Acta* **1984**, *158*, 15–22.
- (9) Guadalupe, A. R.; Abruna, H. D. *Anal. Chem.* **1985**, *57*, 142–149.
- (10) Wier, L. M.; Guadalupe, A. R.; Abruna, H. D. *Anal. Chem.* **1985**, *57*, 2009–2011.
- (11) Kalcher, K. *Anal. Chim. Acta* **1985**, *177*, 175–182.
- (12) O'Riordan, D. M. T.; Wallace, G. G. *Anal. Chem.* **1986**, *58*, 128–131.
- (13) Gehron, M. J.; Brajter-Toth, A. *Anal. Chem.* **1986**, *58*, 1488–1492.
- (14) Baldwin, R. P.; Christensen, J. K.; Kryger, L. *Anal. Chem.* **1986**, *58*, 1790–1798.
- (15) Prabhu, S. V.; Baldwin, R. P.; Kryger, L. *Anal. Chem.* **1987**, *59*, 1074–1078.
- (16) Whiteley, L. D.; Martin, C. R. *Anal. Chem.* **1987**, *59*, 1746–1751.
- (17) Skov, H. J.; Kryger, L. *Anal. Chim. Acta* **1980**, *122*, 1979–191.
- (18) Anderson, L.; Jagner, D.; Josefson, M. *Anal. Chem.* **1982**, *54*, 1371–1376.
- (19) *Statistical Methods in Research and Production*; Davies, O. L.; Goldsmith, P. L., Eds.; Longman (Harlow): Essex, U.K., 1976; Chapter 7.

RECEIVED for review February 24, 1987. Resubmitted June 29, 1987. Accepted September 24, 1987. Our work is currently supported by NATO Scientific Affairs Division (Grant 85/0679 for international collaboration), by the Danish Technical Research Council (Grant 16-4069.K, Research Fellowship (K.N.T.)), and by the Danish Natural Science Research Council (Grant 511-8033 for the computerized electroanalytical device).

# Spectroelectrochemical Response and Optical Geometry Optimization of Thin-Layer Flow Detectors with Long Optical Path Lengths: Theory

Lawrence E. Fosdick<sup>1</sup> and James L. Anderson\*

Department of Chemistry, The University of Georgia, Athens, Georgia 30602

Steady-state current and absorbance are characterized for a thin-layer spectroelectrochemical flow detector with the working electrode on one wall, using complementary Nernst diffusion-layer-approximation and finite difference simulation models. Both models rigorously treat the important effects on the measured absorbance of the electrochemically induced sample inhomogeneity across the optical beam, requiring calculation of absorbance by integrating local transmittances rather than absorbances over the appropriate distance coordinates, except for weakly absorbing samples. Predicted flow rate exponents of current and absorbance are approximately equal and of opposite sign:  $+1/3$  for current and  $-1/3$  for absorbance under fully developed laminar flow or  $+1/2$  for current and  $-1/2$  for absorbance under developing laminar flow. Optimum optical path geometries are predicted, having long optical paths parallel to the electrode surface and either perpendicular or parallel to flow and illuminating the entire electrode length if shot noise is dominant.

Detector selectivity is an important problem for determination of trace species in complex mixtures using flow techniques such as high-performance liquid chromatography (HPLC) or flow injection analysis (FIA). Liquid chromatographic identification and quantitation using a single detector of specific trace species in complex matrices may be subject to interferences by other species which have the same chromatographic retention characteristics and similar detector response. Correlation of two independent detector signals, such as electrochemical current and optical absorbance (spectroelectrochemistry) can be used to improve selectivity by ensuring that a sample component is recognized only when both detection signals yield appropriate responses simultaneously (1).

Previous spectroelectrochemical cell (SEC) designs include thin-layer cells with illumination perpendicular to optically transparent electrodes (2-4), planar thin-layer cells with illumination parallel to the electrode and coupled to a spectrometer beam either indirectly by fiber optics (5, 6) or directly (7), a cell with the optical path inside a narrow hole drilled through a carbon electrode (8), and planar bulk cells, with illumination from a continuum source (9, 10) or a laser (11, 12) passed through a thin layer parallel to the electrode surface. These designs are for static solutions, whose spectroelectrochemical responses are described by semiinfinite (9-12), thin-layer planar (2-7), or concentric cylindrical (8) diffusion. A thin-layer spectroelectrochemical flow detector reported by Heineman and co-workers used a minigridded optically transparent electrode (13). Recently, an electrochemical detector for HPLC and FIA was reported that used photoexcitation to enhance sensitivity (14).

This paper characterizes the steady-state flow-rate dependence of absorbance of a species either generated or consumed

at an electrode on one wall of a thin-layer flow channel, under a wide range of conditions. The feasibility and properties of a correlation detector based on coupled amperometric and absorbance measurements are also considered for this geometry. Earlier work has treated the response of a static thin-layer SEC under equilibrium conditions (5). A cell of the general configuration described here with fiber-optic coupling to a spectrometer is the subject of a patent (6). Experimental verification of the theory for a flow cell with a long optical path is presented in a separate paper (15), which demonstrates the utility of the approach in assessing the physics of flow in practical cells.

## THEORY

**Optical Geometry.** The absorbance response of a thin-layer spectroelectrochemical flow cell (SEFC) depends on the absorbance characteristics of the electrochemical reactant and product, the solution velocity and nature of flow hydrodynamics, and the optical geometry. In the simplest case, for identical reactant and product molar absorptivities, the flow cell is essentially optically homogeneous, and the absorbance can be calculated from Beer's law after subtracting the blank absorbance in absence of sample.

If only the reactant or product of the electrochemical reaction absorbs appreciably, the spatially heterogeneous distribution of absorber within the electrochemical diffusion layer and relative to the optical beam complicates the calculation of absorbance. Absorbance response of the detector will clearly be largest if the electroactive substance absorbs strongly, or much smaller if only the electrode reaction product absorbs while confined to the diffusion layer, traversed by only a portion of the optical beam. However, the latter case does enable the generation of an optical response when one was not initially present.

A rectangular thin-layer SEFC is depicted schematically in Figure 1. The working electrode lies in the  $xy$  plane, serving as one wall of the cell, flow is along the  $x$  axis, and the narrowest dimension is on the  $z$  axis. The light path may have one of three possible geometries, corresponding to incident radiation along the  $z$ ,  $y$ , and  $x$  axes, respectively. The following conventions are used, distinguishing *localized* from *overall* absorbance. Localized absorbance (e.g.  $A(y)_{z,x}$  or  $A(y)_{j,k}$ ) and transmittance (e.g.  $T(y)_{z,x}$  or  $T(y)_{j,k}$ ) refer to a small region of the cell and are denoted by the optical beam axis (in parentheses) and the directions perpendicular to the beam in subscripts. For finite difference calculations, integers  $j$  and  $k$  indicate specific grid coordinates ( $z_j, x_k$ ) on the  $z$  axis (divided into  $J$  increments) and the  $x$  axis (divided into  $K$  increments), respectively. Overall absorbance and transmittance (e.g.  $A_{||,\perp}$  and  $T_{||,\perp}$ ) are denoted by subscripts indicating the orientation of the beam relative to the plane of the working electrode (parallel [ $||$ ] or perpendicular [ $\perp$ ]) and the direction of flow ( $||$  or  $\perp$ ).

In the geometry ( $\perp, \perp$ ), the incident light passes through the cell on the  $z$  axis, perpendicular to both the working electrode surface and the direction of flow, similar to the geometry reported by Heineman and co-workers (13). The

<sup>1</sup>Current address: Hercules Incorporated, Research Center, Wilmington, DE 19894.



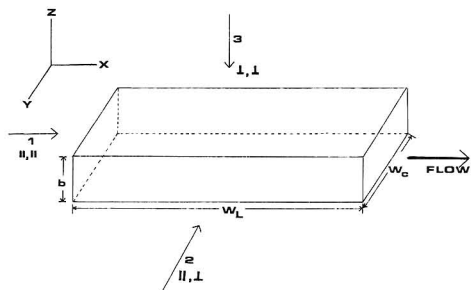


Figure 1. Schematic representation of rectangular flow channel detector and optical beam axes (1-3). Bottom plane of cell is the working electrode.

spectrometric sensitivity of this geometry is low, because of the very short optical path length. This geometry requires an optically transparent or reflective working electrode and reflective or transparent opposite wall.

In the geometry ( $\parallel, \perp$ ), the incident radiation passes along the  $y$  axis, parallel to the electrode surface and perpendicular to flow. This geometry requires transparent cell side walls but provides a much longer optical path length, since the cell width is significantly (often more than 20-fold) greater than the cell height. In the cell geometry ( $\parallel, \parallel$ ), the incident light passes through the cell on the  $x$  axis, parallel to both flow and the electrode surface. This geometry requires optically transparent end windows on the cell and also provides a longer path length than the ( $\perp, \perp$ ) geometry. It differs from the ( $\parallel, \perp$ ) geometry in that the working electrode width is equal to the cell width, but the electrode length may be less than the cell length to allow laminar flow to develop.

**Boundary Value Problem.** The spatial heterogeneity of concentration within the cell requires calculation of concentrations of the reactant and product species everywhere in the cell. For continuous flow of a sample stream through the detector at steady state, the concentration,  $C_i$  ( $i = R$  or  $P$ ), of either the reactant  $R$  or the product  $P$  can be calculated from the solution of one or more convective diffusion equations, of the general form

$$D_i \frac{\partial^2 C_i}{\partial z^2} - V_x(z) \frac{\partial C_i}{\partial x} = 0 \quad (1)$$

where  $D_i$  is the diffusion coefficient. Two cases will be treated: fully developed and developing laminar flow. For the former case, which will be assumed unless explicitly stated otherwise, the velocity of flow along the  $x$  axis,  $V_x(z)$  is represented by

$$V_x(z) = [6U/(bW_c)](z/b)(1 - z/b) \quad (2)$$

Here,  $U$  is the average volume flow rate,  $b$  is the channel height,  $W_c$  is the channel width, and  $z$  is the height in the channel at which the velocity is calculated. The boundary conditions for monitoring both the reactant and product species are

$$\begin{aligned} x = 0, 0 \leq z \leq b: & \quad C_R = C_R^*, C_P = 0 \\ x > 0, z = 0: & \quad C_R = 0, D_R \frac{\partial C_R}{\partial z} = -D_P \frac{\partial C_P}{\partial z} \\ x > 0, z = b: & \quad \frac{\partial C_R}{\partial z} = 0, \frac{\partial C_P}{\partial z} = 0 \end{aligned}$$

where  $C_R^*$  is the initial bulk concentration of the reactant. Two complementary approaches will be developed and compared: a Nernst diffusion layer approximation and a backward implicit finite difference (BIFD) numerical simulation.

**Nernst Diffusion Layer Model.** The absorbance of the cell can be approximated by using a simple Nernst diffusion-layer model, in which reactant and product concentrations

vary linearly with distance between the electrode and a small multiple  $m$  ( $\geq 1$ ) of the diffusion-layer thickness  $\delta_x$  at any position  $x$  along the channel. The multiplier  $m$  ( $m = 1.1779$ , as shown below) is greater than one to compensate for the effect of the finite concentration variation beyond the nominal diffusion-layer thickness.

**Fully Developed Laminar Flow.** For fully developed laminar flow

$$\delta_{x,f} = b\bar{\delta}_x = b \left[ \frac{D_i x W_c}{U b (0.9355 - 0.6018 \bar{\delta}_x)} \right]^{1/3} \approx f(x/U)^{1/3} \quad (3a)$$

where  $\bar{\delta}_x$  is the fraction of the channel height occupied by the diffusion layer,  $D_i$  is the appropriate diffusion coefficient for either reactant or product, and  $f$  is a composite of the other terms, neglecting the  $\bar{\delta}_x$  term in the denominator of the complete expression. This expression is valid where  $[W_c W_c D_i / (U b)] < 0.3337$  (16). For cell dimensions used in this study, where  $W_c = 0.5$  cm,  $W_c = 0.3$  cm, and  $b = 0.0127$  cm, and assuming  $D_i = 7.0 \times 10^{-6}$  cm<sup>2</sup>/s, eq 3a is valid for flow rates above 0.015 mL/min. Equation 3a should be solved iteratively by successive approximations except when the diffusion layer is sufficiently thin.

**Developing Laminar Flow.** The analogous expression for developing laminar flow (where viscous drag is still developing), is given (17) by

$$\delta_{x,d} = b\bar{\delta}_x \approx 2.94 D_i^{1/3} \nu^{1/6} (b W_c x / U)^{1/2} = d(x/U)^{1/2} \quad (3b)$$

where  $\nu$  is the solution kinematic viscosity (cm<sup>2</sup>/s) and  $d$  is a composite term.

**Inviscid Flow.** If flow velocity is assumed invariant across the channel, it can be shown that

$$\delta_{x,iv} = b\bar{\delta}_{x,iv} = [\pi D b W_c x / U]^{1/2} = q(x/U)^{1/2} \quad (3c)$$

where  $q$  is a composite term. The functional dependence of  $\delta_{x,iv}$  on electrode length and flow rate is the same as for developing flow, except that  $q \neq d$ .

At the trailing edge of the electrode, where  $x = W_c$ , the diffusion layer thickness,  $\delta_{W_c}$ , can be represented by  $b\bar{\delta}_{L}$ , where  $\bar{\delta}_L$  is the fraction of the channel height occupied by the diffusion layer at that position.

**Absorbance Calculation.** Since the solution composition is spatially inhomogeneous perpendicular to the optical beam, varying with both  $x$  and  $z$ , the cell absorbance, obtained from the logarithm of the ratio of total transmitted to total incident intensities (transmittance), must be determined by integrating local transmittances (not absorbances!) across the beam. For convenience, the beam intensity is assumed to be uniform and perfectly collimated at all positions across the beam. In contrast, when concentration is homogeneous perpendicular to the beam cross section, but inhomogeneous parallel to the beam path, the absorbances can be integrated. Porter and Kuwana found that integration of absorbance or intensity yielded comparable results under their conditions in SEC's consisting of a hole drilled through glassy carbon for small hole diameters (8). In the present case, integration of local absorbances rather than transmittances across the beam cross section is an acceptable approximation only if absorbance is everywhere less than ca. 0.1, since transmittance varies exponentially with concentration (9, 18).

The approach will be applied for one case, ( $\parallel, \perp$ ), yielding an approximation of absorbance from the relation

$$A_{\parallel, \perp} = -\log \left\{ \frac{1}{b(x_2 - x_1)} \int_{x_1}^{x_2} \left[ \int_0^{m\delta_x} T(y)_{z,x} dz + \int_{m\delta_x}^b T(y)_{z,x} dz \right] dx \right\} \quad (4)$$

where

$$T(y)_{z,x} = 10^{-A(y)_{z,x}} = e^{-A(y)_{z,x} \ln 10} \quad (5)$$

Here,  $A(y)_{z,x}$  is the average absorbance in any volume element  $W_c dx dz$  in the cell, and  $x_1$  and  $x_2$  represent the leading and trailing edges of the region over which the absorbance is measured (e.g.,  $x_1 = 0$  and  $x_2 = W_L$  if absorbance is measured over the entire electrode length). If both reactant R and product P can absorb

$$A(y)_{z,x} = \epsilon_R W_c C_R(z,x) + \epsilon_P W_c C_P(z,x) \quad (6)$$

where  $\epsilon_i$  and  $C_i$  are, respectively, the molar absorptivity ( $M^{-1} \text{ cm}^{-1}$ ) and the concentration (M) of species  $i$  ( $i = R$  or  $P$ ).

Substituting eq 5 and 6 into eq 4, assuming equal diffusion coefficients for reactant and product, and linear concentration gradients, we obtain for total absorbance the expression

$$A_{||,L} = -\log \left\{ \frac{1}{b(x_2 - x_1)} \int_{x_1}^{x_2} \left[ \int_0^{m\delta_L} e^{-(\epsilon_P[1-z/(m\delta_L)] + \epsilon_R z/(m\delta_L)) W_c C_R^* \ln 10} dz + \int_{m\delta_L}^b e^{-\epsilon_R W_c C_R^* \ln 10} dz \right] dx \right\} \quad (7)$$

Equation 7 is perfectly general, independent of the flow physics model used for the diffusion layer. Further development depends on the diffusion layer model selected.

**Fully Developed Laminar Flow.** Substitution of eq 3a (neglecting the  $\delta x$  term in the denominator) into eq 7, followed by integration, yields the general expression

$$A_{||,L} = -\log \left[ e^{-\epsilon_R W_c C_R^* \ln 10} + \frac{3m(x_2\delta_{x2} - x_1\delta_{x1})}{4b(x_2 - x_1)} \left( \frac{e^{-\epsilon_P W_c C_R^* \ln 10} - e^{-\epsilon_R W_c C_R^* \ln 10}}{(\epsilon_R - \epsilon_P) W_c C_R^* \ln 10} - e^{-\epsilon_R W_c C_R^* \ln 10} \right) \right] \quad (8)$$

Product and reactant absorbances or their sum predicted by eq 8 clearly exhibit complex dependence on reactant concentration. The limiting behavior when only product absorbs, with low maximum local product absorbance  $A(P)_{\max} = \epsilon_P W_c C_R^*$  is

$$\lim_{A(P)_{\max} \rightarrow 0} A_{P||,L} = \left[ \frac{3m(x_2\delta_{x2} - x_1\delta_{x1})}{8b(x_2 - x_1)} \right] \epsilon_P W_c C_R^* \quad (9)$$

which reduces when  $x_2 = W_L$  and  $x_1 = 0$  to the expression

$$\lim_{A(P)_{\max} \rightarrow 0} A_{P||,L} = [3m\delta_L/8] \epsilon_P W_c C_R^* = 0.452 \epsilon_P W_c C_R^* [D_P W_L W_c / (bU)]^{1/3} \quad (9a)$$

Equations 9 and 9a, which show a linear dependence of absorbance on reactant concentration, agree with the results of integration of absorbance rather than transmittance, as expected, for low maximum local absorbance.

The limiting behavior for product with high local absorbance is

$$\lim_{A(P)_{\max} \rightarrow \infty} A_{P||,L} = -\log \left[ 1 - \frac{3m(x_2\delta_{x2} - x_1\delta_{x1})}{8b(x_2 - x_1)} \right] \quad (10)$$

which reduces when  $x_2 = W_L$  and  $x_1 = 0$ , to the expression

$$\lim_{A(P)_{\max} \rightarrow \infty} A_{P||,L} = -\log [1 - 3m\delta_L/4] = -\log [1 - 0.903[D_P W_L W_c / (bU)]^{1/3}] \quad (10a)$$

Equations 10 and 10a exhibit saturation. Absorbance as-

ymptotically approaches a limit independent of concentration and dependent only on the thickness of the diffusion layer relative to cell thickness, arising from the effect of unabsorbed light not passing through the diffusion layer.

The limiting behavior for reactant with low maximum local absorbance  $A(R)_{\max} = \epsilon_R W_c C_R^*$  is

$$\lim_{A(R)_{\max} \rightarrow 0} A_{R||,L} = \epsilon_R W_c C_R^* \left[ 1 - \frac{3m(x_2\delta_{x2} - x_1\delta_{x1})}{8b(x_2 - x_1)} \right] \quad (11)$$

which reduces when  $x_2 = W_L$  and  $x_1 = 0$ , to the expression

$$\lim_{A(R)_{\max} \rightarrow 0} A_{R||,L} = \epsilon_R W_c C_R^* [1 - 3m\delta_L/8] = \epsilon_R W_c C_R^* [1 - 0.452[D_P W_L W_c / (bU)]^{1/3}] \quad (11a)$$

Equations 11 and 11a agree with the results of integration of absorbance rather than transmittance, as expected, for low maximum local absorbance.

The limiting behavior for reactant, with high local maximum absorbance, is

$$\lim_{A(R)_{\max} \rightarrow \infty} A_{R||,L} = \log \left[ \frac{4b(x_2 - x_1) \epsilon_R W_c C_R^* \ln 10}{3m(x_2\delta_{x2} - x_1\delta_{x1})} \right] \quad (12)$$

which reduces when  $x_2 = W_L$  and  $x_1 = 0$  to the expression

$$\lim_{A(R)_{\max} \rightarrow \infty} A_{R||,L} = \log [4b \epsilon_R W_c C_R^* \ln 10 / (3m\delta_L)] = \log \{5.77b \epsilon_R W_c C_R^* [D_P W_L W_c / (bU)]^{-1/3}\} \quad (12a)$$

Equations 12 and 12a show that absorbance shifts from linear to logarithmic dependence on reactant concentration at high maximum local absorbance and becomes inversely proportional to the ratio of diffusion layer thickness to channel height. Absorbance should thus be proportional to the bulk concentration of the reactant at low concentrations, with a coefficient that increases for product and decreases for reactant as diffusion layer thickness increases. The coefficient eventually decreases with increasing reactant concentration for both. For typical values of  $m\delta_L$  less than 0.3, product absorbance will be less than 10% of that expected if reactant were coulometrically converted to product. Conversely, reactant absorbance will be decreased by less than 10% from the value expected in absence of an electrochemical reaction for low concentrations, with increasingly negative deviations at high concentrations as local absorbance increases.

The sum of reactant and product absorbances predicted by eq 8–12a can be used in conjunction with the semiempirical expression for the current response of a solid electrode in a rectangular flow channel reported by Weber and Purdy (16), namely

$$i = nFUC_R^* \delta_{Lr}^2 [1.4032 - 0.8024\delta_{Lr}] \quad (13)$$

to provide a complete set of equations to calculate the electrochemical and spectrometric response of the detector. An iterative solution of eq 3a yields the value of  $\delta_L$  for these equations. Both current and absorbance depend on the magnitude of  $\delta_L$ . Thus, eq 13 predicts a limiting cube root dependence on flow rate for current response, and eq 9a–12a predict a limiting inverse cube root dependence on flow rate for absorbance at high flow rates. As with transient time-dependent experiments, absorbance and current are complementary. Their product is, to a first approximation, independent of flow rate.

**Developing Laminar Flow.** Substituting eq 3b into eq 7 and integrating as before, the expression obtained is identical in form with eq 8, except that the coefficient of the second term inside the logarithmic expression is  $2/3$  rather than  $3/4$ , and the functional dependence of  $\delta_L$  on flow rate and other

parameters differs, as seen by comparing eq 3a and 3b. The limiting cases for low absorbance when the optical beam illuminates the entire length of the electrode are respectively

$$\lim_{A(P)_{\max} \rightarrow 0} A_{P||, \perp} = [m\epsilon_P C^* R W_c / (3b)] d(W_L / U)^{1/2} \\ = 0.980 m \epsilon_P C^* R D^{1/3} \nu^{1/6} [W_c^3 W_L / (bU)]^{1/2} \quad (14)$$

and

$$\lim_{A(R)_{\max} \rightarrow 0} A_{R||, \perp} = \epsilon_R C^* R W_c [1 - [m / (3b)] d(W_L / U)^{1/2}] \\ = \epsilon_R C^* R W_c [1 - 0.980 m D^{1/3} \nu^{1/6} [W_c W_L / (bU)]^{1/2}] \quad (15)$$

Unlike fully developed laminar flow, the equations for developing flow reduce to a limiting dependence of absorbance on the inverse square root of flow rate. The value of  $m$  is not as certain as for fully developed laminar flow but may be assumed to be in the range 1.03–1.27, by comparing approximate solutions to known solutions for fully developed laminar flow and stationary diffusion. Electrochemical current for these cases is given by the expression (17)

$$i = 0.68 n F C^* R D^{2/3} \nu^{-1/6} (W_c W_L / b)^{1/2} U^{1/2} \quad (16)$$

**Inviscid Flow.** Functional dependences of absorbance and current on flow rate and channel dimensions are similar to developing flow behavior, except for multiplicative constants. Limiting product absorbance is given by

$$\lim_{A(P)_{\max} \rightarrow 0} A_{P||, \perp} = [m\epsilon_P C^* R / 3] [\pi D W_c^3 W_L / (Ub)]^{1/2} \quad (17)$$

while current is given by

$$i = 2nFC^* R [DW_c W_L U / (\pi b)]^{1/2} \quad (18)$$

**Backward Implicit Finite Difference (BIFD) Model.** The BIFD approach (19) was used both to assess the validity of the Nernst diffusion layer approximation and to model factors influencing signal/noise ratios for several beam geometries. This technique calculates reactant and product concentrations in each three-dimensional rectangular element of a grid with width  $W_c$  on the  $y$  axis, dividing the flow cell in the  $xz$  plane, as seen in Figure 1. The approach has been validated for calculation of current in rectangular flow channels by comparison to existing semiempirical theory for solid electrodes (eq 13) (16) and by comparison to experimental results for solid electrodes and arrays of microelectrodes of varying geometries (20, 21). However, the absorbance calculation depends on concentrations throughout the cell, while the current depends only on concentrations in the immediate vicinity of the working electrode. Errors arising from concentration variation within grid elements can be minimized by employing a high vertical resolution in the BIFD simulation. Figure 2 shows the effect of vertical resolution on absorbance calculations.

The calculated absorbance decreases as vertical resolution increases, reaching a constant value when adequate resolution is achieved. At least 2000 vertical increments are required to calculate absorbance (to an accuracy of at least 0.01%) under the conditions examined if the grid extends across the entire channel height, whereas theoretical and experimental studies have found 200 vertical increments sufficient for calculating current (19–21). When insufficient vertical resolution is used, plots of log absorbance vs log flow rate become nonlinear at high flow rates, primarily because of an inadequate number of grid elements within the diffusion layer, which becomes thinner as flow rate increases.

Spatial resolution parallel to flow is much less critical. For both current (19–21) and absorbance calculations, 50 incre-

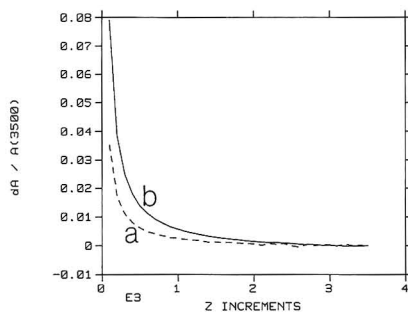


**Figure 2.** Effect of vertical resolution in BIFD simulations for absorbance calculations, cell length = 0.3 cm, width = 0.3 cm, height = 0.0127 cm for Figures 2–7: (a) dotted curve, 0.5 mL/min; (b) solid curve, 5.0 mL/min. "E3" on horizontal axis denotes multiplication by  $10^3$ .

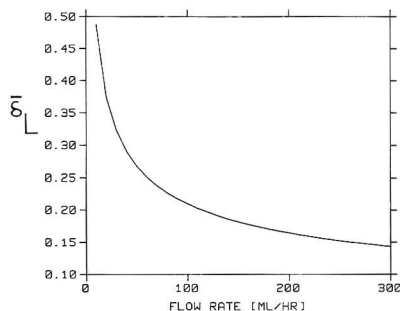


**Figure 3.** Fraction of flow channel occupied by diffusion layer vs flow rate (eq 3a).

ments along the  $x$  axis are sufficient. Differences of less than 0.01% in calculated absorbance were noted when the number of  $x$  axis increments was doubled to 100.

The diffusion layer is typically very thin, seldom extending more than 30% of the cell height from the electrode surface, depending on flow rate as shown in Figure 3. Outside the diffusion layer, the concentration of the reactant is essentially unchanged, while the concentration of the product approaches zero.

Maximization of the vertical resolution and retention of the calculated concentrations of both species within each grid element across the entire channel require a large amount of computer memory and calculation time to calculate the absorbance and signal to noise ratio ( $S/N$ ) values for three beam geometries with a  $2000 \times 50$  grid. Since the concentrations of reactant and product are constant outside the diffusion layer, it suffices to perform the BIFD calculations for the fraction of cell height,  $\mu\delta_L$ , in which concentrations deviate from their bulk values and  $\mu$  is a small multiplier ( $\mu > 1$ ). The calculation is completed by adding the corresponding terms for the fraction of cell height,  $1 - \mu\delta_L$ , where bulk concentrations are observed.

By use of the nomenclature conventions described above, the local absorbance (and transmittance) and overall absorbance for the three optical geometries are defined by eq 19–24.

$$A(x)_{j,k} = -\log T(x)_{j,k} = (W_L/K)(\epsilon_R C_{R,j,k} + \epsilon_P C_{P,j,k}) \quad (19)$$

$$A_{||, \perp} = -\log [\mu\delta_L (\sum_{j=1}^J 10^{-\sum_{k=1}^K A(x)_{j,k}}) / J + (1 - \mu\delta_L) 10^{-\epsilon_R C^* R W_L}] \quad (20)$$

$$A(y)_{j,k} = -\log T(y)_{j,k} = W_c(\epsilon_R C_{R,j,k} + \epsilon_P C_{P,j,k}) \quad (21)$$

$$A_{\parallel,\perp} = -\log \left[ \mu \bar{\delta}_L \left( \sum_{k=1}^K \sum_{j=1}^J 10^{-A(y)_{j,k}} \right) / (JK) + (1 - \mu \bar{\delta}_L) 10^{-\epsilon_R C^* b W_c} \right] \quad (22)$$

$$A(z)_{j,k} = -\log T(z)_{j,k} = (b/J)(\epsilon_R C_{R,j,k} + \epsilon_P C_{P,j,k}) \quad (23)$$

$$A_{\perp,\perp} = -\log \left[ \left( \sum_{k=1}^K 10^{-\sum_{j=1}^J A(z)_{j,k}} \right) / K \right] + (1 - \mu \bar{\delta}_L) \epsilon_R C^* b \quad (24)$$

The optimum value of  $\mu$  was determined by dividing the channel vertically into 2000 increments, and including in the BIFD simulations only those increments falling within a selected multiple of the ratio of diffusion layer thickness to channel height,  $\bar{\delta}_L$ , calculated from eq 3a at flow rates ranging from 10 to 300 mL/h. Figure 4 shows the results comparing multiples of  $\bar{\delta}_L$ , ranging from 0.6 $\bar{\delta}_L$  to 3.0 $\bar{\delta}_L$ , to the results obtained if the entire channel is used. Multipliers  $\mu$  exceeding a value of 1.4 yield negligible errors in calculated absorbance at all flow rates tested. This value is significantly lower than that used in finite difference calculations for stationary diffusion, presumably because of convective shearing of the diffusion layer. This modest change in the model results in substantial (up to 85%) savings in computation times.

In each of the above computations, the absorbances are summed parallel to the direction of the incident light and transmittances are summed perpendicular to the incident light vector. Normalization over the cross section is required when summing local transmittances. Equations 20, 22, and 24 assume that incident light is homogeneously distributed across the beam but can be readily extended to the case of inhomogeneous beam intensity if needed.

**Optical Signal/Noise Ratio.** If absorbance were the only criterion, the optimum geometry would have the longest and narrowest path length through the region containing the highest concentration of absorber. A more valid model considers optical noise in evaluating possible cell geometries.

Ingle and Crouch (22) showed, when transmittance shot noise  $s_T$  is the dominant noise source, for transmittance  $T$ , that

$$s_T = Q[T^2 + T]^{1/2} \quad (25)$$

where  $Q$  is an instrumental shot noise parameter, proportional to total measured light flux (photons per second). For a fixed optical beam geometry, with detected flux proportional to the cell aperture,  $Q$  can be approximated by the relation

$$Q = Q_0 W_T h_T / (W_d h_d) \quad (26)$$

where  $Q_0$  is the shot-noise parameter for the total beam of width  $W_T$  and height  $h_T$  and  $W_d$  and  $h_d$  are the width and height of the beam actually intercepted by the cell and directed to the detector. Thus, the signal/noise ratio (S/N) is dependent only on the value of  $T$  and an instrumental parameter. For the BIFD model, the S/N for absorbance ( $\parallel, \perp$ ) is

$$(S/N)_{A(\parallel,\perp)} = \frac{-W_d H_d}{Q_0 W_T h_T} \left[ \frac{\sum_{j,k} T(y)_{j,k}}{JK + \sum_{j,k} T(y)_{j,k}} \right]^{1/2} \log \left( \frac{\sum_{j,k} T(y)_{j,k}}{JK} \right) \quad (27)$$

where the first term calculates the instrumental shot-noise coefficient for the fraction of the beam entering the cell, the second term is the inverse of noise, the last term represents

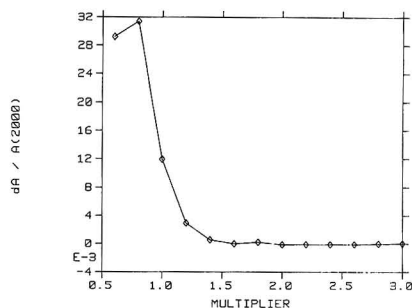


Figure 4. Relative error in calculated  $A_{\parallel,\perp}$  (eq 22) vs multiplier of  $\bar{\delta}_L$ . Constant vertical increment =  $b/2000$ . Flow rate was 0.5 mL/min.

the cell absorbance signal, and the summation is over the entire cell height. Similar expressions can be used to determine the S/N for the other two geometries modeled.

## RESULTS AND DISCUSSION

**Comparison of Models for Fully Developed Laminar Flow.** The Nernst diffusion-layer model (eq 8 and 13) and the BIFD simulations predict that absorbance and current should vary approximately with the inverse cube root of flow rate and the cube root of flow rate, respectively, for fully developed laminar flow. The BIFD simulations predict that the absorbance should actually vary as  $U^{-0.388}$  and current should vary as  $U^{0.340}$  over the range of flow rates investigated, where  $U$  is the average volume flow rate, while eq 8 predicts that absorbance should vary as  $U^{-0.356}$ . The difference between the BIFD method and eq 8 for the absorbance flow dependence is due in part to the linear diffusion layer approximation used to obtain eq 8 and is negligible over the flow rates normally encountered. Since local absorbance is small, and  $\bar{\delta}_L$  is small ( $<0.3$ ) at the flow rates used in this study, eq 8 predicts reactant absorbance exceeding 90% of the value expected when no reaction occurs and product absorbance less than 10% of the value expected when pure product is introduced.

The multiplier  $m$  in eq 8 was determined by a nonlinear least-squares simplex fit of data generated by the BIFD simulations (eq 22), using volume flow rates ranging from 10 to 3000 mL/h and  $A(P)_{\max}$  values ranging from 0.001 to 1. A flow-independent value of 1.1779 was determined for  $m$ , with a sum-of-residuals squared of  $1.26 \times 10^{-4}$  (absorbance units)<sup>2</sup>, indicating good agreement between the models over the flow range studied. All calculations using eq 8 were performed in double precision to prevent the significant round-off errors due to small differences between terms. (Pocket calculators with 10-digit precision have sufficient accuracy.)

**Effects of Concentration Heterogeneity.** An absorption saturation effect may be observed for incident light parallel to the electrode if only the product of an electrochemical reaction absorbs strongly, as predicted by eq 8 and the respective limiting behaviors of eq 10, 10a, 12, and 12a. The absorbance sensitivity for product may be relatively low in this case. Additionally, nonlinearity of measured absorbance with respect to concentration can occur at deceptively low total absorbance values. The effect of the small number of photons transmitted through the thin diffusion layer of the cell is overwhelmed by the preponderance of unabsorbed light transmitted through the much thicker regions of essentially constant absorbance, and the overall measured absorbance is much lower than expected for a cell with homogeneously distributed concentrations. This situation, which is similar to that observed for conventional spectrometers at high absorbance in the presence of significant nonabsorbed stray light,

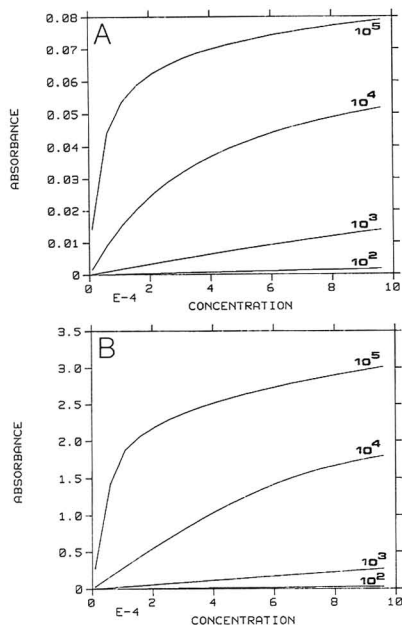


**Figure 5.** Effect of concentration heterogeneity on absorbance vs initial reactant concentration: (A) product absorbance, (B) reactant absorbance. Numbers on curves are molar absorptivities. Flow rate was 0.5 mL/min.

is depicted in Figure 5A, where absorbance is plotted as a function of initial concentration of the reactant for various values of  $\epsilon_P$ .

Marked nonlinearity of product absorbance vs concentration is evident above an absorbance of 0.012 when  $\epsilon_P = 10^4$ , where the initial reactant concentration is  $1.2 \times 10^{-4}$  M. Since the cell width is 0.3 cm, the product absorbance in the region immediately adjacent to the working electrode is ca. 0.48. If  $C^*_{R}$  is 0.001 M, the absorbance immediately adjacent to the working electrode is 3.0, though the overall cell absorbance is only 0.05. Saturation near the electrode surface may block virtually all the incident light in that region, but the overall absorbance will be relatively low because the light passing through the majority of the cell is unattenuated.

This saturation effect also occurs in stationary solution cells with illumination parallel to the electrode surface, except that the concentration gradient is less steep without flow. This saturation effect is less likely to be observed in SEFC's where the light is perpendicular to the working electrode, which have typical path lengths of less than 0.2 mm and hence lower overall absorbances.

An analogous, but less severe, saturation effect is observed when only the reactant absorbs significantly. Here, depletion of the reactant decreases absorbance in the thin diffusion layer near the electrode surface. The absorbance response calculated from eq 11a is linear, since the limiting case for eq 11 and 11a, where  $A(R)_{\max} \rightarrow 0$ , neglects the saturation effect. Deviations from Beer's law become significant only at absorbance values greater than ca. 1. For example, when  $A(R)_{\max} = 1.0$ , the deviation of eq 11a from eq 8 is ca. 10% at 0.5 mL/min, decreasing with increasing flow rate, to less than 5% at 5.0 mL/min. Figure 5B shows plots of absorbance vs initial reactant concentration for several values of  $\epsilon_R$ . Though eq 8 and 22 show slight deviations from linearity at higher  $A$ -

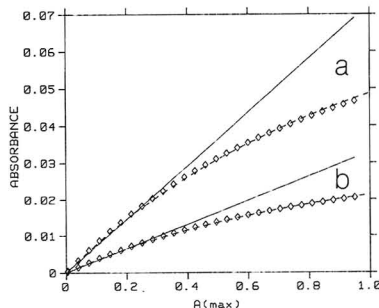


**Figure 6.**  $A_{\perp}$  calculated from several models vs  $A(P)_{\max}$  ( $A(R)_{\max} = 0$ ): solid curves, low absorbance approximation (eq 9a); dashed curves, BIFD (eq 22); diamonds, general approximation (eq 8); (a) flow rate = 0.5 mL/min, (b) flow rate = 5.0 mL/min.

( $R$ ) $_{\max}$  values resulting from the saturation effect, the deviation is not nearly as large as in the case where only the product absorbs, because most of the light intersects the cell outside the thin diffusion layer, where the reactant concentration is essentially unchanged by the electrode reaction. Figure 6 compares the predictions for product absorbance from the BIFD simulations (eq 22) with the full treatment (eq 8) and low absorbance limit (eq 9a) of the diffusion layer model at 0.5 and 5.0 mL/min. The agreement between the BIFD simulations and the full diffusion layer treatment (eq 8) is quite good, as expected from the simplex results. Since eq 9a represents the limiting condition  $A(P)_{\max} \rightarrow 0$ , where the saturation effect can be neglected, deviations are expected between eq 9a and eq 8 and 22 as  $A(P)_{\max}$  increases, and the calculated results agree with these expectations.

It is important to note that the nonlinearity of absorbance vs concentration is a function of  $\epsilon_R W_c C^*_{R}$  and/or  $\epsilon_P W_c C^*_{R}$ , which represents the theoretical maximum absorbance if either the reactant or product is the only significant absorber, respectively, and not simply of  $C^*_{R}$ . The maximum absorbance for the reactant is obtained when no electrochemical reaction occurs; conversely, the maximum absorbance for the product occurs if the reaction proceeds with 100% coulometric efficiency at the leading edge of the working electrode.

**Optimization of Optical Beam Geometry.** Heterogeneity of concentration distribution in the SEFC causes poorer S/N for absorbance measurements than for current measurements if the optical beam fills the complete cell height. However, illumination parallel to the electrode surface substantially improves both signal and S/N relative to the more common perpendicular illumination, due to the longer optical path length. Simulations using a typical cell width of 0.3 cm, cell height of 0.0127 cm, flow rate of 0.5 mL/min, initial reactant concentration of 0.001 M, and product molar absorptivity of 1000, showed that the relative absorbance ratio,  $A_{\perp}/A_{\parallel}$ , was identical with the path length ratio (width/height) of 23.6, following the relative path length. However, the corresponding S/N enhancement,  $(S/N_{\perp})/(S/N_{\parallel})$ , was 20, growing slightly less rapidly than the absorbance signal, due to light losses encountered when illuminating the narrow side walls and due to the greater importance of the saturation effect for a longer path length. The improvement in S/N, though somewhat less than the improvement in absorbance, allows significantly lower detection limits for parallel illumination than for perpendicular illumination. If the cell length and width are equal, the absorbance and S/N calculated using the BIFD simulations are identical for the two beam geometries ( $\parallel$ ,  $\perp$ ) and ( $\parallel$ ,  $\parallel$ ).

The SEFC designs in which the illumination is perpendicular to flow can be modified such that the light beam does

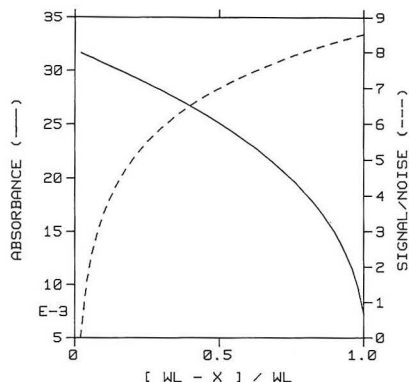


**Figure 7.**  $A_{||}$  and signal/noise ratio vs illumination aperture length, assuming constant total light flux of fixed geometry. Flow rate was 0.5 mL/min. Solid curve denotes absorbance; dashed curve denotes signal/noise.

not intersect the full cell cross section, but rather only a small portion. For an absorbing reactant, absorbance is maximized near the leading edge of the cell, where reactant concentration is largest. Measurement errors resulting from the heterogeneous distribution of reactant in the cell are also less important near the leading edge than at the trailing edge of the working electrode. For an absorbing product, absorbance is maximized near the trailing edge of the electrode, where the product concentration is largest and the diffusion layer is thickest.

A simulation was performed to evaluate the potential benefits of partial cell illumination where the incident light is perpendicular to flow and parallel to the electrode surface. Absorbance was calculated for a cell window of increasing length. The narrowest window is simply the  $x$  axis increment at the trailing edge of the working electrode. The window was progressively widened by including adjacent  $x$  axis increments, to a final width, using the entire cell as in the earlier simulations. The shot noise parameter,  $Q_0$ , was arbitrarily set to 0.001, corresponding to a shot noise level of  $4 \times 10^{-4}$  absorbance unit. Equation 26 was used to calculate the value of  $Q$ , assuming that the total incident flux per unit area was constant. A plot of absorbance and S/N vs the length of this window is shown in Figure 7. Since widening the illuminated window increases the volume of the cell in which no product appears, the total amount of light transmitted increases, decreasing overall absorbance and increasing the importance of the saturation effect.

Since S/N is directly related to the incident flux in the optical train if shot noise is dominant, S/N should be poorest when only the trailing edge is monitored if beam intensity is fixed in space, because most of the available flux is not used. For example, when only the trailing 1% of the electrode is illuminated, 99% of the light is masked from the cell and lost, increasing the effective value of  $Q$ . As the width of the illuminated window increases, the total incident flux increases, and S/N improves. If the incident light could be focused onto the trailing edge, then the degradation of S/N and saturation effects would be minimized. The possible importance of other optical noise sources such as flicker or flow fluctuation noise may significantly alter these conclusions in any specific experiment. Diffusion layer imaging using an optical beam from a laser source (12) confined to a region within the diffusion layer is predicted to afford a very attractive S/N and significantly improved detection limits, without the saturation and nonlinear absorbance/concentration limitations of a beam filling the entire cell. Another promising alternative is pho-

tothermal deflection coupled to the electrode reaction (23) at the trailing edge of the electrode.

## CONCLUSIONS

In summary, a spectroelectrochemical thin-layer flow detector with a long path length has been investigated theoretically. It has been established that illumination parallel to the electrode surface affords significantly better signal and S/N than illumination perpendicular to the electrode. If the optical beam fills the channel thickness and light throughput is limited by aperture dimensions, comparable S/N's will be obtained with illumination parallel to the electrode and either parallel or perpendicular to flow. Alternatively, if light throughput is independent of aperture dimensions, or an optical beam can be focused to dimensions smaller than channel thickness, a narrow beam at the trailing edge of the electrode, parallel to the electrode surface and perpendicular to flow, will afford the best signal and S/N when only the product of the electrochemical reaction absorbs.

The digital simulations confirm the validity of the approximate analytical solution based on the Nernst diffusion layer model. However, potential errors in absorbance measurements due to concentration inhomogeneity in the cell caused by the electrochemical reaction may result in poorer S/N than expected in a conventional absorption detector. Nonlinear dependence of absorbance on concentration may be observed due to a saturation effect if local absorbances are high and the height of the optical beam is greater than the diffusion layer thickness, requiring more extensive calibration for quantitation. The greatest absorbance signals and S/N will be achieved if the electrochemical reactant absorbs strongly. The linear working region of absorbance vs concentration extends to more than one absorbance unit for an absorbing reactant, yielding a wide dynamic range, well-suited for application in a correlation detector.

## LITERATURE CITED

- (1) Clark, G. J.; Goodin, R. R.; Smiley, J. W. *Anal. Chem.* **1985**, *57*, 2223-2228.
- (2) Condit, D. A.; Herrera, M. E.; Stankovich, M. T.; Curran, D. J. *Anal. Chem.* **1984**, *56*, 2909-2914.
- (3) Evans, D. H.; Kelly, M. J. *J. Anal. Chem.* **1982**, *54*, 1727-1730.
- (4) Anderson, C. W.; Halsall, H. B.; Heineman, W. R. *Anal. Biochem.* **1979**, *93*, 366-372.
- (5) Brewster, J. D.; Anderson, J. L. *Anal. Chem.* **1982**, *54*, 2560-2566.
- (6) Anderson, J. L.; Brewster, J. D. U.S. Patent 4,540,280, 1985.
- (7) Zak, J.; Porter, M. D.; Kuwana, T. *Anal. Chem.* **1983**, *55*, 2219-2222.
- (8) Porter, M. D.; Kuwana, T. *Anal. Chem.* **1984**, *56*, 529-534.
- (9) Brewster, J. D.; Anderson, J. L., unpublished work, 1987.
- (10) Tyson, J. F.; West, T. S. *Talanta* **1979**, *26*, 117.
- (11) Jan, C. C.; McCreery, R. L.; Gamble, F. T. *Anal. Chem.* **1985**, *57*, 1763-1765.
- (12) Jan, C. C.; McCreery, R. L. *Anal. Chem.* **1986**, *58*, 2771-2777.
- (13) Pinkerton, T. C.; Hajizadeh, K.; Deutsch, E.; Heineman, W. R. *Anal. Chem.* **1980**, *52*, 1542-1544.
- (14) LaCourse, W. R.; Krull, I. S.; Bratin, K. *Anal. Chem.* **1985**, *57*, 1810-1814.
- (15) Fosdick, L. E.; Anderson, J. L. *Anal. Chem.*, following paper in this issue.
- (16) Weber, S. G.; Purdy, W. C. *J. Anal. Chem.* **1978**, *100*, 531-544.
- (17) Levich, V. G. *Physical Electrochemical Hydrodynamics*; Prentice-Hall: Englewood Cliffs, NJ, 1962; p 91.
- (18) Brewster, J. D. Doctoral Dissertation, University of Georgia, 1987.
- (19) Anderson, J. L.; Moldoveanu, S. J. *Electroanal. Chem. Interfacial Electrochem.* **1984**, *179*, 107-117.
- (20) Fosdick, L. E.; Anderson, J. L. *Anal. Chem.* **1986**, *58*, 2481-2485.
- (21) Fosdick, L. E.; Anderson, J. L.; Baginski, T. A.; Jaeger, R. C. *Anal. Chem.* **1986**, *58*, 2750-2756.
- (22) Ingle, J. D., Jr.; Crouch, S. R. *Anal. Chem.* **1972**, *44*, 1373-1386.
- (23) Pawliszyn, J.; Weber, M. F.; Dignam, M. J.; Mandelis, A.; Venter, R. D.; Park, S. M. *Anal. Chem.* **1986**, *58*, 236-242.

RECEIVED for review April 6, 1987. Accepted October 1, 1987. This work was funded in part by the U.S. Department of the Interior, U.S. Geological Survey, Project G-1011 (02), and the National Science Foundation, Grant No. CHE-8600224. L. E. Fosdick also acknowledges a University of Georgia University-wide Graduate Nonteaching Assistantship.



# Spectroelectrochemical Response and Flow Hydrodynamics in Thin-Layer Flow Detectors with Long Optical Path Lengths and Fiber-Optic or Slab Waveguide Coupling

Lawrence E. Fosdick<sup>1</sup> and James L. Anderson\*

Department of Chemistry, The University of Georgia, Athens, Georgia 30602

Spectroelectrochemical experiments were performed in rectangular thin-layer flow cells with long optical paths, for the oxidation of ferrocyanide to ferricyanide in phosphate buffer. The optical beam was coupled to the cell with fiber optics or thin-slab waveguides as the cell sidewalls. Steady-state amperometric and absorptometric responses both depended critically on cell design, agreeing well with theory for fully developed laminar flow when the cell inlet and outlet were several millimeters upstream and downstream of the working electrode, but agreed better with theory for developing laminar flow when the electrode completely covered one channel wall. The signal to noise ratio was considerably poorer for absorbance measurements than for current but considerably better than for more conventional thin-layer spectroelectrochemical cell designs with short optical paths. Flow injection calibration curves demonstrated much greater absorbance sensitivity when the reactant rather than the product was the primary absorber. Experimental results support the potential use of the cells as correlation detectors.

Thin-layer (TL) spectroelectrochemical flow cell (SEFC) detectors offer intriguing possibilities for enhanced analytical selectivity as well as assessment of flow hydrodynamics and reaction mechanisms in applications such as high-performance liquid chromatography (HPLC) or flow injection analysis (FIA). Although numerous stationary spectroelectrochemical cells (SEC) have been reported (1-5), with both short (1, 2, 6) and long (3-5) optical paths, we are aware of only one flow application of a TL-SEFC having a short optical path length of low sensitivity in an HPLC stopped-flow coulometry configuration (6).

Theory describing the current and absorbance response and optimum optical geometries for a rectangular TL-SEFC is reported elsewhere (7), demonstrating the utility of configurations with long optical paths. The present work experimentally evaluates the steady-state flow response of TL-SEFC detectors with long optical paths parallel to the electrode surface and coupled to the light beam by fiber optics or slab waveguides serving as cell side windows. Experimental data agree well with theoretical predictions. The absorptometric measurements provide a powerful means of confirming observations on the nature of channel flow hydrodynamics derived from amperometric measurements. The results show that a slight change in geometry can shift response and flow rate exponents (8) between fully developed laminar flow behavior and a behavior consistent with developing or stagnating laminar flow. The feasibility of correlation detection based on coupled amperometric and absorptometric measurements is also evaluated.

<sup>1</sup>Current address: Hercules Incorporated, Research Center, Wilmington, DE 19894.

## EXPERIMENTAL SECTION

The thin-layer, long optical path SEFC cell designed for this study is shown in Figure 1. The working electrode substrate consisted of either glass or a silicon wafer with a thin, thermally generated oxide insulating layer, coated with Liquid Bright Gold (Engelhard Industries), and fired in a muffle furnace at 560 °C for 1 h to form a solid gold surface on the substrate. The working electrode was designed to be 0.5 cm in length, with its width equal to the flow channel width. The optical beam was passed through the side walls parallel to the electrode surface and perpendicular to flow. Some electrodes were fabricated by using a microlithographic technique (9). The cell wall opposing the working electrode was made of poly(methyl methacrylate) (PMMA). The cell channel was defined by a 0.14 mm thick microscope cover glass spacer.

The flow channel between the working electrode and the opposite cell wall was made by several techniques to determine the optimum method of producing thin, optically transparent side walls. Two configurations were tested in which the side walls of the channel spacer served as slab optical waveguides. One type was made by epoxying four sections of cover glass to form a rectangular flow channel. A second type was made by ultrasonically drilling a 0.50 cm by 0.30 cm rectangular channel in a single sheet of cover glass with a locally constructed rectangular bit, followed by polishing the inner walls with 0.3- $\mu$ m alumina.

The most successful cell was a fiber-optic thin-layer (FOTL) SEFC. The FOTL-SEFC fabrication method employed a ribbon fiber optic sheet (Edmund Scientific), consisting of parallel 0.003 in. diameter glass fibers, intimately contacting in a single, orderly layer as optical waveguides and cell side walls. The fiber-optic sheet was originally obtained in a 1-in. width, with an overall thickness of 0.0045 in., including the binding material used to produce the fiber sheet. Two sections, each 0.50 cm wide, were cut from the sheet to form the side walls and optical waveguides. An ultrasonically drilled cover glass of the type described above was cut in half and butted to both ends of the fiber sheets, which overlaid the 0.5 cm working electrode. These ends formed the cell inlet and outlet regions to allow laminar flow to develop fully before the solution reached the working electrode and sheet fiber optics. The measured optical path length for this cell was 0.28 cm. This final design is very similar to that reported earlier (4) with the exception that the fibers were obtained in a ribbon form, eliminating the need to align the individual fibers.

The solution inlet and outlet ports were machined into the PMMA cell top. The entire assembly was sealed with epoxy. Cells using microscope cover glass as the optical waveguide were masked with black tape and India ink over both side walls to minimize stray light outside the desired light path.

The dual beam spectrometric system used with cells having microscope cover glass as the optical waveguides consisted of a tungsten filament lamp, an Instruments SA Model H-20 monochromator, and a quartz beam splitter with an aluminum mirror grid pattern (Corion) to separate the sample and reference beams within a large, light-tight sample box. Lenses were used to focus the beams through the sample cell and reference compartment and also onto the dual photomultiplier tubes (Hamamatsu R508-01), as described previously (10).

The FOTL-SEFC (employing the ends of ribbon fiber optic bundles as side walls) was mounted in a light-tight box. The ends of the fiber bundles were sealed into aluminum tubes and placed into xy positioners to optimize the coupling of light from the

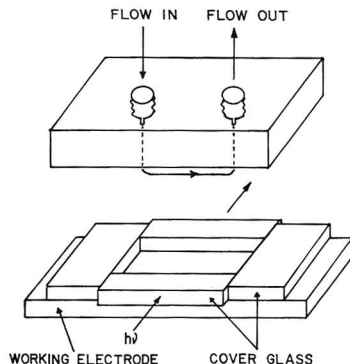


Figure 1. Spectroelectrochemical thin-layer flow cell with long optical path. Side walls (optical light guides) were either sheet fiber optics or microscope cover glass.

monochromator (American Instruments Co.) through the fibers and onto the photomultiplier tubes (Hamamatsu R508-01) (4).

The outputs of the photomultiplier tubes in both spectrometer systems were converted electronically to absorbance by using a logarithmic ratio amplifier (Philbrick Model 4367), and the output was recorded on a strip chart recorder. Some data were digitally recorded with a Nicolet Model 3091 dual beam digital oscilloscope, from which the data were transferred via RS232 connections to an IBM Personal Computer and then to a VAX 11/750 for processing. The output of the logarithmic ratio amplifier, which normally has a band-pass of ca. 1 kHz, was filtered through a low pass filter having a 1-s time constant when monitored by the strip chart recorder and was unfiltered when used with the digital oscilloscope. The monochromator was set at 418 nm, the absorption maximum for ferricyanide (4). Wavelength and photometric calibration of both systems were achieved by filling the cells with 0.5 mM potassium ferricyanide in pH 7.1 0.1 M phosphate buffer and comparing the absorbance spectrum from 400 to 440 nm to that obtained with phosphate buffer in the cell.

Electrochemical measurements were performed with a Model 174A potentiostat (EG&G Princeton Applied Research Corp.) and recorded with a dual pen strip chart recorder (Linear) or the digital oscilloscope. A bundled carbon fiber auxiliary electrode and Ag/AgCl (1.0M KCl) reference electrode were mounted at the exit port. Electrical connections to the cells were made through light-tight connectors which penetrated the walls of the boxes.

Flow injection experiments were carried out with a Varian Model 8500 syringe pump and a pneumatically controlled injector (Valco) with a 1.1-mL injection loop. This large injection volume, combined with a 90- $\mu$ L dead volume between the injector and cell, ensured a steady-state spectroelectrochemical response, with concentration at the center of the peak equal to the injection concentration (9). The 1.1-mL injection loop was replaced with a 50- $\mu$ L loop for calibration curve measurements. The tubing from the injector entered the light-tight boxes through ports masked with black tape and black foam, and the waste solvent containers were placed inside the boxes, to minimize stray light. The mobile phase of pH 7.1 0.1 M phosphate buffer was prepared fresh daily in distilled-deionized water and filtered through 0.2- $\mu$ m nylon filters (Millipore). A used reverse-phase liquid chromatography column, inserted in the flow stream between the pump and injector, reduced solution pump noise. The electroactive species was potassium ferricyanide (reagent grade, used as received) prepared fresh daily in pH 7.1, 0.1 M phosphate buffer. Potassium ferricyanide concentrations ranged from 0.2 to 1.0 mM for steady-state measurements. Calibration curve measurements were performed with 0.42–2.1 mM potassium ferricyanide or 0.036 mM to 4.5 mM potassium ferricyanide.

## RESULTS AND DISCUSSION

**Laminar vs Developing Flow.** The key equations for steady-state, mass transport limited current and absorbance

Table I. Absorbance and Current Equations for Fully Developed and Developing Flow<sup>a</sup>

General Case	
$A_{\perp, L} = -\log \{ (1 - f\delta_L) 10^{-\epsilon W C_R} + f\delta_L (10^{-\epsilon W C_R} - 10^{-\epsilon W C_P}) / [2.303(\epsilon_R - \epsilon_P) S C_R] \}$	(1)
Fully Developed Laminar Flow ( $f = 0.8834$ )	
$\delta_L = 1.022 [D W C_R / (U b (1 - 0.6433 \delta_L))]^{1/3}$	(2)
$i = n F U C_R \delta_L^2 / [1.4032 - 0.8024 \delta_L]$	(3)
Developing or Stagnant Laminar Flow ( $0.667 < f < 0.8487$ ) [assume $f = 0.7853$ ] <sup>b</sup>	
$\delta_L \approx 2.94 D^{1/3} U^{1/6} (W C_R / (U b))^{1/2}$	(4)
$i = 0.68 n F C_R D^{2/3} U^{1/6} (W C_R U / b)^{1/2}$	(5)
Inviscid Flow (assume $f = 0.7853$ ) <sup>b</sup>	
$\delta_L = [\pi D W C_R / (U b)]^{1/2}$	(6)
$i = 2 n F [D W C_R U / (\pi b)]^{1/2}$	(7)

<sup>a</sup> See ref 7 for details and definitions of terms. <sup>b</sup> By analogy to known limits for fully developed laminar flow (7) and stationary diffusion;  $f = 0.7853$  if the same diffusion layer thickness multiplier is used as for fully developed laminar flow (7).

Table II. Flow Rate Dependence of Current and Absorbance

$C_R$ , mM	flow rate exponent <sup>a</sup>	
	current ( $\alpha_i$ )	absorbance ( $\alpha_A$ )
0.20	$0.322 \pm 0.008$	$-0.43 \pm 0.04$
0.50	$0.314 \pm 0.009$	$-0.42 \pm 0.03$
1.00	$0.316 \pm 0.003$	$-0.37 \pm 0.01$
1.00	$0.315 \pm 0.004$	$-0.35 \pm 0.01$
Developing or Stagnating Laminar Flow Cell		
1.20	$0.520 \pm 0.007$	$-0.49 \pm 0.01$

<sup>a</sup> Slopes of log-log plots for current and absorbance of ferricyanide vs flow rate,  $U$ , for oxidation of potassium ferricyanide in phosphate buffer ( $i \propto U^{\alpha_i}$  and  $A \propto U^{\alpha_A}$ ). Theory predicts  $i \propto U^{0.34}$  (BIFD) and  $A \propto U^{-0.368}$  (BIFD) or  $A \propto U^{-0.356}$  (Nernst approximation).

response  $A_{\perp, L}$  with illumination parallel to the electrode and perpendicular to flow are summarized in Table I for both fully developed and developing laminar flow, and inviscid flow, where R and P refer to reactant and product, respectively. Other terms and limiting behaviors are defined in ref 7. Equation 1 describes all three flow cases, depending on the choice of  $f$  and  $\delta_L$  (eq 2, 4, or 6). Equations 2 and 3, or eq 4 and 5, or eq 6 and 7 describe the respective currents. Equations 1–3 and backward implicit finite difference (BIFD) simulations predict that absorbance (7) and current (9, 11, 13) should vary approximately with the inverse cube root and cube root of flow rate, respectively, for fully developed laminar flow (7). Equations 1, 4, and 5 predict inverse square root and square root dependence for developing laminar flow, and eq 1, 6, and 7 predict the same dependence for inviscid flow.

The product of absorbance and current either for fully developed or developing laminar flow or for inviscid flow should be virtually independent of flow rate. The sum of flow exponents of absorbance and current should be constant whether flow is fully developed (7) or developing laminar flow. The magnitudes of the flow exponents for both current and absorbance provide a test of the nature of flow, and their sum a test of the self-consistency of the experimental results.

**Fully Developed Laminar Flow Cell.** Steady-state flow injection experiments using the ferricyanide/ferricyanide couple ( $\Delta\epsilon = 1023 \text{ M}^{-1} \text{ cm}^{-1}$ ) verified that both absorbance and current could be measured, as shown in Figure 2. Absorbance and current were in reasonable agreement with

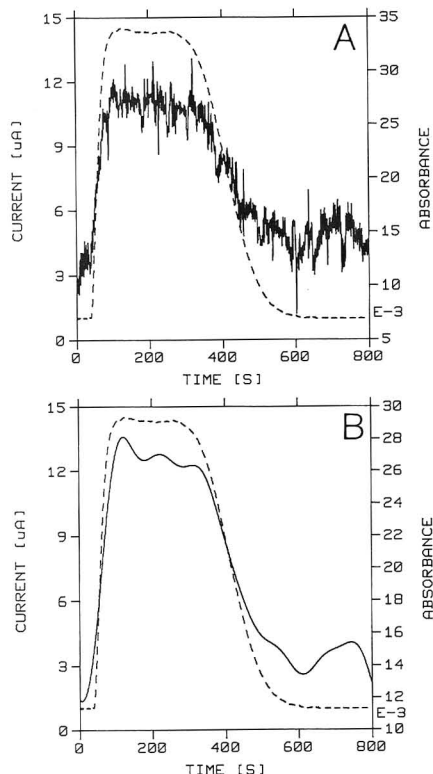


**Figure 2.** Experimental response of a fully developed laminar flow FOTL-SEFC: steady-state current (---) and absorbance (—) of ferriocyanide produced by oxidation of 1.1 mL of 1.00 mM ferrocyanide at 0.17 mL/min; (A) 1-kHz band-pass, (B) after Fourier smooth.

theoretical expectations. Table II summarizes the steady-state flow rate exponents measured for current and absorbance for ferrocyanide solutions ranging from 0.20 to 1.0 mM.

When ferrocyanide solutions of less than 1.0 mM were used, the small absorbances measured had increasingly poor S/N (as low as ca. 3) as flow rate increased. Thus, measurement errors are largely responsible for the uncertainties in flow exponents listed in Table II, and for the higher than expected slopes at ferrocyanide concentrations below 1.0 mM. For example, theoretical absorbance for 0.5 mM concentrations ranged only between 0.015 at 0.17 mL/min and 0.004 at 1.7 mL/min.

Figure 3 compares the experimental response with theoretically simulated response for absorbance and current, respectively, using the BIFD method, for a 1.0 mM ferrocyanide solution using the FOTL-SEFC. The complete diffusion layer approximation presented in eq 1 and 2 yields results virtually identical with the BIFD method, as reported previously, while the low absorbance limiting approximation presented in eq 9a of ref 7 overestimates the absorbance, due to the saturation effect (7). Good agreement is observed between theory and experiment for current response, with the slight negative deviation of experimental response at the higher flow rates consistent with electrode fouling restricting diffusion to the electrode surface (9).

The measured absorbance is ca. 16% lower than predicted, but generally follows the expected trend with flow rate. A

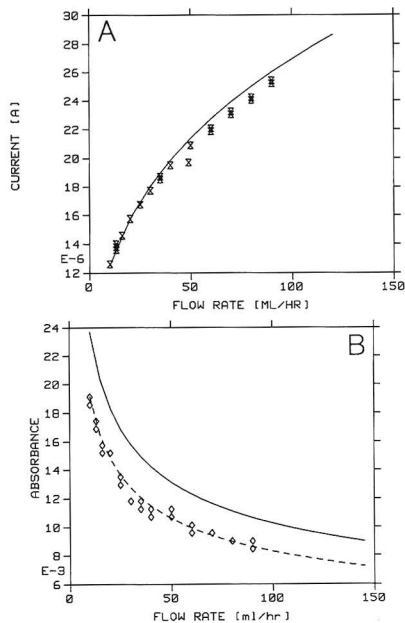


**Figure 3.** Steady-state experimental and theoretical BIFD response vs flow rate of a fully developed laminar flow FOTL-SEFC. Only product absorbance. Conditions are given in Figure 2. (A) Current: solid curve, theoretical; points, experimental. (B) Absorbance: solid curve, theoretical; points, experimental; dashed curve, theoretical response multiplied by 0.84.

gap between the beam and the electrode, a lack of collimation, and the possibility of sheath flow through stagnant eluent, with the sample restricted to a narrower zone than the complete cell width, are the most important nonidealities affecting the measured absorbance, since the model assumes perfectly collimated light filling the entire cell height.

The finite thickness of the optical sheath surrounding the optical fiber core, plus the ribbon binder and the epoxy, may collectively displace the edge of the fiber core as much as 15  $\mu\text{m}$  above the electrode surface. The resulting gap decreases the measured absorbance of product by masking the diffusion layer region where the product concentration is largest. The small tangential circular fiber cross section nearest the electrode also decreases the measured absorbance of product, for the same reason, according to a square-law dependence on cross section when fibers are used for both light input and output.

At fixed flow rate, BIFD simulations assuming collimated light show that absorbance for a finite gap should decrease relative to absorbance for zero gap, and the flow rate exponent should become more negative as the ratio of gap thickness to diffusion layer thickness increases. At fixed gap thickness, the flow rate exponent should become increasingly negative as flow rate increases. For example, the simulated flow rate exponent changes in magnitude from the ideal limiting value of  $-0.368$  at sufficiently low flow rates to a value as negative as  $-0.935$  at high flow rates for a gap of 15  $\mu\text{m}$  between the electrode surface and the fibers, but to a negative limit of only  $-0.447$  for a gap between 3 and 9  $\mu\text{m}$ . The effect of the gap is more pronounced at higher flow rates. For example, for a gap of 15  $\mu\text{m}$ , the gap/product diffusion distance ratio at the trailing edge of the electrode is only 0.23 at 0.17 mL/min but increases to ca. 0.54 at a flow rate of 1.7 mL/min, since

concentration reaches the bulk value at a distance from the electrode of  $1.4b\delta_x$  (7). The analogous gap between the fibers and the top of the cell is predicted to improve the absorbance slightly, by masking off a region containing no absorbing product. These results indicate that the discrepancies between experimental and ideal theoretical absorbance are not due simply to a gap between the electrode surface and the optical fibers in the cell.

Lack of collimation is ensured by the angular dispersion of light entering the fibers from the monochromator, as shown previously (4). Uncollimated rays passing through the diffusion layer tend to increase the absorbance, relative to collimated rays separated by a gap, because more rays are absorbed than expected. Thus the measured absorbance is lower than that predicted by ideal theory for a collimated beam, due to the gap, but not as low as expected, and without significantly altering the flow dependence predicted by ideal theory, due to lack of collimation. The effects of these nonidealities are quantitatively treated elsewhere for time-dependent experiments in static solution (14).

Sheath flow would restrict the sample to a zone occupying only a fraction  $f_s$  ( $f_s \leq 1$ ) of the cell width, assuming that the sample fills the full cell height, decreasing absorbance by factors of  $f_s^{4/3}$  (fully developed laminar flow) and  $f_s^{3/2}$  for developing or inviscid flow and decreasing the current by factors of  $f_s^{2/3}$  and  $f_s^{1/2}$ , respectively. In all cases, the effect of sheath flow on absorbance is much greater than on current.

Both absorbance and current flow exponents deviated at low flow rates from the ideal limits of  $-1/3$  and  $+1/3$ , because the diffusion layer impinged on the opposite cell wall, although the absorbance measurements were improved since the product occupied a larger fraction of the cell. Flow rates higher than ca. 1.7 mL/min were avoided due to very low absorbance values, with unfavorable S/N ratios, making differentiation of values difficult.

The signal/noise ratio (S/N) in the absorbance measurement at the full bandwidth of 1 kHz was much lower than in the current measurement, as seen in Figure 2. BFD simulations predicted that the S/N for absorbance measurements using the FOTL-SEFC and a 1 mM ferrocyanide solution as the analyte should have been 25.8 at 0.5 mL/min, assuming a shot noise level of  $4 \times 10^{-4}$  absorbance unit as the dominant noise source (7). The root mean square noise measured at the full 1-kHz band-pass of the detector was 0.0012 absorbance unit, ca. 3-fold higher than assumed in the model, resulting in an experimental root mean square S/N of ca. 8 at 0.5 mL/min. The peak-to-peak noise, measured from the 1-Hz filtered absorbance signal on the strip chart recorder, was 0.0008 absorbance unit, yielding a peak-to-peak S/N of ca. 10 at 0.5 mL/min. At the highest flow rates used in this study, the absorbance S/N was ca. 4 at the 1-kHz band-pass, based on root mean square noise, for a 1 mM ferrocyanide solution. Fourier smoothing significantly improved the S/N of the absorbance data, as shown in Figure 2b, but the current data still exhibited significantly better S/N.

The difference in S/N can be attributed to noise sources not considered by the simulations, such as source flicker noise, dark current shot noise, and noise associated with solution flow. In addition, only a small fraction of the available light in the sample beam actually entered and passed through the cell. The SEFC with microscope cover glass as the spacer and light guide transmitted ca. 0.1% of the incident light through the cell to the detector. The FOTL-SEFC, based on fiber-optic light guides, transmitted ca. 1% of the incident light. These large light losses are primarily due to limitations on focusing the beam onto the light guide, scattering due to incomplete polishing, and losses of uncollimated light rays refracted from the solution in the cell of low refractive index through the

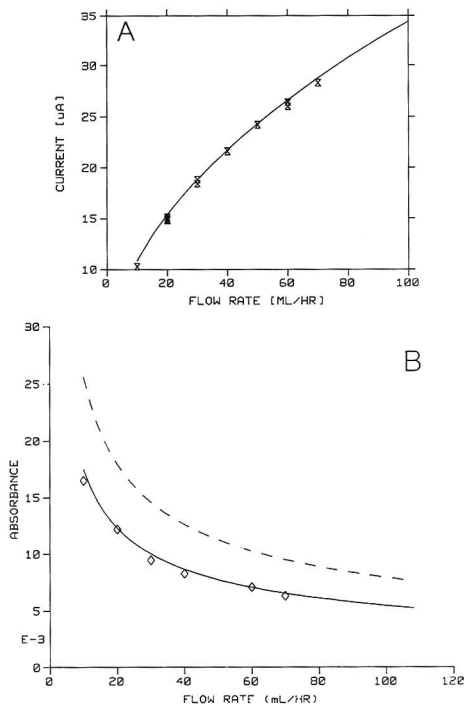


**Figure 4.** Steady-state experimental and theoretical response vs flow rate of a developing or stagnant laminar flow SEFC, 1.2 mM ferrocyanide. (A) Current: solid curve, theoretical; points, experimental. (B) Absorbance: solid curve, theoretical developing flow response, for sheath fraction  $f_s = 0.20$ ; points, experimental; dashed curve, theoretical inviscid flow response for  $f_s = 1.0$ .

transparent cell wall of higher refractive index (4). The latter effect has previously been shown to account for ca. 90% of the light losses using this geometry (4). The large background absorbance resulting from these losses was compensated by a combination of neutral density filters, a bias voltage applied through a simple adder circuit, and increased photomultiplier dynode voltage to deliver adequate photocurrent to the logarithmic ratio amplifier.

**Developing or Stagnating Laminar Flow Cell.** The cell constructed by using the microscope cover glass slab optical waveguide channel with a rectangular 0.5 by 0.3 cm cavity yielded a square-root rather than the expected cube-root flow dependence. The slope of the log current-log flow rate plot was  $0.520 \pm 0.007$ , while the slope for the log absorbance-log flow rate plot was  $-0.492 \pm 0.01$ . The working electrode in this cell completely covered one wall of the flow channel defined by the rectangular drilled hole, including the regions around the flow inlet and outlet ports. The square root flow dependence is inconsistent with fully developed laminar flow but is consistent with behavior expected for developing (11, 12) or stagnating laminar or inviscid flow.

The current response data obtained for this cell showed good agreement with predictions for developing laminar flow (eq 5, ref 12), as shown in Figure 4A, over the flow range studied, indicating that fully developed laminar flow conditions were not dominant. However, the diffusion layer thicknesses predicted for developing flow exceed the cell thickness at most flow rates if the sample fills the entire cell width, indicating that uncomplicated developing flow was

probably not truly attained. The absorbance followed an inverse square root flow dependence, tracking the current response, as predicted by eq 1 and 3. However, the absorbance (Figure 4B) was only ca. 10% of that predicted by eq 1 and 4 if the sample stream flows over the entire width of the electrode.

The low absorbance may result in part from sheath flow, with a shorter than expected optical path and faster than expected linear velocity. Visual observations of the injection of opaque samples showed that the flow filled perhaps half (or less?) of the channel width, confirming the hypothesis that sheath flow was occurring, although the physical dimensions of sample distribution were ill-defined. The developing flow theory fit the observed data well if the sheath fraction  $f_s$  was assumed to be 0.2 (Figure 4B). For this value, the predicted diffusion layer thickness was more plausible, never exceeding the cell thickness at experimental flow rates. However, assumption of such a low value of  $f_s$  should also cause the theoretical current to differ significantly from the observed value. The inviscid flow model with sample filling the entire channel width slightly overestimated experimental absorbance (Figure 4B). Thus there is evidence suggestive of the possible role of sheath flow, but additional experiments are needed. In any case, the flow conditions in the SEFC affected both current and absorbance flow exponents similarly.

Thus, the flow dependence of the absorbance response was more consistent with developing or stagnating than with fully developed laminar flow. The ferrocyanide concentration of 1.2 mM was high enough to provide an adequate S/N, such that the  $U^{-0.492}$  dependence measured for absorbance in this cell can confidently be attributed to flow characteristics and not poor S/N as were some measurements with the FOTL-SEFC. In the latter case, current response was always very close to the predicted cube root flow dependence for laminar flow, but the absorbance response, for low concentrations with poor S/N ratios, in some cases showed a greater flow dependence (Table II), which could be largely accounted for by experimental uncertainty and nonidealities.

Additionally, the background absorbance in this developing or stagnating flow cell tended to drift toward larger values after repeated injections. Rapidly cycling the injector two to three times resulted in a sudden drop in the background absorbance to the original value, indicating the presence of stagnation zones within the cell, which were perturbed by the turbulence accompanying the momentary pressure pulse when flow stopped during the injector cycling. In contrast, neither a drifting background nor a square root flow dependence was observed with the fully developed laminar flow FOTL-SEFC, presumably because the 2-mm distances between the working electrode and the inlet and outlet ports were sufficient to allow full development of laminar flow conditions and to avoid stagnation zones in the measurement region. These results indicate that the cell must be carefully designed to ensure the proper flow characteristics.

These results also provide insight into the diversity of conclusions (8) concerning cube root vs square root dependence on flow rate in electrochemical flow detectors under steady-state conditions. Weber and co-workers have shown clearly (8, 11, 13), and our results agree, that cube root dependence is to be expected if fully developed laminar flow is achieved (9). Weber et al. present arguments that the entrance length for flow development should be negligible for detectors of dimensions such as investigated here (8, 11, 13). However, geometries analogous to our developing flow cell, having the electrode completely covering one wall of the channel, are found in several of the papers cited by Weber (8) as reporting square root dependence, although in some cases inadequate data analyses were also used. If the electrode does not com-

pletely cover one channel wall, with adequate entrance and exit zones and no stagnation zones, the estimates of Weber et al. regarding required entrance length are likely to be valid (8, 11, 13).

**Reactant vs Product Absorption.** *Product Absorption.* Calibration curves for product absorption were carried out by using the fully developed laminar flow FOTL-SEFC, with a 50- $\mu$ L injection loop, a flow rate of 0.17 mL/min, and reactant ferrocyanide concentrations ranging from 2.10 to 0.420 mM. The response for these low injection volumes was significantly less than for the steady-state studies, because axial dispersion in the flow stream prevented attainment of the limiting steady-state concentrations. These curves yielded a linear current/concentration response with a sensitivity (slope) of  $5.72 \pm 0.1 \mu\text{A}/\text{mM}$  and an intercept of  $1.0 \pm 0.5 \mu\text{A}$ . The absorbance/concentration response had a sensitivity of  $0.0049 \pm 0.0001$  absorbance unit/mM and an intercept of  $0.0014 \pm 0.0005$  absorbance unit at a wavelength of 418 nm. The absorbance S/N measured peak to peak on the strip chart recorder was 6 for the 0.42 mM injection, indicating a detection limit of ca. 0.2 mM based on absorbance measurements, while current has been easily measured at nanoampere levels, indicating several orders of magnitude lower detection limits.

A calibration curve for ferrocyanide at 0.33 mL/min yielded a current/concentration slope of  $3.55 \pm 0.1 \mu\text{A}/\text{mM}$  and an absorbance-concentration slope of  $0.0021 \pm 0.0001$  absorbance unit/mM. Since the diffusion layer thickness of the product decreases with increasing flow rate, slow flow rates are best when only the product absorbs, to allow the absorber to diffuse into a larger volume of the flow cell. Even though the sensitivity for product absorbance is poorer than that desired for trace analyses, it is vastly greater than achievable conventionally, since the injected species, ferrocyanide, does not absorb at 418 nm. In addition, the sensitivity is much superior to that obtainable for a more conventional SEFC, using an optically transparent working electrode and very short optical path length. It can be shown that the ratio of absorbance measured perpendicular to the electrode over absorbance measured parallel to the electrode is in the ratio of optical path lengths,  $b/W_c$ , yielding a response for perpendicular illumination only 5% as large as for parallel illumination, ensuring a 20-fold worse detection limit for perpendicular illumination.

*Reactant Absorption.* Calibration curves, using a flow rate of 0.33 mL/min, were obtained for potassium ferricyanide reactant solutions both with and without a potential applied to the cell, to assess the change in absorbance resulting from the conversion of an absorbing reactant to a nonabsorbing product. With no electrochemical reaction occurring, the slope of the absorbance-concentration line was  $0.088 \pm 0.001$  absorbance unit/mM, with an intercept of  $0.005 \pm 0.002$  absorbance unit. The slope changed to  $0.094 \pm 0.002$  absorbance unit/mM when reduction of ferricyanide occurred in the cell. The change in absorbance from the bulk value at any concentration due to reduction of ferricyanide was only slightly larger than the standard deviations of the measurements. The detection limit, based on the experimental absorbance data, is ca. 20  $\mu\text{M}$ , an order of magnitude better than for ferrocyanide, where the product absorbed. These results are due to the nature of a thin-layer amperometric cell, in which only a small fraction of the material in the cell diffuses to the electrode surface and reacts during the analyte residence time in the cell. The slope of the current-concentration line was  $3.72 \pm 0.1 \mu\text{A}/\text{mM}$ , with an intercept of  $0.9 \pm 0.3 \mu\text{A}$ .

Though the absorbance becomes difficult to measure at the higher flow rates and/or lower concentrations, especially when only the product absorbs, it is important to note that the overall sensitivity for absorbance where only the product

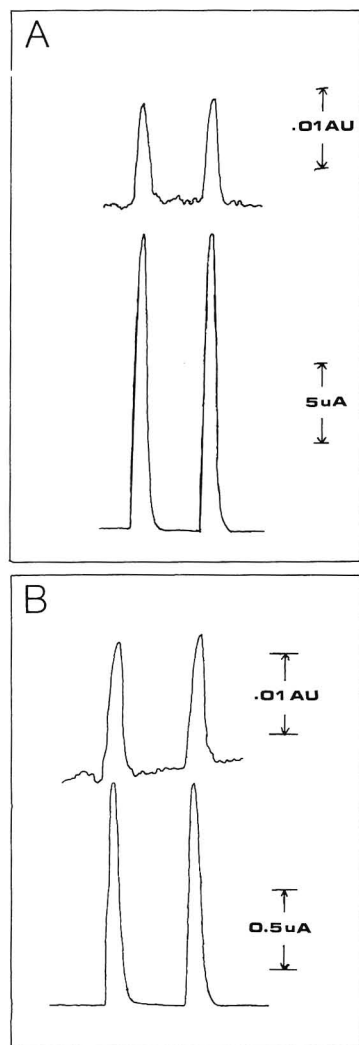


**Figure 5.** FOTL-SEFC flow injection amperometric and optical response under laminar flow conditions, injection volume 50  $\mu$ L: (A) ferricyanide produced by oxidation of 2.10 mM ferrocyanide, flow rate 0.17 mL/min; (B) 0.18 mM ferricyanide during reduction to ferrocyanide, flow rate 0.33 mL/min.

absorbs depends on  $\epsilon_p W_c C_R^*$ , where  $\epsilon_p$  is the molar absorptivity of the product,  $C_R^*$  is the initial concentration of the reactant, and  $W_c$  is the path length. It should be noted that the molar absorptivity of ferricyanide ( $\epsilon = 1023 \text{ M}^{-1} \text{ cm}^{-1}$ ) is not particularly large. Numerous species exist for which product absorbance could be measured successfully at reactant concentrations of 100  $\mu$ M, and the strongest absorbers ( $\epsilon \approx 10^5$ ) should provide measurable absorbance at 10  $\mu$ M. Higher values of  $\epsilon_p$  would increase the sensitivity of the detector, though nonlinear absorbance-concentration response may result due to saturation effects at high concentrations (7). Detection limits for reactant absorbance would be expected

to be ca. 10-fold lower than for product. Presumably better detection limits could also be achieved by using an optical flow detector optimized for low noise, such as found in commercial HPLC detectors.

**Correlation Detection.** A correlation detector based on coupled electrochemical and spectrometric measurements can have at least four distinct modes of operation. The presence of an absorber (either reactant or product) with an adequate absorbance at the appropriate wavelength could be used to "gate" a current measurement, i.e., to determine whether the sample is considered for detection. Alternatively, the presence of a faradaic current could be used to "gate" an absorbance measurement (or an entire spectrum if a scanning spectrometer is used). In a third mode, the product of absorbance and current measurements,  $A_i$ , can be shown to be proportional to  $(C_R^*)^2$ , and to a first approximation, independent of flow rate. If a coeluting species interferes with one of the signals, deviations could be easily detected. Finally, the ratio of absorbance to concentration (or vice versa) can be used to assess identity, independent of sample concentration with the disadvantage that the ratio has a marked dependence on flow rate. The primary shortcoming of a spectroelectrochemical correlation detector based on product absorption is the lower sensitivity provided in the absorbance measurements when only the product absorbs. If the reactant absorbs, or the chromophoric group is not affected by the electrochemical reaction, e.g., if  $\epsilon_p = \epsilon_R$ , the sensitivity is much less a problem, and the approach has significant practical utility.

## CONCLUSIONS

In summary, spectroelectrochemical measurements with a long optical path in a thin-layer flow channel are feasible. Experimental results are in accord with theoretical expectations. The coupling of optical and amperometric measurements allows confirmation that either fully developed or developing or stagnating laminar flow can be observed in a thin-layer channel of typical dimensions, depending on the placement of the electrode relative to the leading and trailing edges of the channel. Flow injection experiments confirm the feasibility of correlation measurements by using both optical and electrochemical signals. The highest sensitivity will be achieved for a correlation detector in which the reactant absorbs significantly, although optical signals not originally present in the sample can be generated when the product absorbs.

## LITERATURE CITED

- (1) Anderson, C. W.; Halsall, H. B.; Heineman, W. R. *Anal. Biochem.* **1979**, *93*, 366-372.
- (2) Condit, D. A.; Herrera, M. E.; Stankovich, M. T.; Curran, D. J. *Anal. Chem.* **1984**, *56*, 2909-2914.
- (3) Zak, J.; Porter, M. D.; Kuwana, T. *Anal. Chem.* **1983**, *55*, 2219-2222.
- (4) Brewster, J. D.; Anderson, J. L. *Anal. Chem.* **1982**, *54*, 2560-2566.
- (5) Porter, M. D.; Kuwana, T. *Anal. Chem.* **1981**, *53*, 529-534.
- (6) Pinkerton, T. C.; Hajizadeh, K.; Deutsch, E.; Heineman, W. R. *Anal. Chem.* **1980**, *52*, 1542-1544.
- (7) Fosdick, L. E.; Anderson, J. L. *Anal. Chem.*, preceding paper in this issue.
- (8) Weber, S. G. *J. Electroanal. Chem.* **1983**, *145*, 1-7.
- (9) Fosdick, L. E.; Anderson, J. L.; Baginski, T. A.; Jaeger, R. C. *Anal. Chem.* **1986**, *58*, 2750-2756.
- (10) Anderson, J. L. *Anal. Chem.* **1979**, *51*, 2312-2315.
- (11) Elbicki, J. M.; Morgan, D. M.; Weber, S. G. *Anal. Chem.* **1984**, *56*, 978-985.
- (12) Levich, V. G. *Physicochemical Hydrodynamics*, Prentice-Hall: Englewood Cliffs, NJ, 1962; p 91.
- (13) Weber, S. G.; Purdy, W. C. *Anal. Chim. Acta* **1978**, *100*, 531-544.
- (14) Brewster, J. D.; Anderson, J. L., unpublished work.

RECEIVED for review April 6, 1987. Accepted October 1, 1987. This work was funded in part by the National Science Foundation, Grant Number CHE-8600224. L. E. Fosdick also acknowledges a University of Georgia University-wide Graduate Nonteaching Assistantship.



# X-ray Photoelectron Spectroscopy of Silica Surfaces Treated with Polyfunctional Silanes

Krishna M. R. Kallury, Ulrich J. Krull, and Michael Thompson\*

Department of Chemistry, University of Toronto, 80 St. George Street, Toronto, Ontario M5S 1A1, Canada

**Results of X-ray photoelectron spectroscopic studies on the surface of silicon wafers silanized with dichlorodimethylsilane, methyltrichlorosilane, ((glycidyloxy)propyl)trimethoxysilane, (aminopropyl)triethoxysilane, *tert*-butyldimethylchlorosilane, and the 12-dichloromonomethylsilyl and 12-monochlorodimethylsilyl ethers of methyl 12-hydroxydodecanoate are reported. The upward shift in the Si (2p) binding energies (by 0.5 eV) of surface silicons treated with silylating agents in the presence of Et<sub>3</sub>N was attributed to hydroxyl functionalities on these atoms. The extent of surface coverage was computed from the surface Si:substrate Si ratios. Large differences in reactivities of the silylating agents were observed in the presence or absence of the base catalyst.**

Silylation of various types of surface with chloro- and alkoxy silanes has been utilized during the last two decades as a method to enhance the applicability of the appropriate surfaces in a number of areas (1-4). Such treatments have also been extended to chromatographic materials like silica to produce modified adsorbent surfaces for specific applications (5-7). In recent years, carbofunctional silanes have been used to immobilize biomolecules (1, 8, 9). Furthermore, this method is the basis for recent attempts at achieving sites for molecular recognition through the so-called template approach (10, 11).

Several reports (6, 12-19) have appeared in recent years on the characterization of silica and other metal oxide surfaces treated with silanizing agents by techniques such as X-ray photoelectron spectroscopy (XPS), X-ray fluorescence (XRF), NMR, ESR, and IR. However, ambiguity still exists regarding the structure of products obtained by treating hydroxylated surfaces with multifunctional silanes. Kinetic studies (20) indicate that the stoichiometry of this reaction is 1.5-1.6 with respect to the number of surface hydroxyls reacting with one molecule of a di- or trihalo/alkoxy silane. However, published reports depict surface species from such reactions as possessing structures resulting from bi- or trimolecular stoichiometry (5, 21). Kinkel and Unger (22) have investigated the role of solvent and base catalysts in the silanization of silica with monofunctional silanes and found that the solvent exerts a more pronounced effect than the base. However, the base enhances the surface coverage even at lower temperatures compared to the uncatalyzed silanizations. Furthermore, the rate of addition and base catalysis also affect surface density as observed during silanizations with binary silylating agent mixtures (6).

We have been investigating the possibilities of binding lipid molecules covalently to silica surfaces through silylation reactions for the purpose of developing selective chemical sensors (23). In this connection, we examined the reactivity of some di- and trichloro/alkoxy silanes with silica under base-catalyzed and noncatalytic conditions to assess the effect of base on the extent of surface coverage and the nature of surface species formed. The results of these studies are presented in the present paper.

## EXPERIMENTAL SECTION

**Materials and Reagents.** Dichlorodimethylsilane (DCDMS), methyltrichlorosilane (MTCS), *tert*-butyldimethylchlorosilane

(BDMCS), ((glycidyloxy)propyl)trimethoxysilane (GOPMS), and (aminopropyl)triethoxysilane (APTES) were obtained from commercial sources (Aldrich) and purified by distillation under nitrogen (for low boiling silanes) or under vacuum (for GOPMS and APTES). The oxide-coated silicon wafers used in the current studies were supplied by the Avrel Co., St. Charles, MO. These possess the following specifications: orientation type, N(100)C<sub>2</sub>; thickness, 0.017 mm; resistivity, 4  $\Omega$ /cm; diameter, 2 in. (5.03 cm). The thickness of the oxide layer was determined by ellipsometry to be about 1100 Å.

**Preparation of 12-((Chlorodimethylsilyl)oxy)dodecanoic Acid Methyl Ester (1) and 12-((Dichloromethylsilyl)oxy)-dodecanoic Acid Methyl Ester (2).** A mixture of methyl 12-hydroxydodecanoate (24) (0.1 mol) and imidazole (0.1 mol) in dry dimethylformamide (DMF) (10 mL) was treated with the appropriate chlorosilane (DCDMS for 1 and MTCS for 2) in DMF solution by dropwise addition at room temperature under nitrogen. The mixture was stirred for a further 24 h. The solvent and excess silylating agent were removed under vacuum. The residue was extracted with CCl<sub>4</sub>, the solution filtered to remove imidazole, and the filtrate concentrated under vacuum to give 1 and 2 in 70-80% yields.

**Surface Reactions.** The silicon wafers were initially refluxed with dry chloroform under nitrogen for 3 h to remove adsorbed hydrocarbon material. The solvent was removed under vacuum and the wafers washed with dry acetone twice before being vacuum dried. The cleaned wafer is refluxed with a solution of 100 mg of the silylating agent in 10 mL of dry toluene under nitrogen for 3 h. In experiments where silylation was done under basic conditions, 0.1 mL of triethylamine (TEA) was added to the mixture prior to refluxing. The solvent was decanted off at the conclusion of the reaction, and the wafer was successively washed several times with chloroform, acetone, and methanol and finally vacuum dried.

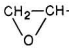
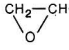
**XPS Measurements.** These were carried out at the Surface Science Lab, University of Western Ontario, London, Canada, on an SSX-100 ESCA Spectrometer with monochromatic Al K $\alpha$  radiation. The sample X-ray source geometry was such that the take-off angle was 55°. Photoelectron spectra were obtained by utilizing 20 scans over a 1000-eV binding energy range. The Si (2p) and C (1s) peaks were deconvoluted on a Hewlett-Packard computer 9836. The N (1s) peaks were also similarly deconvoluted, where applicable.

**Measurement of FTIR Spectra.** The infrared spectra of silicon wafers, treated first with APTES in the presence of TEA and then with monomethyl ester of nonanedioic acid, were recorded on a Nicolet 5-DX FTIR instrument while using a reflectance cell.

## RESULTS AND DISCUSSION

The Si (2p) and C (1s) binding energies along with those for substrate (wafer) silicon (2p) values of wafers treated with various silylating agents are presented in Table I. The binding energies for the substrate remain more or less constant irrespective of the nature of the silylating agent and presence/absence of base. On the other hand, the Si (2p) binding energies of the surface silicon atoms are higher by ~0.5 eV for surface species obtained under base-catalyzed conditions with (aminopropyl)triethoxysilane (APTES) and dichlorodimethylsilane (DCDMS). Surprisingly, the trimethoxysilane-treated wafers exhibit the same Si (2p) binding energy values irrespective of the presence or absence of base. Furthermore, with methyltrichlorosilane (MTCS), the binding energy values of Si (2p) are the same under both sets of

Table I. Binding Energies of Silicon (Substrate and Surface), Carbon, and Nitrogen Atoms from XPS on Silanized Surfaces

reagent	surface Si (2p), eV	substrate Si (2p), eV	C (1s), eV	N (1s), eV
Me <sub>2</sub> SiCl <sub>2</sub>	102.3 (100%)	103.9	285.4 (100%)	
Me <sub>2</sub> SiCl <sub>2</sub> /Et <sub>3</sub> N	103.1 (66%) 102.0 (33%)	104.0	285.4 (86%) 286.6 (14%)	
MeSiCl <sub>3</sub> /Et <sub>3</sub> N	102.9 (92%) 101.7 (8%)	103.8	285.2 (70%) 286.8 (30%)	
MeSiCl <sub>3</sub>	102.8 (100%)	103.8	285.6 (60%) 286.9 (40%)	
H <sub>2</sub> N(CH <sub>2</sub> ) <sub>3</sub> Si(OEt) <sub>3</sub>	102.4 (100%)	103.9	285.1 (66%) 286.2 (22%) 287.1 (12%)	399.9 (15%) 401.8 (85%)
H <sub>2</sub> N(CH <sub>2</sub> ) <sub>3</sub> Si(OEt) <sub>3</sub> /Et <sub>3</sub> N	102.9 (100%)	103.8	285.9 (50%) 286.9 (35%) 287.7 (10%) 288.8 (5%)	400.3 (43%) 402.3 (57%)
MeOOC(CH <sub>2</sub> ) <sub>10</sub> COOH + wafer treated with H <sub>2</sub> N(CH <sub>2</sub> ) <sub>3</sub> Si(OEt) <sub>3</sub> /Et <sub>3</sub> N	102.5 (65%) 103.1 (35%)	103.8	285.5 (57%) 286.5 (24%) 287.7 (11%) 288.8 (9%)	400.4 (77%) 401.7 (23%)
 CH <sub>2</sub> —CH—CH <sub>2</sub> O(CH <sub>2</sub> ) <sub>3</sub> Si(OMe) <sub>3</sub>	102.5 (100%)	103.8	285.8 (15%)	
 CH <sub>2</sub> —CH—CH <sub>2</sub> O(CH <sub>2</sub> ) <sub>3</sub> Si(OMe) <sub>3</sub> , and Et <sub>3</sub> N	102.5 (100%)	103.9	286.7 (86%) 286.0 (30%)	
MeOOC(CH <sub>2</sub> ) <sub>10</sub> CH <sub>2</sub> OSiMe <sub>2</sub> Cl	102.5 (100%)	104.0	286.7 (70%) 284.8 (76%) 285.6 (24%)	
MeOOC(CH <sub>2</sub> ) <sub>10</sub> CH <sub>2</sub> OSiMe <sub>2</sub> Cl/Et <sub>3</sub> N	103.0 (100%)	103.9	285.0 (71%) 286.0 (22%) 287.1 (7%)	
MeOOC(CH <sub>2</sub> ) <sub>10</sub> CH <sub>2</sub> OSiMeCl <sub>2</sub>	102.5 (100%)	103.8	285.4 (70%) 286.6 (18%) 288.8 (4%)	
<i>t</i> -BuMe <sub>2</sub> SiCl	102.5 (100%)	103.9	285.7 (70%) 287.0 (30%)	

conditions, but are in the range of values obtained for APTES and DCDMS under base-catalyzed conditions. Moreover, with DCDMS and MTCS, an additional Si (2p) signal is recorded under base-catalyzed conditions whose binding energy is ~1.0 eV lower than the more intense Si (2p) peak.

The binding energy values of the surface silicon atoms derived from the monochlorosilanes BDMCS and methyl 12-(chlorodimethylsilyloxy)dodecanoate (102.5 eV for both) are close to the reported value of 102.4 eV for surface silicon atoms formed from mono or multifunctional silanes (13, 14). The Si (2p) binding energies of surface silicon atoms derived from DCDMS, GOPMS, and APTES under noncatalytic conditions are also close to 102.4 eV. Therefore, the surface species formed from both the mono- and multifunctional silanes under noncatalytic conditions in the present study seem to possess similar electronic environments. That means that chain branching (as in BDMCS) or a long straight-chain carrying a functional group at the terminus (as in methyl 12-(chlorodimethylsilyloxy)dodecanoate or aminopropyl as in APTES or (glycidyloxy)propyl as in GOPMS) does not alter the surface Si (2p) binding energies significantly. Furthermore, since the three multifunctional silanes mentioned above do not differ much from the monofunctional silanes in their Si (2p) binding energy values, there do not appear to be any dangling chloro or alkoxy moieties on the surface silicon atoms. Alternately, the effect of additional silicon-bound oxygen atoms on the binding energies of surface silicon atoms seems to be negligible.

The upward shift of the Si (2p) binding energies of surface silicon atoms under base-catalyzed conditions with DCDMS, MTCS, and APTES (also under noncatalytic conditions for MTCS) must be attributed to a species that exhibits greater delocalization of the valence electrons of silicon. Such a delocalization can occur in silanols through  $d\pi-p\pi$  interactions,

which make the hydroxylic hydrogen more acidic than the corresponding atom in a carbinol, as observed in solution organosilicon chemistry (25). Accordingly, under base-catalyzed conditions, the surface silicon species formed carries at least one hydroxyl moiety, while under noncatalytic conditions, condensation of the silanol to siloxane structure is rapid and complete (Figure 1a). In fact, results from solution chemistry indicate that silanols can be isolated by the hydrolysis of halo- or alkoxy silanes in inert solvents in the presence of bases such as pyridine and tetraethylammonium hydroxide (25).

Hydrogen bonds formed by silanols with a number of functional groups are known to be very strong. The shift of the Si (2p) peak from 102.5 eV under noncatalytic conditions to 103.0 eV under the catalytic influence of base with 12-((chlorodimethylsilyl)oxy)dodecanoic acid methyl ester is consistent with the formation of such bonds (see Figure 1b) and lends support to the argument put forth above to explain the upward shift of Si (2p) peaks under base catalysis. Part of reagent 1 is hydrolyzed in the presence of the base and the resulting silanol binds to the ether group of the surface-bound silane. It should be noted that the Si (2p) binding energy of the substrate remains the same under both reaction conditions employing 1, indicating that the substrate hydroxyl groups are not involved in this bonding. The low yield of the surface product from 1 is accounted for by the loss of reagent through selfcondensation of the silanol intermediate to siloxane in part, the latter being washed out during the postsilanization treatment.

Additional support for the hypothesis of stable silanol formation under base catalysis stems from the reaction of nonanedioic acid monomethyl ester with the surface species formed from APTES. While the Si (2p) binding energy value of the surface silicon from APTES under base catalysis is 102.9

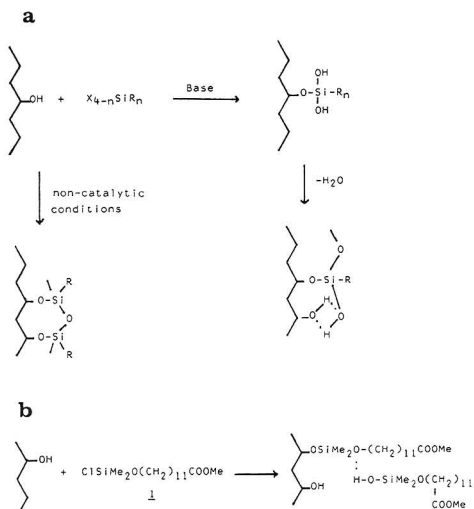


**Figure 1.** (a) Reaction of multifunctional silanes with oxidized silicon surfaces under base-catalysis/noncatalytic conditions. (b) Reaction of methyl 12-((monochlorodimethylsilyl)oxy) dodecanoate (**1**) with silicon surface under base-catalysis.

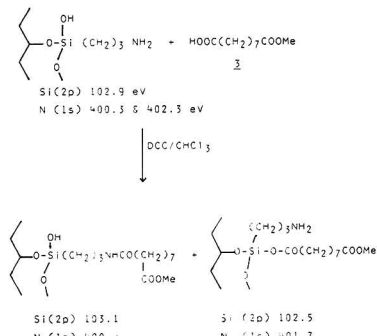


**Figure 2.** Reaction of monomethylazolate with silicon wafer treated with (aminopropyl)triethoxysilane under base catalysis.

eV, treatment with the above mono ester of this same surface species results in two Si (2p) peaks at 102.5 eV and 103.1 eV. These two Si (2p) peaks correspond to the two different silicons obtained by reaction of the amino or the silanol group of the surface species as shown in Figure 2. The two different carbonyls shown in Figure 2 are supported by the fact that reflectance IR of the surface species contains two peaks at 1730 and 1665  $\text{cm}^{-1}$  corresponding to the ester and amide carbonyl moieties, respectively, in addition to the COOMe carbonyl at 1750  $\text{cm}^{-1}$ .

The postulation of stable silanol structures under the influence of base is further supported by the N (1s) binding energies of the product species obtained with APTES. An upward shift of 0.5 eV is noticed for the bonded N (1s) peak in moving from noncatalyzed to base-catalyzed conditions (see Table I), again indicative of strong intramolecular H bonding between the silanol hydrogen and amine nitrogen under the base-catalyzed conditions. An interesting observation is that when the wafer silanized with APTES in the presence of base is treated with the monomethyl ester of nonanedioic acid, the ratio of H-bonded to nonbonded N (1s) peak intensities be-

**Table II.** Surface Si:Substrate Si Ratios from Silanization Reactions (Derived from XPS Data)

reagent	Si <sub>surface</sub> :Si <sub>substrate</sub> (wafer) (atom %)
Me <sub>2</sub> SiCl <sub>2</sub>	1:4
Me <sub>2</sub> SiCl <sub>2</sub> /Et <sub>3</sub> N	1:2 (higher binding energy)
	1:4 (lower binding)
MeSiCl <sub>3</sub>	1:1
MeSiCl <sub>3</sub> /Et <sub>3</sub> N	1:2 (higher binding energy)
	1:20 (lower binding energy)
H <sub>2</sub> N(CH <sub>2</sub> ) <sub>3</sub> Si(OEt) <sub>3</sub>	9:1
H <sub>2</sub> N(CH <sub>2</sub> ) <sub>3</sub> Si(OEt) <sub>3</sub> /Et <sub>3</sub> N	4:1
GOPMS	1:3
GOPMS/Et <sub>3</sub> N	4:1
MeOOC(CH <sub>2</sub> ) <sub>10</sub> CH <sub>2</sub> OSiMe <sub>2</sub> Cl	1:7
MeOOC(CH <sub>2</sub> ) <sub>10</sub> CH <sub>2</sub> OSiMe <sub>2</sub> Cl/Et <sub>3</sub> N	1:7
MeOOC(CH <sub>2</sub> ) <sub>10</sub> CH <sub>2</sub> OSiMeCl <sub>2</sub>	1:9
<i>t</i> -BuMe <sub>2</sub> SiCl	1:6
H <sub>2</sub> N(CH <sub>2</sub> ) <sub>3</sub> Si(OEt) <sub>3</sub> and then MeOOC(CH <sub>2</sub> ) <sub>7</sub> COOH	9:1

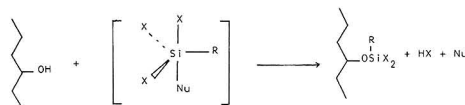


**Figure 3.** Nucleophilic substitution mechanism for surface silanization reactions: Nu = H<sub>2</sub>O for noncatalytic reactions, H<sub>2</sub>N(CH<sub>2</sub>)<sub>3</sub>- for APTES; Nu = Et<sub>3</sub>N for base-catalyzed reactions.

comes 1:3, while for the original wafer the same ratio is about 3:2. The Si (2p) ratio of 2:1 between non-silanol versus silanol type silicon in the monomer treated product is also in agreement with the above N (1s) ratio indicating that both the silanol and amine functions are modified by reaction with the monomethyl ester.

The differences in reactivity between the trimethoxysilane GOPMS and the triethoxysilane APTES, discernable from the surface Si:substrate Si ratios (see Table II), can be attributed to the difference in their rates of hydrolysis. Trimethoxysilane is known (26) to be much more readily hydrolyzed than triethoxysilane in benzene solution upon treatment with a limited quantity of water. Therefore, chances for siloxane formation by cross-linking are greater for the methoxy silane in comparison with the competing surface silanization, which probably proceeds by the S<sub>N</sub>2 mechanism. A similar mechanism was proposed by Kinkel and Unger earlier for surface silanizations (22). The amino group in APTES, on the other hand, may serve as a nucleophile (or base) by itself in aiding the proton abstraction from the substrate silanol (see Figure 3). Thus, due to the slower hydrolysis rate coupled with the reactivity of the amine function, APTES is more effective towards surface silanization under noncatalytic conditions than GOPMS, as reflected by the respective surface Si:substrate Si ratios (Table II). When triethylamine (TEA) is used as a base, the reactivity of both alkoxy silanes becomes the same and the surface Si:substrate Si ratios become equal (see Table II). This is due to the fact that TEA is a stronger base (and nucleophile) than the primary amine in APTES and controls the rate of substitution in both cases. However, H-bonding between TEA and the silanol function (as well as the amino group) can occur in the case of APTES under base catalysis thereby reducing the efficiency of TEA as a nucleophile. Therefore, surface coverage is reduced for APTES under the base catalysis conditions compared to noncatalytic treatment. Since GOPMS does not form stable silanol structures, TEA enhances the rate of the surface reaction.

The same argument holds good for methyltrichlorosilane (MTCS). With this silane, however, the hydrolysis is more

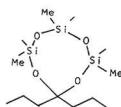


Figure 4. Cyclic siloxane formation with DCDMS and MTCS (Si (2p)  $101.9 \pm 0.1$  eV).

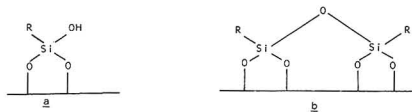


Figure 5. Surface species (major) under base-catalyzed and noncatalytic conditions: (a) under base catalysis; (b) under noncatalytic.

rapid in the presence of a base (27) and hence siloxane formation is more prevalent under base catalysis as reflected by the lower surface Si:substrate Si ratio under these conditions. It is known (28) that the rate of hydrolysis of successive chlorines in MTCS is 1.0:0.2:0.1 under neutral conditions and hence formation of a stable silanol can be expected with this reagent even under neutral conditions, which explains the higher binding energy for the Si (2p) peak under these conditions.

The lower energy Si (2p) peaks observed with surfaces treated with the chlorosilanes MTCS and DCDMS can be attributed to siloxane structures (Figure 4) formed by the reaction of the halogens with substrate centers possessing geminal hydroxyls. This explanation is consistent with the fact that this lower energy peak is more intense for DCDMS than for MTCS due to lesser steric hindrance.

Our results are in good agreement with those of De Haan and co-workers (29) as well as Sindorf and Maciel (18) who have investigated silanization of silica surfaces by solid-state NMR. Both these groups initially observed single surface-to-silane attachment under anhydrous conditions, but higher temperatures and/or exposure to air gradually enhanced the siloxane  $^{29}\text{Si}$  NMR signal. In particular, De Haan et al. (29) have attributed the two principal signals in their  $^{29}\text{Si}$  NMR spectra to structures a and b (Figure 5) formed under anhydrous conditions initially and upon exposure to air subsequently, respectively. The only difference between our results and those of these authors is that under our conditions free hydroxyls (as in a, Figure 5) are stabilized only in the presence of base catalyst (with the exception of MTCS) and under

noncatalytic conditions complete dehydration to b (Figure 5) occurs.

**Registry No.** 1, 111268-11-2; 2, 111268-10-1; DCDMS, 75-78-5; MTCS, 75-79-6; GOPMS, 2530-83-8; APTES, 919-30-2; BDMCS, 18162-48-6;  $\text{Et}_3\text{N}$ , 121-44-8; Si, 7440-21-3.

## LITERATURE CITED

- (1) Chvalovsky, V. In *Carbon-Functional Organosilicon Compounds*; Chvalovsky, V., Bellama, J. M., Eds.; Plenum: New York, 1984; pp 2-34.
- (2) Murray, R. W. In *Electroanalytical Chemistry*; Bard, A. J., Ed.; Marcel Dekker: New York, 1984; Vol. 13, pp 191-368.
- (3) Elwing, H.; Ivarsson, B.; Lundström, I. *Eur. J. Biochem.* **1986**, *156*, 359.
- (4) Huang, M. et al. In *Organosilicon and Biorganosilicon Chemistry*; Sakurai, H., Ed.; Horwood: Chichester, U.K., 1985.
- (5) Tundo, P.; Venturello, P.; Angelletti, E. *Isr. J. Chem.* **1985**, *26*, 283.
- (6) Hannicutt, M. L.; Harris, J. M. *Anal. Chem.* **1986**, *58*, 748.
- (7) Williams, D. E.; Tangney, T. J.; In *Chemically Modified Surfaces*; Leyden, D. E., Ed.; Gordon and Breach: New York, 1986.
- (8) Shiraiishi, S.; Komiya, M.; Hirai, H. *Bull. Chem. Soc. Jpn.* **1986**, *59*, 507.
- (9) Hayward, J. A. and co-workers *Biomaterials* **1986**, *7*, 121, 126, 252.
- (10) Wulff, G.; Heide, B.; Hellmeier, G. *J. Am. Chem. Soc.* **1986**, *108*, 1089.
- (11) Shea, J.; Dougherty, T. K. *J. Am. Chem. Soc.* **1986**, *108*, 1091.
- (12) Cukman, D.; Jednacak-Biscan, J.; Vekslil, Z.; Haller, W. *J. Colloid Interface Sci.* **1987**, *115*, 357.
- (13) Moses, P. R.; Wier, L. M.; Lennox, J. C.; Finklea, H. O.; Lenhard, J. R.; Murray, R. W. *Anal. Chem.* **1978**, *50*, 576.
- (14) Willmann, K. W.; Rocklin, R. D.; Nowak, R.; Kuo, K. N.; Shultz, F. A.; Murray, R. W. *J. Am. Chem. Soc.* **1980**, *102*, 7629.
- (15) Hair, M. L.; Hertl, W. *J. Phys. Chem.* **1969**, *73*, 2372.
- (16) Puglisi, O.; Torris, A.; Marletta, G. *J. Non-Cryst. Solids* **1984**, *68*, 219.
- (17) Ratner, B. D.; Rosen, J. J.; Hoffman, A. S.; Scharpen, L. H. In *Surface Contamination*; Mittal, K. L., Ed.; Plenum: New York, 1979.
- (18) Sindorf, D. W.; Maciel, G. E. *Anal. Chem.* **1983**, *105*, 3767.
- (19) Kelusky, E. C.; Fyfe, C. A. *J. Am. Chem. Soc.* **1986**, *108*, 1746.
- (20) Buzek, F.; Rathousky, J. *J. Colloid Interface Sci.* **1981**, *79*, 47.
- (21) Netzer, L.; Isovici, R.; Sagiv, J. *Thin Solid Films* **1983**, *99*, 235.
- (22) Kinkel, J. N.; Unger, K. K. *J. Chromatogr.* **1984**, *316*, 193.
- (23) Kallury, R. K. M. R.; Krull, U. J.; Thompson, M. J. *Org. Chem.*, in press.
- (24) Mohanraj, S.; Ford, W. T. *J. Org. Chem.* **1985**, *50*, 1616.
- (25) Eaborn, C. *Organosilicon Compounds*; Academic: New York, 1960; Chapter 8.
- (26) Sprung, M. M.; Guenther, F. O. *J. Am. Chem. Soc.* **1955**, *77*, 3990, 3996, 4173.
- (27) Andrianov, K. A.; Vasil'eva, T. V.; D'yachenko, B. I.; Simanovskaya, E. I.; Molchanov, B. V.; Golubtsov, S. A. *Izv. Akad. Nauk SSSR, Ser. Khim.* **1973**, 76.
- (28) Bazant, V.; Chvalovsky, V.; Rathousky, J. *Chemistry of Organosilicon Compounds*; Academic: New York, 1965; p 51.
- (29) De Haan, J. W.; Van Den Bogaert, H. M.; Ponjse, J. J.; Van De Ven, L. J. M. *J. Colloid Interface Sci.* **1986**, *110*, 591.

RECEIVED for review May 22, 1987. Accepted September 14, 1987. We thank the Natural Sciences and Engineering Research Council of Canada and Allied-Signal, Canada, for financial support of this work.

# Evaluation of a Nitrosyl-Specific Gas-Phase Chemiluminescent Detector with High-Performance Liquid Chromatography

Albert Robbat, Jr.,\* Nicholas P. Corso, and Tyng-Yun Liu

Chemistry Department, Tufts University, Medford, Massachusetts 02155

**A gas-phase chemiluminescent detector (CD) used in conjunction with high-performance liquid chromatography (HPLC) has been evaluated. The detector responded linearly from 1000 ng to the detection limit for the nitrated polycyclic aromatic hydrocarbons tested. The relative molar response with respect to 2-nitronaphthalene was within 13%. HPLC with reversed-phase solvents under isocratic and gradient elution conditions is shown to be compatible with the CD.**

Of primary importance to analytical chemists is the ability to identify analytes in complex sample matrices. Often the analytes of interest are present at trace levels, with detection and quantification complicated by high levels of interfering components. Notwithstanding the continuing development of high-resolution gas and high-performance liquid chromatographic columns, the development of chromatographic detectors that are selective, sensitive and specific for a given analyte provides unmatched advantages over exhaustive sample cleanup procedures and universal detectors.

Chemical interactions which produce chemiluminescent optical responses are highly specific since relatively few compounds undergo chemiluminescent reactions. During the past decade, increasing attention has focused on developing chromatographic chemiluminescent optical detection systems (1, 2). Chemical analyses and, as important, sample cleanup prescreening methods based on chemiluminescent detection may be accomplished more easily since only sample components of interest will produce a signal response. In particular, chemiluminescent detectors based on the nitrosyl radical/ozone reaction have been used for the determination of nitrogen-containing organic compounds. Previously, we reported on the design, response, and analytical application of a gas chromatographic chemiluminescent detector (GC/CD) for the analysis of nitrated polycyclic aromatic hydrocarbons (nitro-PAH) (3). The GC/CD responded linearly between 0.050 and 1000 ng. The CD detection limit for most nitro-PAH was 50 pg at a S/N of 3. The detector responded on a mole of NO<sub>2</sub> per mole of compound basis for each nitro-PAH tested (within 8%). The GC/CD has been used to identify and quantify a number of nitro-PAH present in environmentally complex samples, for example, in organic fractions of diesel exhaust particulate matter and waste crankcase oil.

To date, high-performance liquid chromatography with gas-phase chemiluminescent detectors (HPLC/CD) have not been widely used. Reports have appeared in the literature for the determination of *N*-nitroso and other nitrogen containing organic compounds by HPLC/CD based on the nitrosyl radical/ozone chemiluminescent reaction (4-8). Results indicate that the presence of the mobile phase in the NO<sup>•</sup>/O<sub>3</sub> reaction chamber dramatically reduces the CD signal response as compared to GC/CD. For example, when reversed-phase HPLC solvents are employed, the CD signal response is about 5 orders of magnitude less sensitive than our GC/CD.

In the present investigation, the application of our gas-phase chemiluminescent detector with isocratic and gradient elution

**Table I. Comparison of Linear Response and Relative Molar Response of Nitro-PAH**

compd <sup>a</sup>	mol fract	slope	inter	corr	slope/ mol fract	RMR <sup>b</sup>
1,3-dnn	0.422	0.505	-8.34	0.999	1.20	0.98
1-nn	0.266	0.408	-3.86	0.999	1.53	1.24
2-nn	0.266	0.326	-0.03	0.999	1.23	1.00
2-nf	0.218	0.255	-4.29	0.999	1.17	0.95
9-na	0.206	0.206	-2.88	0.999	1.00	0.81
1-np	0.186	0.198	-5.12	0.999	1.07	0.87

<sup>a</sup> Compounds are 1,3-dnn = 1,3-dinitronaphthalene, 1-nn = 1-nitronaphthalene, 2-nn = 2-nitronaphthalene, 2-nf = 2-nitrofluorene, 9-na = 9-nitroanthracene and 1-np = 1-nitropyrene.

<sup>b</sup> The RMR (relative molar response) is based on the ratio of the slope and the mole fraction for each compound relative to the ratio of 2-nitronaphthalene.

high-performance liquid chromatography has been evaluated. The linear dynamic range, the detection limit, and the applicability of reversed-phase solvents are discussed.

## EXPERIMENTAL SECTION

HPLC grade acetonitrile (Fisher Scientific, Medford, MA) was used as received. Water was purified with the Milli-Q Water Purification System (Millipore, Milford MA). All solvents were filtered through a 0.45-μm Nylon-66 filter (Rainin, Woburn, MA) and ultrasonically vacuum degassed prior to use.

Nitro-PAH have been identified elsewhere and were used without further purification (9). Standard solutions were prepared by dissolving the appropriate amount of nitro-PAH in acetonitrile and then performing serial dilutions. The solvent delivery system consisted of a Constametric III pump, a Constametric I pump, and Gradient Master (LDC/Milton Roy, Riviera Beach, FL). A Rheodyne Model 7410 sample injection valve with an internal 2-μL sample loop was used for sample introduction onto the HPLC column. An ODS solvent miser, 25 cm × 2.1 mm, 5-μm particle size reversed-phase column (Alltech Associates, Deerfield, IL) was used.

The dynamic range was determined by using acetonitrile as the mobile phase at a flow rate of 0.2 mL/min. The effect of the mobile phase composition on the detection limit was determined by using acetonitrile and water at a flow rate of 0.2 mL/min. Linear gradient elution experiments were performed from 45/55 to 75/25 acetonitrile/water in 60 min at flow rates of 0.5 mL/min.

The chemiluminescence detector has been described previously (3). The HPLC column was connected to a 7-cm length of stainless steel tubing. The tubing was extended 5 cm into the quartz tubing (34 cm) housed in a pyrolysis oven at 900 °C. A glass solvent trap (100 mL) located at the exit port of the oven and before the CD system was maintained at -75 °C with a dry ice/acetone bath.

## RESULTS AND DISCUSSION

Isocratic HPLC/CD experiments were performed with acetonitrile as the mobile phase at a flow rate of 0.2 mL/min. The dynamic range of the CD for nitro-PAH was evaluated from 1000 ng to the detection limit. The CD responded linearly over the entire concentration range. Table I summarizes the CD response for the nitro-PAH studied. The detection limit for the mononitro-PAH investigated was about 30 ng while that for 1,3-dinitronaphthalene was 10 ng at a S/N of

**Table II. Linear Response and Detection Limits for 1-Nitronaphthalene at Different Mobile-Phase Compositions of Acetonitrile and Water**

% CH <sub>3</sub> CN	slope	inter	corr	detection limit, ng injected
100	0.408	-3.86	0.999	30
90	0.163	-13.20	0.999	30
80	0.090	-7.69	0.999	60
70	0.061	-10.80	0.995	70
60	0.044	-6.59	0.996	125
50	0.036	-5.30	0.997	250

3. In theory and as reported previously (3), the gas-phase chemiluminescent detector is molar responsive, i.e., the CD responds only to the moles of nitro groups per mole of nitro-PAH. Thus, for example, the detector achieves lower detection limits per compound injected for lower molecular weight mononitrated-PAH than higher molecular weight mononitrated-PAH. The HPLC/CD system responded similarly. This is evidenced by the decreasing slope with increasing molecular weight of mononitrated-PAH. Also shown in the table is the relative molar response for each compound relative to 2-nitronaphthalene. The experimental results are in agreement with theory within about 13%.

Isocratic experiments were performed with varying acetonitrile/water mobile phase composition to determine solvent effects on CD signal response. At a given concentration of 1-nitronaphthalene the signal detected at 50/50 acetonitrile/water was about 10 times less than that observed when the mobile phase was acetonitrile. The detection limit of the CD became worse as the percent water in the mobile phase increased. For example, the detection limit for 1-nitronaphthalene increased from 30 ng injected at 100% acetonitrile to 250 ng injected at 50/50 acetonitrile/water. Although the CD detection limit varied with percent acetonitrile, as shown in Table II, the CD responded linearly for all isocratic acetonitrile/water compositions examined. These findings indicate that at any given isocratic experimental condition, concentration calibration curves are not needed for each nitro-PAH measured.

The separation of 10 nitro-PAH by reversed-phase linear gradient HPLC/CD is shown in Figure 1; solvent ramp 45/55 to 75/25 acetonitrile/water over 60 min. The flow rate was 0.5 mL/min. Plots of chromatographic peak area versus analyte injected yielded linear dynamic ranges for these compounds between 70 and 1000 ng. The correlation coefficient in all cases was 0.998. For determination of many nitro-PAH in complex samples, gradient programmed HPLC yields the best separation. The results of this experiment indicate that the CD detection limit was only 2 times less sensitive than isocratic experiments performed in the absence of water. However, it is at least 15 times better than similar nitrosyl/ozone detectors reported in the literature for HPLC (4, 6). Previous attempts to use a NO<sup>+</sup>/O<sub>3</sub> CD in conjunction with solvent programming were unsuccessful due to gas-dynamic problems (10). Other researchers have indicated that the use of polar solvents, organic as well as aqueous, have resulted in NO<sup>+</sup>/O<sub>3</sub> detector instability, i.e., excessively high background noise (7, 11). In contrast, as can be seen in Figure 1, base line stability is achieved even at high mobile-phase water content, i.e., 50% H<sub>2</sub>O, with our HPLC/CD system. For optimum signal-to-noise the HPLC eluent was aspirated into the quartz pyrolysis chamber. The day-to-day reproducibility of the CD for both isocratic and gradient experiments over a 4-month period was about 5%.

It appears that the HPLC/CD detection response is flow rate dependent. For example, in the gradient experiments

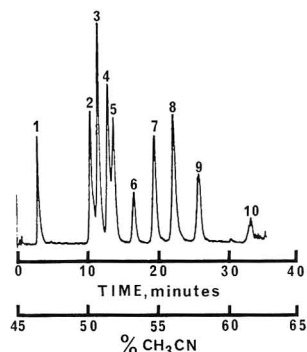


**Figure 1.** Chromatographic profile of a solution of 10 nitro-PAH obtained by using reversed-phase gradient elution with CD. Labeled peaks are (1) 8-nitroquinoline, (2) 1,5-dinitronaphthalene, (3) 1-nitronaphthalene, (4) 2-nitronaphthalene, (5) 2-nitrobiphenyl, (6) 1-nitro-2-methylnaphthalene, (7) 4-nitrobiphenyl, (8) 2-nitrofluorene, (9) 9-nitroanthracene, and (10) 1-nitropyrene.

1-nitronaphthalene elutes at a solvent composition of 51/49 acetonitrile/water with CD detection limit of 125 ng, this result is in contrast to the isocratic experiment where the detection limit was 250 ng at a similar solvent composition.

O'Brien and co-workers (12) have shown that the NO<sup>+</sup>/O<sub>3</sub> reaction is sensitive to changes in sample pressure and flow rate. Pressure variations in the reaction chamber are more likely to occur with HPLC/CD than with GC/CD due to mobile-phase transition from liquid to gaseous state. Moreover, since the solvent composition is constantly changing during gradient elution, pressure changes within the CD reaction chamber are to be expected. Currently, work is in progress to optimize the HPLC/CD with respect to reaction chamber variables such as pressure, temperature, solvent flow rate, and reactant composition for improved detection of nitrated organic compounds. The use of HPLC/CD as a screening tool to obtain organic fractions of nitrogen containing compounds from complex sample matrices should prove applicable. A forthcoming publication will describe nitro-PAH HPLC isocratic and gradient retention characteristics on an octadecylsilane stationary phase.

#### ACKNOWLEDGMENT

The authors thank LDC/Milton Roy for providing the HPLC equipment.

#### LITERATURE CITED

- Hutte, S. R.; Sievers, R. E.; Birks, J. W. J. *Chromatogr. Sci.* **1986**, *24*, 499-505.
- Barth, H. G.; Barber, W. E.; Lochmüller, C. H.; Majors, R. E.; Regnier, F. E. *Anal. Chem.* **1986**, *58*, 211R-250R.
- Robbat, A. Jr.; Corso, N. P.; Doherty, P. J.; Wolf, M. H. *Anal. Chem.* **1986**, *58*, 2078-2084.
- Baker, J. K.; Ma, C. *IARC Sci. Publ.* **1978**, *19*, 19-32.
- Fan, T. Y.; Krull, I. S.; Ross, R. D.; Wolf, M. H.; Fine, D. H. *IARC Sci. Publ.* **1978**, *19*, 3-15.
- Fine, D. H.; Huffman, F.; Rounbehler, D. P.; Belcher, N. M. *IARC Sci. Publ.* **1976**, *14*, 43-50.
- Massey, R. C.; Key, P. E.; McWeeny, D. J.; Knowles, M. E. *IARC Sci. Publ.* **1984**, *57*, 131-136.
- Sen, N. P.; Seaman, S. *IARC Sci. Publ.* **1984**, *57*, 137-143.
- White, C. M.; Robbat, A. Jr.; Hoes, R. M. *Chromatographia* **1983**, *17*, 605-612.
- Oettinger, P. E.; Huffman, F.; Fine, D. H.; Lieb, D. *Anal. Lett.* **1975**, *8*(6), 411-414.
- Kubacki, S. J.; Havery, D. C.; Fazio, T. *IARC Sci. Publ.* **1984**, *57*, 145-155.
- Mehrabzadeh, A. A.; O'Brien, R. J.; Hard, T. M. *Anal. Chem.* **1983**, *55*, 1660-1665.

RECEIVED for review June 22, 1987. Resubmitted August 26, 1987. Accepted September 22, 1987.



# Determination of Ammonium Ion by Fluorometry or Spectrophotometry after On-Line Derivatization with *o*-Phthalaldehyde

Sham S. Goyal,\* Donald W. Rains, and Ray C. Huffaker

Department of Agronomy and Range Science/Plant Growth Laboratory, University of California, Davis, California 95616

A fast, sensitive, simple, and highly reproducible method for routine assay of ammonium ion ( $\text{NH}_4^+$ ) was developed by using HPLC equipment. The method is based on the reaction of  $\text{NH}_4^+$  with *o*-phthalaldehyde (OPA) in the presence of 2-mercaptoethanol. After an on-line derivatization, the resulting  $\text{NH}_4^+$ -OPA product was quantified by using fluorometric or spectrophotometric detection. For fluorometric detection, the excitation and emission wavelengths were 410 and 470 nm, respectively. The spectrophotometric detection was made by measuring absorbance at 410 nm. Results on the effects of OPA-reagent composition and pH, reaction temperature, sample matrix, and linearity of the assay are presented. Even though it took about 2 min from the time of sample injection to the appearance of sample peak, sample injections could be overlapped at an interval of about 1 min. Thus, the actual time needed for analysis was about 1 min per assay. The method can be used in a fully automated mode by using an autosampler injector.

Historically, the methods for quantitative assay of ammonium ion have been relatively insensitive and time-consuming and have poor reproducibility. Most of the earlier methods were based on Nessler's reagent, with which many other inorganic ions interfere. The method currently used by most laboratories is based on the phenol-hypochlorite reaction (Weatherburn, 1967). The Technicon AutoAnalyzer (Technicon Instruments, Tarrytown, NY) and Lachat Quikchem (Lachat Chemicals, Inc., Mequon, WI) are two examples of commercially available equipment used for  $\text{NH}_4^+$  analysis using the phenol-hypochlorite reaction.

Cohn and Lyle (1) first reported the reaction of *o*-phthalaldehyde (OPA) with glutathione in alkaline pH, resulting in the formation of an OPA-glutathione fluorophore. Subsequently, Roth (2) showed that OPA reacted with all primary amines and  $\text{NH}_4^+$ , provided a reducing agent (2-mercaptoethanol) was included in the reaction mixture. This reaction has become popular for assaying picomole levels of amino acids by using HPLC techniques (3-6). The reaction has also been used in a few specialized situations to assay  $\text{NH}_4^+$  (7, 8); however, no focused effort has been made to exploit the potential of this chemistry for measuring  $\text{NH}_4^+$ . The reaction of  $\text{NH}_4^+$  with OPA in the presence of 2-mercaptoethanol is easily carried out and its subsequent measurement by fluorometry makes it a very sensitive method; however, the reaction needs to be characterized. Potentially, it can replace all other methods of  $\text{NH}_4^+$  measurement.

This paper describes a method for assaying  $\text{NH}_4^+$  based on the  $\text{NH}_4^+$ -OPA reaction, which can be used routinely as a fully automated method requiring only about 1 min per assay. The method is simple, highly reproducible, flexible, and very sensitive and has a large linear concentration range, which eliminates the need for sample dilution. So far, the OPA-

$\text{NH}_4^+$  primary amine product has only been measured by fluorometry (2-8). This study reports the possibilities of using spectrophotometry for situations where a fluorometer may not be available. The molar response factor of  $\text{NH}_4^+$ -OPA fluorophore formed in alkaline pH (9.0-10.0) and in neutral pH (ca. 7.0) is at least an order of magnitude lower (2, 5) and higher (7), respectively, than for primary amines and amino acids. Thus, the latter was used in this study. Special care is required since a slight contamination of samples with primary amines and/or amino acids could result in significant overestimation of  $\text{NH}_4^+$  if the reaction is run in alkaline pH. However,  $\text{NH}_4^+$  could be separated by using high-performance liquid chromatography (HPLC) in which case interference from primary amines and/or amino acids would not be a problem (5). But the HPLC procedure usually requires, at least, 20-25 min per sample. The method reported here is presently proposed for nonphysiological fluids, e.g., water samples, acid digests of organic materials, nutrient solutions, soil extracts, inorganic industrial waste, and others. Extension of this method for use with physiological fluids, e.g. blood, urine, green plant extracts, etc., is currently under development and will be reported shortly. Our preliminary results (unpublished data) show that representative primary amines and amino acids did not interfere with  $\text{NH}_4^+$  determination in the reported procedure.

## EXPERIMENTAL SECTION

**Equipment.** The equipment system included a modular HPLC (high-performance liquid chromatography) unit consisting of a pump (Laboratory Data Control, Riviera Beach, FL; Model, Constametric IIIG), a fluorescence detector (Shimadzu Scientific Instruments, Inc., Columbia, MD; Model, RF-530), a UV-vis detector (Shimadzu; Model, SPD-6AV), an injector (Rheodyne, Inc., Cotati, CA; Model 7126; for 0.5-mL injections, Model 7413), an integrator/data processor (Shimadzu; Model, C-R3A), and a constant-temperature water bath (Fisher Scientific, Inc., Santa Clara, CA; Model 730). A coil of 0.5 mm i.d. Teflon tubing (total volume, 4 mL) immersed in the constant temperature bath was used as reaction coil. The flow diagram of the equipment used is shown in Figure 1.

**OPA Reagent.** The reagent was composed of potassium phosphate buffer, OPA, and 2-mercaptoethanol. The concentrations of various components studied were as follows: potassium phosphate, 50, 100, 150, and 200 mM; OPA, 0, 1, 3, 5, 10, 15, 20, 25, and 30 mM; 2-mercaptoethanol, 0.5, 1.25, 2.5, 5.0, 7.5, 10.0, and 12.5, mM. The potassium phosphate buffer ( $\text{K-PO}_4$ ) was prepared by adding equimolar amounts of  $\text{KH}_2\text{PO}_4$  and  $\text{K}_2\text{HPO}_4$ . This resulted in a final pH close to the desired (ca. 7.0). The pH of the reagent was adjusted and then filtered through 0.2- $\mu\text{m}$  filter prior to adding mercaptoethanol. The reagent was generally prepared about one day ahead of use, covered, and left at room temperature and normal laboratory lighted conditions. A freshly prepared reagent could also be used but resulted in a slight continuous drop of base line, presumably due to decay of the  $\text{NH}_4^+$ -OPA product in the reagent itself.

**Procedure.** The OPA reagent was pumped through the HPLC pump and the  $\text{NH}_4^+$  samples (as  $\text{NH}_4\text{Cl}$ ) were injected into the stream. The sample, mixed with the OPA reagent, passed through

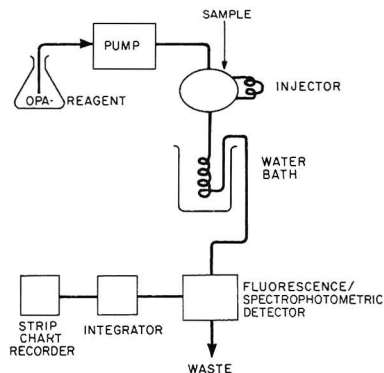


Figure 1. Flow diagram of the system.

the reaction coil immersed in a water bath before entering the detector. For most studies the flow rate of the OPA reagent was adjusted such that the time interval between the injection and appearance of the peak (referred to as residence time, hereafter; since no column was used, it should not be called retention time) was 2 min. For 0.5-, 5-, and 20- $\mu$ L injections a complete loop fill technique was used. A gas-tight syringe, with a 100- $\mu$ L loop on the HPLC injector, was used when varying volumes of sample were injected.

The excitation and emission wavelengths for fluorescence measurements were 410 and 470 nm, respectively. For spectrophotometric studies, the absorbance was measured at 410 nm. The results were based on peak areas except that the absorbance data, reported as "absorbance units" were based on peak heights. For residence time vs. response studies, various residence times were achieved by adjusting the flow rate of the OPA reagent while the reaction coil volume was constant. The response was calculated from peak heights. Ammonium chloride was used as the source of  $\text{NH}_4^+$ .

At the end of each day, the entire system was flushed with deionized water (filtered through 0.2- $\mu$ m filter). To date we have not seen any unusual wear on the system, despite the high salt content of the liquids being pumped.

**Statistical Analysis.** The  $\text{NH}_4^+$  concentration vs. response data were subjected to regression analysis with an IBM (XT) microcomputer and a curve fitting program, "Curve Fitter-PC" (Interactive Microwave, Inc., College Park, PA). Based on the linear regression analysis, "useful linear ranges" were calculated. The useful linear range is defined as that range of  $\text{NH}_4^+$  concentration over which any single data point deviated by no more than 5% from linear regression. In some cases, the useful linear range may be slightly larger than those reported due to the resolution in  $\text{NH}_4^+$  calibration standards. The standard errors in all cases were much smaller than the size of the data points shown in the figures. Thus, the standard error bars are contained within the data points. In general, the maximum variability experienced was always less than  $\pm 0.5\%$ .

**Limit of Quantitation.** The lower limits of quantitation (LOQ), not the detection limit, were calculated under different conditions. The definition of LOQ as suggested by Keith et al. (9) was followed in this study.

## RESULTS AND DISCUSSION

### Effect of OPA Reagent Composition on Fluorescence.

The fluorescence of the OPA- $\text{NH}_4^+$  product increased as the OPA concentration of the reagent increased up to 10 mM. Further increase in the OPA concentration caused a decrease in fluorescence (Figure 2). Taylor et al. (7) also observed an increase in fluorescence with increased OPA concentration; however, the response did not level off even at the highest OPA concentration tested (37.5 mM).

The lowest concentration of 2-mercaptoethanol (0.5 mM) tested in this study gave nearly the maximal fluorescence

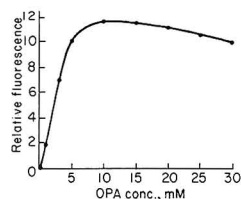


Figure 2. Effect of OPA concentration on the fluorescence of  $\text{NH}_4^+$ -OPA product: 2-mercaptoethanol, 12.5 mM; temperature, 63 °C; residence time, 2 min; pH 6.8; K- $\text{PO}_4$ , 50 mM.

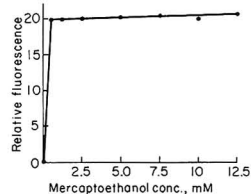


Figure 3. Effect of 2-mercaptoethanol concentration on the fluorescence of  $\text{NH}_4^+$ -OPA product: OPA, 3.75 mM; temperature, 63 °C; residence time, 2 min; pH 6.8; K- $\text{PO}_4$ , 50 mM.

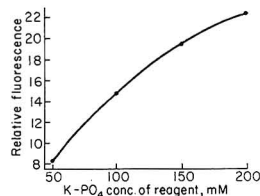


Figure 4. Effect of K- $\text{PO}_4$  concentration on the fluorescence of  $\text{NH}_4^+$ -OPA product: OPA, 3.75 mM; 2-mercaptoethanol, 12.5 mM; residence time, 2 min, temperature, 63 °C; pH 6.8.

(Figure 3). Concentrations higher than 0.5 mM resulted in only a slight increase in fluorescence, e.g., 12.5 mM of 2-mercaptoethanol gave only about 4% higher fluorescence compared to a concentration of 0.5 mM. The response agrees with that reported by Taylor et al. (7) in the sense that a very low concentration of 2-mercaptoethanol gave the maximal fluorescence; however, the decrease in fluorescence that they observed, due to higher concentrations of 2-mercaptoethanol (7) did not occur in this study (Figure 3).

An increase in the buffer concentration of the OPA reagent resulted in increased fluorescence (Figure 4). A polynomial regression analysis revealed that K- $\text{PO}_4$  concentration vs. fluorescence was a second order function (Figure 4). This agrees well with the results of Taylor et al. (7). The mechanism by which this might occur is not clear; however, an increase in the reactivity of OPA with increasing ionic strength of the reagent may be a strong possibility.

### Effect of Reaction Temperature and Time on Fluorescence.

The fluorescence of the OPA- $\text{NH}_4^+$  product increased with increasing temperature at which the reaction was carried out. Similar findings were reported by Taylor et al. (7) but no quantitative data on the effect of temperature were presented. In the present study when the reaction time (residence time) was 1.5 min, the fluorescence leveled off at about 63 °C and was essentially constant between 63 and 66 °C. Further increase in temperature led to a decrease in fluorescence (Figure 5). With a 2-min reaction time, the maximal fluorescence was obtained at 61 °C and the plateau span was only 2 °C instead of 4 °C with 1.5 min (Figure 6).

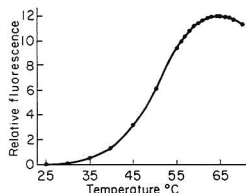


**Figure 5.** Effect of reaction temperature on the fluorescence of  $\text{NH}_4^+$ -OPA product with 1.5 min residence time: OPA, 3.75 mM; 2-mercaptoethanol, 12.5 mM; pH 6.8;  $\text{K-PO}_4$ , 50 mM.

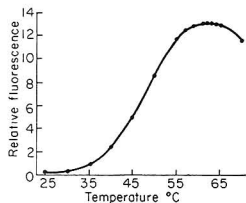


**Figure 6.** Effect of reaction temperature on the fluorescence of  $\text{NH}_4^+$ -OPA product with 2 min residence time. The other conditions were same as in Figure 5.

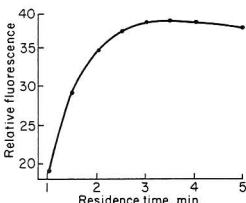


**Figure 7.** Effect of residence time on the fluorescence of  $\text{NH}_4^+$ -OPA product: OPA, 3.75 mM; 2-mercaptoethanol, 12.5 mM; temperature, 63 °C; pH 6.8;  $\text{K-PO}_4$ , 50 mM.

Hence, it should be possible to further reduce the reaction time required for maximal fluorescence by further increasing the reaction temperature. Conversely, it should be possible to reduce the temperature required by increasing the residence time.

When the reaction temperature was held constant at 63 °C, the fluorescence increased with increasing time allowed for the reaction up to 3 min and remained essentially constant up to 4 min (Figure 7). A further increase in time led to a slight decrease in fluorescence. At room temperature, a 30-min reaction time was required to achieve maximal fluorescence (7).

**Effect of OPA Reagent pH on Fluorescence.** The effect of OPA reagent pH on fluorescence of OPA- $\text{NH}_4^+$  product is shown in Figure 8. The highest fluorescence was obtained at a pH of 6.8. Unfortunately, no apparent plateau for the pH effect occurred; hence pH control in this assay becomes very important. In contrast, Taylor et al. (7) reported the maximal fluorescence at pH 7.3 with a plateau of  $\pm 0.1$  pH units. Hence, for samples with high acid content, the volume of the sample injected should be minimized and the buffer concentration should be increased to provide higher buffering capacity.

**Effect of Sample Matrix on Fluorescence.** The effect of sample matrix (ionic content) on the fluorescence of OPA- $\text{NH}_4^+$  product is shown in Figure 9. Potassium sulfate ( $\text{K}_2\text{SO}_4$ ) was chosen as a representative salt to vary the sample matrix (background ionic content) of samples. Other salts were also tested for specific ionic effects and the results are

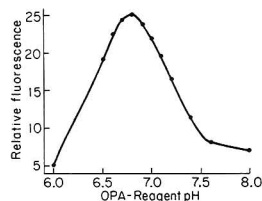


**Figure 8.** Effect of OPA reagent pH on the fluorescence of  $\text{NH}_4^+$ -OPA product: OPA, 3.75 mM; 2-mercaptoethanol, 12.5 mM; temperature, 63 °C; residence time, 2 min;  $\text{K-PO}_4$ , 50 mM.

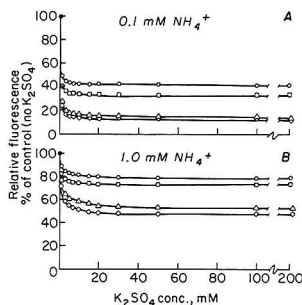


**Figure 9.** Effect of sample matrix on the fluorescence of  $\text{NH}_4^+$ -OPA product from (a) 0.1 mM and (b) 1.0 mM  $\text{NH}_4^+$  solutions: 50 mM  $\text{K-PO}_4$  in OPA reagent, 5- $\mu\text{L}$  ( $\Delta$ ) and 20- $\mu\text{L}$  ( $\circ$ ) samples injected; 200 mM  $\text{K-PO}_4$  in OPA reagent, 5- $\mu\text{L}$  ( $\diamond$ ) and 20- $\mu\text{L}$  ( $\square$ ) samples injected. The other conditions are given in Figure 4.

reported later in this section. An increased concentration of  $\text{K}_2\text{SO}_4$  in the sample decreased fluorescence dramatically, up to about 20 mM, and leveled off at 50 mM. This was a rather perplexing observation, especially considering that the OPA reagent (which serves as a reactant as well as a carrier) had up to 200 mM  $\text{K-PO}_4$ . The effect seemed to be related to three factors:

A. The  $\text{NH}_4^+$  concentration of the sample to be analyzed; the lower the  $\text{NH}_4^+$  concentration, the greater was the effect. For example, addition of 1 mM  $\text{K}_2\text{SO}_4$  to a 0.1 mM  $\text{NH}_4^+$  solution decreased the fluorescence by about 72% (5- $\mu\text{L}$  injection using a 200 mM  $\text{K-PO}_4$ , OPA reagent) whereas the response of 1 mM  $\text{NH}_4^+$  solution decreased only by about 30% when analyzed under the same conditions.

B. The volume of the sample injected; the larger the sample, the lower the effect and vice versa (Figure 9). For instance, addition of 1 mM  $\text{K}_2\text{SO}_4$  to a 1 mM  $\text{NH}_4^+$  solution decreased the response by 29% and 17%, respectively, when 5- and 20- $\mu\text{L}$  samples were injected.

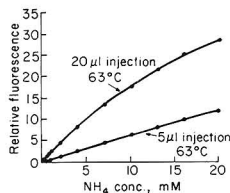
C. The  $\text{K-PO}_4$  concentration of the OPA reagent; the higher the concentration, the greater the effect and vice versa (Figure 9).

The mechanism by which the ionic content of the sample might be affecting the fluorescence is not clear; however, two possibilities exist: (1) A partial loss of absorbed energy through collisions with ions (10) such that the energy emitted as light is lowered and/or (2) The ions interfere in the synthesis of the  $\text{NH}_4^+$ -OPA fluorophore. Tests showed that the addition of  $\text{K}_2\text{SO}_4$  to  $\text{NH}_4^+$  solutions decreased the absorbance ( $A_{410}$ ) of the OPA- $\text{NH}_4^+$  product in the same proportion as it did the fluorescence (results not shown). Hence, the ionic content of sample interfered with the synthesis of the  $\text{NH}_4^+$ -OPA fluorophore and not the emission process.

As to why the salt concentration of the sample lowered the synthesis of the fluorophore, it was possible that the sample

**Table I. Effect of Various Salts in the  $\text{NH}_4^+$  Solution on the Fluorescence**

sample composition	response, % of $\text{K}_2\text{SO}_4$
1 mM $\text{NH}_4^+$ + 20 mM $\text{K}_2\text{SO}_4$	100
1 mM $\text{NH}_4^+$ + 20 mM $\text{Na}_2\text{SO}_4$	100.36
1 mM $\text{NH}_4^+$ + 20 mM NaCl	99.86
1 mM $\text{NH}_4^+$ + 20 mM KCl	100.11
1 mM $\text{NH}_4^+$ + 20 mM $\text{CaCl}_2$	96.82
1 mM $\text{NH}_4^+$ + 20 mM $\text{Ca}(\text{NO}_3)_2$	95.11
1 mM $\text{NH}_4^+$ + 10 mM $\text{CaCl}_2$	98.98
1 mM $\text{NH}_4^+$ + 10 mM $\text{Ca}(\text{NO}_3)_2$	99.02

**Figure 10.** Effect of  $\text{NH}_4^+$  concentration on the fluorescence of  $\text{NH}_4^+$ -OPA product. The  $\text{K}-\text{PO}_4$  was at 200 mM and the other conditions were as in Figure 4. See Table II for statistical analysis. 50 mM  $\text{K}_2\text{SO}_4$  was included in all samples.

band did not fully mix with the OPA reagent. Thus, the ionic concentration of the sample band remained different from that of the OPA reagent surrounding it on both sides. Due to the osmotic effects, then, the salt content of the sample band controlled the mixing of the sample with the reagent. When a mixing chamber was inserted in the fluid stream (to force complete mixing), the results remained unchanged. Moreover, the addition of sucrose instead of  $\text{K}_2\text{SO}_4$  did not decrease the fluorescence (results not shown). These observations show that the effect of sample ionic concentration on fluorescence was not due to mixing or osmotic reasons. Instead, it was probably related to the decreased activity of  $\text{NH}_4^+$  ion in the sample due to ionic strength.

The effect of sample ionic concentration on the formation of OPA- $\text{NH}_4^+$  fluorophore has not been reported previously. It is possible that the OPA-primary amines/amino acids product may also be affected; however, it is difficult to assess at this time whether the effect was caused only under the conditions used in this study. Taylor et al. (7) carried out the reaction in a test tube at room temperature. Judging from the similarities in the effect of ionic concentration of the OPA reagent on the fluorescence observed in this study and those reported by Taylor et al. (7), the effect of the ionic concentration of the sample remains a strong possibility under many conditions involving OPA reagent.

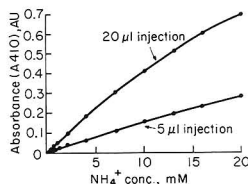
**Effect of Various Inorganic Salts in Sample on the Fluorescence.** Four salts, out of six tested, namely  $\text{K}_2\text{SO}_4$ ,  $\text{Na}_2\text{SO}_4$ , NaCl, and KCl, affected the fluorescence of OPA- $\text{NH}_4^+$  chromophore similarly. This shows that there were no specific ionic interactions involved in the formation of  $\text{NH}_4^+$ -OPA chromophore. The other two,  $\text{CaCl}_2$  and  $\text{Ca}(\text{NO}_3)_2$ , had slightly greater effect than any one of the other four, at equimolar concentrations (Table I). The effect of the latter two salts was about the same as the former four at half the concentration (Table I). This suggests that the anions contributed more to the observed salt effect.

**Ammonium Concentration vs Fluorescence.** The  $\text{NH}_4^+$  concentration of the sample (from 0 to 20 mM) vs fluorescence (5- and 20- $\mu\text{L}$  injections at 63 °C) is shown in Figure 10. Basically, the response was curvilinear and represented a second-order function. Such a response is generally expected of fluorometric methods over a large concentration range (11).

**Table II. Useful Linear Ranges of  $\text{NH}_4^+$  Concentration under Different Conditions with Fluorescence Measurements**

concn range, mM	corr coeff (r)	concn range, mM	corr coeff (r)
5- $\mu\text{L}$ Injections, 63 °C			
0.001 <sup>a</sup> -4	0.999 85	5- $\mu\text{L}$ Injections, 37 °C	
1-7	0.999 83	0.002 <sup>a</sup> -10	0.999 98
4-20	0.999 70	1-20	0.999 97
20- $\mu\text{L}$ Injections, 63 °C			
0.0002 <sup>a</sup> -2	0.999 76	0.5- $\mu\text{L}$ Injections, 63 °C	
1-4	0.999 89	0.002 <sup>a</sup> -13	0.999 99
7-20	0.995 76	0.75-20	0.999 95

<sup>a</sup>Represents the lower limit of quantitation (LOQ).

**Figure 11.** Effect of  $\text{NH}_4^+$  concentration on absorbance ( $A_{410}$ ): moderation of linear concentration range by sample injection volume. Conditions are the same as those given in Figure 10. See Table III for statistical analysis.  $\text{K}_2\text{SO}_4$  (50 mM) was included in all samples.

In this study an attempt was made to enlarge the linear concentration range by varying different parameters. The response for 0-20 mM  $\text{NH}_4^+$  concentration was essentially linear, when the assay was done at 37 °C, 5- $\mu\text{L}$  injections ( $y = 0.04 + 1.749X$ ,  $r = 0.99997$ ;  $y = -0.009 + 1.788X - 0.00228X^2$ ,  $r = 0.99999$ ), and at 63 °C, 0.5- $\mu\text{L}$  injections ( $y = -0.0292 + 1.205X$ ,  $r = 0.99995$ ;  $y = 0.010 + 1.273X + 0.0018X^2$ ,  $r = 0.99998$ ) (data not shown). Useful linear concentration ranges (see Experimental Section), under different conditions, are listed in Table II. In general, the linear concentration range was extended by changing a parameter such that it resulted in decreased intensity of fluorescence (response). For example, a decrease in the volume of sample injected from 20 to 5  $\mu\text{L}$  resulted in extending the linear range from 0.0002-2 mM to 0.001-4 mM (Figure 10 and Table II). Injection of a 0.5- $\mu\text{L}$  sample yielded a linear range of 0.002-13 mM (Table II). Similarly, with a decrease of the temperature at which reaction was carried out from 63 to 37 °C (5- $\mu\text{L}$  injections), the linear range increased from 0.001-4 mM to 0.002-10 mM (Figure 10, Table II). Thus, the system is quite flexible and the individual investigators may choose the conditions suited for their application. A LOQ of 2 pmol of  $\text{NH}_4^+$  was possible under the conditions of maximal sensitivity ( $\text{K}-\text{PO}_4$ , 200 mM; OPA, 10 mM; mercaptoethanol, 12.5 mM; temperature, 63 °C; residence time, 2 min). The fluorescence sensitivity of  $\text{NH}_4^+$ -OPA product relative to quinine sulfate was calculated to be about 1:25 at 63 °C.

**Ammonium Concentration vs Absorbance.** Photometric response ( $A_{410}$ ) of the OPA- $\text{NH}_4^+$  product was similar to the fluorometric response in characteristics and was curvilinear (over a concentration range of 0-20 mM), even though the maximum absorbance was well below a value of 2.0 (Figure 11). The useful linear concentration ranges were also similar to the fluorescence method (Table III). A change in conditions that resulted in lower absorbance increased the linear concentration range. The nonlinearity in concentration vs response (fluorometric or absorbance) may be related to the efficiency of derivatization or OPA- $\text{NH}_4^+$  reaction kinetics.

Table III. Useful Linear Ranges of  $\text{NH}_4^+$  Concentration under Different Conditions with Absorbance ( $A_{410}$ ) Measurements<sup>a</sup>

concn range, mM	corr coeff (r)	concn range, mM	corr coeff (r)
5- $\mu\text{L}$ Injections, 63 °C		20- $\mu\text{L}$ Injections, 63 °C	
0.05 <sup>b</sup> -4	0.999 89	0.02 <sup>b</sup> -4	0.999 85
1-10	0.999 95	1-7	0.999 34
2-16	0.999 94	2-10	0.999 26
4-20	0.999 66	7-20	0.995 92

<sup>a</sup> Data from Figure 12. <sup>b</sup> Represents the lower limit of quantitation (LOQ).

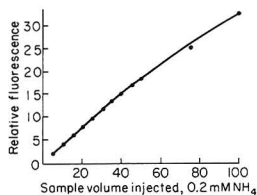


Figure 12. Effect of sample volume injected on the fluorescence of  $\text{NH}_4^+$ -OPA product. Conditions are the same as those given in Figure 10.  $\text{K}_2\text{SO}_4$  (50 mM) was included in the sample.

The use of spectrophotometry (instead of fluorometry) attempted in this study, to measure OPA- $\text{NH}_4^+$  product, seemed quite feasible. This has not been possible in the past primarily due to sensitivity problems. However, the modern spectrophotometric detectors made for HPLC are about an order of magnitude more sensitive than the older models. In this study we measured an absorbance of about 0.1 absorbance units (optical density) for 40 nmol of  $\text{NH}_4^+$  (20  $\mu\text{L}$  of 2 mM). An average "specific absorbance" of  $2.41 \times 10^6 \pm 0.028 \times 10^6$  absorbance units (AU) per mole of  $\text{NH}_4^+$  was calculated from solutions containing 0.1-4 mM  $\text{NH}_4^+$  (20- $\mu\text{L}$  injections). Therefore, assaying  $\text{NH}_4^+$  quantities of up to 1 nmol, using spectrophotometry, should not be a problem.

**Effect of Sample Volume on Fluorescence.** In this system, the fluorometric response increased linearly with the sample volume (0.2 mM  $\text{NH}_4^+$ ) injected up to 30  $\mu\text{L}$  (6.0 nmol of  $\text{NH}_4^+$ , Figure 12). When 20- $\mu\text{L}$  samples were injected, the linearity occurred up to a concentration of 2 mM (40 nmol, Figure 10); therefore, the deviation from linearity observed with injection volumes greater than 30  $\mu\text{L}$  of 0.2 mM  $\text{NH}_4^+$  was probably not due to the mass of  $\text{NH}_4^+$  injected, per se. Instead, it seems that the sample volume affected the efficiency of derivatization independently. In our system, the sample volume generally remains constant. Thus, this factor should not be of any consequence; however, the sample volume effect may be related to the mixing of the sample and the reagent. This in turn may be related to the length of "sample plug", which is a function of the internal diameter of the tubing used. It may be possible to reduce this effect by choosing a larger internal diameter tubing, if variable and larger sample volumes are to be injected.

**Reproducibility.** The analysis of a 1 mM  $\text{NH}_4^+$  solution 40 times in 1 h gave a relative standard error (RSE) of  $\pm 0.0015$ . When the assay was done at 37 °C, the RSE was slightly higher ( $\pm 0.0023$ , results not shown). This was expected because a slight fluctuation in reaction temperature at 37 °C caused relatively a greater change in response, than at 63 °C (Figures 5 and 6).

**General Comments and Suggested Procedure.** An OPA reagent composed of 100 mM K- $\text{PO}_4$ , 3 mM OPA, and 10 mM 2-mercaptoethanol, pH 6.8, is suggested for routine purposes. For higher sensitivity, the OPA concentration may be increased up to 10 mM. If greater buffering is needed (depending on the sample pH), the K- $\text{PO}_4$  concentration of the OPA reagent may be increased to 200 mM. For samples with high acid content (e.g. acid digests of organic materials), injection of small volumes (0.5  $\mu\text{L}$ ) would eliminate the need for an additional step of sample dilution. We have analyzed acid digests of plant materials (ca. 1.25 M  $\text{H}_2\text{SO}_4$ ) with high reproducibility ( $\pm 0.5\%$ ), without any sample dilution, by injecting 0.5- $\mu\text{L}$  samples. High correlation coefficients ( $r = > 0.94$ ) were found when the present method was compared to the conventional methods (distillation of  $\text{NH}_4^+$  into boric acid solution followed by titration and phenol-hypochlorite method) of  $\text{NH}_4^+$  detection, by using acid digests of several plant materials (an assay for total nitrogen). If an injector capable of injecting small volumes is not available, the acid digests must be diluted such that the sample pH does not effect the response. For samples with low salt background ( $< 50$  mM), a small aliquot (about 1% of the sample volume) of a concentrated salt solution (e.g. 5 M  $\text{Ca}(\text{NO}_3)_2$ ) to an approximate sample volume, can be added to alleviate the salt effects. More rigorous volumetric additions should be made for greater accuracy. The volume of the sample to be injected would largely depend on factors such as sensitivity, linear range required, and the sample pH. A minimum of 2 min residence time is recommended. Overlapping injections at an interval of about 1 min can be made such that 50-60 samples can be analyzed per hour.

**Registry No.** OPA, 643-79-8;  $\text{NH}_4^+$ , 14798-03-9;  $\text{K}_2\text{SO}_4$ , 7778-80-5;  $\text{Na}_2\text{SO}_4$ , 7757-82-6; NaCl, 7647-14-5; KCl, 7447-40-7;  $\text{CaCl}_2$ , 10043-52-4;  $\text{Ca}(\text{NO}_3)_2$ , 10124-37-5; 2-mercaptoethanol, 60-24-2.

## LITERATURE CITED

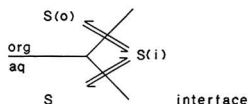
- (1) Cohn, V. M.; Lyle, J. *Anal. Biochem.* **1966**, *14*, 434.
- (2) Roth, M. *Anal. Chem.* **1971**, *43*, 880-882.
- (3) Benson, J. R.; Hare, P. E. *Proc. Natl. Acad. Sci. U.S.A.* **1975**, *72*, 619-622.
- (4) Hill, D. W.; Walters, F. H.; Wilson, T. D.; Stuart, J. D. *Anal. Chem.* **1979**, *51*, 1338-1341.
- (5) Lindroth, P.; Mopper, K. *Anal. Chem.* **1979**, *51*, 1667-1674.
- (6) Roth, M.; Hampai, A. *J. Chromatogr.* **1973**, *83*, 353-356.
- (7) Taylor, S.; Ninjor, V.; Dowd, D. M.; Tappel, A. L. *Anal. Biochem.* **1974**, *60*, 153-162.
- (8) Corbin, J. L. *Appl. Environ. Microbiol.* **1984**, *47*, 1027-1030.
- (9) Keith, L. H.; Crummett, W.; Deegan, J., Jr.; Libby, R. A.; Taylor, J. K.; Wentling, G. *Anal. Chem.* **1983**, *55*, 2210-2218.
- (10) Pecsok, R. L.; Shields, L. D.; Cairns, T.; McWilliam, I. G. *Modern Methods of Chemical Analysis*; Wiley: New York, 1976.
- (11) Knox, J. H.; Done, J. N.; Fell, A. F.; Gilbert, M. T.; Pryde, A.; Wall, R. A. *High-Performance Liquid Chromatography*; Edinburgh University Press: Edinburgh, 1979; pp 112-113.

RECEIVED for review April 14, 1987. Accepted September 17, 1987.

## CORRESPONDENCE

## Exchange of Comments on the Role of the Interface in Solvent Extraction Processes

Sir: In 1982, we demonstrated that the use of a microporous Teflon phase separator (MTPS) could be used to sample just the bulk organic phase (*I*) from an organic-aqueous-phase mixture stirred so rapidly that an average droplet size as small as 200  $\mu\text{m}$  resulted (2). Consequently, we could quantitatively account for changes in distribution equilibrium resulting from the presence of a third, interfacial phase of significant area (3). The basis for our calculations was that of a simple, classical heterogeneous equilibrium approach in which all three phases are in mutual equilibrium. While it is certainly true that the measurement technique involves the coalescence of the organic droplets passing through the phase separator to form the stream of bulk organic phase that leads to the flow-through cell of the spectrophotometer cell and then returned to the mixing flask, the resulting loss of interfacial area is only a small fraction ( $\sim 1\%$ ) of the total. The consequent loss in interfacial area caused by such sampling is so small that the question raised by Persaud, Tian, and Cantwell (4) of the possible loss of adsorbed solute from the interface to either of the bulk phases during the phase separation in such an experiment is below experimental error and hence is not relevant to the evaluation of the published applications of the technique. The experiment described by Persaud et al. does not in any way extend existing knowledge of extraction systems involving appreciable interfacial areas. Since the three (two bulk and interfacial) phases are in mutual equilibrium, elementary thermodynamic considerations ("when each of two phases is in equilibrium with a third, they must be in equilibrium with each other" (5) require that



the distribution ratio ( $D = [S]_o/[S]$ ) of the solute *S* between the two bulk phases must be independent of the presence or absence of a significant interface. Moreover, the associated distribution ratios between the interface and bulk organic,  $D_{io}$ , and bulk aqueous,  $D_{iw}$ , can be seen to be related to each other by the value of *D*. Thus

$$D_{io} = [S]_i/[S]_o \quad (1)$$

and

$$D_{iw} = [S]_i/[S] \quad (2)$$

where  $[S]_i$  is an interfacial concentration in appropriate units from which it may be seen that

$$\frac{D_{iw}}{D_{io}} = \frac{[S]_i/[S]}{[S]_i/[S]_o} = [S]_o/[S] = D \quad (3)$$

Not surprisingly, the adsorption of a solute to the interface will depend on its relative solubility in the bulk phases, i.e.

$$D_{iw} = D \times D_{io} \quad (4)$$

shows that adsorption of a solute having a high *D* from the aqueous phase will be greater than that from the organic phase

Table I. Relationship between  $D$ ,  $D_{io}$ ,  $D_{iw}$ ,  $D_{io}/D_{iw}$ , and Methylene Blue Concentration

methylene blue concn, $\times 10^7$ M	<i>D</i>	$D_{io}$	$D_{iw}$	$D_{io}/D_{iw}$
1.53	3.67 <sup>a</sup>	1.98 <sup>a</sup>	6.64 <sup>a</sup>	3.36 <sup>a</sup>
3.06	2.24	0.953	2.43	2.55
4.59	2.04	0.896	1.85	2.07
6.12	2.12	0.684	1.59	2.32
7.65	2.18	0.671	1.44	2.14
9.18	1.95	0.583	1.19	2.05
mean (SD)	2.11 (+0.16)			2.22 (+0.21)

<sup>a</sup> These data, obtained at the lowest concentration, are probably not as reliable as the remainder and were not used in calculating the mean values.

(in which they are more soluble). Further, these equations are readily verified from data in Table I of (4). In the following,  $A_o$  and  $A_w$  represent absorbances of methylene blue perchlorate (MB) in organic and aqueous phases when no stirring occurs, and  $A_o'$  and  $A_w'$  represents these values under stirring conditions. If the molar absorbances of MB in both bulk phases are essentially the same, not an exact hypothesis but once adequate for the level of data reliability in this case (see Table I), then the value  $A_i$  may be taken as the sum of  $\Delta A$  values, or

$$A_i = (A_o - A_o') + (A_w - A_w') \quad (5)$$

with  $D$ ,  $D_{io}$ , and  $D_{iw}$  defined as  $A_o/A_w$ ,  $A_i/A_o$ , and  $A_i/A_w$ . The values in Table I are calculated by using these equations. Thus, the identity of  $D$  and  $D_{iw}/D_{io}$  is experimentally verified. (Once again, this reflects that the fraction of the total interface disturbed in any way by the sampling procedure is well below experimental error.)

What is discussed but not experimentally addressed in the Persaud paper is what happens to the adsorbed solute in the "two" equilibrium layers" when the droplets coalesce with the wetting layer. The authors discuss what happens during coalescence to interfacially adsorbed solute based on a detailed theoretical treatment of well-established principles of surface chemistry. We have shown experimentally, using exhaustive removal of bulk organic phase from the high speed stirring mixture through the MTPS (6) that when the drops coalesce on the phase separator, the corresponding collapse or reduction of interfacial area releases adsorbed solute to the reaction mixture in the flask, where it redistributes between the phases, rather than carrying it through the MTPS with the coalesced organic phase. Such an effect could not be detected by either our earlier or Persaud's current experimental configuration in which (a) only a small fraction of the bulk organic phase is removed at any one time, and (b) the bulk organic phase portions are returned continuously to the reaction vessel. It is tempting to predict that if one performed the same experiment (exhaustive bulk aqueous phase removal) by using the hydrophilic phase separator an analogous effect, i.e., adsorbed analyte returning to the reaction vessel for phase re-



distribution rather than moving with the removed bulk aqueous phase, would be found.

This virtual desorption of solute must be faster than the rate of passage of the organic phase through the MTPS. In any event, such a steady state is achieved very rapidly (<1 min). Persaud's experiment duration is of the order of 15 min. The discussion relating to the rate of establishment of a steady state or that of desorption accompanying droplet coalescence cannot be supported by such experiments. Of course, with other aspects of the overall phase-transfer process, such as chelate formation (6), dissociation (7), or disaggregation of colloidal aggregates of ion association complexes (8), transfer rates in the high-speed stirring apparatus can be significantly slower (half lives of more than 1 h are fairly common).

#### LITERATURE CITED

- (1) Watarai, H.; Cunningham, L.; Freiser, H. *Anal. Chem.* **1982**, *54*, 2390-2392.

- (2) Aprahamian, E.; Cantwell, F. F.; Freiser, H. *Langmuir* **1985**, *1*, 79-82.
- (3) Watarai, H.; Freiser, H. *J. Am. Chem. Soc.* **1983**, *105*, 191-194.
- (4) Persaud, G.; Tian, Xiu-min; Cantwell, F. F. *Anal. Chem.* **1987**, *59*, 2-7.
- (5) Noyes, A. A.; Sherrill, M. S. *An Advanced Course of Instruction in Chemical Principles*; Macmillan: New York, 1936; p 76.
- (6) Chamupathi, V. G.; Freiser, H. *Langmuir*, in press.
- (7) Ohashi, K.; Freiser, H. *Anal. Chem.* **1980**, *52*, 2214.
- (8) Cantwell, F. F.; Freiser, H. Presented at the Pacific Basin Conference, Honolulu, HI, 1984.

Henry Freiser

Strategic Metals Recovery  
Research Facility  
Department of Chemistry  
University of Arizona  
Tucson, Arizona 85721

RECEIVED for review February 17, 1987. Accepted September 18, 1987.

Sir: The criticism by Freiser (1) of our work on the behavior of solute adsorbed at the liquid-liquid interface in systems involving porous membrane phase separators (2) is based largely on a misinterpretation of our work. Briefly stated, in a rapidly stirred liquid-liquid mixture there might be a total of, e.g.,  $10^4 \text{ cm}^2$  of interface, only a few square centimeters of which lies adjacent to the porous membrane. In our paper we are dealing with nonequilibrium effects occurring *locally* in those few square centimeters of interface. Freiser incorrectly interprets our comments when he applies them to the *total* liquid-liquid interface. Since the liquid passing through the porous membrane to the detector necessarily comes from the immediate vicinity of the membrane, the processes accompanying the *local* coalescence in this vicinity are the ones that influence the composition of the liquid reaching the detector. Specific criticisms are addressed below.

First, we agree with the "... simple, classical heterogeneous equilibrium approach in which all three phases are in mutual equilibrium." This describes what is happening in the vast majority of the liquid-liquid mixture in the container.

Second, we agree that the "loss of interfacial area" compared to the *total* in the flask is very small. We never said otherwise, nor do we even refer to the fractional loss of interfacial area in the *total* system. We did not raise a question "of the possible loss of adsorbed solute from the interface" to the bulk phase in the *total* system which, most certainly, would be below experimental error. In the second paragraph of our paper we do refer to the possibility that "some of the adsorbed solute would dissolve into the adjacent bulk liquid phases thereby raising their solute concentrations *locally*". (That is, in the portions of the bulk phases immediately adjacent to the interface overlying the porous membrane, rather than in the *total* bulk phases in the system.) Our meaning should be clear not only from this comment in the introduction, but also from the descriptions in the Results and the Discussion sections of our paper, particularly Figure 4.

Third, starting with the expression  $D = [S]_o/[S]$ , Freiser sets out to prove the truth of the very same claim that we make in the section headed Distribution Isotherm. He states that "the distribution ratio ... of the solute S between the two bulk phases must be independent of the presence or absence of a significant interface." This is exactly the point that we are making in our paper. His derivation, through eq 4, is

implicitly assumed to be true in our paper. His eq 5 neglects the adsorption of a small amount of the solute onto interfaces other than the liquid-liquid interface (which we discuss in the section Adsorption of MB-ClO<sub>4</sub>). This omission is a relatively minor matter, the effects of which would be included in the approximately  $\pm 10\%$  relative uncertainties for the mean values in his table. The fact that he finds  $D$  and  $D_{iw}/D_{io}$  to be equal to one another is merely another way of saying that the isotherm through the open symbols in our Figure 3 is the same as that through the closed symbols. (The small amount of adsorption to other interfaces, which Freiser has ignored, is correctly reflected in the nonzero intercept in our Figure 3.)

Fourth, contrary to Freiser's claim, our model correctly predicts the results that he reports from his experiment employing "exhaustive removal of bulk organic phase" (3). According to our model, during the coalescence taking place in the immediate vicinity of the porous membrane there is not sufficient time for adsorbed solute to be "released" into either aqueous or organic bulk phase. After the "patch" of adsorbed solute (whose interfacial concentration is different from the equilibrium value) has been swept across the face of the membrane, detachment of the wetting liquid occurs, creating more interface. After detachment, the solute then reestablishes equilibrium in the three-phase mixture away from the immediate vicinity of the membrane. Thus, solute that was interfacially adsorbed at the time of coalescence at the porous membrane *stays in the extraction vessel* and does not pass through the porous membrane. This is what Freiser observed in his exhaustive removal of organic phase (3). We predict that the same effect would be observed if one were to do an exhaustive removal of aqueous phase with a porous cellulose membrane.

Fifth, in the section Distribution Isotherm (2) we say "Absorbances were monitored ... until they remained constant for at least 15 min." We did not say that 15 min were required to reach steady state (equilibrium). In fact, steady state was achieved in <3 min. This is longer than the <1 min observed by Freiser because we were using a much slower pumping rate of 0.5 mL/min than the 5.0 mL/min used by Freiser (4). Thus, flushing out of liquid in peristaltic pump tubing, connecting tubing and detector cell (which are responsible for most of the time required to achieve steady state is such

systems (5) took longer in our system. However, in any event, the time required to achieve steady state after turning on the stirrer is *not relevant* to the discussion. This is because all reported absorbances were measured after the achievement of steady state. The relevant question is as follows: To what extent does the absorbance measured for the solution at steady state (equilibrium) contain a contribution from solute that was released from the interface into the bulk solution during coalescence in the vicinity of the porous membrane? This is determined by the rates of desorption and diffusion, by the thickness of the Nernst film, and by the residence time of a "patch" of interface above the membrane, as we discuss in our paper, and is essentially independent of pumping rate and of "volume" of pump tubing, connecting tubing, and detector cell.

We find nothing in the criticism of Freiser (1) to alter in any way the model that we have proposed to explain the

behavior of solute adsorbed at the liquid-liquid interface in systems involving porous membrane phase separators.

### LITERATURE CITED

- (1) Freiser, H. *Anal. Chem.* **1987**, *59*, 000.
- (2) Persaud, G.; Tian, X.-M.; Cantwell, F. F. *Anal. Chem.* **1987**, *59*, 2-7.
- (3) Chamupathi, V. G.; Freiser, H. *Langmuir*, in press.
- (4) Watarai, H.; Cunningham, L.; Freiser, H. *Anal. Chem.* **1982**, *54*, 2390-2392.
- (5) Cantwell, F. F.; Freiser, H. *Anal. Chem.*, in press.

Frederick F. Cantwell

Department of Chemistry  
University of Alberta  
Edmonton, Alberta, Canada T6G 2G2

RECEIVED for review September 3, 1987. Accepted September 29, 1987.

## Simultaneous Enhancement of Fluorescence and Thermal Lensing by Reversed Micelles

*Sir:* Fluorescence and thermo-optical measurements, i.e., thermal lens (1) and photothermal deflection (2-4), are often used in trace chemical analysis. The fluorescence technique is based on the measurement of emitted photons of an excited analyte. It is, therefore, particularly well suited for the detection of substances that have high fluorescence quantum yields. Conversely, the thermo-optical technique is based on the measurement of the heat generated by the nonradiative relaxation of an excited analyte. It has been successfully employed for trace detection of nonfluorescent substances. Thus, the two techniques are complementary and have been used to determine fluorescent as well as nonfluorescent substances at concentrations as low as  $10^{-11}$  M (5, 6).

Fluorescence can be enhanced by increasing the radiative processes of a molecule. In particular, isolation of the fluorescence molecule from quenching impurities and/or solvent molecules can be used to achieve this enhancement (5, 6).

The thermo-optical technique is based on the temperature rise that is produced in an illuminated sample by nonradiative relaxation of the energy absorbed from a laser. Thus, its intensity can be enhanced by improving the nonradiative relaxation processes of the analyte and more significantly the thermal physical properties of the solvent. When a modulated laser beam, which has a Gaussian intensity distribution, is used to excite the sample, the heat generated will be strongest at the center of the beam since this is where the beam intensity is greatest. Consequently, a lenslike optical element is formed in the sample due to the temperature gradient between the center of the beam and the bulk sample. The effect of the thermal lens is generally measured as a relative change in the beam center intensity,  $\Delta I_{bc}/I_{bc}$ , in the far field. When a sample is located  $3^{1/2}Z_c$  beyond the beam waist, this change is given by

$$\frac{\Delta I_{bc}}{I_{bc}} = 2.303EA + \frac{(2.303EA)^2}{2} \quad (1)$$

where

$$E = -\frac{P(dn/dT)}{(1/91)\lambda k} \quad (2)$$

is the enhancement in sensitivity over a conventional trans-

Table I. Thermo-optical Properties of Solvents for Thermal Lens Measurements

solvent	$k, ^\circ\text{mW cm}^{-1} \text{K}^{-1}$	$10^4 dn/dT, ^\circ\text{K}^{-1}$	$E/P, ^\circ\text{mW}^{-1}$
$\text{CCl}_4$	1.03	-5.9	4.7
<i>n</i> -pentane	1.13	-5.5	4.0
cyclohexane	1.24	-5.4	3.6
<i>n</i> -heptane	1.26	-5.0	3.3
<i>n</i> -nonane	1.29	-4.4	2.8
dioxane	1.39	-4.6	2.7
1-pentanol	1.37	-3.7	2.2
1-butanol	1.52	-3.9	2.1
methanol	2.02	-4.2	1.7
water	6.11	-0.8	0.1

<sup>a</sup>Data taken from Harris and Dovichi (1), Tsederberg (7), Timmermans (8), Ishibashi (9), and Spirin (10). <sup>b</sup>Enhancement per unit laser power in mW;  $\lambda = 632.8$  nm.

mission measurement,  $dn/dT$  is the temperature coefficient of the index of refraction,  $A$  is the sample absorption,  $\lambda$  is the wavelength of the excitation radiation, and  $k$  is the thermal conductivity of the solvent (1, 5, 6). It is clear from eq 2 that the sensitivity of the thermal lens technique also depends on the thermal physical properties of the solvent in which the analyte dissolves. Higher sensitivity per unit excitation laser power, i.e., high  $E/P$  value, can be achieved by choosing solvents with high  $dn/dT$  and low thermal conductivity values. The thermal physical and  $E/P$  values of some commonly employed solvents are summarized in Table I (7-10). Aqueous solutions are the worst medium for thermal lens techniques owing to water's low  $dn/dT$  value and high  $k$  value. Generally, nonpolar solvents such as carbon tetrachloride and hydrocarbons are good thermo-optical solvents because they have high  $dn/dT$  and low  $k$  values. At the same applied laser intensity, thermal lens measurements in *n*-pentane and  $\text{CCl}_4$  are estimated to be 40-47 times more sensitive than those in water (Table I). It is thus possible to enhance the fluorescence as well as thermal lens signals of an analyte by improving its radiative relaxation processes and performing the measurement in a solvent which has high  $dn/dT$  and low  $k$  values, respectively.

Amphiphilic surfactant molecules form micelles in aqueous solution and reversed micelles in nonpolar solvents. The term

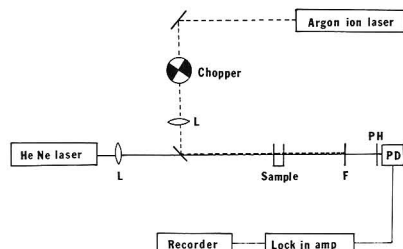


**Figure 1.** Schematic diagram of the thermal lens apparatus. L is a lens, F is a filter, PH is a pinhole, and PD is a pin photodiode.

"reversed" is used as these nonpolar solvent micelles are reversed in relation to that in aqueous micellar solution. The surfactant's polar head groups define the water-soluble polar core region of the micelle shielded by its nonpolar hydrocarbon tails. Consequently, the reversed micelle contains a small water pool in which water-soluble analytes can be dissolved. This solubilization process can be used to enhance or to quench the radiative processes of the analyte. In fact, micelles have been used to enhance fluorescence, phosphorescence, and chemiluminescence (11–15) or to quench the fluorescence interference to facilitate the Raman scattering measurement of highly fluorescent analytes (16). An important additional advantage provided by reversed micelles is their ability to improve the thermal physical properties of the solvent. Namely, the size of the water pool containing the dissolved analyte is relatively small (less than 20 Å) so that the thermal physical properties of a reversed micellar solution are expected to be similar to those of the bulk nonpolar solvent (17). Consequently, reversed micellar solution should provide an ideal medium for enhanced thermal lens for solubilized polar analytes. In spite of its great potential, reversed micelles have not been previously exploited to enhance the sensitivity of the thermal lens measurement.

Such considerations prompted the present study, which aims to develop a chemical method to enhance the sensitivity of fluorescence as well as thermooptical measurements. It will be demonstrated for the first time that reversed micelles simultaneously enhance the fluorescence and thermal lens of solubilized analytes. The mechanism for the enhancements, the analytical utility, and implications of this finding will be discussed.

## EXPERIMENTAL SECTION

The schematic diagram of the pump and probe configuration thermal lens apparatus is shown in Figure 1. In this system, a Coherent Innova 100-10 argon ion laser operated in the ultraviolet multilines (333.6, 351.1, and 363.8 nm) was used as a pump beam. The ultraviolet excitation beam, which was amplitude modulated by a mechanical chopper (Stanford Research Systems Model SR 540 variable speed chopper) was focused onto the sample cell by a quartz lens with 50-mm focal length. A He-Ne laser (Spectra-Physics Model 154) was used as a probe beam. The pump and probe beams were aligned to overlap inside the sample cell by means of a dichroic filter. The heat generated by the sample absorption of the pump beam changes the intensity of the probe beam. The intensity fluctuation of the probe beam was measured by a pin photodiode (United Detector Technology Pin, 10 DP) placed behind a 0.1-mm pinhole and demodulated and amplified by a lock-in amplifier (Stanford Research Systems Model SR 510). A lens with 50-mm focal length was used to focus the probe beam and its relative distance from the sample was adjusted to give a maximal signal. Signal intensity was obtained from the digital reading on the lock-in amplifier whose time constant was maintained as 1 s. The whole apparatus was vibrationally isolated by means of an optical table. Each measurement was performed at least in triplicate and their average values are reported.

Absorption spectra were taken on a Perkin-Elmer 320 spectrophotometer. Fluorescence spectra were measured on a Perkin-Elmer LS-5 spectrofluorometer interfaced with a Perkin-Elmer 3600 data station.

Terbium chloride hexahydrate (Aldrich Gold Label 99.999%), cetyltrimethylammonium bromide (CTAB, Kodak) and sodium dodecyl sulfate (SDS, Kodak, gel electrophoresis grade) were used without further purification. Sodium bis(2-ethylhexyl)sulfosuccinate (AOT) was purchased from Sigma and purified as previously described (18). Typically, the AOT was dissolved in carbon tetrachloride (Burdick & Jackson, Muskegon, MI) containing activated charcoal and stirred while heated at 35 °C for 1 h. The solution was filtered and the solvent was rotary evaporated. The pure AOT was dried in vacuo at 98 °C to constant weight (2 days).

A 3.0 M stock solution of  $\text{Tb}^{3+}$  in water was prepared by dissolving terbium chloride hexahydrate in water with a few drops of hydrochloric acid. Its concentration was determined spectrophotometrically (19).

Reversed micellar solution was prepared by injecting the  $\text{Tb}^{3+}$  aliquot into the solution of surfactant (AOT) in nonpolar solvent. An appropriate amount of water was then added in order to obtain the required concentration. If necessary, the mixture was sonicated by means of a sonication bath (Bransonic Model 2200) to clarify. The clear reversed micellar solution was filtered through a Spartan-25 Teflon filter with 0.20- $\mu\text{m}$  pore size prior to any measurement.

## RESULTS AND DISCUSSION

Terbium chloride was chosen for this study because of its high hydrophilicity. It is very soluble in water, sparingly soluble in polar solvents such as alcohols, and insoluble in nonpolar solvents, e.g., carbon tetrachloride and hydrocarbons. An aqueous solution of the  $\text{Tb}^{3+}$  ions emits weak luminescence with a quantum yield of  $4.4 \times 10^{-5}$  upon excitation (20). Therefore, both fluorescence and thermal lens measurements can be carried out on this complex with the results providing an insight into the mechanism of these processes.

The ultraviolet lines of the argon ion laser (power 35 mW) were modulated at 10 Hz and used as an excitation beam to measure the thermal lens of  $\text{Tb}^{3+}$  in various solvents. As expected based on the  $dn/dT$  and  $k$  values in Table I, thermal lens signal intensities of  $\text{Tb}^{3+}$  in polar organic solvents such as methanol and 1-butanol are appreciably higher than that in pure water. These values are listed in Table II as the relative intensity  $(\text{RI})_{\text{exptl}}$ , which is defined as

$$(\text{RI})_{\text{exptl}} = \frac{S_{\text{sample}} - S_{\text{blank}}}{S_{\text{water}}}$$

where  $S_{\text{sample}}$  and  $S_{\text{water}}$  are the thermal lens signals of equal concentrations of  $\text{Tb}^{3+}$  in the sample and in water, respectively, and  $S_{\text{blank}}$  is the blank signal.

Compared to that in water, the thermal lens signal amplitude is enhanced 10 times when  $\text{Tb}^{3+}$  is dissolved in methanol. The enhancement is further increased to 15 times when  $\text{Tb}^{3+}$  is in 1-butanol. Interestingly, the thermal lens intensities of  $\text{Tb}^{3+}$  in the anionic sodium dodecyl sulfate (SDS) as well as in the cationic cetyltrimethylammonium bromide (CTAB) aqueous micelles are the same as that in water (Table II). The lack of thermal lens enhancement in these aqueous micelles can be explained in terms of the location of the  $\text{Tb}^{3+}$  ions. In CTAB aqueous micellar solution, the  $\text{Tb}^{3+}$  ions are located well in the bulk water because of the hydrophilicity of the lanthanide ions and the electrostatic repulsion between the micellar cationic headgroups and the  $\text{Tb}^{3+}$  cation. The  $\text{Tb}^{3+}$  ions are also exposed to the water in the SDS micellar solution even though there may be electrostatic attractions between the ions and the anionic micellar headgroups. Consequently, the thermal lens intensities of  $\text{Tb}^{3+}$  in these two aqueous micellar systems are the same as that in water because it has been shown above that the thermal lens depends

**Table II. Relative Thermal Lens Signal Intensity of TbCl<sub>3</sub> in Different Media**

surfactant <sup>a</sup>	solvent	(RI) <sub>exptl</sub> <sup>b</sup>	(RI) <sub>calcd</sub> <sup>c</sup>
	water	1	1
	methanol	10	17
	1-butanol	15	21
	dioxane	22	27
AOT	dioxane	25	27
AOT	<i>n</i> -nonane	15	28
AOT	<i>n</i> -heptane	21	33
AOT	<i>n</i> -pentane	23	40
AOT	cyclohexane	20	36
AOT	CCl <sub>4</sub>	38	47
SDS	water	1	1
CTAB	water	1	1

<sup>a</sup>Concentrations of surfactants used were [AOT] = 0.2 M, [SDS] = 0.15 M, and [CTAB] = 0.1 M. <sup>b</sup>(RI)<sub>exptl</sub> = (S<sub>sample</sub> - S<sub>blank</sub>)/S<sub>water</sub>, where S<sub>sample</sub> and S<sub>water</sub> are thermal lens signals of equal concentration of Tb<sup>3+</sup> in a sample and in water, respectively and S<sub>blank</sub> is the blank signal. <sup>c</sup>(RI)<sub>calcd</sub> is calculated as (RI)<sub>calcd</sub> = (E/P)<sub>soln</sub>/(E/P)<sub>water</sub>, where the values for thermal lens enhancement per unit laser power in solvent (E/P)<sub>soln</sub> and in water (E/P)<sub>water</sub> are obtained from Table I.

on the thermo-optical property of the solvent surrounding the Tb<sup>3+</sup> ions which is water in SDS as well as CTAB.

Due to its hydrophilicity, terbium chloride is insoluble in nonpolar solvents. The Tb<sup>3+</sup> aqueous solution can be, however, solubilized in a nonpolar solvent such as carbon tetrachloride or hydrocarbons if surfactant molecules such as Aerosol-OT (AOT) are present. This is due to the fact that these surfactant molecules form reversed micelles in the nonpolar solvent (11, 12). In the reversed micelle, the surfactant's polar headgroups outline a water-soluble polar core region of the micelles which is shielded by its nonpolar hydrocarbon tails. Consequently, the reversed micelle contains a small water pool which includes the Tb<sup>3+</sup> aqueous solution. Table II lists the relative thermal lens signal intensity of Tb<sup>3+</sup> solubilized in anionic AOT reversed micelles formed in different nonpolar solvents, i.e., CCl<sub>4</sub>, *n*-pentane, *n*-heptane, and *n*-nonane.

It is interesting to note that in spite of the fact that the Tb<sup>3+</sup> ions are in the water pool of the reversed micelles, the thermal lens signal intensities of the Tb<sup>3+</sup> are much higher than that in pure water. This appears to be the first observation of an enhancement of thermal lens phenomena by reversed micelles. The enhancements were found to be dependent on the particular nonpolar solvent in which the reversed micelles are formed. Under identical conditions, Tb<sup>3+</sup> exhibits 38-fold enhancement when it is solubilized in AOT/CCl<sub>4</sub> reversed micelles compared to that in pure water. This enhancement factor decreases to 23 in AOT/*n*-pentane, 20 in AOT/cyclohexane, 21 in AOT/*n*-heptane, and 15 in AOT/*n*-nonane.

Taking advantage of the fact that AOT forms reversed micelles in dioxane (21) and terbium chloride is soluble in this solvent, thermal lens measurements were also performed for Tb<sup>3+</sup> in pure dioxane and for Tb<sup>3+</sup> solubilized in the water pool of AOT/dioxane reversed micelles. The thermal lens of Tb<sup>3+</sup> in pure dioxane is 22 times more than that in pure water and is the same, within experimental error, as that of Tb<sup>3+</sup> in AOT/dioxane (25X, Table II). These results suggest that the thermal lens of Tb<sup>3+</sup> in AOT reversed micellar systems is governed by the thermal physical properties of the bulk nonpolar solvent even though the complex is solubilized in the micellar water pool. This observation can be explained in terms of the relative size of the water pool and the laser beam spot size. The concentrations of the solubilized water in the reversed micellar systems used in this work were kept very low ( $w = [H_2O]/[AOT] < 4$ ) so that the diameter of the

**Table III. Relative Fluorescence Intensity of TbCl<sub>3</sub> in Different Media**

surfactant <sup>a</sup>	solvent	RI <sub>550nm</sub> <sup>b</sup>	RI <sub>590nm</sub> <sup>b</sup>
	water	1.3	1.8
	methanol	3.6	3.3
	1-butanol	2.2	2.6
	dioxane	3.2	2.4
AOT	dioxane	3.6	2.9
AOT	<i>n</i> -heptane	3.2	3.6
AOT	<i>n</i> -nonane	2.9	3.5
AOT	<i>n</i> -pentane	2.5	3.0
AOT	CCl <sub>4</sub>	2.5	3.8

<sup>a</sup>Concentration of surfactant used was [AOT] = 0.2 M. <sup>b</sup>Relative fluorescence intensities, excited at 370 nm.

water pools is estimated to be less than 20 Å (11). This value is smaller than the spot size of the laser beam at the sample which is estimated to be 0.10 mm. Therefore, the measured thermal lens is strongly affected by the physical properties of the bulk nonpolar solvent of the reverse micelle.

Table II also lists the relative intensity values calculated in terms of the enhancement per unit laser power values listed in Table I, assuming that Tb<sup>3+</sup> had been soluble in these nonpolar solvents and that its photophysical properties are the same as those in pure water (RI)<sub>calcd</sub>. The relative enhancement for Tb<sup>3+</sup> in AOT/CCl<sub>4</sub> was found to be 38 times which is relatively lower than the 47 times enhancement expected from the calculation. In fact, the experimental values for Tb<sup>3+</sup> in AOT in a variety of different nonpolar solvents are always lower than the corresponding calculated values; i.e., (RI)<sub>exptl</sub> values were 20, 23, 21, and 15 while (RI)<sub>calcd</sub> values were 36, 40, 33, and 28 for Tb<sup>3+</sup> in AOT/cyclohexane, AOT/*n*-pentane, AOT/*n*-heptane, and AOT/*n*-nonane, respectively. A variety of reasons might account for this discrepancy. The most likely are the invalidity of such assumptions as the use of the thermal conductivity value of a pure solvent for the AOT reversed micellar systems and the similarity in the photophysical properties of Tb<sup>3+</sup> in different media to that in pure water.

In fact, the thermal conductivity is known to be directly proportional to the order of a mixture. Therefore, the use of the thermal conductivity value of a pure solvent for that of an AOT reversed micellar system is probably not valid because the two systems have different structures. However, the fact that similar discrepancies were also found for Tb<sup>3+</sup> in pure methanol, 1-butanol, and dioxane (the (RI)<sub>exptl</sub> values were 10, 15, and 22 while (RI)<sub>calcd</sub> values were 17, 21, and 27 for methanol, 1-butanol, and dioxane, respectively) suggested that the contribution of this effect to the discrepancy is rather small. Consequently, the photophysical properties of Tb<sup>3+</sup> in different media are probably different from those in pure water. This possibility was further investigated by fluorescence measurement.

Excitation of Tb<sup>3+</sup> solution at 370 nm resulted in weak emissions, centered at 420, 495, 550, and 590 nm (uncorrected). The relative intensities of the two highest bands, 495 and 550 nm for Tb<sup>3+</sup> in different media, are listed in Table III. Interestingly, the fluorescence intensities were found to be enhanced by a factor of 2 or greater when Tb<sup>3+</sup> is dissolved in an organic solvent such as methanol, 1-butanol, or dioxane as compared to that in pure water. Similar enhancements were also observed when Tb<sup>3+</sup> is solubilized in the water pool of AOT/CCl<sub>4</sub>, AOT/*n*-pentane, AOT/*n*-nonane, AOT/*n*-heptane, and AOT/dioxane reversed micellar systems. A variety of reasons might account for these enhancements, including the increase in viscosity of the micellar media compared to that in pure water (18). However, the most likely one is the quenching effect of water. In bulk water, the excited Tb<sup>3+</sup>

is quenched by the high-frequency OH vibrations of the surrounding water molecules (22-25) and this quenching leads to the low fluorescence quantum yield ( $\Phi = 4.4 \times 10^{-3}$ ) (20). The fluorescence intensity is enhanced when  $Tb^{3+}$  is in organic solvents because the high-frequency OH vibrations are not present in these media. Similarly, the high-frequency OH vibrations were not available in the reversed micellar systems in spite of the fact that there were substantial water pools present in these micellar systems. This is because the hydration number for the surfactant polar head groups are 10 and the amount of added water was kept very low ( $w = [H_2O]/[AOT] < 4$ ) so that all added water molecules were bound to the charged surfactant headgroups (25, 26). The  $Tb^{3+}$  ions are solubilized in these small water pools probably because of the strong interactions between the trications and the surfactant's anionic headgroups and between the  $Tb^{3+}$  ions and the bound water molecules which are not efficient fluorescence quencher (23, 24).

Taken together, these results provide clear evidence for the simultaneous enhancement of the fluorescence and thermal lens signal of  $Tb^{3+}$  by reversed micellar systems. The fluorescence is enhanced because the reversed micelles isolate and protect the analyte from water quencher molecules whereas the thermal lens enhancement is due to modification of the thermal physical properties of the solvent by reversed micelles, i.e., increased  $dn/dT$  and decreased thermal conductivity,  $k$ , values. However, because of the change in the radiative processes of the analyte in going from pure water to organic solvents and/or reversed micelles, the observed thermal lens values are less than the calculated ones.

The calibration curve for  $Tb^{3+}$  ion solubilized in a 0.2 M AOT/ $CCl_4$  reversed micellar system was measured on the thermal lens apparatus using the 35-mW multilines ultraviolet excitation laser beam modulated at 10 Hz as an excitation source. The calibration plots exhibited a linear response (correlation coefficient,  $r = 0.994$ ) over a concentration range of  $3 \times 10^{-6}$  to  $3 \times 10^{-4}$  M. The limit of detection, LOD, defined as the amount of the sample that yielded a signal twice the standard deviation of the blank, is estimated to be  $4.5 \times 10^{-7}$  M which corresponds to an absorbance of about  $1.3 \times 10^{-7}$ . This LOD value is comparable with the  $5.0 \times 10^{-7}$  value obtained for iodine in pure carbon tetrachloride solvent (27) and is 2 orders of magnitude lower than the LOD values obtained for neodymium and praseodymium in  $HClO_4$  solution (28).

It has been demonstrated that the sensitivity of two fundamentally different techniques, fluorescence and thermal lens, can be enhanced simultaneously by reversed micelles. This enhancement facilitates the use of these techniques as a complementary means for the detection and identification of fluorescent as well as nonfluorescent trace chemical species.

Experiments are now in progress to expand the application of these techniques in the area of general trace chemical analysis.

**Registry No.** AOT, 577-11-7; Tb, 7440-27-9;  $CCl_4$ , 56-23-5; water, 7732-18-5; methanol, 67-56-1; 1-butanol, 67-56-1; dioxane, 123-91-1; *n*-nonane, 111-84-2; *n*-heptane, 142-82-5; *n*-pentane, 109-66-0; cyclohexane, 110-82-7.

## LITERATURE CITED

- (1) Harris, J. M.; Dovichi, N. J. *Anal. Chem.* **1980**, *52*, 695A-706A.
- (2) Tran, Chieu D. *Anal. Chem.* **1986**, *58*, 1714-1716.
- (3) Tran, Chieu D. *Appl. Spectrosc.* **1986**, *40*, 1108-1110.
- (4) Tran, Chieu D. *Appl. Spectrosc.* **1987**, *41*, 512-516.
- (5) Klier, D. S. *Ultraviolet Laser Spectroscopy*; Academic: New York, 1983.
- (6) Piegmeier, E. H. *Analytical Applications of Lasers*; Wiley: New York, 1986.
- (7) Tseberg, N. V. *Thermal Conductivity of Gases and Liquids*; MIT Press: Cambridge, 1965.
- (8) Timmermans, J. *Physics—Chemical Constants of Pure Organic Compounds*; Elsevier: Amsterdam, 1965; Vol. 1 and 2.
- (9) Mori, K.; Imasaka, T.; Ishibashi, N. *Anal. Chem.* **1982**, *54*, 2034-2038.
- (10) Spirin, G. G. *Inzh.-Fiz. Zh.* **1978**, *35*, 445-449.
- (11) Fendler, J. H. *Membrane Mimetic Chemistry*; Wiley: New York, 1982.
- (12) Hinze, W. L. *Solution Chemistry of Surfactants*; Mittal, K. L., Ed.; Plenum: New York, 1979; Vol. 1, pp 79-127.
- (13) Armstrong, D. W. *Sep. Purif. Methods* **1985**, *14*, 213-304.
- (14) Cline Love, L. J.; Dorsey, J. G.; Habarta, J. G. *Anal. Chem.* **1984**, *56*, 1132A-1148A.
- (15) Hoshino, H.; Hinze, W. L. *Anal. Chem.* **1987**, *59*, 496-504.
- (16) Armstrong, D. W.; Spino, L. S.; Ondras, M. R.; Findsen, E. W. J. *J. Am. Chem. Soc.* **1986**, *108*, 5646-5647.
- (17) Lalanne, J. R.; Poullgny, B.; Sein, E. J. *Phys. Chem.* **1983**, *87*, 696-707.
- (18) Calco-Perez, V.; Beddard, G. S.; Fendler, J. H. J. *Phys. Chem.* **1981**, *85*, 2316-2319.
- (19) Escabi-Perez, J.; Nome, F.; Fendler, J. H. J. *Am. Chem. Soc.* **1977**, *99*, 7749.
- (20) Stein, G.; Wurzbach, E. J. *Chem. Phys.* **1975**, *62*, 208.
- (21) Eicke, H. F.; Christen, H. J. *Colloid Interface Sci.* **1974**, *46*, 417-427.
- (22) Kropp, J. L.; Whinston, M. W. J. *Chem. Phys.* **1967**, *71*, 477-482.
- (23) Eicke, H. F.; Shepherd, J. C. W.; Steinemann, A. J. *Colloid Interface Sci.* **1976**, *56*, 168-176.
- (24) Sunamoto, J.; Hamada, T.; Seto, T.; Yamamoto, S. *Bull. Chem. Soc. Jpn.* **1980**, *53*, 583-589.
- (25) Gelade, E.; De Schryver, F. C. J. *Am. Chem. Soc.* **1984**, *106*, 5871-5875.
- (26) Wong, M.; Thomas, J. K.; Nowak, T. J. *Am. Chem. Soc.* **1977**, *99*, 4730-4736.
- (27) Jansen, K. L.; Harris, J. M. *Anal. Chem.* **1985**, *57*, 2434-2436.
- (28) Berthoud, T.; Delorme, N. *Appl. Spectrosc.* **1987**, *41*, 15-19.

Chieu D. Tran

Department of Chemistry  
Marquette University  
Milwaukee, Wisconsin 53233

RECEIVED for review June 17, 1987. Accepted September 22, 1987. Acknowledgment is made to the donors of the Petroleum Research Fund, administered by the American Chemical Society, and to the Marquette University Committee on Research for financial support of this research.

## Influence of Porphyrin Structure on Anion Selectivities of Manganese(III) Porphyrin Based Membrane Electrodes

*Sir:* Although highly selective polymeric membrane electrodes are now routinely used for in situ determinations of various cations, the development of similar devices for detection of anions has been hampered by the inability to identify appropriate membrane active components. To date, the vast majority of anion selective liquid/polymer membrane electrodes have been formulated with tetraalkylammonium

or phosphonium salts (1, 2). Such sensors respond via a classical ion-exchange mechanism in which the counter-anions in the membrane are dissociated from the mobile, lipophilic, positively charged sites. Thus, selectivity is dictated by the relative solubility of individual anions in the membrane solvent (i.e., plasticizer) (3). This results in the so-called Hofmeister pattern (4) ( $ClO_4^- > IO_4^- > I^- > Br^- > Cl^- > HCO_3^-$ ) in which



more lipophilic anions are preferred.

Recent studies have shown that anti-Hofmeister behavior can only be achieved if anions in the sample can selectively interact with components of the membrane phase. These components may be charged or neutral (5). Both the unusual selectivities of trifluoroacetophenone derivatives for carbonate (6), and alkyltin compounds for thiocyanate (7), have been attributed to neutral carrier type mechanisms. On the other hand, it has been postulated that the unique selectivity of lipophilic vitamin B<sub>12</sub> derivatives toward nitrite involves an associated charged carrier mechanism in which the nitrite selectively coordinates as an axial ligand to the central Co(III) atom of a positively charged metallocorine (8, 9).

While several groups have studied the use of metalloporphyrins as membrane active components for the transport of gases, ions, and molecules (10–14), relatively few efforts have focused on the potential analytical utility of such membranes. However, in recent preliminary studies it has been shown that polymeric membranes based on Mn(III) porphyrins yield anion responses which differ somewhat from classical Hofmeister behavior (15, 16). Since potentiometric response of these metalloporphyrin doped membranes is likely to involve direct interaction of the anion as an axial ligand of the Mn(III), we were interested in examining whether changes in the porphyrin structure, both in terms of initial ligation as well as substitution on the porphine ring, can influence the ability of given anions to bind as axial ligands and thereby alter potentiometric anion selectivity. Results presented here demonstrate that such structural changes do indeed have a significant effect on the selectivities observed and that these variations in selectivity can be partly explained based on the coordination chemistry of the metalloporphyrins examined.

### EXPERIMENTAL SECTION

**Apparatus.** For all potentiometric measurements reported, the following galvanic cell was employed: Hg/Hg<sub>2</sub>Cl<sub>2</sub>(s), KCl-saturated/MES (0.05 mol/L), pH 5.5/sample solution/PVC-porphyrin membrane/KCl (0.1 mol/L), AgCl(s)/Ag.

The external reference electrode was a double-junction cracked-bead SCE electrode. The outer filling solution was 0.05 mol/L 2-morpholinoethanesulfonic acid (MES), adjusted to pH 5.5 with NaOH solution. The polymeric membrane composition was as follows: 1 wt % of porphyrin, 66 wt % of dibutyl sebacate (DBS) (Eastman Kodak, Rochester, NY), and 33 wt % of poly(vinyl chloride) (PVC) (Polysciences, Inc., Warrington, PA). All membranes were cast as described in (7); however, absolute amounts of the casting reagents were adjusted somewhat to obtain membranes that were 100-μm thick (40 mg PVC, 80 mg DBS, 1.2 mg porphyrin). With this formulation, there was no visual evidence suggesting porphyrin crystallization or aggregation in the membrane phase. Membranes were mounted in Phillips electrode bodies (IS-561) (Glasblaseri Moller, Zurich). The internal reference solution was 0.1 mol/L KCl. There was no conditioning of the membranes unless otherwise indicated.

Cell potentials were measured in a thermostated cell at 25 °C in 50 mL of sample solution. The electrodes were connected through a high impedance amplifier to a Zenith Z-100 PC computer equipped with an analog-to-digital converter (DT2801, Data Translation, Inc., Marlborough, MA).

**Reagents.** The porphyrin compounds, chloro(5,10,15,20-tetraphenylporphyrinato)manganese(III) [Mn(TPP)Cl] (2), azido(5,10,15,20-tetraphenylporphyrinato)manganese(III) [Mn(TPP)N<sub>3</sub>] (3), chloro(5,10,15,20-tetramesitylporphyrinato)manganese(III) [Mn(TMP)Cl] (4), α,α,α,α-chloro(5,10,15,20-tetrakis(8-bromo-1-naphthyl)porphyrinato)manganese(III) [Mn(TBrNP)Cl] (5), α,α,α,α-chloro(5,10,15,20-tetrakis(8-chloro-1-naphthyl)porphyrinato)manganese(III) [Mn(TCINP)Cl] (6), and α,α,α,β-chloro(5,10,15,20-tetrakis(8-bromo-1-naphthyl)porphyrinato)manganese(III) (7), were synthesized according to methods we have described elsewhere (17, 18). Chloro(β-5,15-[2,2'-(dodecathienyloxy)diphenyl]-α-10,20-(2,2'-(3,3'-(pyridine-3,5-diyl)dipropoxy)diphenyl]porphyrinato)manganese(III), [Mn(DDPP)Cl] (8), and chloro(β-5,15-[2,2'-(dodecathienyloxy)diphenyl]-α-10,20-[2,2'-(6-imidazole)diphenyl]porphyrinato)-manganese(III) [Mn(MDIP)Cl] (9) were graciously provided by Dr. M. Mometeau, Institut Curie, Centre Universitaire, Orsay, France.

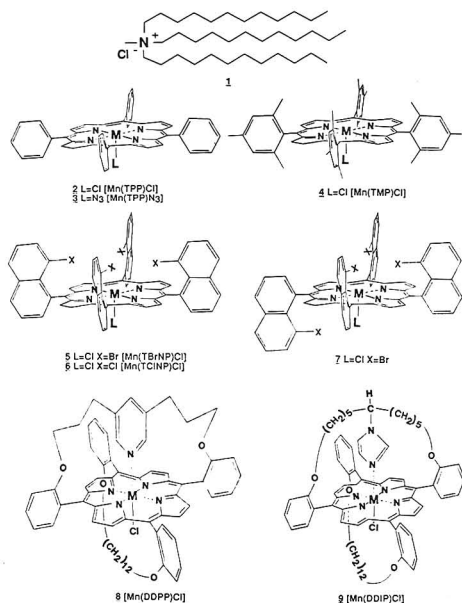


**Figure 1.** Structures of a quaternary ammonium (1) and manganese(III) (2–9) metalloporphyrin species used to prepare membranes.

oxy)diphenyl]-α-10,20-[2,2'-(6-imidazole)diphenyl]porphyrinato)-manganese(III) [Mn(MDIP)Cl] (9) were graciously provided by Dr. M. Mometeau, Institut Curie, Centre Universitaire, Orsay, France.

**Determination of emf Response and Selectivity of Membranes.** Anion selectivity coefficients were determined by the separate solution method (19) from cell emf values obtained at anion levels of 10 mmol/L. Activity coefficients were estimated by using the extended Debye–Hückel equation.

Response toward different anions was evaluated by making standard additions of a 0.1 mol/L solution of the sodium salt of each anion to 50 mL of 0.05 mol/L MES buffer, pH 5.5. The response of the membranes toward pH was determined by additions of 0.1 mol/L NaOH to 50 mL of 0.05 mol/L phosphoric acid. The pH of this sample solution was monitored simultaneously with a conventional glass pH electrode.

In all experiments, the response of the membranes toward the anions or pH changes was quite rapid, reaching relatively stable emf values within 100 s after the additions. The emf values were recorded every 4 s and the average potential over the last 20 s of the 100 s response period was used for subsequent calculations.

### RESULTS AND DISCUSSION

Table I summarizes the potentiometric anion selectivity coefficients, relative to chloride, for polymeric membranes prepared with the eight Mn(III) porphyrins shown in Figure 1. For comparison purposes, data is also presented for a membrane containing a typical anion exchanger, TDMA-Cl (1), evaluated under the exact same experimental conditions.

When relatively simple unhindered porphyrin structures are employed as active membrane components (Mn(TPP)Cl (2), Mn(TPP)N<sub>3</sub> (3)), moderate deviations from the Hofmeister pattern are evident. Indeed, salicylate becomes the preferred species, although selectivity for this anion is only marginal over those normally favored in the Hofmeister series. In general, the range of selectivity coefficient values is considerably suppressed when compared to that obtained with TDMA-Cl. This is in good agreement with earlier preliminary studies involving Mn(III) porphyrins (15, 16) and suggests that



**Table I. Logarithm of Anion Selectivity Coefficients for Mn(III) Porphyrin Based Membranes<sup>a-c</sup>**

anion	1	2	3	4	5	6	7	8	9
Cl <sup>-</sup>	0.0	0.0	0.0	0.0	0.0	0.0	0.0	0.0	0.0
Br <sup>-</sup>	0.6	0.3	0.5	0.2	0.2	0.4	0.3	0.4	0.6
I <sup>-</sup>	2.8	1.5	1.5	1.5	1.6	1.5	1.7	2.1	2.5
Sal	2.7	2.1	2.4	3.2	2.0	2.4	2.4	2.4	2.3
SCN <sup>-</sup>	3.0	1.3	1.6	2.5	3.5	3.0	3.2	2.0	2.0
IO <sub>4</sub> <sup>-</sup>	4.0	1.8	2.1	1.7	0.6	1.5	1.0	3.0	2.6
ClO <sub>4</sub> <sup>-</sup>	4.6	1.5	1.7	1.5	0.4	1.2	0.8	3.5	3.3

<sup>a</sup> Selectivity coefficients determined relative to chloride, log  $k_{\text{Cl}^+/\text{X}^-}^{\text{pot}}$ , using the separate solution method (14), in a 0.05 M MES/NaOH buffered solution, pH 5.5. <sup>b</sup> Membrane compositions: 1 wt % of compound; 33 wt % PVC; 66 wt % dibutyl sebacate. Internal electrolyte was 0.1 M KCl for all electrodes. <sup>c</sup> See Figure 1 for structures of compounds 1-9.

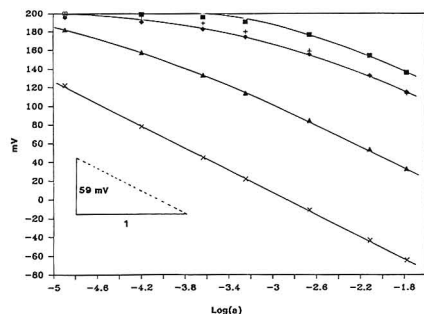


**Figure 2.** Potentiometric response of Mn(TBrNP)Cl (5) doped polymeric membrane to Cl<sup>-</sup> (■), Br<sup>-</sup> (+), ClO<sub>4</sub><sup>-</sup> (◆), Sal (▲), and SCN<sup>-</sup> (X) in 50 mL 0.05 mol/L MES/NaOH solution, pH 5.5.

these metalloporphyrins are not behaving primarily as classical dissociated ion-exchange molecules in the membrane. That is, there must be some association of the anion with the central Mn(III) metal, and it is the relative affinity of the anion as a fifth or sixth ligand which dictates selectivity. Perchlorate and IO<sub>4</sub><sup>-</sup> are known to be weak Mn(III) porphyrin axial ligands (20) and this may account for the dramatic loss in response toward these lipophilic species. Note that altering the initial fifth site ligation (Cl<sup>-</sup> to N<sub>3</sub><sup>-</sup>) has relatively little effect on the overall pattern observed.

When additional hydrophobic character in the form of methyl groups is added around the coordination sites (Mn(TMP)Cl (4)), a marked increase in the response to both salicylate and SCN<sup>-</sup> is observed (see Table I). Such increases occur without concomitant changes in the response toward other lipophilic anions (ClO<sub>4</sub><sup>-</sup>, IO<sub>4</sub><sup>-</sup>, I<sup>-</sup>). This implies that the coordination of salicylate and SCN<sup>-</sup> ions are stabilized by the presence of the methyl groups.

To gain further insight into the mechanism by which the Mn(III) porphyrins are functioning within the membranes, Mn(III) porphyrin structures were examined in which anion accessibility to one side of the metal is partly or totally impaired. When certain tetrahalonaphthylporphyrins were used (5, 6, and 7), response toward ClO<sub>4</sub><sup>-</sup> and IO<sub>4</sub><sup>-</sup> is reduced up to 10-fold, whereas response toward SCN<sup>-</sup> is enhanced (relative to Mn(TMP)Cl and Mn(TPP)Cl). In the case of ClO<sub>4</sub><sup>-</sup> and IO<sub>4</sub><sup>-</sup>, the degree of response correlates to the cavity size as determined by X-ray structures ( $\alpha,\alpha,\alpha,\alpha$ -Mn(TBrNP)Cl, 1.64 Å;  $\alpha,\alpha,\alpha,\alpha$ -Mn(TCINP)Cl, 3.2 Å (18)). This data suggests that the anions are capable of binding as sixth ligands and that selectivity can be varied by controlling which anions can coordinate at this site. Indeed, binding of anions with tetrahedral structures (ClO<sub>4</sub><sup>-</sup> and IO<sub>4</sub><sup>-</sup>) is probably restricted by

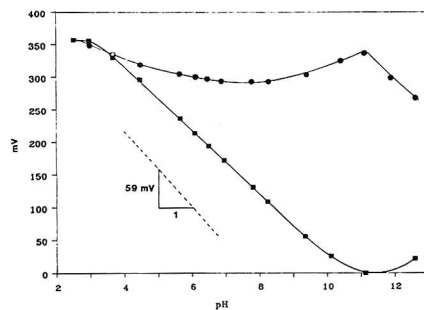


**Figure 3.** Potentiometric pH response of Mn(TPP)Cl (2) doped polymeric membrane before (●) and after (■) 4 day treatment in 0.01 mol/L NaOH solution.

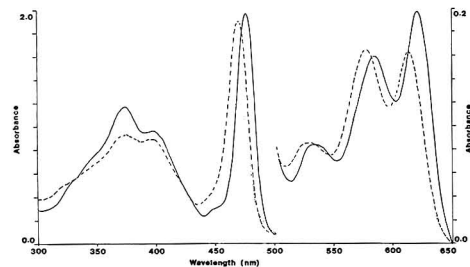


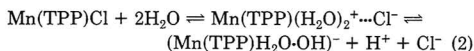
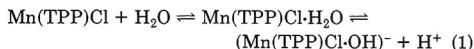
**Figure 4.** UV-vis absorption spectra of 0.015 mol/L Mn(TPP)Cl (2) in polymeric membrane before treatment (—), after 4 day water treatment (---), and after 4 day treatment in 0.1 mol/L NaOH (— · —).

the geometry of the axial cavity created by the halogen atoms. Linear SCN<sup>-</sup> can easily fit within this cavity and its coordination affinity to Mn(III) is apparently enhanced. In general, the total response toward a given anion is likely to depend on its relative strength as an axial ligand (e.g. association constant at sixth coordination site). Typical calibration curves for several of the anions obtained by using membranes doped with Mn(TBrNP)Cl (5) are shown in Figure 2. Near Nernstian behavior is observed for the preferred anion (SCN<sup>-</sup>), while weakly ligated anions (e.g. Cl<sup>-</sup>, ClO<sub>4</sub><sup>-</sup>, Br<sup>-</sup>) yield very small responses (sub-Nernstian).

As Table I indicates, when one side of the Mn(III) is totally blocked (capped) with an intramolecularly bound neutral axial ligand (compounds 8 and 9) selectivity essentially reverts back to the classical Hofmeister pattern. It is well-known that imidazole and pyridine are strong  $\sigma$  electron donating ligands and such strong intramolecular coordination on one side of the metal generally weakens the interactions of ligands at the other axial site (21). Thus, within the membrane phase, the chloride ions are likely to be dissociated from such porphyrin structures yielding a positively charged lipophilic ion-exchange type species. Consequently, analyte anions can enter the membrane phase predominately as solvated counter ions with little or no affinity for the central Mn(III) atom.

The pH response of the various Mn(III) porphyrin based membranes was also investigated. For example, upon initial testing, membranes doped with Mn(TPP)Cl show little response to pH (Figure 3). However, when those same membranes are conditioned for prolonged periods (4 days) in water or NaOH solutions, the pH response dramatically increases, becoming nearly Nernstian in the range of pH 4-10 (see Figure 3). Similar results were obtained immediately with unconditioned membranes when small amounts of concentrated NaOH were added to the THF membrane casting solution.

As the response to pH changes upon conditioning or pretreatment, there is relatively little alteration in the potentiometric response to the various anions in buffered solutions. There is, however, a change in the visible absorption spectra of the membrane (Figure 4), suggesting a change in axial coordination (either H<sub>2</sub>O or OH<sup>-</sup>) at the fifth and/or sixth sites. Two reaction sequences are possible:



In the first instance, one water molecule simply adds as a sixth ligand, and pH response for the resulting complex can occur due to dissociation of a water proton yielding a negatively charged metalloporphyrin-OH<sup>-</sup> complex. In the second case, two waters can add to the Mn(III), one displacing the initial Cl<sup>-</sup>, forming a dissociated ion-exchanger type system in which Cl<sup>-</sup> is solvated in the membrane but not coordinated to the metal. The data suggests that the latter is unlikely since Mn(TPP)Cl membranes conditioned in water still exhibit anti-Hofmeister behavior with regard to anion response. In addition, as shown in Figure 3, at very high pHs, potentiometric responses level off and actually reverses. This behavior has been observed previously in neutral carrier based systems in which the membrane becomes overloaded with charge at high analyte ion levels (6, 22). In this case, we believe that the first reaction sequence more readily explains such behavior; i.e., loss of a proton in basic solution makes the membrane more negatively charged, giving rise to cation response. Similarly, replacement of a single water by an anion at the membrane/sample interface would result in the formation of a six-coordinate anion complex and could explain the anion responses observed with compounds 2-7 (e.g., Mn(TPP)Cl·H<sub>2</sub>O + Y<sup>-</sup> ⇌ Mn(TPP)Cl·Y<sup>-</sup>).

While further spectroscopic studies are required to definitively explain the mechanism by which Mn(III) porphyrin based membranes respond to pH and anions, the data presented here clearly illustrates that potentiometric selectivity toward anions can be varied significantly by altering the structure of the porphyrin used to prepare the membrane. Further manipulation of selectivity may be achieved by using even more unique and hindered porphyrin structures (including membrane soluble aggregates) as well as porphyrins with metal centers other than Mn(III). Indeed, ongoing studies with Sn(IV) porphyrins have yielded membranes that appear to offer adequate selectivity for use in the measurement

of blood salicylate levels (23).

## LITERATURE CITED

- (1) Arnold, M. A.; Solsky, R. L. *Anal. Chem.* **1986**, *58*, 84R-101R.
- (2) Yu, R.-Q. *Ion-Sel. Electrode Rev.* **1986**, *3*, 153-171.
- (3) Morf, W. E. *The Principles of Ion-Selective Electrodes and Membrane Transport*; Elsevier: Amsterdam, 1981; Chapter 11.
- (4) Hofmeister, F. *Arch. Exp. Pathol. Pharmacol.* **1988**, *24*, 247-260.
- (5) Oesch, U.; Ammann, D.; Pham, H. U.; Wuthier, U.; Zund, R.; Simon, W. *J. Chem. Soc., Faraday Trans. 1* **1986**, *82*, 1179-1186.
- (6) Meyerhoff, M. E.; Pretsch, E.; Welti, D. G.; Simon, W. *Anal. Chem.* **1987**, *59*, 144.
- (7) Wuthier, U.; Pham, H. V.; Zund, R.; Welti, D.; Funk, R. J. J.; Bezegh, A.; Ammann, D.; Pretsch, E.; Simon, W. *Anal. Chem.* **1984**, *56*, 535-538.
- (8) Schulthess, P.; Ammann, D.; Krautler, B.; Caderas, C.; Stepanek, R.; Simon, W. *Anal. Chem.* **1985**, *57*, 1397-1401.
- (9) Schulthess, P.; Ammann, D.; Simon, W.; Caderas, C.; Stepanek, R.; Krautler, B. *Helv. Chim. Acta* **1984**, *67*, 1026-1032.
- (10) Shimidzu, T.; Iyoda, T.; Segawa, H.; Honda, K. *Nouv. J. Chim.* **1986**, *10*, 213-215.
- (11) Nishide, H.; Ohyanagi, M.; Okada, O.; Tsuchida, E. *Macromolecules* **1986**, *19*, 494-496.
- (12) Tsuchida, E.; Nishide, H.; Yuasa, M. *J. Chem. Soc., Dalton Trans.* **1985**, 275-278.
- (13) Nishide, H.; Ohyanagi, M.; Okada, O.; Tsuchida, E. *Macromolecules* **1987**, *20*, 417-422.
- (14) Tsuchida, E. *J. Macromol. Sci., Chem.* **1979**, *A13*(4), 545-571.
- (15) Chang, Q.; Meyerhoff, M. E. *Anal. Chim. Acta* **1986**, *186*, 81-90.
- (16) Ammann, D.; Huser, M.; Krautler, B.; Rusterholz, B.; Schulthess, P.; Lindemann, B.; Halder, E.; Simon, W. *Helv. Chim. Acta* **1986**, *69*, 849-854.
- (17) Groves, J. T.; Chasser, A. M., submitted for publication in *J. Org. Chem.*
- (18) Chasser, A. M. Ph.D. Dissertation, University of Michigan, 1986.
- (19) Guilbault, G. G.; Durst, R. A.; Frant, M. S.; Freiser, H.; Hansen, E. H.; Light, T. S.; Pungor, G. A.; Rechnitz, G. A.; Rice, N. M.; Rohm, T. J.; Simon, W.; Thomas, J. D. R. *Pure Appl. Chem.* **1976**, *48*, 127-131.
- (20) Hill, C. L.; Williamson, M. M. *Inorg. Chem.* **1985**, *24*, 2836-2841.
- (21) Kelly, S. L.; Kadish, K. M. *Inorg. Chem.* **1982**, *21*, 3631-3639.
- (22) Morf, W. E.; Ammann, D.; Simon, W. *Anal. Lett.* **1974**, *7*, 9-22.
- (23) N. A. Chaniotakis and M. E. Meyerhoff, unpublished results, 1987.

N. A. Chaniotakis  
A. M. Chasser  
M. E. Meyerhoff\*

Department of Chemistry  
The University of Michigan  
Ann Arbor, Michigan 48109

J. T. Groves

Department of Chemistry  
Princeton University  
Princeton, New Jersey 08544

RECEIVED for review June 12, 1987. Accepted October 1, 1987.  
M.E.M. and N.A.C. gratefully acknowledge support from the National Institutes of Health (GM-28882). J.T.G. and A.M.C. gratefully acknowledge support from the National Science Foundation (CHE-8706310).

## TECHNICAL NOTES

### Fabrication of Platinum-Disk Ultramicroelectrodes

C. D. Baer,\* N. J. Stone, and D. A. Sweigart\*

Department of Chemistry, Brown University, Providence, Rhode Island 02912

Platinum, gold, and graphite ultramicroelectrodes having at least one dimension less than 25 μm have been intensively investigated during the past few years. Such electrodes have been fabricated as disks, cylinders, rings, and various arrays. Compared to conventional electrodes of diameter on the order of 1 mm, microelectrodes offer several significant advantages in voltammetric experiments. These include (1) a steady-state

response at appropriately low sweep rates, (2) the ability to determine moderately fast heterogeneous electron-transfer rate constants (*k*<sub>s</sub>) as well as rate constants for very rapid homogeneous chemical reactions through steady-state measurements, (3) decreased distortion from *i*R drop, which allows less polar solvents, lower electrolyte concentrations, and faster sweep rates to be used, (4) rapid measurement of faradaic

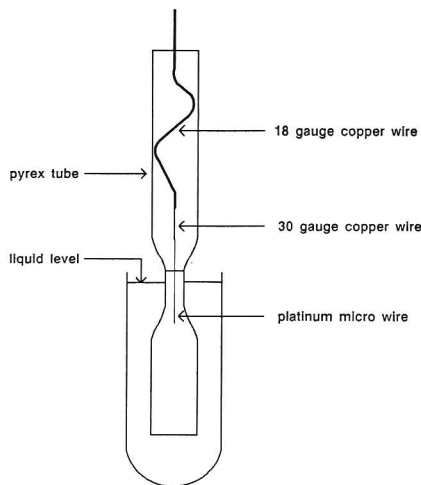


**Figure 1.** Diagram showing the Wollaston wire and connected copper wires in Pyrex tubing. The silver is etched off the Wollaston wire by nitric acid in the test tube.

processes due to a very small RC time constant, and (5) a favorable faradaic to charging current ratio.

Several groups have reported the construction of platinum-disk ultramicroelectrodes having dimensions from 25 to  $0.6\ \mu\text{m}$  (1–15). The general procedure involves heat sealing the platinum wire in glass and making electrical contact via silver epoxy to a wire of copper or some other metal. [The platinum may also be sealed with epoxy, but this method produces an inferior electrode (4).] For larger platinum wire (diameter  $\geq 10\ \mu\text{m}$ ) the reported procedure is quite adequate. However, for smaller diameters the technique is difficult and a “fairly high failure rate” is reported (1, 2). This is unfortunate since the smaller electrodes are the ones that best exemplify the properties listed above and are preferred in mechanistic studies involving rapid heterogeneous electron transfer and/or chemical reactions. Using the reported procedure, we were unable to fabricate any functional platinum electrodes with a diameter less than  $5\ \mu\text{m}$ . For this reason we developed an alternative method that is simple, highly successful, and produces very rugged platinum electrodes with diameters as small as  $1\ \mu\text{m}$ . The details are reported herein.

## EXPERIMENTAL SECTION

**Microelectrode Fabrication.** Platinum wire, 99.9%, was purchased from Goodfellow Metals as Wollaston wire in 5-, 2-, and  $1\text{-}\mu\text{m}$  diameters. A 2–3-cm length of the Wollaston wire was soldered to a short (ca. 2 cm) piece of 30-gauge copper wire that was in turn soldered to 8 cm of 18-gauge copper wire. A 20-cm piece of 4-mm-i.d. by 6-mm-o.d. Pyrex tubing was drawn out along a 2-cm section to give a constriction as illustrated in Figure 1. The wire was rinsed with acetone and placed in the tubing with the Wollaston wire positioned in the constriction; the 18-gauge copper wire had been bent sufficiently to keep it firmly positioned in the tubing. The assembly was then lowered into a test tube of 50% nitric acid in order to remove the silver coating from the platinum wire (Figure 1). The dissolution process was monitored with a magnifying glass and normally was complete within 15 min. The wire was carefully rinsed, *without removing the test tube*, with a 30-, 10-, 10-, and 10-mL sequence of distilled water, dilute ammonia, distilled water, and acetone, respectively applied to the top of the Pyrex tubing. The overflow from the test tube was collected in a beaker. (Rinsing the assembly after removal from the test tube is unnecessary and undesirable since it was found that this can lead to breakage of the platinum; reimmersion into

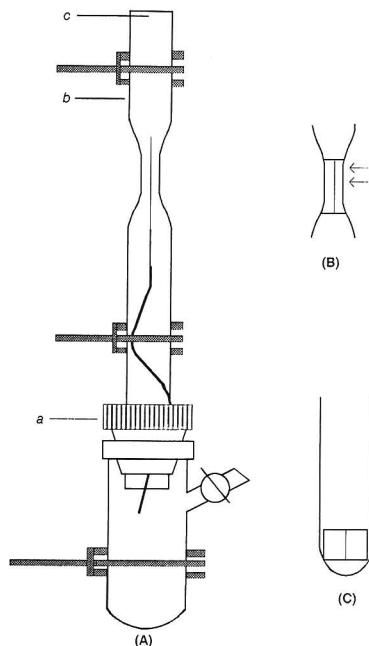


**Figure 2.** (A) Pyrex tubing assembly ready for sealing of the platinum wire at the constriction. (B) Tubing constriction after sealing; arrows indicate a possible segment containing unbroken platinum microwire. (C) A cylinder cut from the sealed segment in B and placed in Pyrex tubing.

the test tube almost always caused the wire to break at the point on the platinum where the etching stopped.) After rinsing, the test tube was discarded and the entire assembly oven dried at  $90\ ^\circ\text{C}$  for 15 min and examined under a stereoscope to ensure that the silver was completely removed and that the platinum wire was intact.

The end of the Pyrex tubing containing the copper wire was firmly fitted to a small flask via a Kontes universal adaptor (a in Figure 2A). The entire assembly was then clamped firmly in a vertical position with the platinum wire pointing up, and a section (b) of the tubing above the constriction was heated to softness to relieve any strain. A vacuum was applied to the upper part of the tubing (c) and the constricted region, was sealed around the platinum wire with an oxygen-methane flame. The latter operation was performed rapidly without allowing the glass to distort any more than necessary. Distortion was usually minimal provided the strain was first relieved as described above. Next the vacuum was broken by opening the stopcock in Figure 2A and the copper wire was pulled away from the platinum, removed from the tubing, and reserved for later use. The sealed part of the pyrex tubing was carefully examined under a stereoscope for a region where the platinum wire was continuous. (It is not uncommon for the platinum wire to break in several places during the sealing process; this is especially true of 1- and  $2\text{-}\mu\text{m}$  wire.) A 3–6-mm section of the sealed glass containing unbroken platinum wire (e.g., between the arrows in Figure 2B) was marked and cut on one end with a glass saw. The cut surface was polished, first with 240-, 600-, and 1200-grade emery paper and then with 5-, 0.3-,  $0.05\text{-}\mu\text{m}$  alumina (Buehler) on microcloth. The other end of the 3–6-mm section was cut free with a glass saw to give a cylinder of height 3–6 mm. Frequently, additional cylinders can be cut from the remaining sealed glass so that several electrodes can be fabricated from the original length of Wollaston wire. (After as many cylinders as possible are cut, the final section of the sealed glass together with the attached tubing can be converted into an electrode by a procedure similar to that used with the cylinders.)

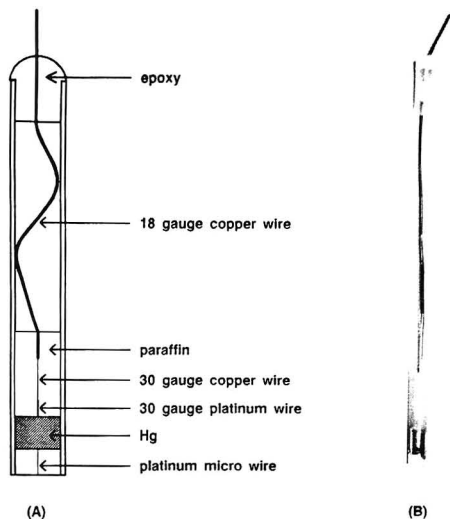


Figure 3. (A) Diagram of finished microelectrode. (B) A photograph of a 2-μm-diameter platinum disk microelectrode.

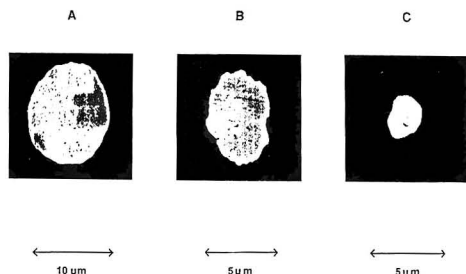


Figure 4. Scanning electron micrographs of (A) 10-, (B) 5-, and (C) 2-μm-diameter platinum-disk microelectrodes.

A new 12 cm section of Pyrex tubing of internal diameter just large enough to allow insertion of the cylinder was sealed on one end and the cylinder placed inside with the polished end of the cylinder facing the open end of the tubing as shown in Figure 2C. A vacuum was applied to the tubing and it was sealed to the cylinder with an oxygen-methane torch. The surface of the platinum wire was exposed by cutting and grinding the bottom of the tubing with a glass saw followed by the polishing steps given above. The surface of the cylinder inside the tubing was etched with 49% HF (CAUTION—avoid inhalation or exposure to skin) which was then thoroughly rinsed out. (This ensures that the platinum wire is well-exposed.) Electrical contact was made with the platinum surface by the addition of a small amount of mercury followed by evacuation to remove any trapped air. At this point, a length of copper wire was put in contact with the mercury and the electrode response checked by running a cyclic voltammogram of ferrocene in dichloromethane (0.1 M TBAP) (TBAP = tetra-*n*-butylammonium perchlorate) under steady-state conditions. If the electrode response was not satisfactory the grinding/polishing and/or etching steps were repeated. When the response was satisfactory, a more permanent electrical connection was made by soldering a 1-cm piece of 30-gauge platinum wire to the previously reserved copper wire, inserting half of the platinum end into the mercury, and adding a layer of paraffin to seal the wire and mercury in place. (Having platinum rather than copper in contact with the mercury prevents amalgamation.) The upper end of the copper wire was epoxied into position at the top of the tube to give a finished electrode. A schematic drawing and

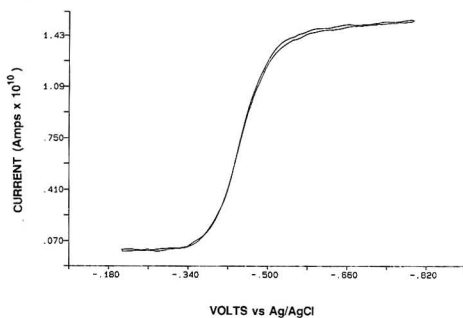


Figure 5. A cyclic voltammogram of  $1.0 \times 10^{-3}$  M  $\text{Fe}(\text{OEP})(N\text{-MeIm})_2^+$  in dichloromethane with 0.1 M TBAP at 25 °C. The working electrode was a 1-μm-diameter platinum disk and the sweep rate was 20 mV/s; the scan started at -0.20 V. OEP is the dianion of octaethylporphyrin and *N*-MeIm is *N*-methylimidazole (the latter present at 1.0 M).

a photograph of a finished electrode are shown in Figure 3. The fabrication technique was highly successful: for each 2-cm section of Wollaston wire at least one functional platinum ultramicroelectrode (2 μm or 1 μm diameter) was produced.

**Voltammetry.** Voltammetric experiments with the ultramicroelectrodes were done with a two-electrode configuration. The reference electrode was either Ag/AgCl in  $\text{CH}_2\text{Cl}_2/0.1$  M TBAP or a platinum-wire pseudoreference. The electrochemical cell was placed inside a solid aluminum Faraday cage. Nitrogen was used to blanket the solution in the cell. An EG&G Model 175 universal programmer was used to generate the voltage ramp and a Keithley Model 427 current amplifier was used to convert current to a voltage signal that was fed to a Nicolet 3091 digital oscilloscope and then to an IBM AT computer for display and analysis by using Asystant+ software (Macmillan Software Co., New York).

## DISCUSSION

Scanning electron micrographs (SEM's) were obtained for several of the ultramicroelectrodes. The SEM's of 10-, 5-, and 2-μm-diameter electrodes are given in Figure 4, which shows that the platinum surface is fairly defect free and is roughly circular in shape. It is also apparent that the platinum is well sealed to the glass. Standard calibrations confirm that the platinum wire diameter is fairly close to the manufacturer's specifications. Steady-state cyclic voltammograms at room temperature were recorded for ferrocene, several (methylcyclopentadienyl)manganese and -rhenium complexes, and several metalloporphyrins. High-quality results were obtained in all solvents tried:  $\text{CH}_2\text{Cl}_2$ ,  $\text{CH}_3\text{CN}$ ,  $(\text{CH}_3)_2\text{CO}$ , dimethylformamide (DMF), and propylene carbonate; a typical room temperature result is given in Figure 5. Although the SEM's showed that the electrodes are not perfectly circular, the steady-state limiting currents were fairly accurately described ( $\pm 10\%$ ) by the theoretical expression  $i_L = 4nFDCr$  where  $r$  is the nominal electrode radius. We also found that good voltammograms were readily obtained at -70 °C in  $\text{CH}_2\text{Cl}_2$  and  $(\text{CH}_3)_2\text{CO}$ , showing that microelectrodes can be used to advantage at low temperature in fairly nonpolar solvents (16-18). The microelectrodes behaved well at sweep rates of several hundred volts per second where (as expected) linear diffusion made a noticeable (i.e., non-steady-state) contribution to the current response. (Much faster scan rates are required to increase the linear diffusion to the point where it dominates, e.g., the 90% level requires about 5000 V/s at a 5-μm-diameter electrode).

In comparison to other published methods of ultramicroelectrode fabrication we believe that our method offers several significant advantages. Foremost is the much higher success rate. As mentioned above, we had great difficulty making any 1- and 2-μm electrodes by published procedures. In contrast, our method represents an efficient use of ex-

pensive Wollaston wire—a single 2-cm length of Wollaston wire frequently can be used to produce several microelectrodes by our fabrication technique (vide supra). A higher success rate also means a savings in time. In addition, we found that the steps leading to the point where it can be determined if the electrode will be functional are simpler and less time consuming compared to other methods.

Another advantage is the ruggedness of our electrodes. Due to sealing of the cylinder in glass tubing (Figure 2C), the insulating glass surrounding the electrode tip is much thicker than in previously described microelectrodes. It is also worth noting that the electrical connection of the platinum microwire is via a mercury pool and does not depend on a solder connection to another (thicker) wire.

#### ACKNOWLEDGMENT

We are grateful to M. Sosnowski of the Physics Department, Brown University, for obtaining the scanning electron micrographs. C.D.B. is grateful to Providence College for granting a sabbatical leave (1986-1987).

**Registry No.** Pt, 7440-06-4; Hg, 7439-97-6; Fe(OEP)(N-MeIm)<sub>2</sub><sup>+</sup>, 60151-09-9; HNO<sub>3</sub>, 7697-37-2.

#### LITERATURE CITED

- (1) Bond, A. M.; Fleischmann, M.; Robinson, J. J. *Electroanal. Chem. Interfacial Electrochem.* **1984**, *168*, 299.
- (2) Fleischmann, M.; Lasserre, F.; Robinson, J.; Swan, D. J. *Electroanal. Chem. Interfacial Electrochem.* **1984**, *177*, 97.

- (3) Cassidy, J.; Khoo, S. B.; Pons, S.; Fleischmann, M. J. *Phys. Chem.* **1985**, *89*, 3933.
- (4) Bixler, J. W.; Bond, A. M.; Lay, P. A.; Thormann, W.; van den Bosch, P.; Fleischmann, M.; Pons, B. S. *Anal. Chim. Acta* **1986**, *187*, 67.
- (5) Dibble, T.; Bandyopadhyay, S.; Ghoroghchian, J.; Smith, J. J.; Sarfarazi, F.; Fleischmann, M.; Pons, S. J. *Phys. Chem.* **1986**, *90*, 5275.
- (6) Montenegro, M. I.; Pletcher, D. J. *Electroanal. Chem. Interfacial Electrochem.* **1986**, *200*, 371.
- (7) Feldman, B. J.; Ewing, A. G.; Murray, R. W. J. *Electroanal. Chem. Interfacial Electrochem.* **1985**, *194*, 63.
- (8) Ewing, A. G.; Feldman, B. J.; Murray, R. W. J. *Phys. Chem.* **1985**, *89*, 1263.
- (9) Geng, L.; Ewing, A. G.; Jernigan, J. C.; Murray, R. W. *Anal. Chem.* **1986**, *58*, 852.
- (10) Geng, L.; Reed, R. A.; Longmire, M.; Murray, R. W. J. *Phys. Chem.* **1987**, *91*, 2908.
- (11) Howell, J. O.; Wightman, R. M. *Anal. Chem.* **1984**, *56*, 524.
- (12) Wehmeyer, K. R.; Wightman, R. M. *Anal. Chem.* **1985**, *57*, 1989.
- (13) Scharifker, B.; Hills, G. J. *Electroanal. Chem. Interfacial Electrochem.* **1981**, *130*, 81.
- (14) Aoki, K.; Akimoto, K.; Tokuda, K.; Matsuda, H.; Osteryoung, J. J. *Electroanal. Chem. Interfacial Electrochem.* **1984**, *171*, 219.
- (15) Fitch, A.; Evans, D. H. J. *Electroanal. Chem. Interfacial Electrochem.* **1986**, *202*, 83.
- (16) O'Brien, P.; Sweigart, D. A. J. *Chem. Soc., Chem. Commun.* **1986**, 198.
- (17) Bond, A. M.; Sweigart, D. A. *Inorg. Chim. Acta* **1986**, *123*, 167.
- (18) Stone, N. J.; Sweigart, D. A.; Bond, A. M. *Organometallics* **1986**, *5*, 2553.

RECEIVED for review August 7, 1987. Accepted September 14, 1987. This work was supported by grants to D.A.S. from the National Institutes of Health (DK30145) and the National Science Foundation (CHE-8521189). D.A.S. is the recipient of a NIH Research Career Development Award (1983-1988).

## Automated Cryogenic Collection of Carbon Dioxide for Stable Isotope Analysis and Carbon-14 Accelerator Mass Spectrometry Dating

C. A. M. Brenninkmeijer

*Institute of Nuclear Sciences, Department of Scientific and Industrial Research, Private Bag, Lower Hutt, New Zealand*

Manipulation of gases and vapors is often done in glass vacuum systems. The incompatibility of glass systems with the recent demand for laboratory automation has been a major drawback. With the development of a pneumatically operated glass high-vacuum valve (1) this problem was largely overcome. Thus by using automated glass valves, and an automated variable temperature cold trap (2), a process like converting organic matter to H<sub>2</sub> for <sup>2</sup>H mass spectrometric analysis could be automated (3). The more recent invention of a vacuum-powered high-vacuum glass valve (4) not only offers an elegant alternative to the pneumatic high-vacuum glass valve, but in addition makes it possible to fit gas sample bottles with automated taps. This allows automated gas collection in glass bottles (5).

In order to quantitatively collect CO<sub>2</sub> in a gas sample bottle, the bottle is commonly immersed in liquid nitrogen. This step can be automated by placing a Dewar with liquid nitrogen on a motorized labjack. Yet, when a larger number of sample bottles is involved this procedure becomes impracticable. Such an instance arose when we had to recover CO<sub>2</sub> samples after mass spectrometric <sup>13</sup>C analysis in order to perform <sup>14</sup>C TAMS (tandem accelerator mass spectrometry).

A sample bottle as depicted in Figure 1 can be used successfully for automated CO<sub>2</sub> collection. It consists of a mass spectrometer sample bottle fitted with a 5-mm-bore Vacutap. Vacutaps are vacuum operated, seatless, O-ring-type, high-vacuum glass valves. (Vacutaps are manufactured by Louwers Hapert, 5527 ZG Hapert, The Netherlands.) Inside the bottle is a tube through which liquid nitrogen can be passed. By reducing the pressure at the exhaust tube, liquid nitrogen is

drawn into this tube and a small quantity is collected in the bottom. Sufficient liquid nitrogen can be collected to last for several minutes, thus allowing CO<sub>2</sub> to be frozen into the bottle.

Although the principle is simple, the procedure had to be optimised and its limitations established. With the bottle shown, and by using a 1-m-long plastic filling tube of 1.6-mm bore (urethane tubing 1/8 × 1/16 in.) while pumping the exhaust at a rate of roughly 30 L/min, the tube can be filled with 1.7 cm<sup>3</sup> of liquid nitrogen, up to level A indicated in Figure 1, in less than 1 min. This amount of nitrogen will last for 6 min. in an evacuated tube. If CO<sub>2</sub> is present, this will form an insulating and reflective layer around the liquid nitrogen, stretching this time to about 12 min. Not much condensation of water vapor on the outside of the bottle occurs and the condensation of CO<sub>2</sub> can be observed. It appears that the height difference between the bottle and the liquid nitrogen supply has no significant effect on the performance. However, increasing the length of the filling tube rapidly increases the time it takes to collect the nitrogen. The reason is that boiling of liquid nitrogen in the filling tube creates so much nitrogen gas that the pressure drop is insufficient. The use of a larger diameter filling tube does not necessarily improve this situation, and often merely cold nitrogen gas was sucked through the assembly. Therefore, for bridging larger distances, a thermally insulated tube with a bore diameter of 3 mm or more is recommended.

Two laboratory compressors have been used during experiments. A Thomas Model 917CD18 (34 L/min) was satisfactory, whereas Model 004CD33 (12 L/min) did not always provide enough suction.

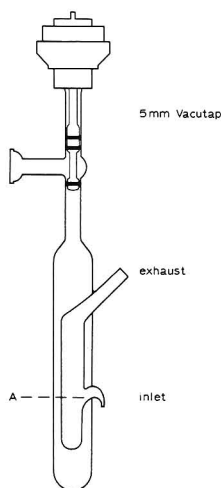


**Figure 1.** Vacutap sample bottle with cooling insert. The inlet tube diameter was about 1 mm. The inlet tube points slightly downward on the inside. The exhaust tube diameter was 5 mm. The cooling tube diameter was 10 mm.

As mentioned above, the cooling time was less than 1 min. For automating the procedure, suction can be applied for a fixed period of 1–1.5 min. After the tube is filled with liquid nitrogen up to level A, a mixture of gas and liquid flows from the inlet tube straight into the exhaust tube. When pumping is interrupted, no liquid remains above level A. Further suction only causes unnecessary loss of liquid nitrogen but eventually the pump may be damaged by embrittlement of interior parts. After completing a sample freeze-back it takes

about 1 min for the filling tube and the plastic tube connected to the exhaust to warm up sufficiently to be detached from the sample bottle.

For testing the freeze-back procedure we used a Vacutap freeze-back bottle on our automated Nuclide stable isotope mass spectrometer. One sample of 10 cm<sup>3</sup> CO<sub>2</sub> gas was analysed and frozen back automatically for 28 times. The spread in  $\delta^{13}\text{C}$  (1 $\sigma$ ) was 0.02‰, and no systematic change in isotopic ratio could be detected. The loss of CO<sub>2</sub>, primarily due to pumping of the sample after freezing back, amounted to 3%, equivalent to 0.1%/cycle. The cause of this loss of CO<sub>2</sub> is that part of the CO<sub>2</sub> is condensed near level A indicated in the figure. As the system is pumped some CO<sub>2</sub> escaping from this position due to a lowering of the liquid nitrogen level is pumped away instead of condensing on the lower part. If this is considered undesirable, some additional liquid nitrogen can be drawn into the tube during pumping. The consumption of liquid nitrogen was 30 cm<sup>3</sup>/cycle.

The bottle described also can be used to automatically collect condensable gases such as CO<sub>2</sub> and SO<sub>2</sub> from preparation systems. Another useful application can be achieved by constructing U-shaped sample bottles with two Vacutaps and a cooling insert. Such sample bottles can be used to automatically trap the condensables from the effluent gas of gas chromatographs.

**Registry No.** CO<sub>2</sub>, 124-38-9.

#### LITERATURE CITED

- (1) Brenninkmeijer, C. A. M. *Int. J. Appl. Radiat. Isot.* **1981**, *32*, 679–680.
- (2) Brenninkmeijer, C. A. M. *Anal. Chem.* **1982**, *54*, 2622.
- (3) Brenninkmeijer, C. A. M. Thesis, University of Groningen, The Netherlands, 1983.
- (4) Brenninkmeijer, C. A. M.; Louwers, M. C. *Anal. Chem.* **1985**, *57*, 960.
- (5) Brenninkmeijer, C. A. M.; Morrison, P. D. *Isot. Geosc.* **1987**, in press.

RECEIVED for review July 15, 1987. Accepted September 14, 1987.

#### CORRECTION

##### Ion-Pair Chromatographic Determination of Anions Using an Ultraviolet-Absorbing Co-Ion in the Mobile Phase

Brian A. Bidlingmeyer, Carmen T. Santasania, and F. Vincent Warren, Jr. (*Anal. Chem.* **1987**, *59*, 1843–1849).

In the Results and Discussion section, the first two sentences of the second paragraph should read as follows: The conductometric monitoring of the separation shown in Figure 1B is similar to one previously reported that used a "dynamically coated" reversed-phase column with a tetramethylammonium salicylate (TMA-SAL) eluent (33). In that work cetylpyridinium chloride was used to "coat" the bonded phase column prior to using the low conductivity, aqueous eluent of 0.5 mM TMA-SAL at pH 6.3.

The following reference corrections should also be noted: (3) Dreux, M.; LaFosse, M.; Pequignot, M. *Chromatographia* **1982**, *15*, 653. (15) Vera-Avila, L. E.; Caude, M.; Rosset, R. *Analysis* **1982**, *10*, 36. (33) Cassidy, R. M.; Elchuk, S. J. *Chromatogr.* **1983**, *262*, 311.



# For Excellence in Chemical Publishing, Look to Publications from the American Chemical Society

## ACCOUNTS OF CHEMICAL RESEARCH

Editor, F.W. McLafferty  
Cornell University  
12 issues a year. ISSN 0001-4842  
Member \$23 Nonmember \$105

## ANALYTICAL CHEMISTRY

Editor, George H. Morrison  
Cornell University  
24 issues a year. ISSN 0003-2700  
Member \$25 Nonmember \$38

## BIOCHEMISTRY

Editor, Hans Neurath  
University of Washington  
26 issues a year. ISSN 0006-2960  
Member \$75 Nonmember \$439

## CHEMICAL & ENGINEERING NEWS

Editor, Michael Heylin  
51 issues a year. ISSN 0009-2347  
Nonmember \$49

## CHEMICAL RESEARCH IN TOXICOLOGY

Editor, Lawrence J. Marnett  
Wayne State University  
6 issues a year. ISSN 0893-228X  
Member \$46 Nonmember \$269

## CHEMICAL REVIEWS

Editor, Josef Michl  
University of Texas  
8 issues a year. ISSN 0009-2665  
Member \$22 Nonmember \$129

## CHEMTECH

Editor, Benjamin J. Lubertoff  
12 issues a year. ISSN 0009-2703  
Member \$34 Nonmember (Pers.) \$55  
Nonmember (Inst.) \$252

## ENERGY & FUELS

Editor, John W. Larsen  
Lehigh University  
6 issues a year. ISSN 0887-0624  
Member \$46 Nonmember \$269

## ENVIRONMENTAL SCIENCE & TECHNOLOGY

Editor, William H. Glaze  
University of California, Los Angeles  
12 issues a year. ISSN 0013-936X  
Member \$30 Nonmember (Pers.) \$55  
Nonmember (Inst.) \$192

## INDUSTRIAL & ENGINEERING CHEMISTRY RESEARCH

Editor, Donald R. Paul  
University of Texas, Austin  
12 issues a year. ISSN 0888-5885  
Member \$52 Nonmember \$299

## INORGANIC CHEMISTRY

Editor, M. Frederick Hawthorne  
University of California, Los Angeles  
26 issues a year. ISSN 0020-1669  
Member \$79 Nonmember \$443

## JOURNAL OF AGRICULTURAL AND FOOD CHEMISTRY

Editor, Irvin E. Liener  
University of Minnesota  
6 issues a year. ISSN 0021-8561  
Member \$24 Nonmember \$131

## JOURNAL OF THE AMERICAN CHEMICAL SOCIETY

Editor, Allen J. Bard  
University of Texas, Austin  
26 issues a year. ISSN 0002-7863  
Member \$70 Nonmember \$399

## JOURNAL OF CHEMICAL AND ENGINEERING DATA

Editor, Bruno J. Zvolinski

Call Toll Free (U.S.)

# 800-227-5558

Telex: 440159 ACSP UI or

892582 ACSPUBS

Cable Address: JIECHEM

Telecopier (SANYO Group 1,2,3): 202-872-4615

**American Chemical Society  
Marketing Communications  
Department  
1155 Sixteenth St., N.W.  
Washington, D.C. 20036  
U.S.A.**

Texas A&M University

4 issues a year. ISSN 0021-9568  
Member \$29 Nonmember \$171

## JOURNAL OF CHEMICAL INFORMATION AND COMPUTER SCIENCES

Editor, Thomas L. Isenhour  
Utah State University  
4 issues a year. ISSN 0095-2338  
Member \$17 Nonmember \$90

## JOURNAL OF MEDICINAL CHEMISTRY

Editor, Philip S. Portoghesi  
University of Minnesota  
12 issues a year. ISSN 0022-2623  
Member \$40 Nonmember \$234

## THE JOURNAL OF ORGANIC CHEMISTRY

Editor, Frederick D. Greene  
Massachusetts Institute of Technology  
26 issues a year. ISSN 0022-3263  
Member \$53 Nonmember \$309

## JOURNAL OF PHYSICAL AND CHEMICAL REFERENCE DATA

Editor, David R. Lide, Jr.  
National Bureau of Standards  
4 issues a year. ISSN 0047-2689  
Member \$60 Nonmember \$265

## THE JOURNAL OF PHYSICAL CHEMISTRY

Editor, Mostafa A. El-Sayed  
University of California, Los Angeles  
26 issues a year. ISSN 0022-3654  
Member \$65 Nonmember \$432

## LANGMUIR

Editor, Arthur W. Adamson  
University of Southern California  
6 issues a year. ISSN 0743-7463  
Member \$55 Nonmember \$342

## MACROMOLECULES

Editor, Field H. Winslow  
AT&T Bell Laboratories  
12 issues a year. ISSN 0024-9297  
Member \$53 Nonmember \$342

## ORGANOMETALLICS

Editor, Dietmar Seyferth  
Massachusetts Institute of Technology  
12 issues a year. ISSN 0276-7333  
Member \$55 Nonmember \$360

# HP offers you more ways to do organic analysis than the EPA has methods.

And your analytical options keep growing.

For example, we've just added an infrared detector, an FPD, 601/602 water analyzer, and MS software specifically tailored to the newest EPA-reporting requirements.

These further expand what is already one of the broadest selections of analytical instruments and automation systems available for organic analysis. They reflect, too, HP's continuing commitment to provide the application solutions you need for your organic environmental analysis methods—and the EPA's.

Our support of your environmental laboratory needs includes a full range of automated systems for data analysis, management and EPA-approved reporting. Whether you need general or application specific instrumentation, GC/MS, GC/FTIR, or LC, HP has a data system to fit.

Breadth of line also means HP can give you the bonus of one-source support. You know the value of that if you've ever had to track down and coordinate multiple vendor support teams! Contrast those complexities and frustrations with the comprehensive across-the-board response that a

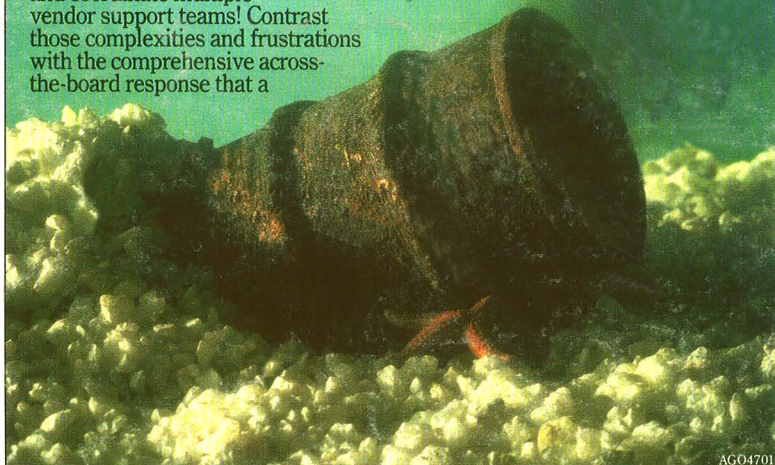
single phone call to HP can provide.

Plus, there's HP's time-proven quality and reliability. It's reflected in tens of thousands of HP analytical instruments that are working day-in, day-out around the world. You also see it in the 99% uptime guarantee available for our industry standard HP 5890A GC.

Quality, breadth of line and support are all a result of our "What If..." approach that sets your needs, always, as our starting point.

See for yourself.

Call the HP office listed in your telephone directory white pages and ask for an analytical products representative. Or write to Hewlett-Packard Analytical Group, 1820 Embarcadero Rd., Palo Alto, CA 94303.



HEWLETT  
PACKARD

AGO4701